



BENJAMIN EDWARDS

EDITOR

NANOTECHNOLOGY
SCIENCE AND TECHNOLOGY

SILVER
NANOPARTICLES

Advances in Research
and Applications

NOVA

Complimentary Contributor Copy

Complimentary Contributor Copy

NANOTECHNOLOGY SCIENCE AND TECHNOLOGY

SILVER NANOPARTICLES

ADVANCES IN RESEARCH AND APPLICATIONS

No part of this digital document may be reproduced, stored in a retrieval system or transmitted in any form or by any means. The publisher has taken reasonable care in the preparation of this digital document, but makes no expressed or implied warranty of any kind and assumes no responsibility for any errors or omissions. No liability is assumed for incidental or consequential damages in connection with or arising out of information contained herein. This digital document is sold with the clear understanding that the publisher is not engaged in rendering legal, medical or any other professional services.

Complimentary Contributor Copy

NANOTECHNOLOGY SCIENCE AND TECHNOLOGY

Additional books in this series can be found on Nova's website
under the Series tab.

Additional e-books in this series can be found on Nova's website
under the e-book tab.

NANOTECHNOLOGY SCIENCE AND TECHNOLOGY

SILVER NANOPARTICLES

ADVANCES IN RESEARCH AND APPLICATIONS

BENJAMIN EDWARDS
EDITOR



Complimentary Contributor Copy

Copyright © 2017 by Nova Science Publishers, Inc.

All rights reserved. No part of this book may be reproduced, stored in a retrieval system or transmitted in any form or by any means: electronic, electrostatic, magnetic, tape, mechanical photocopying, recording or otherwise without the written permission of the Publisher.

We have partnered with Copyright Clearance Center to make it easy for you to obtain permissions to reuse content from this publication. Simply navigate to this publication's page on Nova's website and locate the "Get Permission" button below the title description. This button is linked directly to the title's permission page on copyright.com. Alternatively, you can visit copyright.com and search by title, ISBN, or ISSN.

For further questions about using the service on copyright.com, please contact:

Copyright Clearance Center

Phone: +1-(978) 750-8400

Fax: +1-(978) 750-4470

E-mail: info@copyright.com.

NOTICE TO THE READER

The Publisher has taken reasonable care in the preparation of this book, but makes no expressed or implied warranty of any kind and assumes no responsibility for any errors or omissions. No liability is assumed for incidental or consequential damages in connection with or arising out of information contained in this book. The Publisher shall not be liable for any special, consequential, or exemplary damages resulting, in whole or in part, from the readers' use of, or reliance upon, this material. Any parts of this book based on government reports are so indicated and copyright is claimed for those parts to the extent applicable to compilations of such works.

Independent verification should be sought for any data, advice or recommendations contained in this book. In addition, no responsibility is assumed by the publisher for any injury and/or damage to persons or property arising from any methods, products, instructions, ideas or otherwise contained in this publication.

This publication is designed to provide accurate and authoritative information with regard to the subject matter covered herein. It is sold with the clear understanding that the Publisher is not engaged in rendering legal or any other professional services. If legal or any other expert assistance is required, the services of a competent person should be sought. FROM A DECLARATION OF PARTICIPANTS JOINTLY ADOPTED BY A COMMITTEE OF THE AMERICAN BAR ASSOCIATION AND A COMMITTEE OF PUBLISHERS.

Additional color graphics may be available in the e-book version of this book.

Library of Congress Cataloging-in-Publication Data

ISBN : ; 9: /3/75832/7: 8/7"*gDqmqm-

Published by Nova Science Publishers, Inc. † New York

Complimentary Contributor Copy

CONTENTS

Preface		vii
Chapter 1	Green Synthesis of Silver Nanoparticles – Nature Cannot Be Left Out <i>Anyik John Leo and Oluwatobi S. Oluwafemi</i>	1
Chapter 2	Tailoring PET Substrates with Collagen-Silver Nanoparticles <i>Mioara Drobeta and Magdalena Aflori</i>	31
Chapter 3	Synthesis of Ag Nanostructures in Mesoporous Silica Using Supercritical CO ₂ and Co-solvent <i>Qin-Qin Xu and Jian-Zhong Yin</i>	55
Chapter 4	Fabrication of Porous Silicon with Silver Nanoparticles by Ion Implantation <i>A. L. Stepanov, V. V. Vorobev, V. I. Nuzhdin, V. F. Valeev and Y. N. Osin</i>	73
Chapter 5	Antifungal Activities of Silver Nanoparticles Obtained by Pulsed Laser Ablation in Liquid <i>E. T. Aréchiga-Carvajal, J. M. Adame-Rodríguez, E. L. Lee-Bazaldua, B. Krishnan and S. Shaji</i>	89
Chapter 6	Silver Nanoparticles: Advances in Research and Applications Is Approaching <i>I. Alghoraibi and R. Zein</i>	105

Chapter 7	Risks and Benefits of Silver Nanoparticles for Nanomedicine Applications <i>Elisa Panzarini, and Luciana Dini</i>	145
Index		189

PREFACE

Nanotechnology is a ground breaking scientific innovation with significant activities that includes the production and application of nanostructures. It is an emerging technology that will contribute to economic prosperity by providing solutions to challenges that face modern day economies for the sustainability of mankind's development. Its applications cut across many scientific boundaries, from electronics to medicine, to advance manufacturing, to cosmetics. Silver nanoparticles are the most widely produced and marketed nanoparticles. This is due to their outstanding plasmonic activity, anti-cancer activity, disinfectant, bacterial inhibitory and bactericidal effects compared with the other metal nanoparticles. This book provides new research on the advances and the many applications of silver nanoparticles.

Chapter 1 - Research interest towards the synthesis of silver nanoparticles has grown tremendously in the recent years due to their application in the biomedical field, catalysis, optics, electronic to mention a few. These applications have triggered the synthesis of silver nanoparticles via several chemical and biological methods. The chemical methods can lead to absorption of hazardous chemicals on the surface of the nanoparticles thus, causing undesired toxicity issues and limit their biomedical applications. Owing to the important attributes silver nanoparticles has in the biomedical field such as disinfectant, antimicrobial, and as anti-cancer agents, their synthesis via a sustainable process is paramount for their usefulness in all these diverse applications. These sustainable processes take advantage of the green chemistry principles by employing green reagents to avoid the use of hazardous substances and in support of environmental sustainability. Nature has blessed the earth with an immense diversity of natural endowments such as plants of different species, DNA, RNA, proteins, and microbes which are readily available as biomaterials

towards a more sustainable green synthesis of nanomaterials. However, among all these naturally occurring material, extracts of diverse range of plant species have been preferentially used in synthesising silver nanoparticles. This is due to their vast availability in nature which can be easily incorporated into large-scale production of nanomaterials and their rich source of phytochemicals with added medicinal values. These phytochemicals have the natural tendency to reduce silver ions to silver nanoparticles. In addition, plant's materials are biodegradable with little or no adverse effect on the environment and are important as medicines, flavours, fragrances, pigments, insecticides and other fine chemicals. Many research groups have reported the synthesis of silver nanoparticles using plant extract of different species and their applications mostly in the biomedical field. This chapter will look into silver nanoparticles synthesis, characterization, and application in the different biomedical field.

Chapter 2 - Polyethylene terephthalate (PET) was selected in this work based on excellent properties, being widely used in many applications. Various strategies of surface modification have been developed over the time, because the response of the devices is largely controlled by surface chemistry and structure of the material.

In this chapter, PET was studied regarding the interactions at the polymer surface after plasma functionalization and immobilization of proteins in order to improve the adhesion properties. Obtaining the semisynthetic materials has enabled the generation of devices for medical applications, finding the optimal compatibility between two materials: one synthetic (polyester) and one natural (collagen). Biomolecules derived from or part of the extracellular matrix (e.g., gelatin, collagen, fibronectin) such as anti-inflammatory agents, anti-coagulant agents were immobilized. Collagens are by far the most abundant proteins that constitute up to 90% of the extracellular matrix of a tissue, thus imparting its structural integrity. Type I collagen is the major component of the extracellular matrix, and numerous reports have shown that collagen promotes higher cell adhesion and proliferation on the material. That can be subsequently used for the immobilization of biologically active molecules, furthermore, cellular growth (stem cells) on new supports.

Synthesis of metal nanoparticles (NPs) is an expanding research area due to the wide range of their applications in various fields. The controlled manner of silver nanoparticles release from polymer/metal nanocomposites can be useful for biotechnological applications, antibacterial and coating for biomedical activities. Conjugated polymers could induce nano-Ag to form compact structure, fill up the vacancy between nano-Ag, and enhance not only electron-transfer between nano-Ag and also adhesion on PET substrate.

In this chapter the interaction between PET/collagen and silver ions was investigated by FTIR spectroscopy, atomic force microscopy (AFM), X-ray photoelectron spectroscopy (XPS), SAXS spectrometry. The new results obtained the PET/collagen complex silver ions open offer new possibilities for applications in biotechnology and nanomedicine.

Chapter 3 - Ordered mesoporous silica have often been used as supports for various metal nanoparticles due to their high specific surface areas, high pore volumes and narrow pore size distributions. However, it is hard to obtain homogeneous metal dispersion and distribution due to low support-precursor interactions when the traditional impregnation method is used. This chapter reviews a new developed method of preparing supported Ag nanoparticles and nanowires in supercritical CO₂. Cheap inorganic salt AgNO₃ is used as precursor, mesoporous SBA-15 and KIT-6 are used as substrates, supercritical CO₂ is used as solvent and ethanol or the mixture of ethanol and ethylene glycol are used as co-solvents. Superior to traditional impregnation method, large aggregates of nanoparticles outside of the nanochannels could be usually avoided due to the near-zero surface tension of supercritical fluids. The operating parameters of interest including the deposition pressure, temperature, time and the amount of the precursor are summarized to demonstrate the optimum parameters influencing the deposition results. The thermodynamics and kinetics of AgNO₃ adsorption on SBA-15 from scCO₂ and co-solvent are investigated to further understand the experimental process and the mechanism. Finally, the underlying mechanism of supercritical fluid deposition method based on AgNO₃ and a specific co-solvent is described.

Chapter 4 - Porous silicon (PSi) have attracted remarkable concerns and found tremendous importance widespread in both fundamental research and industrial applications. At modern time PSi is considering as a key material in many industrial sectors such as electronics, sensors and photonics. Additionally, the interest to PSi nanostructures containing noble metal nanoparticles was recently found. Silver nanoparticles are the subject of specific increasing features due to their strongest plasmon resonance in the visible spectrum. Such materials could be widely used for variety applications as solar cells, absorbents, lightings, catalysts, and for biological sensors. At the present report a novel technological approach based on low-energy ion implantation is suggested and realized to create PSi layers with silver nanoparticles on the crystalline surface of Si wafers. It is demonstrated that using high-dose Ag-ion implantation of silicon with the energy of 30-60 keV the surface PSi structures with silver nanoparticles can be successfully fabricated. Also the fabricated plasmonic

material - Ag:PSi is tested for Surface Enhanced Raman Scattering - SERS sensor application.

Chapter 5 - Nanostructures of noble metals are being investigated for their applications in areas of biology and biotechnology, biological labeling, photothermal, photonics, optoelectronics, catalysis, surface-enhanced Raman scattering (SERS) detection etc. Among the metal nanoparticles, silver nanoparticles are well known for their size dependent properties as well as antibacterial activities. Pulsed laser ablation in liquid (PLAL) is a physical synthesis technique to obtain ultra-pure nanoparticles of metals, semiconductors and ceramics which is a green synthesis compared to other chemical methods. In this chapter, we describe antifungal activities of silver nanoparticles produced by pulsed laser ablation of a high purity silver target in distilled water. The chapter includes details of the synthesis of silver nanocolloids using PLAL and their characterization using various techniques. Antifungal activities of these silver nanocolloids on fungi such as *Aspergillus niger* and *Penicillium spp* are explained. These filamentous fungi are responsible for the deterioration of storage life of fruits and vegetables worldwide. The effects of heterogeneous shaped silver nanoparticles produced by PLAL in these two fungal species probed in vitro are discussed. The nanoparticle concentrations from 31.8 to 74.2 mg/L were able to delay mycelium growth and sporulation in both species at the conditions probed. These results open up more biological applications of nanoparticles synthesized by PLAL.

Chapter 6 - The field of nanotechnology has gained momentum over the past two decades with a broad range of potential applications, such as increasing bioavailability of a drug, biological labeling, cancer treatment, biosensing, antibacterial activity, antiviral activity, detection of genetic disorders and gene therapy. Advances in this field are mainly dependent on the ability to form nanoparticles of various materials, sizes, and shapes, and to efficiently assemble these particles into complex architectures. Nanoparticles are particles with a maximum size of 100 nm. These particles have unique properties, which are quite different than those of larger particles. The most prominent nanoparticles for medical uses are noble metal nanoparticles such as nanosilver which are well recognized for their remarkable physical, chemical, optical, electronic, magnetic, catalytic and anti-microbial properties of silver nanomaterial allows for their utilization in various scientific applications such as sensors, nanophotonics devices biology, drug delivery, cancer treatment, photothermal therapy, diabetic healing, solar cells, catalysis, cooling system, surface-enhanced Raman spectroscopy, inkjet-printer, imaging sensing, biology and medicine, optoelectronics and magnetic devices. There are many methods for

the synthesis of silver nanoparticles such as chemical reduction, electrochemical reduction, photochemical reduction, microemulsion, chemical vapor deposition, microwave assisted, hydrothermal method, spray pyrolysis, laser ablation, radiolysis and sonochemical method, etc.

From a practical point of view, the method of chemical reduction from aqueous silver nitrate solution is most preferable for obtaining silver nanoparticles which involve the reduction of relevant metal salts in the presence or absence of surfactants, which is necessary in controlling the growth of metal colloids through agglomeration.

The synthesized nanoparticles were characterized using Atomic Force Microscopy (AFM), UV-visible spectrophotometer; X-ray diffraction (XRD) and Fourier transform infrared spectrometry (FTIR).

Chapter 7 - The unique physicochemical characteristics of metal nanoparticles (NPs) (i.e., catalytic activity, optical properties, electronic properties, antibacterial properties, magnetic properties) are gaining the interest of scientists for their wide applications (from microelectronics to human health). In particular, silver (that is the most studied and used), gold, titanium, zinc, etc. NPs are largely exploited for nanomedicine applications. The AgNPs antibacterial and antifungal properties allow them to be extensively used in medical devices and to be also present in several daily use commercialized products such as food and cosmetics. Indeed, silver and AgNPs are largely applied in the preparation of skin ointments and creams to prevent infection of burns and bloody wounds and silver-impregnated polymers are nowadays present in several implants. The most recent AgNPs applications for human health, are in the field of high sensitivity biomolecular detection, diagnostics, antimicrobials and therapeutics. During recent years, AgNPs have received significant attention in cancer management, being also suitable as theranostic agents.

Regardless of the broad potentiality of the AgNPs use, there is still a lack of information concerning the increase exposure to AgNPs of humans, animals, plants and environments and their eventual short- and long-term toxicity. Indeed, *in vitro* studies indicate toxicity of AgNPs for skin, liver, lung, blood, and germ mammalian cells, by inducing cell cycle progression genes, Reactive Oxygen Species (ROS) production, DNA damage and cell deaths that suggest the application of AgNPs as anticancer agent. It is known that AgNPs have a better cytotoxic effects on liver cancer cell lines compared to normal ones. AgNPs in *in vivo* studies in adult rats and mice can reach several organs and cause toxicity while elicit developmental and structural malformations in non-mammalian embryos. Thus, to overcome toxicity (largely due to the release of Ag ions from

the NPs) and improve AgNPs performance a particular attention has been paid to the modality of synthesis. There is an increasing demand for *green synthesis* that ensures the absence of toxic byproducts. In fact, the approach used to synthesize AgNPs influences the response of cells by influencing the NPs surface characteristics. The NPs coating with molecules chosen among starch, glycans, PVP (poly(N-vinyl-2-pyrrolidone), citrate, polymers, etc. is pivotal to block the release of Ag ions.

In this work we will discuss the risks and the benefits of AgNPs to human health, in relation to nanomedicine by reviewing *in vitro* literature data and current applications in cancer theranostic.

Chapter 1

**GREEN SYNTHESIS OF SILVER
NANOPARTICLES – NATURE CANNOT BE
LEFT OUT**

Anyik John Leo^{1,2} and Oluwatobi S. Oluwafemi^{1,2,}*

¹Department of Applied Chemistry, University of Johannesburg,
Doornfontein, Johannesburg, South Africa

²Centre for Nanomaterials Science Research, University of Johannesburg,
Johannesburg, South Africa

BACKGROUND

Research interest towards the synthesis of silver nanoparticles has grown tremendously in the recent years due to their application in the biomedical field, catalysis, optics, electronic to mention a few. These applications have triggered the synthesis of silver nanoparticles via several chemical and biological methods. The chemical methods can lead to absorption of hazardous chemicals on the surface of the nanoparticles thus, causing undesired toxicity issues and limit their biomedical applications. Owing to the important attributes silver nanoparticles has in the biomedical field such as disinfectant, antimicrobial, and as anti-cancer agents, their synthesis via a sustainable process is paramount for their usefulness in all

* Corresponding author: Oluwatobi S. Oluwafemi. Department of Applied Chemistry, University of Johannesburg, P.O. Box 17011, Doornfontein 2028, Johannesburg, South Africa. Centre for Nanomaterials Science Research, University of Johannesburg, Johannesburg, South Africa. E-mail: Oluwafemi.oluwatobi@gmail.com.

these diverse applications. These sustainable processes take advantage of the green chemistry principles by employing green reagents to avoid the use of hazardous substances and in support of environmental sustainability. Nature has blessed the earth with an immense diversity of natural endowments such as plants of different species, DNA, RNA, proteins, and microbes which are readily available as biomaterials towards a more sustainable green synthesis of nanomaterials. However, among all these naturally occurring material, extracts of diverse range of plant species have been preferentially used in synthesising silver nanoparticles. This is due to their vast availability in nature which can be easily incorporated into large-scale production of nanomaterials and their rich source of phytochemicals with added medicinal values. These phytochemicals have the natural tendency to reduce silver ions to silver nanoparticles. In addition, plant's materials are biodegradable with little or no adverse effect on the environment and are important as medicines, flavours, fragrances, pigments, insecticides and other fine chemicals. Many research groups have reported the synthesis of silver nanoparticles using plant extract of different species and their applications mostly in the biomedical field. This chapter will look into silver nanoparticles synthesis, characterization, and application in the different biomedical field.

1. INTRODUCTION

Nanotechnology has revolutionised the scientific community ever since the concept was introduced by physics Nobel laureate Richard P Feynman in his famous lecture entitled 'There's plenty of room at the bottom' at the December 1959 meeting of the American Physical Society (Feynman, 1960). Nano-sized materials (1-100 nm) such as nano-rods, nanowires, nanotubes, and nanoparticles are being considered building blocks of nanotechnology for designing materials with unique and interesting optical, electronic and catalytic properties (Mohan et al., 2014) due to their small sizes and large surface area to volume ratio. These properties have made nano-sized materials unique and different from their corresponding bulk counterparts (Burda et al., 2005). Nanotechnology comes with its own challenges, as it generates waste products that undermined the safety of the environment with lack of appropriate policies to manage these new risks. The major concern includes potential reactivity and exposure to nanomaterials that have been dispersed into the environment (Justo-Hanani and Dayan, 2015). The extensive applications of this new technology in cosmetics, personal care products, paints and coatings, household products like detergents, catalysts and lubricants, sports products and textiles, medical and

healthcare products, food and nutritional ingredients, food packaging and agrochemicals, veterinary medicines, construction materials and consumer electronics (Golovina and Kustov, 2013; Benelmekki Maria, 2015) have eventually opened a lot of possibilities for the subsequent release of these waste into the environment (Figure 1). This has become a big source of concern for the safety of the environment and human health. The studies on the toxicity of various engineered nanomaterials (Beer et al., 2012; Maurer-Jones et al., 2013; Hadrup and Lam, 2014; Wang et al., 2014) suggest the need for caution though there is currently no sufficient information on their adverse effects on humans despite evidence of their presence in the environment (Kaegi et al., 2010). The need to steer the development of nanomaterials towards more sustainable practices is a pressing issue for the future of nanotechnology (Cinelli et al., 2015). This has also put pressure on researchers to integrate green chemistry towards the synthesis of nanomaterials. Green chemistry (GC) is a set of principles or rather a chemical philosophy that encourages the design of products and processes that reduce or eliminate the use and generation of hazardous substances (Lu and Ozcan, 2015). The first-hand book of green chemistry was published by Prof. Paul Anastas and John Warner in 1998 in which they exposed the GC objectives, visions, and challenges and also illustrated the 12 principles of GC, a set of “design rules” to help chemists in developing GC (Epicoco et al., 2014). Green chemistry is aimed at thwarting waste, minimizing energy use, employing renewable materials, and applying methods that minimize risk (Rauwel et al., 2015). Utilization of non-toxic chemicals, environmentally benign solvents, and renewable materials are some of the key issues that merit important consideration in a green synthetic strategy due to their advantage in reducing environmental risks (Mohan et al., 2016a). The synthesis of nanomaterials from a natural organism has become a major research area in the field of nanotechnology and has led to a sub-branch called green nanotechnology. Greener approach in nanotechnology for synthesising nanoparticles has various advantages such as simplicity, cost effectiveness, compatibility for bio-medical and pharmaceutical applications as well as for large-scale commercial production.

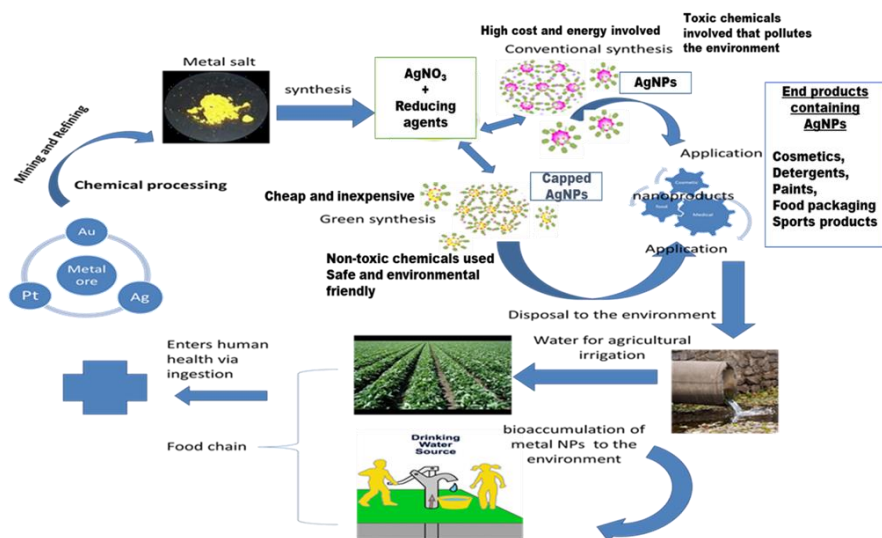


Figure 1. Possible pathway for the disposal of metal nanoparticles to the environment.

1.1. Significance of Nanotechnology

Nanotechnology is a ground breaking scientific innovation (Mura et al., 2013) with significant activities that includes the production and application of nanostructures. It is an emerging technology that will contribute to economic prosperity by providing solutions to challenges that face modern day economy for the sustainability of mankind's development. Its applications cut across many scientific boundaries, from electronics to medicine, to advance manufacturing, to cosmetics. In fact, nanotechnology has the potential to dramatically change lifestyles, jobs, and whole economies (Virikutyte and Varma, 2011). According to Fleischer and Grunwald (2008), nanotechnology cannot provide "magic bullets" that will solve all sustainability problems but a critical enabling component for a sustainable development when they are used wisely and when the social context of their application is considered. Many research groups have reported the synthesis of silver nanoparticles using plant extract of different species and their application mostly in the biomedical field. This chapter will look into their synthesis, characterization, and applications.

1.2. Silver Nanoparticles

The recent development of nanotechnology has triggered research interest towards the synthesis of noble metal nanoparticles such as gold, silver, and platinum due to their unique and attractive, optical and electronic properties. Among these noble nanomaterials, silver nanoparticles are the most widely produced (Piccinno et al., 2012) and marketed nanoparticles. This is due to their outstanding plasmonic activity, anti-cancer activity, disinfectant, bacterial inhibitory and bactericidal effects compared with the other metal nanoparticles (Mohan et al., 2014; Saha et al., 2014). Since historical times, utensils were fabricated with a silver lining, silver vessels were utilized for the preservation of perishable items, silver was used as an effective antimicrobial agent for the treatment of diseases as well as for disinfection and purification of water (Silver, 2003; Pradeep, 2009). This was purposely due to the fact that, silver ions and their related compounds had low toxicity toward animal cells but present a high toxicity to microorganisms like bacteria and fungi (Rauwel et al., 2015). Silver-containing materials can be applied in medicine for reduction of infections on the burn treatment, prevention of bacteria colonization on catheters and elimination of microorganisms on the textile fabrics as well as disinfectant in water treatment (Oluwafemi et al., 2013). However, silver in nano form possess a relatively much higher antimicrobial activity, anti-cancer and antioxidant properties compared to its macroscopic counterpart (Rajan et al., 2015) due to their small sizes and large surface area to volume ratio. Generally, silver nanoparticles (Ag-NPs) have been synthesised using the conventional route (physical and chemical method) which requires higher cost and higher energy with the aid of radiation and reducing agents. The physical method involves radiation techniques such as ultrasound irradiation, c-radiation, and microwave irradiation (Krishna et al., 2015) while the chemical methods make use of reducing agents such as sodium borohydrides, hydroxylamine hydrochloride, trisodium citrates, dimethyl formamide, hydrazine hydrate, thiols, etc. (Cheviron et al., 2014; Mohan et al., 2014). These conventional methods make use of highly toxic reagents which may lead to absorption of hazardous chemicals onto the surfaces of nanoparticles, making it difficult to use them for the biomedical application (Shankar et al., 2004). Furthermore, the by-products of these chemicals are potentially hazardous to the environment (Ahmed et al., 2015). Since silver nanoparticles are widely used in biomedical applications, and in order to enhance their efficacy toward this field, their synthesis via a sustainable process that is clean, reliable, safe, and eco-friendly is very important. This has triggered the scientific community to dedicate extensive

efforts toward developing suitable synthetic techniques for producing green and sustainable silver nanoparticles. The recent development of green nanotechnology which is an intersection of nanotechnology and biotechnology has enabled the synthesis of Ag-NPs using natural resources of biological origin. Biosynthesis of nanoparticles is a kind of bottom-up approach where the main reaction is reduction/oxidation (Durán et al., 2011). The interception of green nanotechnology has helped to maximise the safety, efficiency and minimise the environmental and societal impact of the synthesized materials. This serves as viable alternative to the conventional approaches for the synthesis of nanoparticles.

2. NATURALLY OCCURRING BIOMATERIALS FOR SYNTHESIS OF SILVER NANOPARTICLES

Nature has blessed the earth with an immense diversity of natural endowments with numerous chemical substances that can serve as suitable reducing agents for the synthesis of nanoparticles (Lu and Ozcan, 2015). The bright side of utilising these natural resources (biomaterials) is their environmental friendliness, abundances in nature and financially inexpensive process compare to the higher costs and higher energy required for the synthesis of nanoparticles via the conventional routes. In addition, these biomaterials have the potential to lower the toxicity of the resulting nanomaterial and thereby improving their biocompatibility and making them suitable for biomedical application.

2.1. Types of Materials

Naturally, renewable resources such as microorganisms, plants and biopolymers (DNA, RNA, proteins, starch, dextrose and gelatine) have the potential to serve as raw materials for making sustainable nanomaterial. The use of micro-organisms such as bacteria, fungi, and yeast have emerged as a good source with considerable potential for synthesizing silver nanoparticles (Jeyaraj et al., 2013; Ahluwalia et al., 2014; Anthony et al., 2014). The major draw-back for microbe-mediated green synthesis is the slow synthesis rate hence, the synthesis is time-consuming. In addition, industrial production of silver nanoparticles (Ag-NPs) via this route is not very feasible because microbes need

to be maintained under high aseptic conditions (Balavigneswaran et al., 2014) which are relatively expensive. The other natural biopolymers only suffer from cost-related challenges in acquiring these raw materials and thus are ill-suited for the large-scale production.

2.2. Plants Materials and Phytochemicals

Among the biological system that nature has provided, plant's materials are considerably preferred for biosynthesis of silver nanoparticles due to the following attributes.

1. The rich diversity of plant kingdom that provides varieties of phytochemicals which has the natural tendency to function as a reducing and capping agents (Hebbalalu et al., 2013),
2. The easy availability of plants in nature which is very cost effective and suitable for large-scale biosynthesis of nanoparticles that are free of contamination with well-defined size, and morphology (Mittal et al., 2013).
3. The presence of phytochemicals with high medicinal values in plants which when incorporated in to the nanoparticles enhance their functionality and marketability.
4. Plant material is environmentally friendly and biodegradable
5. Plants extracts from different species have been used for centuries for various purposes such as traditional medicine, food preservatives, flavors, fragrances, pigments, insecticides and other fine chemicals (Facchini et al. 2012) largely due to their antimicrobial properties (Busquet et al. 2006).

These attributes have encouraged scientists to use plant extracts in the synthesis of silver nanoparticles in support of environmental sustainability. Extracts from a number of different plants species have been successfully used for the preparation of Ag-NPs (Kajani et al., 2014) and in most cases, plants with medicinal properties have been employed (Table 1). The use of plant extracts to synthesize noble metal nanoparticles began with the pioneering work of Gardea-Torresdey et al. (2002), Jose-yacamann et al. (2003) and Shankar et al. (2004).

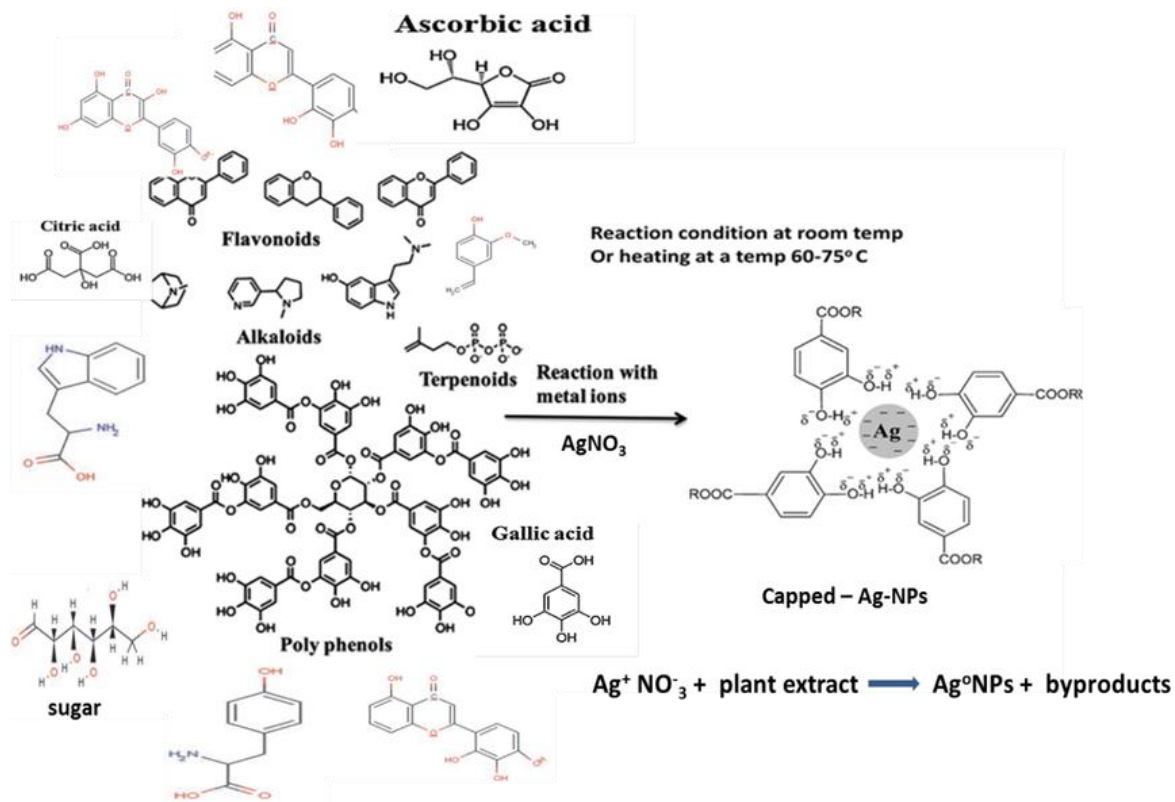


Figure 2. Formation of stable and capped silver nanoparticles in the presence of plant extracts (phytochemicals) and silver salts.

Table 1. Different plant species with medicinal properties used for green synthesis of silver nanoparticles

Plants species	Plant parts	Sizes (nm)	shapes	Biomolecules responsible for reduction and capping process	application	References
Acacia leucophloea	stem barks	17–29	spherical	amines, aldehyde/ketone, aromatic, azo, and nitro compounds	antibacterial activity	Murugan et al., 2014
Alternanthera dentate	Leaves	50–100	Spherical	Proteins	Anti-bacterial	Kumar et al., 2014
Acalypha indica	Leaves	20–30	Spherical	Quercetin	Antibacterial activity against water borne pathogens	Krishnaraj et al., 2010
Aegle marmelos	leaves	~60	Spherical	alkaloids, phenylpropanoids, terpenoids and other polyphenols		Rao and Paria, 2013
Psidium guajava L.	Leaves	~60	spherical	phenols, flavonoid, terpenoid	Anti-microbial	Gupta et al., 2014
green tea	leaves	20-90	Almost spherical	extracts	Anti-bacterial	Sun et al., 2014
Morinda citrifolia	roots	32-52	Spherical and oval	Flavanoids, terpenoids	cytotoxicity	Suman et al., 2013
Ananas comosus	leaves	12.4	spherical	Sucrose, glucose	Anti-bacterial	Emeka et al., 2014
Dalbergia spinosa	leaves	14-22	spherical	Reducing sugar and flavonoids	Anti-bacterial and catalytic activity	Muniyappan and Nagarajan, 2014

Table 1. (Continued)

Plants species	Plant parts	Sizes (nm)	shapes	Biomolecules responsible for reduction and capping process	application	References
<i>Petroselinum crispum</i>	leaves	30-32	spherical	Ascorbic acid, alcohols and aldehydes	Anti-bacterial	Roy et al., 2014
<i>Ziziphora tenuior</i>	leaves	8-40	spherical	Alkaloids, phenolic, terpenoids		Sadeghi et al., 2015
<i>Caesalpinia coriaria</i>	Leaves	40-50 78-98	Triangular hexagonal spherical	Tannic acid	Anti-bacterial activity	Jeeva et al., 2014
Olive plant	leaves	20-25	spherical	Plants phytochemicals	antibacterial activity	Kahlil et al., 2014
Citrus limon	Peels	17.3-62.2	spherical	Plants phytochemicals	Anti-dermatophytic activity	Nisha et al., 2014
<i>Agrimoniae herba</i>		11	spherical	flavonoids and phenols	antineoplastic evaluation	Qu et al., 2014
<i>Naringi crenulata</i>	leaves	72-98	Spherical and cubic shape.	alkaloids, phenols, saponins and quinines	Biomedical application	Bhuvaneswari et al., 2014
<i>Brucea javanica</i> (L.)	Rind parts	8-50	spherical	Organic compounds		Notriawan et al., 2013
Satsuma mandarin	Peels	5–20	spherical	Flavonoid glycosides,		Basavegowda and Lee, 2013
<i>Ammannia baccifera</i>	aerial part	10-30	spherical, triangle and hexagonal	Proteins, phenolic compounds	Larvicidal activity	Suman et al., 2013

Since then, several research groups have used plants extracts of different species for their synthesis. Phytochemicals in plants crude such as alkaloids, flavonoids, carbohydrate, saponins, phenolic acids, phenyl propanoids, terpenoids, polyphenols, glucosinolates, polyamines, polysaccharides, vitamins, amino acids, etc. with hydroxyl, carbonyl, carboxylic or amine functional groups have been proposed as the active ingredients which are solely responsible for the reduction of silver ions to silver nanoparticles (Chiguvere et al., 2016; Singh et al., 2016). Typically, phenolic derivatives with hydroxyl and carboxyl functional groups have the ability to bind to metals (Ahmad et al., 2010) during synthesis to form bio-compatible and stable nanoparticles of desired shapes and sizes. Consequently, the antimicrobial, antioxidant and anticancer properties of the as-synthesized silver nanoparticles are also enhanced significantly (Rajan et al., 2015). The plant extracts obtained from various parts of the plant such as leaves, stems, roots shoots, flowers, and barks, of different plant species, contains different types of phytochemicals which vary in concentration. In most cases, not all of these phytochemicals present in the plant extract participate in the reduction and capping process during the synthesis of silver nanoparticles. Figure 2 is a schematic diagram showing the formation of stable and capped silver nanoparticles in the presence of silver salts and plants biomolecules. According to Rajan et al. (2015), phytochemicals such as protein, flavonoids, polyphenols, alkaloids, phenols, essential oils and polyols present in the plant extracts play a major role in the bio-reduction and capping of the nanoparticles.

3. GREEN SYNTHESIS OF SILVER NANOPARTICLES AND THEIR CHARACTERISATION TECHNIQUES

According to Raveendran et al. (2003), the three main steps in the preparation of nanoparticles that should be evaluated from a green chemistry perspective are the choice of the solvent medium used for the synthesis, the choice of an environmentally benign reducing agent, and the choice of a nontoxic material for the stabilization of the nanoparticles. For the green synthesis of silver nanoparticles using plant extract, water is preferable as the choice of environmentally benign solvent throughout the preparation while the reducing and stabilising agents are the active phytochemicals present in the plant biomass (Singh et al., 2016). The protocol for silver nanoparticle syntheses using plants extracts is simple and straightforward. It involves the collection of

the plants part of interest (leaves, roots or stem), and then obtain the crude extract containing the phytochemicals which are the active ingredients for the reduction and capping process. The next step is mixing the required volumes of metal salts with plants extracts and allows the mixture to reacts under room temperature or heating to produce the nanoparticles which usually takes few minutes or hours. For the synthesis of silver nanoparticles, the formation is indicated visually by a change in colour of the solution due to excitation of the surface plasmon resonance (SPR) in the silver nanoparticles. The resulting silver nanoparticles are then further characterised using spectroscopic and electron microscopy techniques (Figure 3). The main challenges frequently encountered in the biosynthesis of nanoparticles is the control of the shape and size as well as monodispersity in solution phase (Akhtar et al., 2013). To circumvent these challenges, certain synthetic parameters need to be optimised such as pH, temperature, concentration of extract, incubation time to mention a few. pH plays an important role in the reduction of metal ions to metal nanoparticles. According to Mochochoko et al. (2013), smaller particles sizes with high degree of monodispersity are more favoured in basic medium than acidic medium. The main influence of the reaction pH is its ability to change the electrical charges on the biomolecules which might affect their capping and stabilizing abilities and subsequently the growth of the nanoparticles (Kahlil et al., 2014). Therefore, shape and size of the nanoparticles synthesized using plants can be controlled and modulated by changing the pH. The increase in temperature (30°C-90°C), increases the rate of Ag-NPs synthesis and also promotes the synthesis of smaller size (Shrikar et al., 2016). Extract concentration plays an important role in the synthesis of silver nanoparticles. A concentration variation study of AgNO₃ using *S. lycopersicums* fruit extract was carried out with various volumes of *S. lycopersicums* fruit extract (Umadevi et al., 2013). When a large volume of the fruit extract was used for the synthesis of silver nanoparticles, an increase in the intensity of the SPR band was observed at around 444 nm which can be correlated with an enhancement in the number of nanoparticles in the reaction medium. In another study reported by Sosa et al. (2003), a comparatively higher extract ratio is responsible for the synthesis of symmetrical nanoparticles.

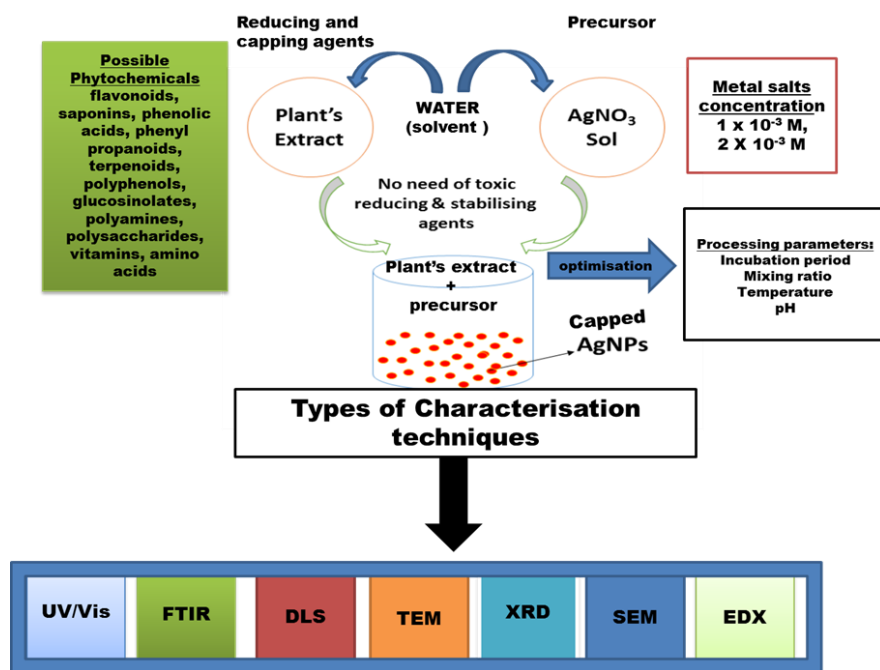


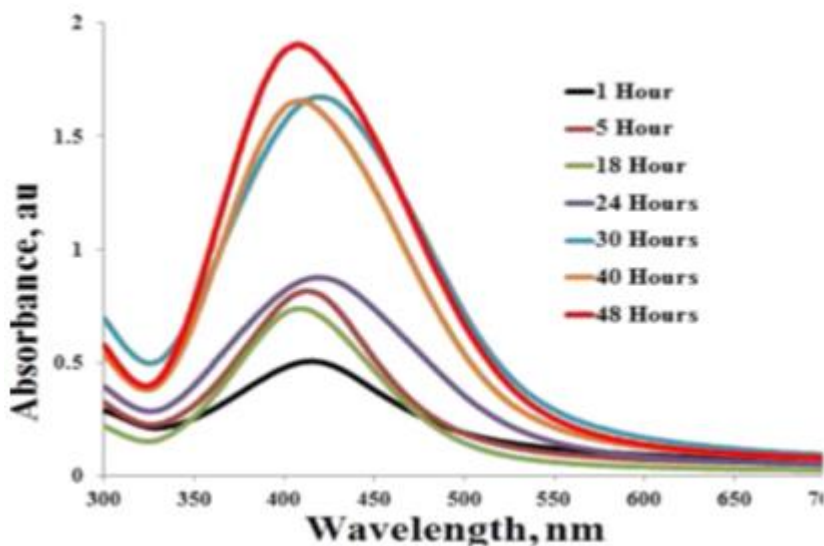
Figure 3. Systematic approach for the synthesis of silver nanoparticles using plant extracts and the various techniques for the characterisation of the as-synthesised Ag-NPs.

Application of nanoparticles is based on the information obtained from their properties which can be elucidated through various characterisation techniques. This is often based on their shape, size, surface area and disparity (Jiang et al., 2009). Below are the common techniques used:

UV-Vis (Ultraviolet/visible Spectroscopy): This characterization technique uses electromagnetic radiation between 190 nm and 800 nm. It is divided into the ultraviolet (190-400 nm) and visible (400-800 nm) regions which are aimed at studying the changes in the energy levels within a molecule during the promotion of electrons from occupied lower energy levels to unoccupied high energy levels (either non-bonding or π orbital). This technique is based on the absorption of surface plasmon resonance (SPR) generated by free electrons on the surface of the nanoparticles which interact with the electromagnetic field and it is usually the first technique used in monitoring the synthesis of nanoparticles (Pal et al., 2007). Noble metals nanoparticles such as gold and silver has strong absorption in the visible region of the electromagnetic spectrum

and spectrophotometric absorption measurements in the range of 400–450 nm corresponds to silver nanoparticles (Huang and Yang, 2004) while 500–550 nm corresponds to gold nanoparticles (Shankar et al., 2004). These wavelength regions are used in characterizing silver and gold nanoparticles, respectively.

Useful information such as the particle size can also be obtained from the UV/Vis techniques which are reflected on SPR band obtained for the nanoparticle synthesised. The increase in particle size causes the increase in maximum wavelength known as the red shift and the reduction in particle size leads to the decrease in maximum wavelength called blue shift (Noruzi, 2015). Mohan et al. (2016b), reported the green synthesis of silver nanoparticles using dextrose and starch as the reducing and capping agent respectively with reaction mixture at different time interval. The UV/Vis spectral (Figure 4) of the as-synthesised Ag-NPs displayed absorption maxima peak at 421 nm which is characteristic of SPR band for silver. The absorption maximum peak was gradually blue-shifted from 421 nm to 412 nm with an increase in intensity as the reaction time increased indicating a decrease in particle size. The increase in the intensity of the SPR peak as the reaction time increased indicates a continued reduction of silver ions and an increase in the concentration of smaller sized Ag-NPs present in the solution.



A

Figure 4. (A) Absorption spectra of dextrose reduced starch-capped Ag-NPs at different reaction time.

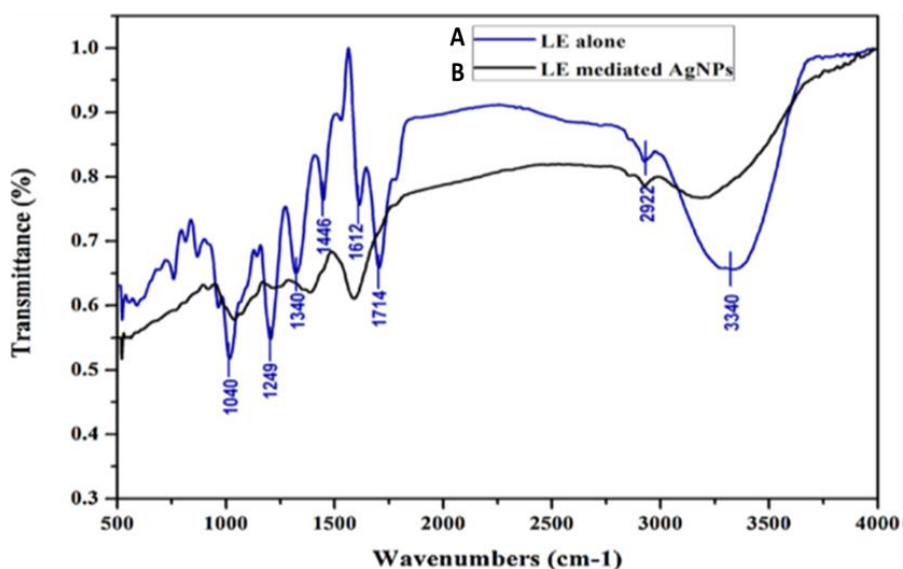


Figure 5. FTIR spectra of leaf extract (LE) alone (A) and synthesized AgNPs using *R. officinalis* L. (B).

FTIR (Fourier Transform Infrared Spectroscopy): This is a technique which gives information about the vibrations and rotations of molecules known as normal modes. These vibrational transitions are as a result of quantized energy levels influenced by the bonds that join the molecules (Skoog et al., 2004). FTIR measurements are employed to identify the possible biomolecules or functional groups that are bound to the surface of nanoparticles.

Das and Velusamy (2013), reported the green synthesis of silver nanoparticles using water extract from *Rosmarinus officinalis* L leaves. FTIR measurement were carried out as shown in Figure 5 to identify the possible biomolecules present in the leaf extract of *R. officinalis* which was exploited as reducing agent for nanoparticle synthesis. Prominent IR bands were observed at 1012, 1249, 1352, 1446, 1612, 1714, 2922, and 3340 cm^{-1} which are mostly characteristic of flavonoids and terpenoids present in the leaf extract and were responsible for the reduction and stabilization of the as-synthesised material.

Electron microscopy techniques; This technique includes SEM (Scanning electron microscopy) and TEM (Transmission electron microscopy), and are used for the identification of surface morphology and size of the nanoparticles. TEM is widely used over SEM as it has greater magnification and resolution for identifying the morphology and average size of the nanoparticle. Another advantage of TEM over SEM is that TEM can be used to distinguish crystalline

structures from amorphous structures using the selected area electron diffraction (SAED) technique (Noruzi, 2015). Green synthesized silver nanoparticles using *Abelmoschus esculentus* (L.) pulp extract was studied and the TEM image revealed that the particles were spherical in shape and were uniformly distributed without significant agglomeration. The nanoparticles were crystalline in nature with particle size ranges from 3 to 11 nm (Mollick et al., 2015). In a recent report by Mohan et al. (2016b), the TEM images (Figure 6) for silver nanoparticles synthesised at different reaction time indicates that the particles are well dispersed and spherical in shape with average particle diameter of 19.41 ± 3.44 nm (1 h), 8.13 ± 1.9 nm (24 h) and 6.27 ± 1.63 nm (48 h). The decrease in the size distribution as the reaction time increases was consistent with the increase in the intensity observed in the absorption spectra (Figure 4).

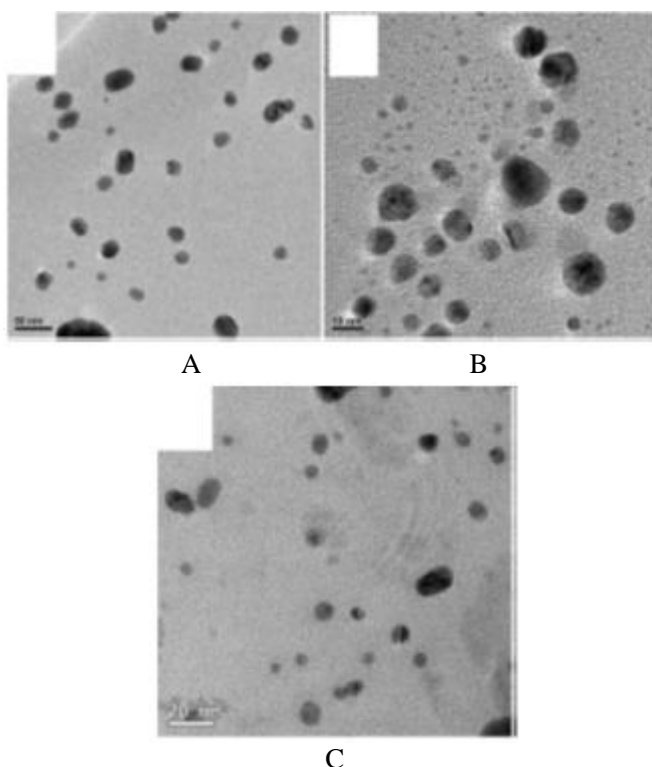


Figure 6. TEM images at 1 h (A), 24 h (B) and 48 h (C) of dextrose reduced starch-capped Ag-NPs.

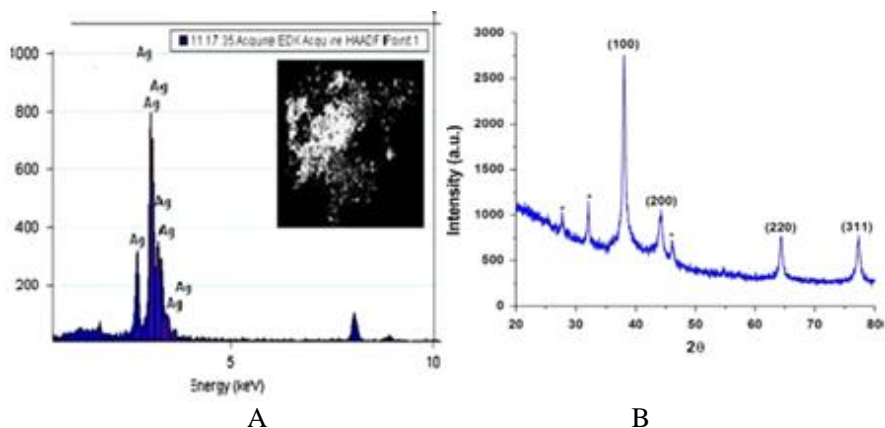


Figure 7. EDX spectra (A) illustrating the formation of Ag-NPs and XRD patterns (B) of Ag-NPs.

Diffraction Techniques: These include EDX (energy-dispersive X-ray spectroscopy) and XRD (X-Ray Diffractometer). EDX technique is used for elemental analysis while XRD, on the other hand, is a non-destructive technique that has wide application in the field of nanostructure for the determination of the chemical composition, crystallography and size distribution of nanoparticles in the range of 1 to 200 nm.

Basavegowda and Lee, (2013) reported the synthesis of silver nanoparticles using peel extract from Satsuma mandarin fruits. The presence of elemental silver was proven by EDX analysis (Figure 7 A) and the XRD results (Figure 7B) shows that silver ions has been reduced to elemental silver due to the presence of four peak at 38.10° , 44.24° , 64.44° , and 77.43° corresponding to the (111), (200), (220) and (311) planes of silver. The intense peak at 38.10° indicated a high degree of crystallinity.

DLS (Dynamic light scattering): This technique is used to study the hydrodynamic size of (Z-average diameter) the particles when they are dispersed in a liquid medium and to find out the surface charge and aggregation condition of the colloidal nanoparticles. Silver nanoparticles synthesised using *Sambucus nigara L.* fruit extract by Moldovan et al. 2016, showed a sharp peak at a negative value of -20.9 mV. The negatively charged surface of the nanoparticles indicates that anionic capping agents such as polyphenols from the *S. nigara* fruits extract are coordinated to the surface of silver nanoparticles metallic shells. The determined Zeta potential value is commonly associated to sufficient mutual repulsion to ensure the stability of the colloidal silver dispersion.

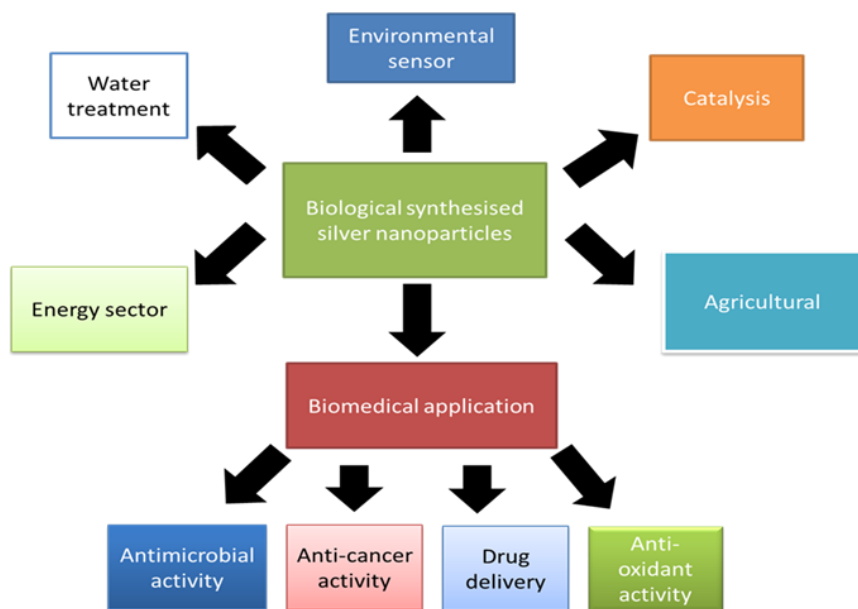


Figure 8. Schematic diagram showing applications of plant extract synthesized silver nanoparticles.

4. BIOMEDICAL APPLICATIONS OF PLANT EXTRACTS SYNTHESISED SILVER NANOPARTICLES

With the advancement of nanotechnology, application of biosynthesized metal nanoparticles has been extended tremendously in various sectors ranging from biomedical field, water treatment (Pradeep, 2009), agriculture (Dasgupta et al., 2015), energy sector (Ali, M and Ali, A., 2011), catalysis and to the environmental sector where it can be used as sensor. Ag-NPs have been extensively used as environmental sensors to detect heavy metal ions due to their tunable size and distance-dependent optical properties with high extinction coefficients at the visible region (Annadhasan et al., 2014). Nanotechnology is seen as the technology that will help in alleviating some of the challenges facing the modern day economy. For instances, in the environmental sector, the use of nanomaterials has offered some potential solutions for the removal and detection of severely toxic contaminants found in both aquatic environment and biological systems (Mohan et al., 2016b). In the biomedical field, they can be used for diagnosing and providing alternative therapy for diseases such as

cancer. Biosynthesised silver nanoparticles are mostly used in the biomedical field due to their antimicrobial functionality (Schröfel et al., 2014) as it has good antimicrobial efficacy against bacteria, viruses and other eukaryotic microorganisms (Logeswari et al., 2012). Their antimicrobial property is dependent on size, shape, surface oxidation or charge, and dispersion degree in medium (Huang et al., 2015). Most studies carried out with plant-mediated silver nanoparticles are geared towards evaluating their antimicrobial and anti-cancer activities as discussed below.

4.1. Anti-Microbial Activity

Currently, microorganisms are becoming increasingly resistant to antibiotics which reduce their effectiveness. To overcome these challenges, colloidal silver nanoparticles have been seen as an important alternative to the use of antibiotics (Gaillet and Roaunet, 2014) because they show improved activity against multi-drug resistant bacteria (Lokina et al., 2014). The antimicrobial action of Ag-NPs against bacteria and other pathogens is widely believed to be through the alteration of cell membrane permeability and the interaction with their macromolecules like proteins and DNA thereby affecting their replication machinery and cellular processes (Gupta et al., 2014). Due to the proven efficiency of colloidal silver nanoparticles, it has been extensively used for analysing antimicrobial activities against different microbes such as the Gram-negative, Gram-positive bacteria and other pathogens. Gupta et al. (2014) reported one-step green synthesis of silver nanoparticles using *Psidium guajava* L. leaf extract and evaluate the antibacterial activity on *Staphylococcus aureus*, *Escherichia coli* and *Candida albicans*. The result revealed prominent ability to inhibit the biofilms formed by these micro-organisms. In another report by Emeka et al. (2014) Ag-NPs synthesised using pineapple leaf extract was used to evaluate the antibacterial activity of *Staphylococcus aureus*, *Streptococcus pneumoniae*, *Proteus mirabilis* and *Escherichia coli* by Agar-well diffusion method. The results showed evidence of inhibition towards bacteria growth while using Gentamycin as the control experiment. Silver nanoparticles obtained from *Acacia leucophloea* extract had been tested against common bacteria pathogens such as *Staphylococcus aureus*, *Bacillus cereus*, *Listeria monocytogenes*, and *Shigella flexneri* via *in-vitro* agar well diffusion method. The results showed effective inhibitory action against these common pathogens (Murugan et al., 2014). Gum extracted from neem (*Azadirachta indica*) was used to synthesis Ag-NPs and tested against clinical isolates of Salmonella

enteritidis and *Bacillus cereus* by Kirby–Bauer disk diffusion method (Velusamy et al., 2015). In a recent report, Nayak et al. (2016) obtained silver nanoparticles from the bark of two plant extracts (*F. benghalensis* and *A. indica*) and tested them against Gram negative (*Escherichia coli*, *Pseudomonas aeruginosa* and *Vibrio cholerae*) and Gram positive (*Bacillus subtilis*) bacteria. The antibacterial potential of the synthesized nanoparticles was investigated using the agar well diffusion assay and a promising anti-microbial activity was observed. The antibacterial activity of Ag-NPs on both *Escherichia coli* and *Staphylococcus aureus* was studied by Krishna et al. (2015) using Ag-NPs synthesised from *salmalia malabarica gum* extract. The results showed antibacterial effectiveness while using Ampicillin as a positive control.

4.2. Anti-Cancer Activity

Cancer is one of the most severe and deadly diseases which account for the death of 7.6 million people worldwide (Lokina et al., 2014) and according to WHO, approximately 13.1 million people may die in 2030 if immediate actions are not taken. Moreover, the traditional techniques used for the treatment of cancer such as surgery, chemotherapy and radiotherapy results in huge side effects on humans due to other important cells which are being damaged in the process. With the emergence of nanotechnology, it has raised the possibilities for using therapeutic nanoparticles to inhibit the growth of cancerous cells with mild or no side effects on human. Several studies have been carried out to demonstrate the efficacy of biosynthesized silver nanoparticles against various cancer cell lines. Jeyaraj et al. (2013) reported the biological synthesis of silver nanoparticles using *Podophyllum hexandrum* plant extract and evaluated the anti-cancer activity on human cervical carcinoma cells. The overall result showed that Ag-NPs can selectively inhibit the cellular mechanism of the cancer cell by causing DNA damage resulting in cell death. In another report by Prabhu et al. 2013, silver nanoparticles obtained from *Vitex negundo* extracts was used to evaluate the anti-cancer activity on human colon cancer cell line HCT15. The results suggested that Ag-NPs exerted its antiproliferative effects on the colon cancer cell line by suppressing its growth, reducing DNA synthesis and inducing apoptosis. As previously mentioned, Nayak et al. 2016, utilised plant extracts from the bark of *F. benghalensis* and *A. indica* to synthesise silver nanoparticles which were tested against Osteosarcoma. The synthesized Ag-NPs showed anti-proliferative activity against osteosarcoma cell line in a dose-dependent manner. Silver nanoparticles synthesised using aqueous extract from *Taxusbaccata* plant

was tested against human breast cancer cell line via MTT assay (Kajani et al., 2014). Significant differences in the viability of the cancer cells were observed in the presence of different concentrations of silver nanoparticles and different exposure times. The results showed an enhancement of cytotoxic activity with the increasing of silver nanoparticle concentration and exposure time.

CONCLUSION

The uncontrolled release of nanoparticles to the environment through waste disposal is critical to the future of nanotechnology and to circumvent this challenge, nature has provided a good back-up through the synthesis of nanoparticles using natural biomaterials that are less toxic and environmental friendly. The utilisation of plant material towards the synthesis of silver nanoparticles has enhanced its application in the biomedical field where its relevance is highly noticeable. Several plant species have been successfully used for the synthesis of silver nanoparticles and the advantages of using plant material are huge as elaborated in this chapter. The major draw-back with plant mediated synthesis is the identification of the particular chemical components in all these different plant species responsible for the capping and reduction process during the synthesis. Further studies are required to ensure that this aspect is satisfied which will also help to address seasonal challenges for large scale production of nanoparticles as plant phytochemicals may vary due to change in weather conditions.

ACKNOWLEDGMENT

This work was supported by National Research Foundation (NRF), South Africa under the Nanoflagship programme (Grant no: 97983).

REFERENCES

- Ahamed, M., Alsalhi, M.S. and Siddiqui, M.K.J., 2010. Silver nanoparticle applications and human health. *Clinica Chimica Acta*, 411, pp. 1841-1848.
- Ahmad, N., Sharma, S., Alam, M.K., Singh, V.N., Shamsi, S.F., Mehta, B.R. and Fatma, A., 2010. "Rapid synthesis of silver nanoparticles using dried

- medicinal plant of basil,” *Colloids and Surfaces B: Biointerfaces*, 81, pp. 81-86.
- Ahmed, S., Ahmad, M., Swami, B. L., and Ikram, S., 2015. A review on plants extract mediated synthesis of silver nanoparticles for antimicrobial applications: A green expertise. *Journal of Advanced Research*.
- Ahluwalia, V., Kumar, J., Sisodia, R., Shakil, N.A. and Walia, S., 2014. Green synthesis of silver nanoparticles by *Trichoderma harzianum* and their bio-efficacy evaluation against *Staphylococcus aureus* and *Klebsiella pneumoniae*. *Industrial Crops and Products*, 55, pp. 202-206.
- Akhtar, M.S., Panwar, J. and Yun, Y.S., 2013. Biogenic synthesis of metallic nanoparticles by plant extracts. *ACS Sustainable Chemistry and Engineering*, 1, pp. 591-602.
- Ali, M. and Ali, A., 2011. Nanotechnology for sustainable energy. *Science Vision*, 16, pp. 1-12.
- Annadhasan, M., Muthukumarasamy Vel, T., Sankar Babu, V. R., and Rajendiran, N. (2014). Green synthesized silver and gold nanoparticles for colorimetric detection of Hg^{2+} , Pb^{2+} , and Mn^{2+} in aqueous medium. *ACS Sustainable Chemistry and Engineering*, 2, pp. 887-896.
- Anthony, K.J.P., Murugan, M. and Gurunathan, S., 2014. Biosynthesis of silver nanoparticles from the culture supernatant of *Bacillus marisflavi* and their potential antibacterial activity. *Journal of Industrial and Engineering Chemistry*, 20, pp. 1505-1510.
- Balavigneswaran, C.K., Kumar, T.S.J., Packiaraj, R.M. and Prakash, S., 2014. Rapid detection of Cr (VI) by AgNPs probe produced by *Anacardium occidentale* fresh leaf extracts. *Applied Nanoscience*, 4, pp. 367-378.
- Basavegowda, N. and Lee, Y.R., 2013. Synthesis of silver nanoparticles using Satsuma mandarin (*Citrus unshiu*) peel extract: a novel approach towards waste utilization. *Materials Letters*, 109, pp. 31-33.
- Beer, C., Foldbjerg, R., Hayashi, Y., Sutherland, D. S., and Autrup, H., 2012. Toxicity of silver nanoparticles—nanoparticle or silver ion? *Toxicology letters*, 208, pp. 286-292.
- Benelmekki, M., 2015. Designing binary nanoparticles. Morgan and Claypool publisher.
- Burda, C., Chen, X., Narayanan, R., and El-Sayed, M. A., 2005. Chemistry and properties of nanocrystals of different shapes. *Chemical reviews*, 105, pp. 1025-1102.
- Busquet, M., Calsamiglia, S., Ferret, A., Kamel, C., 2006. Plant Extracts Affect *In Vitro* Rumen Microbial Fermentation. *Journal of dairy Science*, 89, pp. 761-771.

- Chevion, P., Gouanvé, F., and Espuche, E., 2014. Green synthesis of colloid silver nanoparticles and resulting biodegradable starch/silver nanocomposites. *Carbohydrate polymers*, 108, pp. 291-298.
- Chiguvare, H., Oyedeji, O.O., Matewu, R., Aremu, O., Oyemitan, I.A., Oyedeji, A.O., Nkeh-Chungag, B.N., Songca, S.P., Mohan. S. and Oluwafemi, O.S., 2016. Synthesis of Silver Nanoparticles Using Buchu Plant Extracts and Their Analgesic Properties, *Molecules*, 21, p. 774.
- Cinelli, M., Coles, S. R., Nadagouda, M. N., Błaszczczyński, J., Słowiński, R., Varma, R. S., and Kirwan, K., 2015. A green chemistry-based classification model for the synthesis of silver nanoparticles. *Green Chemistry*, 17, pp. 2825-2839.
- Dasgupta, N., Ranjan, S., Mundekkad, D., Ramalingam, C., Shanker, R. and Kumar, A., 2015. Nanotechnology in agro-food: from field to plate. *Food Research International*, 69, pp. 381-400.
- Durán, N., Marcato, P.D., Durán, M., Yadav, A., Gade, A., Rai, M., 2011. Mechanistic aspects in the biogenic synthesis of Extracellular metal nanoparticles by peptides, bacteria, fungi, and plants. *Appl. Microbiol. Biotechnol.* 90, pp. 1609-1624.
- Epicoco, M., Oltra, V. and Saint Jean, M., 2014. Knowledge dynamics and sources of eco-innovation: Mapping the Green Chemistry community. *Technological Forecasting and Social Change*, 81, pp. 388-402.
- Emeka, E. E., Ojiefoh, O. C., Aleruchi, C., Hassan, L. A., Christiana, O. M., Rebecca, M., ... and Temitope, A. E., 2014. Evaluation of antibacterial activities of silver nanoparticles green-synthesized using pineapple leaf (*Ananas comosus*). *Micron*, 57, pp. 1-5.
- Facchini, P. J., Bohlmann, J., Covello, P.S De Luca, V., Mahadevan, R., Page, J. E., Ro, D.K., Sensen, C. W., Storms, R. and Martin, V.J., 2012. Synthetic bio-systems for the production of high-value plant metabolites. *Trend in biotechnology*, 30, pp. 127-131.
- Feynman. R. P., 1960. There's plenty of room at the bottom. *Engineering and Science*, 23, pp. 22-36.
- Fleischer, T. and Grunwald, A., 2008. Making nanotechnology developments sustainable - A role for technology assessment. *Journal of Cleaner Production*, 16, pp. 889-898.
- Gaillet, S., Rouanet, J-M., 2014. Silver nanoparticles: Their potential toxic effects after oral exposure and underlying mechanisms – A review. *Food and Chemical Toxicology*, 77, pp. 58-63.

- Gardea-Torresdey, J.L., Parsons, J.G., Dokken, K., Peralta-Videa, J., Troiani, H.E., San-tiago, P., Jose-yacamann, M., 2002. Formation and growth of Au nanoparticles inside line Alfalfa plants. *Nano Lett.* 2, pp. 397-401.
- Gupta, K., Hazarika, S. N., Saikia, D., Namsa, N. D., and Mandal, M., 2014. One step green synthesis and anti-microbial and anti-biofilm properties of Psidium guajava L. leaf extract-mediated silver nanoparticles. *Materials Letters*, 125, pp. 67-70.
- Hadrup, N., and Lam, H. R., 2014. Oral toxicity of silver ions, silver nanoparticles and colloidal silver – A review. *Regulatory Toxicology and Pharmacology*, 68(1), 1-7.
- Hebbalalu, D., Lalley, J., Nadagouda, M. N., and Varma, R. S. (2013). Greener techniques for the synthesis of silver nanoparticles using plant extracts, enzymes, bacteria, biodegradable polymers, and microwaves. *ACS Sustainable Chemistry and Engineering*, 1, pp. 703-712.
- Huang, J., Lin, L., Sun, D., Chen, H., Yang, D. and Li, Q., 2015. Bio-inspired synthesis of metal nanomaterials and applications. *Chemical Society Reviews*, 44, pp. 6330-6374.
- Hussein, A.K., 2015. Applications of nanotechnology in renewable energies— A comprehensive overview and understanding. *Renewable and Sustainable Energy Reviews*. 42, pp. 460-476.
- Jeeva, K., Thiagarajan, M., Elangovan, V., Geetha, N. and Venkatachalam, P., 2014. Caesalpinia Coriaria leaf extracts mediated biosynthesis of metallic silver nanoparticles and their antibacterial activity against clinically isolated pathogens. *Industrial Crops and Products*, 52, pp. 714-720.
- Jeyaraj, M., Varadan, S., Anthony, K.J.P., Murugan, M., Raja, A. and Gurunathan, S., 2013. Antimicrobial and anticoagulation activity of silver nanoparticles synthesized from the culture supernatant of Pseudomonas aeruginosa. *Journal of Industrial and Engineering Chemistry*, 19, pp. 1299-1303.
- Jeyaraj, M., Rajesh, M., Arun, R., Alic, D.M., Sathishkumar, G., Sivanandhan, G., Deva, G.K., Manickavasagam, M., Premkumar, K., Thajuddin, N., and Ganapathi, A., 2013. An investigation on the cytotoxicity and caspase-mediated apoptotic effect of biologically synthesized silver nanoparticles using Podophyllum hexandrum on human cervical carcinoma cells. *Colloids and Surfaces B: Biointerfaces*, 102, pp. 708-717.
- Jose-yacamann, M., Gardea-Torresdey, J.L., Gomez, E., Peralta-Videa, J., Parsons, J.G., Troiani, H.E., 2003. Alfalfa sprout: a natural source for the synthesis of silver nanoparticles. *Langmuir* 19, pp. 1357-1361.

- Justo-Hanani, R., Dayan, T., 2015. European risk governance of nanotechnology: Explaining the emerging regulatory policy. *Research Policy*, 44, pp. 1527-1536.
- Kaegi, R., Sinnet, B., Zuleeg, S., Hagendorfer, H., Mueller, E., Vonbank, R., and Burkhardt, M., 2010. Release of silver nanoparticles from outdoor facades. *Environmental pollution*, 158, pp. 2900-2905.
- Kajani, A.A., Bordbar, A.K., Esfahani, S.H.Z., Khosropour, A.R. and Razmjou, A., 2014. Green synthesis of anisotropic silver nanoparticles with potent anticancer activity using *Taxus baccata* extract. *RSC Advances*, 4, pp. 61394-61403.
- Khalil, M.M., Ismail, E.H., El-Baghdady, K.Z. and Mohamed, D., 2014. Green synthesis of silver nanoparticles using olive leaf extract and its antibacterial activity. *Arabian Journal of Chemistry*, 7, pp. 1131-1139.
- Kumar, D. A., Palanichamy, V., and Roopan, S. M., 2014. Green synthesis of silver nanoparticles using *Alternanthera dentata* leaf extract at room temperature and their antimicrobial activity. *Spectrochimica Acta Part A: Molecular and Biomolecular Spectroscopy*, 127, pp. 168-171
- Krishnaraj, C., Jagan, E.G., Rajasekar, S., Selvakumar, P., Kalaichelvan, P.T., Mohan, N., 2010. Synthesis of silver nanoparticles using *Acalypha indica* leaf extracts and its antibacterial activity against waterborne pathogens. *Colloids Surf. BBiointerfaces*, 76, 50-56.
- Logeswari, P., Silambarasan, S. and Abraham, J., 2015. Synthesis of silver nanoparticles using plants extract and analysis of their antimicrobial property. *Journal of Saudi Chemical Society*, 19, pp. 311-317.
- Lokina, S., Stephen. A., Kaviyaran, V., Arulvasu, C., Narayanan, V., 2014. Cytotoxicity and antimicrobial activities of green synthesized silver nanoparticles. *European Journal of Medicinal Chemistry*, 76, pp. 256-263.
- Lu, Y., and Ozcan, S., 2015. Green nanomaterials: On track for a sustainable future. *Nano Today*.
- Maurer-Jones, M. A., Gunsolus, I. L., Murphy, C. J., and Haynes, C. L., 2013. Toxicity of engineered nanoparticles in the environment. *Analytical chemistry*, 85, pp. 3036-3049.
- Mittal, A. K., Chisti, Y., and Banerjee, U. C., 2013. Synthesis of metallic nanoparticles using plant extracts. *Biotechnology advances*, 31, pp. 346-356.
- Mochochoko, T., Oluwafemi, O. S., Jumbam, D. N., and Songca, S. P., 2013. Green synthesis of silver nanoparticles using cellulose extracted from an aquatic weed; water hyacinth. *Carbohydrate polymers*, 98, pp. 290-294.

- Mohan, S., Oluwafemi, O.S., George, S.C., Jayachandran, V.P., Lewu, F.B., Songca, S.P., Kalarikkal, N. and Thomas, S., 2014. Completely green synthesis of dextrose reduced silver nanoparticles, its antimicrobial and sensing properties. *Carbohydrate Polymers*, 106, pp. 469-474.
- Mohan, S., Oluwafemi, O.S., Songca, S.P., Rouxel, D., Miska, P., Lewu, F.B., Kalarikkal, N., Thomas, S., 2016(a). Completely green synthesis of silver nanoparticle decorated MWCNT and its antibacterial and catalytic properties. *Pure Appl. Chem.*, 88, pp. 71-81.
- Mohan, S., Oluwafemi, O.S., Songca, S.P., Jayachandran, V.P., Rouxel, D., Joubert, O., Kalarikkal, N., Thomas, S., 2016(b). Synthesis, antibacterial, cytotoxicity and sensing properties of starch-capped silver nanoparticles. *Journal of Molecular Liquids*, 213, pp. 75-81.
- Moldovan, B., David, L., Achim, M., Clichici, S. and Filip, G.A., 2016. A green approach to phytomediated synthesis of silver nanoparticles using *Sambucus nigra* L. fruits extract and their antioxidant activity. *Journal of Molecular Liquids* 221, pp. 271-278.
- Mollick, M.M.R., Rana, D., Dash, S.K., Chattopadhyay, S., Bhowmick, B., Maity, D., Mondal, D., Pattanayak, S., Roy, S., Chakraborty, M. and Chattopadhyay, D., 2015. Studies on green synthesized silver nanoparticles using *Abelmoschus Esculentus* (L.) pulp extract having anticancer (*in vitro*) and antimicrobial applications. *Arabian Journal of Chemistry*.
- Muniyappan, N., and Nagarajan, N. S., 2014. Green synthesis of silver nanoparticles with *Dalbergia spinosa* leaves and their applications in biological and catalytic activities. *Process Biochemistry*, 49, pp. 1054-1061.
- Murugan, K., Senthilkumar, B., Senbagam, D., Al-Sohaibani, S., 2014. Biosynthesis of silver nanoparticles using *Acacia leucophloea* extract and their antibacterial activity. *International Journal of Nanomedicine*, 9, pp. 2431-2438.
- Nayak, D., Ashe, S., Rauta, P.R., Kumari, M., Nayak, B., 2016. Bark extract mediated green synthesis of silver nanoparticles: Evaluation of antimicrobial activity and antiproliferative response against osteosarcoma. *Materials Science and Engineering: C*, 58, pp. 44-52.
- Nisha, N.S., Aysha, O.S., Rahaman, J.S.N., Kumar, P.V., Valli, S., Nirmala, P. and Reena, A., 2014. Lemon peels mediated synthesis of silver nanoparticles and its antidermatophytic activity. *Spectrochimica Acta Part A: Molecular and Biomolecular Spectroscopy*, 124, pp. 194-198.
- Notriawan, D., Angasa, E., Suharto, T.E., Hendri, J. and Nishina, Y., 2013. Green synthesis of silver nanoparticles using aqueous rinds extract of

- Brucea javanica (L.) Merr at ambient temperature. *Materials Letters*, 97, pp. 181-183.
- Piccinno, F., Gottschalk, F., Seeger, S., Nowack, B., 2012. Industrial production quantities and uses of ten engineered nanomaterials for Europe and the world. *J. Nanopart. Res.* 14, pp. 1109-1120.
- Prabhua, D., Arulvasu, C., Babua, G., Manikandan, R., Srinivasan, P., 2013. Biologically synthesized green silver nanoparticles from leaf extract of *Vitex negundo* L. induce growth-inhibitory effect on human colon cancer cell line HCT15. *Process Biochemistry* 48, pp. 317-324.
- Oluwafemi, O.S., Ncapayi, V., Scriba, M., and Songca, S.P., 2013. Green controlled synthesis of monodispersed, stable and smaller sized starch-capped silver nanoparticles. *Materials Letters*, 106, pp. 332-336.
- Pradeep, T., 2009. Noble metal nanoparticles for water purification: a critical review. *Thin solid films*, 517, pp. 6441-6478.
- Prakash, P., Gnanaprakasam, P., Emmanuel, R., Arokiyaraj, S., Saravanan, M., 2013. Green synthesis of silver nanoparticles from leaf extract of *Mimusops elengi*, Linn. for enhanced antibacterial activity against multi drug resistant clinical isolates. *Colloids Surf. B: Biointerfaces*, 108, pp. 255-259.
- Qu, D., Sun, W., Chen, Y., Zhou, J., Liu, C., 2014. Synthesis and *in vitro* antineoplastic evaluation of silver nanoparticles mediated by *Agrimoniae herba* extract. *International Journal of Nanomedicine*, 9, pp. 1871-1882.
- Rajana, R., Chandran, K., Harperc, S.L., Yun, S.L. and Kalaichelvana, P.T., 2015. Plant extract synthesized silver nanoparticles: An on-going source of novel biocompatible materials. *Industrial Crops and Products*, 70, pp. 356-373.
- Rao, K.J. and Paria, S., 2013. Green synthesis of silver nanoparticles from aqueous *Aegle marmelos* leaf extract. *Materials Research Bulletin*, 48(2), pp. 628-634.
- Rauwel, P., Küüinal, S., Ferdov, S., and Rauwel, E., 2015. A Review on the green synthesis of silver nanoparticles and their morphologies studied via TEM. *Advances in Materials Science and Engineering*.
- Raveendran, P., Fu, J. and Wallen, S.L., 2003. Completely "green" synthesis and stabilization of metal nanoparticles. *Journal of the American Chemical Society*, 125, pp. 13940-13941.
- Roy, K., Sarkar, C. K., and Ghosh, C. K., 2014. Plant-mediated synthesis of silver nanoparticles using parsley (*Petroselinum crispum*) leaf extract: spectral analysis of the particles and antibacterial study. *Applied Nanoscience*, 5, pp. 945-951.

- Sadeghi, B., and Gholamhoseinpoor, F. (2015). A study on the stability and green synthesis of silver nanoparticles using *Ziziphora Tenuior* (Zt) extract at room temperature. *Spectrochimica Acta Part A: Molecular and Biomolecular Spectroscopy*.
- Saha, S., Malik, M.M. and Qureshi, M.S., 2014. Comparative Study of Synergistic Effects of Antibiotics with Triangular Shaped Silver Nanoparticles, Synthesized Using UV-Light Irradiation, on *Staphylococcus aureus* and *Pseudomonas aeruginosa*. *Journal of Biomaterials and Nanobiotechnology*, 5(3), p. 186.
- Schröfel, A., Kratošová, G., Šafařík, I., Šafaříková, M., Raška, I. and Šor, L.M., 2014. Applications of biosynthesized metallic nanoparticles - A review. *Actabiomaterialia*, 10, pp. 4023-4042.
- Shankar, S.S., Rai, A., Ahmad, A., Sastry, M., 2004. Rapid synthesis of Au, Ag, and bimetallic Au core–Ag shell nanoparticles using Neem (*Azadirachta indica*) leaf broth. *J. Colloid Interface Sci.*, 275, pp. 496-502.
- Shrikar, S.K., Giri, D.D., Pal, D.B., Mishra, P.K, and Upadhyay, S.N., 2016. Green Synthesis of Silver Nanoparticles: A Review. *Green and Sustainable Chemistry*. 6, p 34.
- Singh, P., Kim, Y.J., Zhang, D. and Yang, D.C., 2016. Biological synthesis of nanoparticles from plants and microorganisms. *Trends in biotechnology*.
- Suman, T.Y., Elumalai, D., Kaleena, P.K. and Rajasree, S.R., 2013. GC–MS analysis of bioactive components and synthesis of silver nanoparticle using *Ammannia baccifera* aerial extract and its larvicidal activity against malaria and filariasis vectors. *Industrial crops and products*, 47, pp. 239-245.
- Suman, T. Y., Rajasree, S. R., Kanchana, A., and Elizabeth, S. B. (2013). Biosynthesis, characterization and cytotoxic effect of plant mediated silver nanoparticles using *Morinda citrifolia* root extract. *Colloids and surfaces B: Biointerfaces*, 106, 74-78.
- Sun, Q., Cai, X., Li, J., Zheng, M., Chen, Z., and Yu, C. P. (2014). Green synthesis of silver nanoparticles using tea leaf extract and evaluation of their stability and antibacterial activity. *Colloids and Surfaces A: Physicochemical and Engineering Aspects*, 444, 226-231.
- Sosa, I.O., Noguez, C., Barrera, R.G. (2003) Optical properties of metal nanoparticles with arbitrary shapes. *J. Phys. Chem. B*, 107, pp. 6269-6275.
- Umadevi, M., Bindhu, M.R. and Sathe, V., 2013. A Novel Synthesis of Malic Acid Capped Silver Nanoparticles using *Solanum lycopersicum* Fruit Extract. *J. Mater. Sci. Technol.*, 2013, 29, pp. 317-322.
- Varma, R. S., 2012. Greener approach to nanomaterials and their sustainable applications. *Current Opinion in Chemical Engineering*, 1, p. 123-128.

- Virkutyte, J and Varma, R.S., 2011. Green synthesis of metal nanoparticles: biodegradable polymers and enzymes in stabilization and surface functionalisation. *Chemical Science*, 2, pp. 837-846.
- Wang, T., Long, X., Cheng, Y., Liu, Z., and Yan, S. (2014). The potential toxicity of copper nanoparticles and copper sulphate on juvenile *Epinephelus coioides*. *Aquatic Toxicology*, 152, pp. 96-104.
- Yildiz, I., Shukla, S. and Steinmetz, N. F., 2011. Application of nanoparticles in medicine. *Current opinion in biotechnology*, 22, pp. 901-908.

BIOGRAPHICAL SKETCH

Name: Prof. Samuel Oluwatobi Oluwafemi

Affiliation: University of Johannesburg

Education: PhD

Business Address: Department of Applied Chemistry, University of Johannesburg, Doornfontein Campus P.O Box 17011, Doornfontein 2028, Corner Beit and Nind Street

Complimentary Contributor Copy

Chapter 2

TAILORING PET SUBSTRATES WITH COLLAGEN-SILVER NANOPARTICLES

Mioara Drobota and Magdalena Aflori¹*

Department of Polymeric Materials Physics, Petru Poni Institute
of Macromolecular Chemistry, Iasi, Romania

ABSTRACT

Polyethylene terephthalate (PET) was selected in this work based on excellent properties, being widely used in many applications. Various strategies of surface modification have been developed over the time, because the response of the devices is largely controlled by surface chemistry and structure of the material.

In this chapter, PET was studied regarding the interactions at the polymer surface after plasma functionalization and immobilization of proteins in order to improve the adhesion properties. Obtaining the semisynthetic materials has enabled the generation of devices for medical applications, finding the optimal compatibility between two materials: one synthetic (polyester) and one natural (collagen). Biomolecules derived from or part of the extracellular matrix (e.g., gelatin, collagen, fibronectin)

* Mioara Drobota: Department of Polymeric Materials Physics, Petru Poni Institute of Macromolecular Chemistry, 41 A Gr. Ghica Voda Alley, Iasi, Romania. Email: miamiara@icmpp.ro.

¹Magdalena Aflori: Department of Polymeric Materials Physics, Petru Poni Institute of Macromolecular Chemistry, 41 A Gr. Ghica Voda Alley, Iasi, Romania. Email: maflori@icmpp.ro.

such as anti-inflammatory agents, anti-coagulant agents were immobilized. Collagens are by far the most abundant proteins that constitute up to 90% of the extracellular matrix of a tissue, thus imparting its structural integrity. Type I collagen is the major component of the extracellular matrix, and numerous reports have shown that collagen promotes higher cell adhesion and proliferation on the material. That can be subsequently used for the immobilization of biologically active molecules, furthermore, cellular growth (stem cells) on new supports.

Synthesis of metal nanoparticles (NPs) is an expanding research area due to the wide range of their applications in various fields. The controlled manner of silver nanoparticles release from polymer/metal nanocomposites can be useful for biotechnological applications, antibacterial and coating for biomedical activities. Conjugated polymers could induce nano-Ag to form compact structure, fill up the vacancy between nano-Ag, and enhance not only electron-transfer between nano-Ag and also adhesion on PET substrate.

In this chapter the interaction between PET/collagen and silver ions was investigated by FTIR spectroscopy, atomic force microscopy (AFM), X-ray photoelectron spectroscopy (XPS), SAXS spectrometry. The new results obtained the PET/collagen complex silver ions open offer new possibilities for applications in biotechnology and nanomedicine.

Keywords: polyethylene terephthalate, collagen, helium plasma, silver nanoparticle

1. INTRODUCTION

The generation of surfaces for protein adsorption is an important issue for the production of medical devices (catheters, dialysers, vascular grafts) and for applications in pharmaceutical and food industries [1-8]. Many approaches have been used to prepare different surfaces for biomaterials applications. Plasma can be presented as an ionised gas and is produced by discharge either at high temperatures or strong magnetic/electromagnetic fields to a gas. The gases used (O_2 , He, N_2) in producing plasma can be selected to give a wide assortment of new chemical groups [9-11] at the treated polymer surface. Plasma treatment is an extremely versatile technique for functionalizing polymer surfaces of different shapes [12-16]. These processes are happening determinate of the nature of the polymeric substrate and the plasma gases [17-23]. In plasma process, atoms are excluded from the surface of the polymer and new chemical

groups are formed thus can produce a strong wettable effect or crosslinked skin [24].

It has been reported that plasma treatment can improve polymer adhesion and the surface properties. Moreover, plasma activation produced transformation and changes in the hydrophobic/hydrophilic character of the polymeric support [25-26].

The surface properties of polymeric materials play an important role in determining the overall biocompatibility of the materials, because the surface of the polymers should first come into interaction with the biological environment [27-28]. The nature of the polymeric substrate plays an important role and determines the surface properties applications. Hence, these treatments could modify the surface or thin layer coating on the polymeric surface, the control of surface chemical compositions and physical topography of the polymers could be monitored. The activation energy used in these techniques is insignificant because the surface deterioration is not desired to happen. Our strategy has been firstly to create hydrophilic groups onto PET surface by plasma-treatment in a controllable way, by adjusting the plasma parameters (time, power). The surface modification introduces functional groups and the surface roughness can be controlled, the topography being the first important parameter that could be essential for a good biocompatibility and immobilization of the proteins [29-30].

Based on these studies, the preset work is extending the investigations further on support interactions with collagen, one of the important proteins, for investigations of molecular damages induced by direct exposures with He plasma and exposures with UV photons from the He plasma on the basis of chemical bonding states analysis using XPS.

In the present study collagen has been selected as a test material because collagen has the simplest molecular structure among all the proteins and therefore is considered as model material to study fundamental processes in plasma medicine.

Recent studies have demonstrated that polyester-based polymers several naturally have been used in medical applications and in especially in dermal patches [31].

2. IMPROVING POLY(ETHYLENE TEREPHTHALATE) FILM SURFACE PROPERTIES

PET films of 5x15 mm size were treated by helium plasma in an Emitech K1050X device. The plasma device has 110 mm diameter x 155 mm deep quartz chamber horizontally mounted with a convenient slide-out specimen drawer and viewing window. Evacuation of the chamber is achieved by an optional 50 L/m rotary vacuum pump. The standard RF power available is 13.56 MHz. Automatic tuning of forward and reflected power is standard. Forward power and vacuum levels are shown by the digital display. During plasma process the 'autotune' facility ensures that the RF power is automatically impedance-matched to any variation in the system or loading. This means conditions in the chamber are always maintained at their optimum ensuring faster reaction times and greater reproducibility of results. The treatments were performed in helium discharges. Input power value was 30 and 50 W and the discharge times 3 min, 5 min respectively.

After plasma treatment the samples were introduced in a wet chemical solution, prepared once in the presence of collagen and in absence of silver (the samples noted with A) and second in presence of both collagen and silver (the samples noted with B), as described in the following sections.

3. PHYSICO-CHEMICAL CHARACTERIZATION

The aim of this work was to investigate the effect of power and time plasma treatment on the surface of PET film. In our work, FTIR spectroscopy, X-ray Photoemission spectroscopy (XPS), Contact Angle (CA) and Atomic Force Microscopy (AFM) test measurements, were used.

Fourier transform infrared spectroscopy (FTIR) spectra were obtained on a spectrometer Bruker Vertex 70 equipped with a reflectance device (Attenuated Total Reflexion) ATR, with diamond crystal and single reflection, at incidence angle of 45°, that operates at ambient temperature.

The spectra of the polymeric samples were analyzed at 4 cm⁻¹ resolution and 64 scans were performed between 4000-600 cm⁻¹.

The measurements were performed in air, at room temperature (22-24°C) using a Solver PRO-M NT-MDT (Russia) setup, in tapping mode with cantilever oscillating frequency and 11.5 Nm⁻¹ constant forces. The tapping

mode was chosen to minimize damage to the sample's surface. The average values of the surface relief parameters were obtained from all images.

Elemental compositions X-Ray photoelectron spectroscopy (XPS) measurements were taken on KRATOS Axis Nova (Kratos Analytical, Manchester, United Kingdom) equipped with a high-resolution hemispherical electron energy analyzer. The exposed and analyzed area had a 0.7×0.3 mm area of the surface.

The X-ray photoelectron spectroscopy (XPS) were analyzed collected in the range of -10 to 1200 eV, with a resolution of 1 eV, at pass energy of 160eV. The high resolution spectra for all the elements identified in the survey spectra were collected using pass energy of 40eV, and a step size of 0.2eV. The compositions in atomic percentage (at. %) were determined from the survey spectra.

The small-angle X-ray scattering experiments (SAXS) were performed on a Nanostar U-Bruker system equipped with Vantec 3000 detector (diameter of 200 mm) and an X-ray I microsource. The wavelength of the incident X-ray beam was 1.54 \AA (Cu $K\alpha$) and the beam was collimated by three pinholes. The sample-to-detector distance was 107 cm allowing measurements with the values between 0.01 \AA^{-1} and 0.15 \AA^{-1} . An area integration was employed to reduced the data to a one-dimensional q ($4\pi\sin\theta/\lambda$) versus $\ln(\text{Intensity})$ trace.

In order to quantify the surface treatment modifications, contact angle measurements were carried out with water (as liquid) on a goniometer (KSV Instruments, Helsinki, Finland). This measurement system is equipped with a CAM-101 with a liquid dispenser, video camera, and drop-shape analysis software, at room temperature. Double-distilled water was used as solvent for these studies. Wetting force between the sample and the liquid, and also the variation of the liquid weight that goes through the fabric length during a given time, were measured. During measurements, a rectangular- film sample was connected to the goniometer at the weighing position, and was then brought into contact with the liquid placed in a syringe, which moved vertically up-down.

As soon as the sample surface was in contact with the bliquid surface, we obtain an estimate of the contact angle. The contact angle (WCA) which provides of wettability was determined. The untreated PET foil had a contact angle of which pointed out film hydrophobicity. After He-plasma treatment the WCA decreased for all samples down. The treatment reduced contact angle from 80° to 30° (Figure 1).

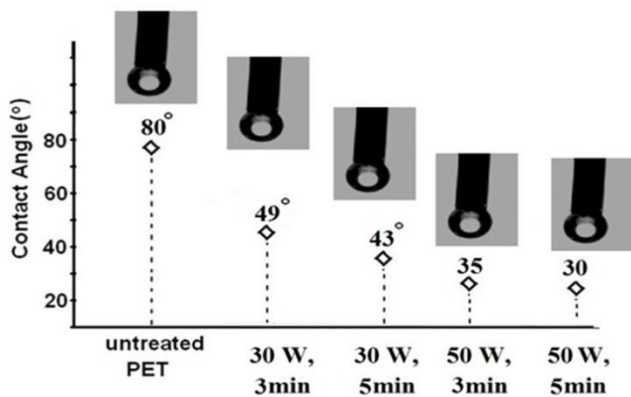


Figure 1. Static contact angle values of water after plasma He action samples.

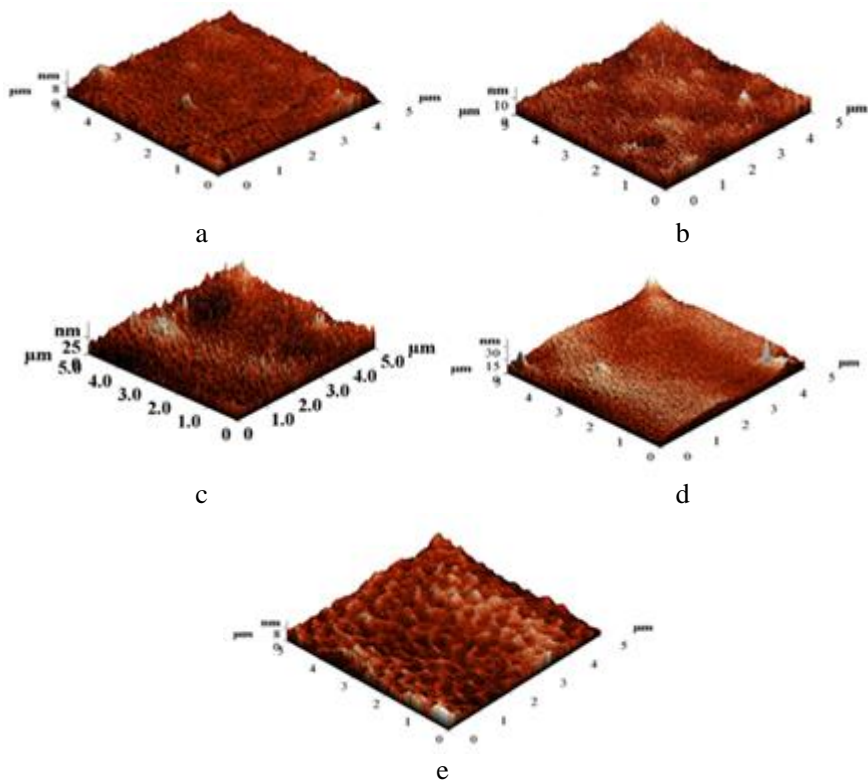


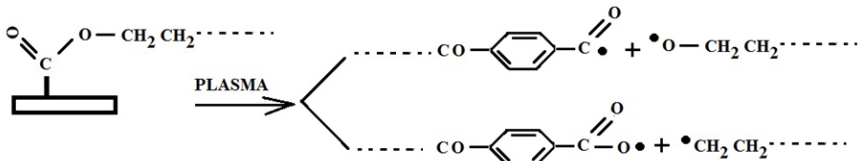
Figure 2. AFM images of pristine PET (a) and PET treated under various conditions of He plasma treatment: 30 W/3 min (b), 30 W/5 min (c), 50W/3 min (d) and 50 W/5 min (e).

The reduction of contact angle in the case of all plasma treated samples was explained by the increase of the proportion of polar functional groups. Moreover, with plasma treatment besides creating hydrophilic polar groups, surface roughness was increasing, which in turn also increased PET surface wettability. These results had proved by AFM techniques for these samples.

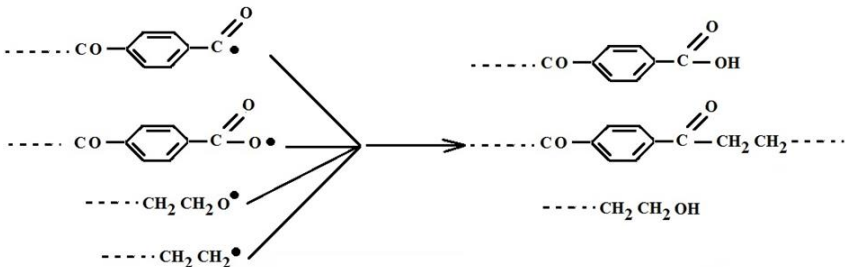
The most important thing was that all of the PET-functionalized samples remained hydrophilic.

Results of the AFM are used to obtain detailed information about the topographical changes of PET film induced by plasma He treatment process. It clearly shows in Figure2 that the surface no remains unchanged field [32-34].

The change in surface morphology induced by the plasma processing might affect the surface properties by simple physical adsorption or/and by diffusion. The surface roughness of the film was increased substantially from 1.4 nm for blank sample to 3.5 nm and 3.9 nm using 3 min and 5 min at 30W parameters treatment while for 3 min and 5min at 50W parameters the roughness between 4.7 and 7.9 nm.



(a). Scissions of chains formed from the PET surface after the action plasma treatment on the surface of film. The bonds are broken when high-energy electrons and particles collide the polymer surface



(b). Radicals react with activated oxygen species formed

Figure 3. Schematic mechanism reaction after He plasma action onto polyethyleneterephthalate film (a) and (b).

Newly formed functional groups on PET films surface, as a consequence of plasma surface modification, were studied by XPS which provided further insight onto the surface. The plasma treatment of PET generated polymer chain-scissions for some of the polymer bonds, which was proved by the decrease in C % content.

The results confirm that the PET polymer surface plasma treatments generate polymer chain, after scissions of the superficial bonds of PET by the plasma treatment. When action with plasma gases, create of very reactive chain-ends the reactions occurred at the surface of PET film.

These reactions present in Figure 3 will create at the chain-ends some oxidized groups like carbonyl, carboxyl and hydroxyl groups presents on the surfaces after plasma action [35].

The plasma-treated films, consequently, had more carboxyl groups at the surface, which increased with the electrical power of the plasma treatment from 30W to 50W.

4. INTERACTIONS OF COLLAGEN-AG COMPLEX WITH ACTIVATED PET SURFACE

4.1. Immobilization of Collagen Molecules After the Plasma Action on the Pet Film Surfaces

After functionalisation on the film surfaces, these were introduced in a solution of 3 mg/ml type I collagen/buffered solution (PBS, pH 3.4) for 24 hours at 24°C.

Due the treatment of plasma action new carbonyl groups are located on surface of polymer; these interact with amines from collagen structures and on the surface promote formation a protonated form positive charge. After incubation in collagen solutions the surface were rinsed sequentially in deionized water and ethanol to remove the unbound proteins.

4.2. Mechanism of Interaction of Pet Surface with Collagen

The collagen molecules present attached after films functionalized were evaluated by FTIR-ATR spectroscopy in Figure4. FTIR-ATR spectra present at 1644 cm^{-1} , reveal the presence of amide I band, which plays a main stretching

vibration ν (C = O). The vibration band of amide II is represented mainly a complex band by the vibration deformation of the link δ (N-H) and the elongation of the relationship ν (C-N) of the amide groups, occurring at about 1563 and 1540 cm^{-1} assigned to groups NH_3^+ existing in the collagen molecules [36-37].

FTIR-ATR studies it was found that the intensity of normalized peak for the vibrations of amide I and II increased significantly with the functionalization time.

4.3. The AFM Measurements of the Untreated Sample and the Collagen-Immobilized Pet Films

Following immobilization the collagen molecules on films activated plasma, the AFM images shows the distribution of collagen molecules, evidencing irregular sphere aspect. Figure 5 shows AFM images of collagen molecules immobilized.

AFM analysis method allowed the estimation of the average diameter of the formations (37 ± 5 nm) density formations (formations 310/3 x 3 mm^2) as images showed for 30 W/3 min. The roughness values and the average height is 6.8 nm.

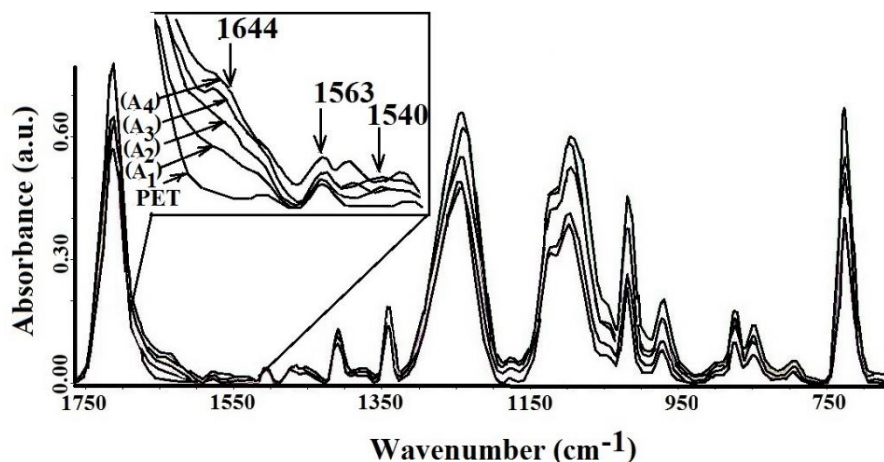


Figure 4. FTIR-ATR spectrum of untreated sample and collagen molecules immobilized on PET films after plasma functionalized.

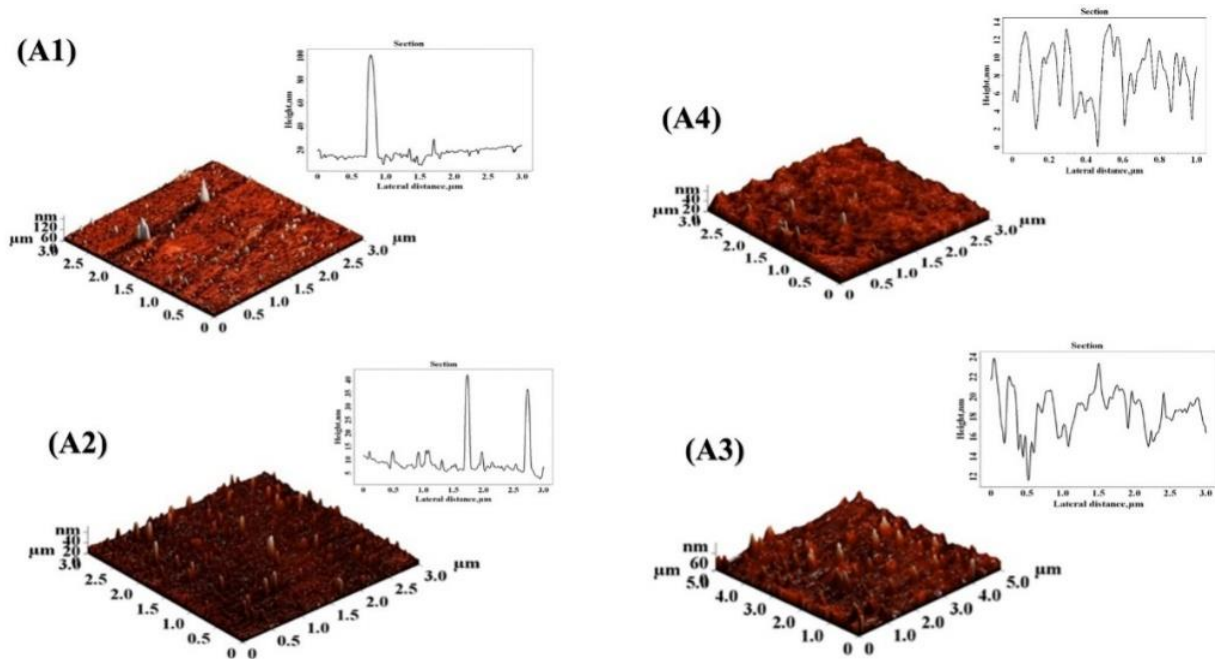


Figure 5. AFM analysis of the collagen immobilized and cross-section profiles from 3D images after He plasma-treated PET at: 30 W/3 min (A1), 30 W/5 min (A2), 50 W/3 min (A3) and 50 W/5 min (A4).

AFM measurements for film plasma treated with immobilized collagen at 30 W/5 min indicative of surface structures with small spherical formations that have a tendency to associate [38-41].

They are shown in cross section profiles of small particles.

Using the particle size, the average diameter of 25 ± 5 nm with a formation density of about $290/3 \times 3$ mm² were obtained.

However, the large number of small parties considered and their uniformity seem to have affected the texture parameters the interaction with the substrate, and decreasing the mobility of molecules. The roughness values and the average height is 4.4.

A general trend can be extracted from these results: the tendency of collagen to assemble is stronger on more hydrophobic substrates, it seems that the collagen-substrate interaction may influence the availability of collagen segments for assembly.

Adsorbed collagen at 50 W/3 min, it formed a surface structure with small diameter and also a tendency to agglomeration [42-43].

In Figure 5 are cross-sectional profiles of the structure the surface was then progressively covered with small filamentous structures. In this case the roughness values is 4.9 nm. Use size distribution showed an average diameter of 45 ± 10 nm and a formation density of about $224/3 \times 3$ mm².

4.4. Interaction Pet Film with Colloidal Solution Collagen-AgNPs After Plasma Action

4.4.1. Treatment Films with Colloidal Solution Collagen-AgNPs

The interaction of the functionalized PET films under the action of the plasma by immersing in collagen sol Ag-nanoparticles, was studied.

Colloidal solution Collagen Ag-nanoparticles: 1 mg/ml collagen was prepared in distilled water; 1 ml of AgNPs solution formed was added to the collagen solution, the solution was homogenized in continue stirring for 1 hour (B₁ and B₂ films for 30 W/3min and 5min; B₃ respectively B₄ films for 50W/3min and 5min) - The films were treated in colloidal solution.

4.4.2. FTIR-ATR Analysis on Pet Film Surface Treated with Colloidal Solution After Plasma He Action

From FTIR spectra we developed the conjugated structures, monitoring the interaction of AgNPs nanoparticles and collagen molecules, through binding mechanism, on the surface functionalized polyester.

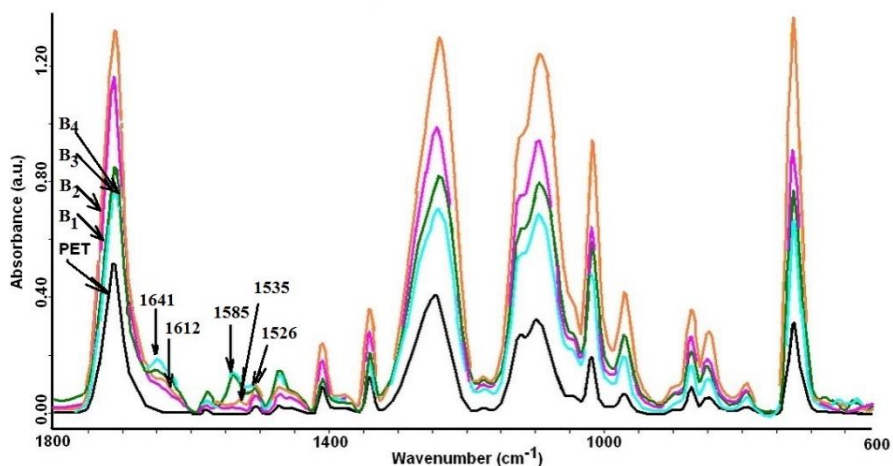


Figure 6. FTIR-ATR spectra of the PET surfaces after treatment with colloidal solution collagen-AgNPs.

The surfaces interact with collagen-AgNPs show a peak at 1612 cm^{-1} and 1384 cm^{-1} (Figure 6). Moreover, the spectra of the treated films ascribed the vibrations of the anions carboxylate are located to 1526 , and 1585 cm^{-1} , that means due to the transfer of the proton from of carboxyl groups/Ag [44-46]. This process involves ionic interactions, which occur between the silver ions and the carboxylate form, new groups on surface after functionalization from support.

A remarkable change can be seen in position of bands of the carboxylate group $\nu_{\text{as}}(\text{C}=\text{O})$ and $\nu_{\text{s}}(\text{C}=\text{O})$.

This indicates implies the carboxyl ends are involved in a conjugate structure with silver. Also, this mechanism favors adsorption and formation of certain interactions collagen-Ag + . . . COO-.

The molecular ability by attachment involves a mechanism, shown in Figure 7, based on the molecular interaction with -COO silver particle. Therefore, a new band in spectrum at 1635 cm^{-1} (attributed to complex formation between carboxyl groups on the surface of PET and complex collagen-AgNPs) confirmed interaction with functionalized support. Vibration $\nu(\text{C}=\text{O})$ component from the amide I present to 1635 cm^{-1} indicates coordination between AgNPs-collagen and carboxyl groups of the substrate.

This fact occurs due the electrons present in the NH bond groups, participating at the formation of the chelate with Ag^+ to Ag^0 , before the reduction, which was immediately stabilized by complexing [47].

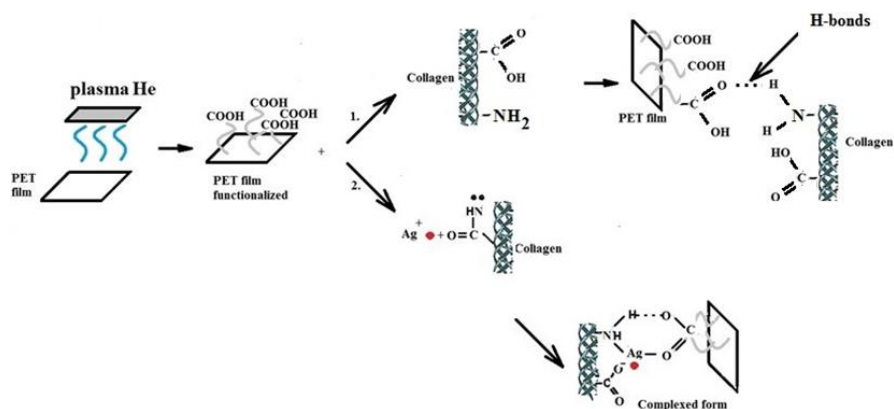


Figure 7. Schematic mechanism representing (1) collagen molecules immobilization onto PET functionalized; (2) interaction PET film with colloidal solution collagen-AgNps.

Interaction collagen-Ag with surface functionalized of PET appear in spectrum at 1535 cm^{-1} (attributed to deformation vibrations δ bond (N-H) and stretching vibrations ν (C-N) of the amide groups).

For a better understanding of the collagen molecules interaction mechanism in colloidal solution Ag-Collagen (the samples B1 and B2), FTIR spectroscopy and AFM microscopy methods were employed.

The film formed after drying using a small amount of solution directly onto the crystal was recorded in the range $4000\text{--}600\text{ cm}^{-1}$, at constant temperature about 25°C .

ATR-FTIR spectroscopy was used to relieve the changes in secondary structure of the collagen molecules interacting with AgNPs. Amide I band located to $1700\text{--}1600\text{ cm}^{-1}$ is the most sensitive for detecting changes in protein secondary structures. In Figure 8 the appearance of different types of secondary structures can be observed for samples with AgNPs. Thus, the spectrum of vibration bands of molecules of the collagen at 1454 , 1404 , 1334 , 1282 , 1240 and 1205 cm^{-1} , which could be attributed δ (CH₂), δ (CH₃), ν (CN) and δ (NH) can be observed. The intensity signal for the vibration characteristic amide I in the region $1700\text{--}1600\text{ cm}^{-1}$ is stronger for the treated samples. The Amide I vibration at 1649 cm^{-1} is attributed ν (C = O) the groups which belongs in peptide structure. The spectrum FTIR-ATR (Figure 8) shows important changes in both the intensity and position of the absorption peak due to the formation of the complex between collagen and silver nanoparticles [48-50]. These changes

suggest significant changes in secondary structures of collagen, when interacting with AgNPs.

The deconvolution and second derivative of the region $1700\text{-}1600\text{ cm}^{-1}$ were presented in order to study in detail the interactions. For processing was used Gaussian/Lorentz profile, each spectrum to be depicted into seven bands in amide I region (Figure 9).

After identification of all vibrations in envelope band, the percentage of the secondary structures components was calculated by integrative areas of the amide I and amide II bands, summed and reported at the total area [51-52]. The resulting number gives as a proportion in the polypeptide chains in that conformation.

The procedure for fitting to determine the curves the secondary structure of the collagen I is described in [48]: 1690 cm^{-1} (antiparallel β sheet), β -turns (1676 cm^{-1}) α -helix (1665 and 1653 cm^{-1}) coil, disposed at random (1642 cm^{-1}), side links (1615 cm^{-1}); the band at 1615 cm^{-1} is a result of the intermolecular β -strand. The band at 1629 cm^{-1} corresponds to the intramolecular β -strand structure.

After the addition of Ag nanoparticles in the solution of collagen, a new absorption band scanned at 1585 cm^{-1} (Figure 9) was observed. The spectrum of the complex collagen-AgNPs shows a modification of the band at 1585 cm^{-1} and also with a increasing intensity band at 1400 cm^{-1} . That vibration located at 1400 cm^{-1} could indicate interaction between AgNPs collagen (antiparallel – β sheet) [53].

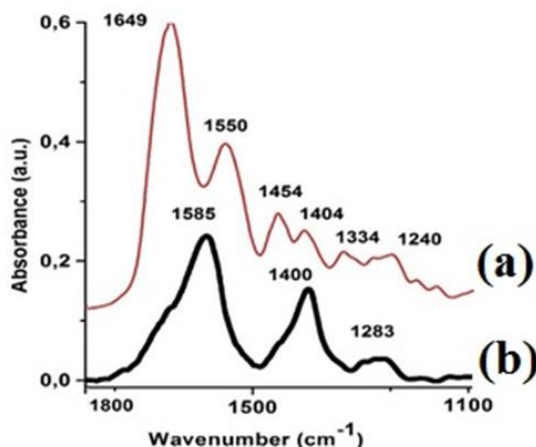


Figure 8. FTIR-ATR spectra of: (a) collagen I and (b) collagen I conjugated with AgNPs.

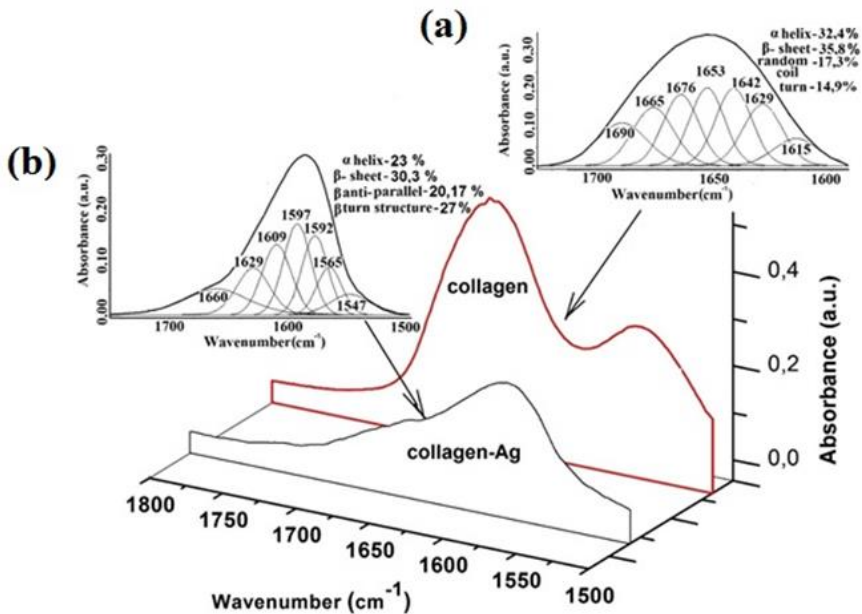


Figure 9. FTIR-ATR spectrum of collagen molecules and collagen conjugated–AgNPs in 1800–1500 cm⁻¹ region (a) deconvoluted band of Amide I region of collagen molecules (b) deconvoluted band of Amide I region of collagen conjugated –AgNPs.

Thus, the α -helix content in collagen decreases from 32% to 23%, while the β structures and anti-parallel β sheet are increase. The peak position from 1615 (β -extended intramolecular) moved to 1609 cm⁻¹, due to the intermolecular β -turns resulting from the unfolded protein structure.

The structure stabilized of the COO- and NH₂ groups from collagen with silver nanoparticles prevents precipitation and aggregation of nanoparticles. The FTIR spectra suggest that conjugations of AgNPs with collagen molecules favoured the formation of a compact structure.

The results from FTIR spectra indicate a strong interaction between the carboxyl groups (COO-) and amine (NH₂⁺) from collagen molecules and of AgNPs nanoparticles. The presence of AgNPs determines a conformational change in the protein structure, dominant growth to be in β conformation. The reduction in α -helix structures in favour of β structure indicates an unfolded of the protein structure in the presence AgNPs leads to structured form [54-56].

The conformational changes occurred as a result of exposure to more hydrophobic cavities to hydrophilic environments, which cause an improvement in the microenvironment polarity.

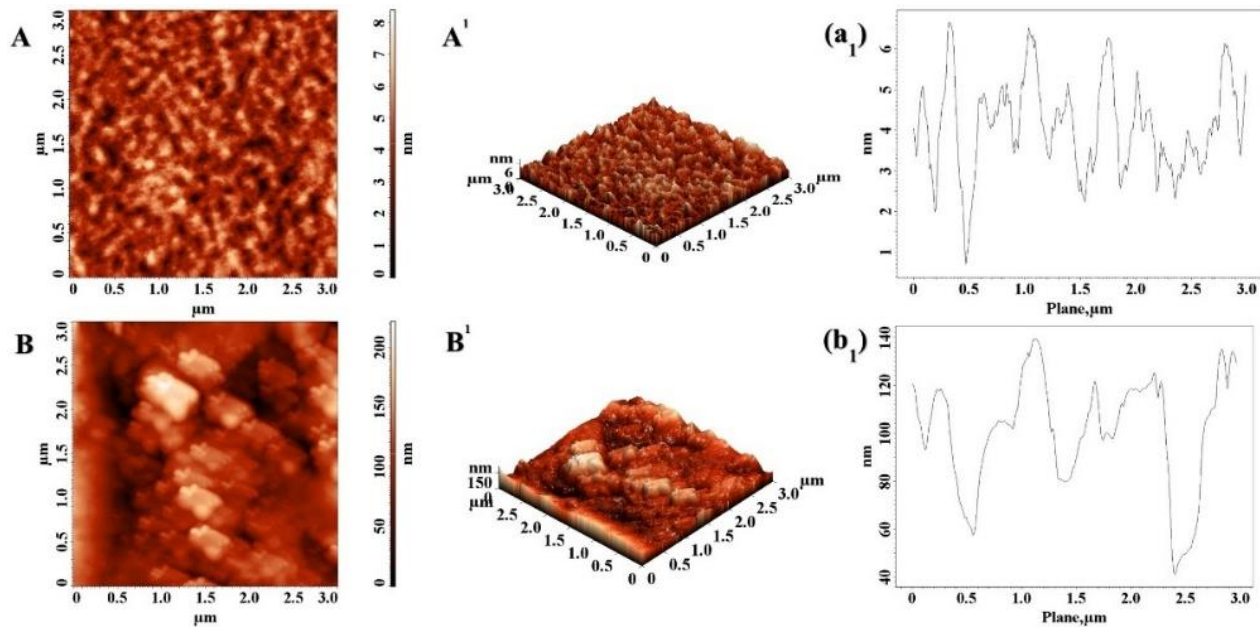


Figure 10. AFM analysis 2D images of collagen molecules (A) and collagen I conjugated with AgNP (B); 3D images of collagen molecules (A¹) and collagen I conjugated with AgNPs (B¹); cross-section profiles from 3D height images (a₁ and b₁).

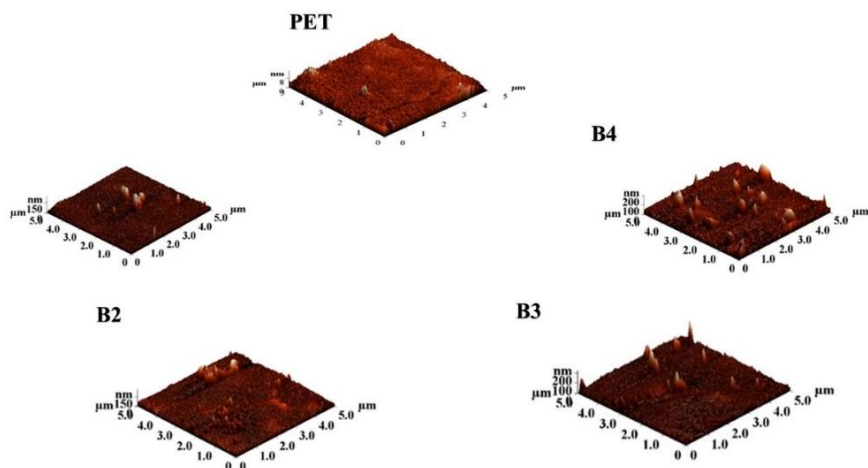


Figure 11. 3D AFM measurements for the untreated PET and treated samples.

More information about the binding of AgNPs in interaction with collagen, were obtained from AFM tapping mode measurements (Figure 10). The topography and morphology describes the collagen molecules and collagen-AgNPs adsorbed onto polymer surfaces in images. The root-mean-square roughness (RMS) was calculated as the average value for each set of AFM measurements. The RMS value of samples containing collagen and AgNPs is 1.4 (for sample B1) and 38 nm (for sample B2), respectively. These values and the image topography confirmed the stable structure obtained from FTIR-ATR methods. That showed the formation of a complex conformation of a structure which becomes compact due the interaction collagen molecules with silver nanoparticles.

4.5. AFM Measurements of Pet Films After Treatment with Colloidal Solution Collagen-AgNPs

In general, the collagen molecules adsorbed on very hydrophobic substrates are composed of elongated structures, and are smoother on less hydrophobic substrates [57].

AFM images of samples B1-B4 are shown in Figure 11. From those pictures, important changes can be noticed for samples treated with collagen –AgNps solution: images the diameter of the silver nanoparticles were between 60-80 nm for B1; 70-90 nm for B2; 50-60 nm for B3 and 60-80nm for B4. For both

treatments, the collagen molecules conjugated with silver in complex form have diameters between 250–450 nm on the PET surfaces.

Roughness values and average height has found 5.9 nm and 50 nm for B1; 5.5 nm and 25 nm for B2; 22 nm and 50 nm for B3; 17 nm or 47 nm to B4.

4.6. SAXS Measurements of Pet Films After Treatment with Colloidal Solution Collagen-AgNPs

The SAXS pattern from Figure 12 present the changes after plasma followed by silver nitrate treatments. This figure shows morphological changes within the sample, indicating the embedded Ag nanostructures can rearrange themselves depending upon counterionic environment [58-60].

From the Gaussian spherical model (Bruker NanoFit software) the values of AgNP sizes were obtained: 65 nm for B1, 85 nm for B2, 55nm for B3 and 75 nm for B4.

The chemical changes induced onto surface treated were investigated using XPS measurements shows in Figure 13.

Elemental composition and the ratio of elements are shown in Table 1. The untreated PET film and the entire treated samples ratio O/C are increased trend from 0.33 to 0.42, suggesting that the new oxygen-containing polar groups are formed on the PET film surface after plasma treatment [61-63].

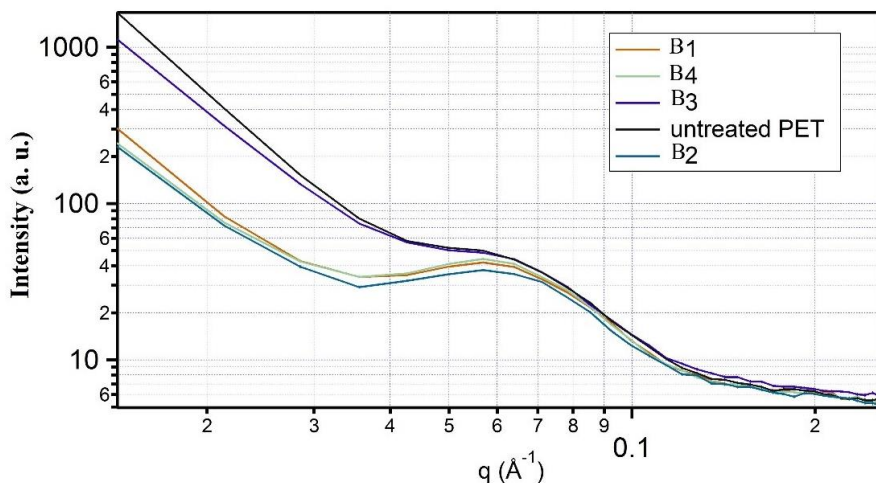


Figure 12. SAXS measurements of all samples.

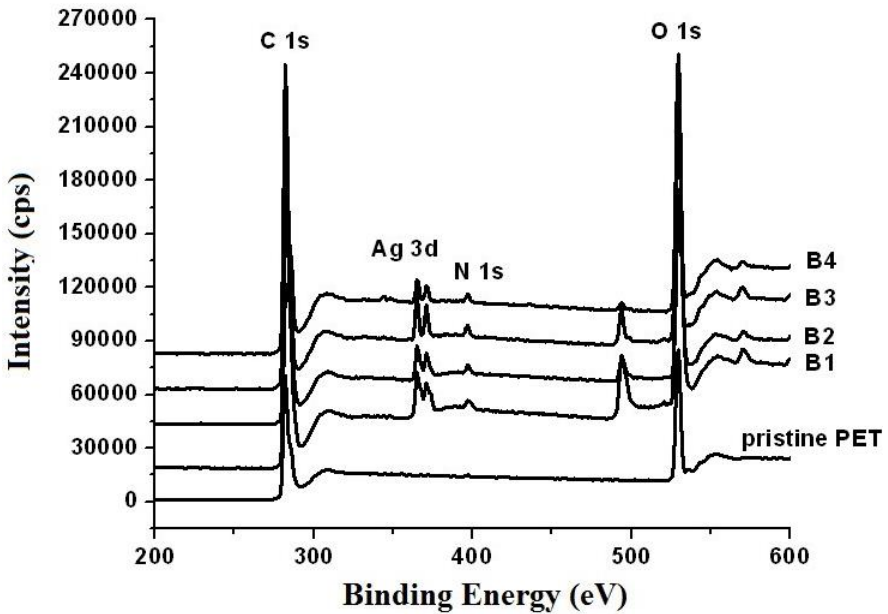


Figure 13. XPS measurements of the untreated and treated PET surfaces.

Table 1. The elemental surface compositions of non-treated and treated PET samples as calculated from the XPS survey spectra

PET/Element	Elemental composition (%)				Ratio		
	O	C	Ag	N	O/C	N/C	Ag/C
PET	25.24	74.76	-	-	0.33	-	-
B1	26.19	62.39	0.96	10.46	0.41	0.17	0.02
B2	26.01	61.93	1.07	10.99	0.42	0.18	0.02
B3	24.64	59.17	0.58	15.61	0.42	0.26	0.01
B4	24.20	60.62	0.52	14.66	0.40	0.24	0.01

XPS measurements confirm that quantity onto the surface treatment leads to an increase of the atomic ratio N/C of 0.17 to 0.26. There are, the functional groups containing the nitrogen are formed on the surfaces onto films after plasma activation and treatment with of collagen-Ag complex.

The higher value of the nitrogen concentration was obtained for B2, the sample fonded to have a lot of collagen molecules in different shapes and dimensions in AFM images. For sample B3 on the surface the higher concentration in Ag was found.

CONCLUSION

This chapter is concerning on the plasma surface treatments of PET film surfaces that contain reactive chemical groups useful for the subsequent immobilization, by solution chemical reactions, of molecules that can exert bio-specific interfacial responses. PET films were treated by helium RF plasma and subsequently were introduced in a wet chemical solution, prepared once in the presence of collagen and in absence of silver and second in presence of both collagen and silver. Various surface characterization techniques (AFM, FTIR, XPS, SAXS) were employed in order to study the chemical and morfological modifications of the films surfaces. From AFM images and SAXS measurements, important changes can be noticed for samples treated with collagen–AgNps solution, the diameter of the silver nanoparticles were obtained between 60-90 nm. For both treatments, the collagen molecules conjugated with silver in complex form have diameters between 250-450 nm on the PET surfaces. The mechanism of collagen secondary structure modifications after interacting with AgNPs was presented in this chapter.

REFERENCES

- [1] Homsy, C. A.; McDonald, K. E.; Akers, W. W.; Short, C.; Freeman, B. S. *J. Biomed. Mater. Res.*1968, 2, 215-230.
- [2] Klinge, U.; Klosterhalfen, B.; Conze, J.; Limberg, W.; Obolenski, B.; Öttinger, A.; Schumpelick, V. *Eur. J. Surg.*1998, 164, 951-960.
- [3] Soares, B.; Guidoin, R.; Marois, Y.; Martin, L.; King, M.; Laroche, G.; Zhang, Z.; Charara, J.; Girard, J. *J. Biomed. Mater. Res.*1996, 32, 293-305.
- [4] Francioni, G.; Ansaldo, V.; Magistrelli, P.; Pari, A.; Rinaldi, P.; Sani, C.; Rafaeli, W.; Pari, G. *Chir. Ital.*1999, 51, 21-27.
- [5] Vinard, E.; Eloy, R.; Descotes, J.; Brudon, J.; Guidicelli, H.; Magne, J.; Patra, P.; Berruet, R.; Huc, A.; Chauchard, J. *J. Biomed. Mater. Res.*1988, 22, 633-648.
- [6] Riepe, G.; Loos, J.; Imig, H.; Schröder, A.; Schneider, E.; Petermann, J.; Rogge, A.; Ludwig, M.; Schenke, A.; Nassutt, R.; Chakfe, N.; Morlock, M. *Eur. J. Vasc. Endovasc. Surg.*1997, 13, 540-548.
- [7] Lindenauer, S.; Weber, T.; Miller, T.; Ramsburgh, S.; Salles, C.; Kahn, S.; Wojtalik, R. *Biomed. Eng.*1976, 11, 301-306.

- [8] Von Recum, A. F. *J. Biomed. Mater. Res.* 1984, 18, 323-336.
- [9] Harkins, W. B.; Jackson, J. M. *J. Chem. Phys.* 1933, 1, 37-39.
- [10] Harkins, W. B. *Trans. Faraday Soc.* 1934, 30, 221-227.
- [11] Conrad, R. *Trans. Faraday Soc.* 1934, 30, 215-220.
- [12] Médard, N.; Soutif, J. C.; Poncin-Epaillard, F. *Surf. Coat. Tech.* 2002, 160, 197-205.
- [13] Kumar, D. S.; Fujioka, M.; Asano, K.; Shoji, A. Jayakrishnan, A.; Yoshida, Y. *J. Mater. Sci.* 2007, 18, 1831-1835.
- [14] Pandiyaraj, K. N.; Selvarajan, V.; Deshmukh, R. R.; Gao, C. *Vacuum.* 2008, 5, 332-339.
- [15] Vesel, A.; Junkar, I.; Cvelbar, U.; Kovac, J.; Mozetic, M. *Surf. Interface Anal.* 2008, 40, 1444-1453.
- [16] Guruvenket, S.; Rao, G. M.; Komath, M. *Appl. Surf. Sci.* 2004, 236, 278.
- [17] Hollahan, J. R.; Stafford, B. B.; Falb, R. D.; Payne, S. T. *J. Appl. Polym. Sci.* 1969, 13, 807-816.
- [18] Mason, M. K.; Vercruyse, P.; Kirker, K. R.; Frisch, R.; Marecak, D. M.; Prestwich, G. D. Pitt, W. G. *Biomaterials.* 2000, 21, 31-36.
- [19] Chatelier, R. C.; Xie, X.; Gengenbach, T. R.; Griesser, H. J. *Langmuir* 1995, 11, 2585-2591.
- [20] Meyer-Plath, A. A.; Finke, B.; Schroder, K.; Ohl, A. *Surf. Coat. Technol.* 2003, 174, 877-881.
- [21] Favia, P.; Stendardo, M. V.; d'Agostino, R. *Plasmas Polym.* 1996, 1, 91-112.
- [22] Bryjak, M.; Gancarz, I.; Pozniak, G.; Tylus, W. *Eur. Polym. J.* 2002, 38, 717-726.
- [23] Grace, J. M.; Gerenser, L. J. *J. Dispersion Sci. Technol.* 2003, 24, 305-341.
- [24] Dai, L.; StJohn, H. A.W.; Bi, J.; Zientek, P.; Chatelier, R. C.; Griesser, H. J. *Surf. Interface Anal.* 2000, 29, 46-55.
- [25] Bonakdar, S.; Orang, F.; Rafienia, M.; Imani, R. *Iran. J. Pharm. Res.* 2008, 4, 37-44.
- [26] Nowak, S.; Küttel, O.M. *Mater. Sci. Forum.* 1993, 140-142, 705-726.
- [27] Ramires, P.A.; Mirengi, L.; Romano, A.R.; Palumbo, F.; Nicolardi, G. *J. Biomed. Mater. Res.* 2000, 51, 535-539.
- [28] Poncin-Epaillard, F.; Vrlicnic, T.; Debarnot, D.; Mozetic, M.; Coudreuse, A.; Legeay, G.; Moualij, B. E.; Zorzi, W. *J. Funct. Biomater.* 2012, 3, 528-543.

- [29] Drobota, M.; Persin, Z.; Zemljic, L. F.; Mohan, T.; Stana-Kleinschek, K.; Doliska, A.; Bracic, M.; Ribitsch, V.; Harabagiu, V.; Coseri, S. *Cent. Eur. J. Chem.* 2013, *11*, 1786-1798.
- [30] Drobota, M.; Aflori, M.; Gradinaru, L. M.; Coroaba, A.; Butnaru, M.; Vlad, S.; Vasilescu, D. S. *High Perform. Polym.* 2015, *27*, 646-654.
- [31] Drobota, M.; Gradinaru, L. M.; Ciobanu, C.; Stoica, I. *J. Adhes. Sci. Technol.* 2015, *29*, 2208-2219.
- [32] Chen, Q.; Xu, S.; Li, R.; Liang, X.; Liu, H. *J. Colloid Interf. Sci.* 2007, *316*, 1-9.
- [33] Woodcock, S. E.; Johnson, W. C.; Chen, Z. J. *J. Colloid Interf. Sci.* 2005, *292*, 99-107.
- [34] Gurdak, E.; Rouxhet, P. G.; Dupont-Gillain, C. C.; *Colloids Surf. B.* 2006, *52*, 76-88.
- [35] Aflori, M.; Drobota, M.; Dimitriu, D. Gh.; Stoica, I.; Simionescu, B.; Harabagiu, V. *Mater. Sci. Eng. B.* 2013, *178*, 1303-1310.
- [36] Bryan, M. A.; Brauner, J. W.; Anderle, G.; Flach, C. R.; Brodsky, B.; Mendelsohn, R. *J. Am. Chem. Soc.* 2007, *129*, 7877-7884.
- [37] Ozaki, Y.; Mizuno, A.; Kaneuchi, F. *Applied Spectroscopy.* 1992, *46*, 626-630.
- [38] Shouhong, X.; Aiping, L.; Qibin, C.; Mingyu, L.; Masakastu, Y.; Honglai, L. *Colloids Surf. B.* 2009, *70*, 124-131.
- [39] Dupont-Gillain, C. C. *Colloids Surf. B.* 2014, *124*, 87-96.
- [40] Qibin, C.; Shouhong, X.; Rong, L.; Xiaodong, L.; Honglai, L. *J. Colloid Interf. Sci.* 2007, *316*, 1-9.
- [41] Zhang, Y.; Chai, C.; Jiang, X. S.; Teoh, S. H.; Leong, K. W. *Mater. Sci. Eng. C.* 2007, *27*, 213-219.
- [42] Steven, F. *Plast. Reconstr. Surg.* 2000, *105*, 362-373.
- [43] Cooperman, L.S.; Mackinnon, V.; Bechler, G.; Pharriss, B. B.; Alto, P. *Aesth. Plast. Surg.* 1985, *9*, 145-151.
- [44] Porel, S.; Venkatram, N.; Rao, D. N.; Radhakrishnan, T. P. *J. Nanosci. Nanotechno.* 2007, *7*, 1887-1892.
- [45] Barth, A.; Zscherp, C. *Rev. Biophys.* 2002, *35*, 369-430.
- [46] Zou, Y.; Li, Y.; Hao, W.; Hu, X.; Ma, G. *J. Phys. Chem. B.* 2013, *117*, 4003-4013.
- [47] Drobota, M.; Grierosu, I.; Radu, I.; Vasilescu, D. S. *Key Eng. Mater.* 2015, *638*, 8-13.
- [48] Petitbois, C.; Gousspillou, G.; Wehbe, K.; Delage, J.P.; Deleris, G. *Anal. Bioanal. Chem.* 2006, *386*, 1961-1966.

- [49] Goormaghtigh, E.; Ruyschaert, J. M.; Raussens, V. *Biophys. J.* 2006, *90*, 2946-2957.
- [50] Byler, M.; Susi, H. *Biopolymers*. 1986, *25*, 469-487.
- [51] Sarver, R.W.; Krueger, W.C. *Anal. Biochem.* 1991, *194*, 89-100.
- [52] Mandal, A.; Meda, V.; Zhang, W. J.; Farhan, K.; Gnanamani, M. A. *Colloids Surf. B.* 2012, *90*, 191-196.
- [53] Chalal, S.; Haddadine, N.; Bouslah, N.; Benaboura, A. *J. Polym. Res.* 2012, *19*, 24-31.
- [54] Yin, J.; Yang, Y.; Hu, Z. Q.; Deng, B. *J. Membrane Sci.* 2013, *441*, 73-82.
- [55] Kim, J. S.; Kuk, E.; Yu, K.; Park, J. H.; Lee, S. J.; Kim, H. J.; Park, S. H.; Park, Y. K.; Hwang, Y.H.; Kim, C.Y.; Lee, Y. S.; Jeong, D. H.; Cho, M. H. *Nanomed. Nanotechnol.* 2007, *3*, 95-101.
- [56] Reznickova, A.; Novotna, Z.; Kolska, Z.; Svorcik, V. *Nanoscale Res. Lett.* 2014, *9*, 305-311.
- [57] Xingguo, C.; Umut, A.; Gurkan, C.; Dehen, J.; Tate, M. P.; Hillhouse, H. W.; Simpson, G. J.; Akkus, O. *Biomaterials*. 2008, *29*, 3278-3288.
- [58] Gunda, P.; Ralf, M.; Roland, W.; Gert, R.; Frye, K. J.; Royer, C. A. *J. Mol. Biol.* 1998, *275*, 389-402.
- [59] Sousa, S. R.; Moradas-Ferreira, Melo, P. L.; Saramago, V. B.; Barbosa, M. A. *Langmuir*. 2004, *20*, 9745-9754.
- [60] Rujitanaroj, P.; Pimpha, N.; Supaphol, P. *Polymer*. 2008, *49*, 4723-4732.
- [61] Wang, Y.Y.; Lu, L. X.; Shi, J. C.; Wang, H. F.; Xiao, Z. D.; Huang, N. P. *Biomacromolecules*. 2011, *12*, 551-559.
- [62] Surdu-Bob, C.C.; Sullivan, J. L.; S.O. Saied, R. Layberry, Aflori, M. *Appl. Surf. Sci.* 2002, *202*, 183-198.
- [63] Ramires, P. A.; Mirengi, L.; Romano, A.R.; Palumbo, F.; Nicolardi, G. *J. Biomed. Mater. Res.* A2000, *51*, 535-539.

Complimentary Contributor Copy

Chapter 3

SYNTHESIS OF AG NANOSTRUCTURES IN MESOPOROUS SILICA USING SUPERCRITICAL CO₂ AND CO-SOLVENT

*Qin-Qin Xu and Jian-Zhong Yin**

State Key Laboratory of Fine Chemicals, School of Chemical Machinery,
Dalian University of Technology, Dalian, P. R. China

ABSTRACT

Ordered mesoporous silica have often been used as supports for various metal nanoparticles due to their high specific surface areas, high pore volumes and narrow pore size distributions. However, it is hard to obtain homogeneous metal dispersion and distribution due to low support-precursor interactions when the traditional impregnation method is used. This chapter reviews a new developed method of preparing supported Ag nanoparticles and nanowires in supercritical CO₂. Cheap inorganic salt AgNO₃ is used as precursor, mesoporous SBA-15 and KIT-6 are used as substrates, supercritical CO₂ is used as solvent and ethanol or the mixture of ethanol and ethylene glycol are used as co-solvents. Superior to traditional impregnation method, large aggregates of nanoparticles outside of the nanochannels could be usually avoided due to the near-zero surface tension of supercritical fluids. The operating parameters of interest including the deposition pressure, temperature, time and the amount of the precursor are summarized to demonstrate the optimum parameters

* Corresponding Author : jzyin@dlut.edu.cn.

influencing the deposition results. The thermodynamics and kinetics of AgNO_3 adsorption on SBA-15 from scCO_2 and co-solvent are investigated to further understand the experimental process and the mechanism. Finally, the underlying mechanism of supercritical fluid deposition method based on AgNO_3 and a specific co-solvent is described.

Keywords: supercritical carbon dioxide; mesoporous silica; silver; inorganic precursor

INTRODUCTION

Nanometer-scale silver has fascinating optical, electronic, magnetic and thermal properties and is widely used in the field of catalysis, electronics, medicine, sensing etc (Hong et al., 2001; Lei et al., 2010; Nowack, 2010; Pyayt et al., 2008; Sun and Xia, 2002). The specific properties mainly depend on the size and the morphology of the nanostructure (Zheng and Dickson, 2002). Mesoporous silica with well-defined pore geometries and large surface areas have often been used as hosts to prevent the aggregation of nanostructures or to make their size or size distribution controllable. There are many methods to prepare these supported Ag nanocomposites, such as impregnation (Huang et al., 2000), sol-gel processing (Bekyarova and Kaneko, 2000), chemical vapor impregnation (Miller et al., 1997) and so on. Supercritical fluid deposition (SCFD) is an effective and environmentally benign technique to synthesize supported nanocomposites. This method involves the dissolution of metal precursor in supercritical fluids (SCFs), the diffusion and impregnation of SCF solution into the pores of the substrates and adsorption of metal precursor onto the walls of the channels, followed by thermal or chemical reduction in or after depressurization process. The low surface tension of SCFs will favor the impregnation of precursors into the nano-scale channels of the substrates. Furthermore, the ordered pores of the substrate won't be collapsed because no organic solvents are left after depressurization, and the post-treatment process is quite simply compared to other preparing methods.

Supercritical carbon dioxide (scCO_2) is the most widely used SCF due to its abundance, low cost, non-flammability, non-toxicity and in particular the mild critical pressure and temperature ($T_c = 31.1^\circ\text{C}$, $P_c = 7.38 \text{ MPa}$). SCFD method was first proposed by Watkins based on chemical vapor deposition (CVD) technique in 1995 (Watkins and McCarthy, 1995). After that, it has attracted growing attentions by many researchers. They used this method to deposit thin metal films (Cu, Au, Pt, Pd, Co, Ni etc.) onto a wide range of substrates such as

silicon wafer, metal, ceramic, polymer and so on(Blackburn et al., 2001; Cabanas et al., 2004; Haruki et al., 2016; Karanikas and Watkins, 2010; Miller et al., 1997; Morere et al., 2011)or incorporate metallic nanoparticles (Pt, Pd, Au etc.) on different inorganic substrates such as carbon aerogel, carbon black, Al₂O₃, silica aerogel(Erkey, 2009; Saquing et al., 2004; Sun et al., 2006; Zhang et al., 2005), mesoporous silica(Morere et al., 2011; Yin et al., 2010), carbon nanotubes(An et al., 2008; Chen et al., 2011; Do et al., 2011; Zhang et al., 2016), graphene(Meng et al., 2015; Zhao et al., 2014) etc.

However, organometallic compounds were usually used as precursors because they have relatively large solubilities in scCO₂. In order to overcome the limitation of using the expensive and toxic organometallic compounds, inorganic salt was used as precursor with the addition of appropriate co-solvent by some groups. Liu and coworkers used metal nitrates dissolved in scCO₂/ethanol system to deposit metal and metal oxides on carbon nanotubes(Liu and Han, 2009; Sun et al., 2007; Sun et al., 2006). Hu et al. prepared 4A-zeolite supported silver nanoparticles with the assistance of scCO₂ and hydrogen reduction using AgNO₃ as precursor(Hu et al., 2016). Yin and his co-workers have made much effort towards the cheap SCFD process based on inorganic precursors and appropriate co-solvents in recent years (Xu et al., 2012a; Xu et al., 2012b; Xu et al., 2014a; Xu et al., 2014b; Yin et al., 2010). This review aims to systematically introduce the synthesis of Ag nanoparticles and nanowires in SBA-15 and KIT-6 using AgNO₃ as precursor, scCO₂ as solvent and different organic solvents as co-solvents. Firstly, the experimental process and the mechanism of SCFD method are discussed. And then the operating parameters of interest including the deposition pressure, temperature, time and the amount of the precursor are summarized to demonstrate the optimum parameters influencing the deposition results. After that, the adsorption isotherms and kinetics of AgNO₃ (adsorbate) on SBA-15 (adsorbent) in scCO₂ are discussed to further understand the experimental process and the mechanism. Finally, the underlying mechanism of SCFD methods based on AgNO₃ and a specific co-solvent is described in detail.

PROCESS OF SCFD WITH INORGANIC SALTS AS PRECURSORS

In a typical SCFD method, the precursors are usually put at the bottom of the reactor, keeping a distance from the substrates held on the upper of the

reactor(Saquing et al., 2004; Xu et al., 2014a). The substrates are held in a filter bag or in a steel stainless basket on a stage. When the inorganic salts are used as precursors, co-solvents are required for the solubility enhancement of the precursors for the reason that the inorganic salts are usually not soluble in scCO_2 . Some organic solvents such as methanol, ethanol, acetone, ethylene glycol, dichloromethane and so on can be acted as co-solvents to enhance the ability of scCO_2 to dissolve some polar compounds. Yin et al.(Xu et al., 2012b)explained the schematic of Ag nanophas formation when AgNO_3 was used as precursor in scCO_2 and co-solvent system, as shown in Figure 1.

The schematic of Ag nanostructures formation in mesoporous silica using supercritical CO_2 and co-solvent is shown in Figure 1. Firstly, the precursor dissolves in scCO_2 and co-solvent system so that the bulk phase becomes a single phase of precursor, CO_2 and co-solvent. Then the scCO_2 solution diffuses into the pores of mesoporous silica. Thirdly, the precursor and scCO_2 solution are adsorbed onto the substrate. Fourthly, CO_2 and co-solvent are desorbed and depart from the substrate by slow depressurization with the precursor left onto the walls of the pores within the substrate. The distribution of the precursors in the nanoscale channels varies according to different deposition conditions, and the morphologies of the nanostructures in the nanocomposites after thermal treatment are quite different.

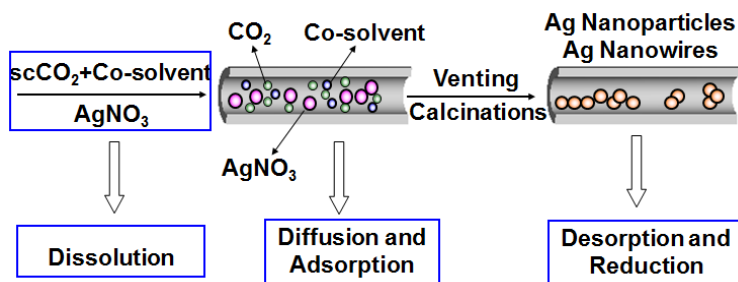


Figure 1. Schematic of Ag nanostructures formation in mesoporous silica using supercritical CO_2 and co-solvent.

The formation of the nanophase could be divided into five stages along with the deposition time. Firstly, a few precursors deposit onto the channels after a short deposition time and small nanoparticles are formed after the thermal treatment. Secondly, nanoparticles tend to aggregate and short nanorods are formed. Thirdly, a large amount of small nanoparticles aggregate and short nanorods connect with one another to form nanowires. Fourthly, the nanowires

break due to a high percentage of channel-filling after the thermal treatment, thus leading to the formation of big nanoparticles or nanorods with a larger diameter. Finally, only big nanoparticles are found instead when the deposition time is quite too long.

However, when the co-solvent is changed, the mechanism will be changed too. Yin and his co-workers (Xu et al., 2012a; Xu et al., 2014a) found that when the mixture of ethanol and ethylene glycol are used as co-solvent to prepare Ag@SBA-15 nanocomposites, the metal loading could achieve the maximum within very short time of deposition and nanowires instead of small nanoparticles were formed in all the samples. As shown in Figure 2, for the synthesis of Ag@SBA-15 in $scCO_2$ using ethylene glycol as the co-solvent, $AgNO_3$ is first dissolved in $scCO_2$ with the assistance of the co-solvent and then it diffuses into the nanochannels of SBA-15. In the nanopores a small amount of $AgNO_3$ is reduced to Ag^0 by ethylene glycol, then the reduced Ag^0 serves as nuclei to attract a large amount of $AgNO_3$, leading to a significant decrease of $AgNO_3$ concentration inside the pores. Because of the large difference of the $AgNO_3$ concentration inside and outside the pores, $AgNO_3$ diffuses rapidly into the nano-scale channels and thus a rapid non-equilibrium sorption occurs. That is the reason why a high metal loading is obtained in a very short deposition time.

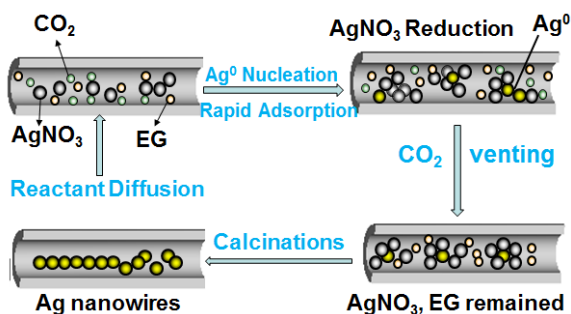


Figure 2. The mechanism of Ag growth in SBA-15 by using ethylene glycol as co-solvent.

THE OPERATING PARAMETERS

In a typical SCFD process, metal precursors first dissolve in $scCO_2$ with the assistance of co-solvent, then the mixture of the precursors, co-solvent and CO_2 diffuse into the nanochannels and adsorb onto the substrates. After

depressurization, CO₂ and co-solvent are removed and nanocomposites are obtained. Thus, there are several controllable steps in the whole preparation process and there is more than one operating parameter to be controlled for each step. Generally speaking, there are four important parameters including the deposition pressure, temperature, time and the mass ratio of substrate to precursor influencing the experimental results in the SCFD method(Xu et al., 2012a).

Yin et al.(Xu et al., 2012a) prepared Ag@SBA-15 (Figure 3a) using AgNO₃ as precursor, scCO₂ as solvent and ethanol as co-solvent in the temperature range of 30-80 °C, pressure range of 8-24 MPa, deposition time of 0.5-28 h. The mass ratio of substrate to precursor was tuned from 2:1 to 0.5:1. It was found that for the sample prepared at the deposition temperature of 30 °C, there were very weak peaks assigned to (111) and (200) reflections of metallic Ag in the XRD pattern. In contrast, the XRD pattern of the sample prepared at 80 °C presented four weak and broad peaks. Moreover, the XRD peaks became much stronger for the sample prepared at 50°C. They suggested that 50 °C should be the proper temperature since it was mild and beneficial to the adsorption. When the deposition pressure was 8 MPa, neither nanoparticles nor nanowires were found in the TEM image. When the pressure was increased to 17 MPa, several nanoparticles could be seen in the TEM image while a large amount of nanoparticles and short nanorods were obtained at the deposition pressure of 24 MPa.

The dependence of nanowire or nanoparticle growth on the deposition time was studied at 50 °C and 24 MPa. When the deposition time was only 1 h, no any Ag nanoparticle or nanowire was observed from TEM image. As the deposition time was prolonged while the other parameters were kept unchanged, different morphologies of nanostructures could be observed. Short nanorods, long nanowires and uniformly dispersed nanoparticles were formed respectively at the deposition time of 3 h, 6-12 h, and 19-28 h. They found that the deposition time affected the morphology of nanostructures in a similar way when using Cu(NO₃)₂ as the precursor to prepare Cu@SBA-15 nanocomposites via a SCFD process (Yin et al., 2010). Besides, the metal loading changed from 3.99 wt% to 19.6 wt% as the deposition time varied from 3 h to 12 h while it kept almost constant after 12 h (19.6 wt% for 12 h, 19.2 wt% for 19 h and 20.4 wt% for 28 h). This indicated that the adsorption reached equilibrium after 12 h of deposition and the adsorbed amount wouldn't increase with deposition time after this equilibrium.

When Ag@KIT-6 (Figure 3b) was synthesized using SCFD method(Xu et al., 2014b), with the mixture of 1mL ethanol and 1 mL ethylene glycol as co-

solvent, the Ag loading of the nanocomposites was increased as the deposition time increased from 1h to 6h (11.89 wt% for 1h, 12.84 wt% for 3h and 15.30 wt% for 6h), but it was slightly decreased when the deposition time was increased to 12h (13.74 wt%). The influence of deposition time on the metal loading is similar to that when preparing Ag@SBA-15 using SCFD method. In addition, When the deposition time was 1h, some nanoparticles were impregnated in the nanochannels of KIT-6 while there were several big nanoparticles outside the channels. As the deposition time increased from 3h to 6h, more nanoparticles and nano-network could be seen inside the nanochannels instead.

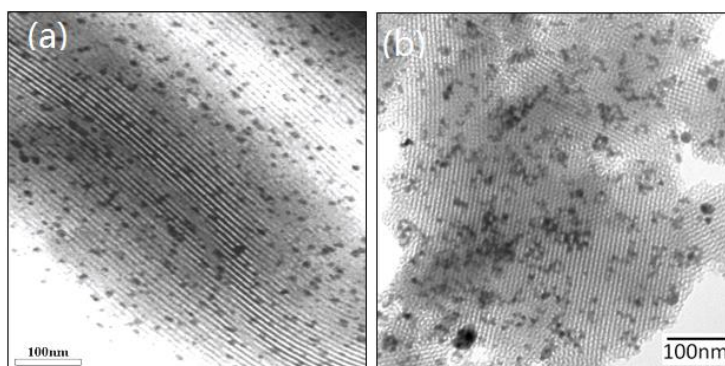


Figure 3. Typical TEM images of (a) Ag@SBA-15 and (b) Ag@KIT-6 prepared using SCFD method.

INFLUENCE OF CO-SOLVENT AND THE UNDERLYING MECHANISM

Yin and his co-workers(Xu et al., 2012b) found that compared to the case of only ethanol as the co-solvent, the employment of dual co-solvent of ethylene glycol and ethanol led to the significant reduction of deposition pressure and time. In their subsequent work(Xu et al., 2014a), they found that well dispersed and continuous nanowires were anchored into the nanochannels of SBA-15 in only 5 minutes at 8.5 MPa with a metal loading of 5.8 wt%. Furthermore, the metal loading increased with the increase of deposition time while the morphology was not changed. They drew a conclusion that the formation of nanowire morphology was independent of deposition time, pressure and metal loading when the dual co-solvent of ethylene glycol and ethanol were used.

As stated above, the deposition process of Ag nanowires in the channels of mesoporous silica can be described as four steps: (i) dissolution of AgNO_3 in scCO_2 ; (ii) diffusion and impregnation of scCO_2 solution into the pores of the substrates and adsorption of AgNO_3 onto the walls of the channels; (iii) depressurization and phase separation; and (iv) thermal reduction. Therefore, Yin and his co-workers (Xu et al., 2014a) investigated the underlying reason for the ethylene glycol co-solvent in consideration of these four steps.

Firstly, the solubility of AgNO_3 in ethylene glycol is nine times larger than that in ethanol at room temperature and the standard atmospheric pressure. Therefore, the solubility of precursor in scCO_2 would be enhanced, facilitating the deposition of AgNO_3 with a higher loading and the more complete filling of the channels, thus leading to the formation of nanowires. Contrast experiments with water and pyridine as the co-solvent were performed then. AgNO_3 has a very high solubility in the three co-solvents (34g in ethylene glycol, 455g in water and 29g in pyridine at 20, 50 and 30 °C respectively). It was unexpected that when the mixture of ethanol and deionized water was used as co-solvent, several nanoparticles were observed and the metal loading was only 0.15 wt%. When the mixture of ethanol and pyridine was used as the co-solvent, a lot of nanoparticles instead of nanowires formed on the substrate even though the metal loading was as high as 15.9 wt%. Therefore, Yin and his co-workers (Xu et al., 2014a) argued that the enhancement of solubility was not the primary reason for the formation of nanowire morphology when ethylene glycol was used as the co-solvent.

Secondly, the diffusion process of precursor into the nanochannels of the substrate probably will change after the addition of ethylene glycol. Yin and his co-workers (Xu et al., 2012a) studied the phase behavior of binary system of ethanol/ scCO_2 and ternary system of ethylene glycol/ethanol/ scCO_2 . They found that for the binary system of ethanol/ CO_2 , only liquid phase was found after calculations; the viscosity was 2.58 mPa·s and the surface tension was 0.11 $\text{N}\cdot\text{m}^{-1}$. For the ternary system, the ratio of the vapor volume to the liquid volume was 69:1, so the vapor phase was the bulk phase in the deposition process (Xu et al., 2012a; Xu et al., 2014a). The viscosity of the vapor phase was 0.081 mPa·s and the surface tension was 0 $\text{N}\cdot\text{m}^{-1}$ according to the calculations. Therefore, smaller viscosity and surface tension of the bulk phase were obtained when the mixture of ethylene glycol and ethanol was used as the co-solvent, which was beneficial for the penetration of precursor into the nanoscale channels.

Thirdly, the interaction among the precursor, the solvent and the substrate will influence the adsorption of AgNO_3 on SBA-15 from scCO_2 /co-solvent, thus

affect the metal loading and the morphology of the nanophase. The adsorption of inorganic precursor on the substrate mainly depends on the adsorption of co-solvent on the substrate. It was reported that the relative effectiveness of hydrogen-bonding formation between the compounds and the silanol surface reflected the adsorption capacity (Ralph, 1979). If dimethoxytetraethylene glycol is used as standard compound, the relative molar effectiveness for ethanol, pyridine, and ethylene glycol is 5, 42, and 0. The bigger the relative molar effectiveness of hydrogen-bonding, the stronger the adsorption between the solvent and the substrate is. However, the zero relative molar effectiveness for ethylene glycol indicates weak adsorption between the co-solvent and silica, which conflicts with the fact that a large amount of AgNO_3 was adsorbed onto the silica in a short deposition time of 5 minutes.

Fourthly, a small amount of AgNO_3 was proved to reduce to Ag^0 during the deposition process by TEM and XAFS analysis. Then the reduced Ag^0 served as nuclei to attract a large amount of AgNO_3 , leading to a significant decline of the precursor concentration inside the pores. Because of a large difference of the AgNO_3 concentration inside and outside the pores, AgNO_3 diffused rapidly from the bulk phase into the nano-scale channels and thus a rapid non-equilibrium sorption occurred. Yin and his co-workers (Xu et al., 2014a) contributed the high metal loading to this reason. This deposition process with the addition of ethylene glycol is quite different from that using other co-solvents. When using ethanol, water or pyridine as the co-solvent, the deposition process could be attributed to the adsorption of precursor on SBA-15 which was determined by the interaction between co-solvent and the silanol groups.

THERMODYNAMICS AND KINETICS OF AgNO_3 ADSORPTION ON SBA-15 FROM scCO_2 AND CO-SOLVENT

As mentioned above, there are four procedures including dissolution of metallic precursor in SCF, the diffusion and adsorption of precursor in the channels of substrates as well as depressurization in a SCFD process. Among the four procedures, the adsorption of the precursor from scCO_2 solution on the substrate is the essential step which influences the metal loading and the distribution of the precursor directly. Erkey et al. (Zhang et al., 2008) and Yin et al. (Xu et al., 2012a) used the classical Langmuir model to investigate the adsorption of the solute on adsorbent from scCO_2 .

$$q = \frac{KQ_0C}{1 + KC} \quad (1)$$

It can be represented by Eq. (1) where q is the amount adsorbed of AgNO_3 on SBA-15 (mmol/g), K is the Langmuir adsorption constant (L scCO_2 /mmol AgNO_3), Q_0 is the adsorption capacity (mmol AgNO_3 /g scCO_2) and C is the concentration of AgNO_3 in scCO_2 (mmol AgNO_3 /L scCO_2). KQ_0 represents the relative affinity of the AgNO_3 towards the surface of the adsorbent. The value of K and Q_0 are obtained from another description of the equation (1) shown as equation (2).

$$\frac{1}{q} = \frac{1}{Q_0KC} + \frac{1}{Q_0} \quad (2)$$

The fitting results are shown in Figure 4a. It can be seen that a good agreement is obtained between the model fitting and the experimental data. As the temperature increases, the adsorbed amount decreases at the same concentration of AgNO_3 . Figure 4b illustrates the difference of the adsorption when different co-solvents are used. When ethanol was used as the co-solvent, it takes about 20 h to achieve the equilibrium while it takes only about 2.8 h to approach the equilibrium when the mixture of ethanol and glycol was used as the co-solvent.

Erkey and co-workers reported a mass transfer model based on diffusion inside the pore volume to describe the kinetics of adsorption of ruthenium and platinum precursors onto carbon aerogels and carbon blacks from scCO_2 solutions (Bozbag et al., 2011; Zhang et al., 2008). Yin et al. (Xu et al., 2012a) applied this method to the system of inorganic salt and scCO_2 /co-solvent system. The equation of the adsorption kinetics model originating from Fick's second law is given below:

$$\varepsilon_p \frac{\partial C_A}{\partial t} + \rho_p \frac{\partial q}{\partial t} = D_{e,p} \left(\frac{\partial^2 C_A}{\partial r^2} + \frac{2}{r} \frac{\partial C_A}{\partial r} \right) \quad (3)$$

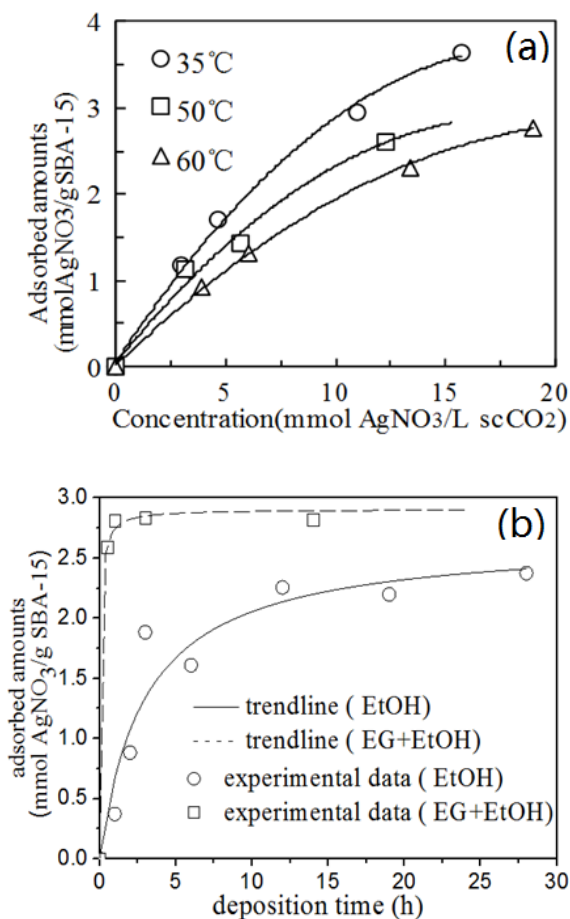


Figure 4. (a) Adsorption isotherms for AgNO₃ on SBA-15 using dual co-solvent (experimental data and Langmuir fitting) (b) AgNO₃ adsorption on SBA-15 using different co-solvents at 50°C and 24 MPa.

Where C_A is the concentration of AgNO₃ in scCO₂ (mol/m³), q is the uptake amount of AgNO₃ on the adsorbent (mol/kg) and t is the time (s). $\partial C_A / \partial t$ represents the accumulation term, $\partial q / \partial t$ represents the adsorption term and $\partial C_A / \partial r$ represents the flux term. ρ_p is the density of adsorbent particles (kg/m³), ε_p is the porosity of adsorbent particles, $D_{e,p}$ is the effective pore volume diffusivity and r is the diameter of the adsorbent particles. The two boundary conditions for Eq. (3) are

$$\frac{\partial C_A}{\partial r} = 0 \quad \text{at} \quad r = 0 \quad (4)$$

$$-V \frac{\partial C_A}{\partial t} = mSD_{e,p} \frac{\partial C_A}{\partial r} \quad \text{at} \quad r = R \quad (5)$$

Where V is the volume of scCO_2 , m is the mass and S is the external surface area of SBA-15 particles. The initial conditions are that the adsorbent is solute free when the time is zero and the bulk fluid concentration is fixed, shown by equations (6) and (7):

$$C_A = 0 \quad \text{at} \quad t = 0, \quad 0 \leq r < R, \quad (6)$$

$$C_A = C_{A0} \quad \text{at} \quad t = 0, \quad r = R, \quad (7)$$

To solve Eq. (3) numerically, the adsorption term $\partial q/\partial t$ in this equation is rewritten in terms of the uptake change with concentration $\partial q/\partial C_A$ and the concentration change with time $\partial C_A/\partial t$ using the chain rule as shown in equation (8)

$$\frac{\partial C_A}{\partial t} = \frac{D_{e,p}}{\varepsilon_p + \rho_p (\partial q / \partial C_A)} \left(\frac{\partial^2 C_A}{\partial r^2} + \frac{2}{r} \frac{\partial C_A}{\partial r} \right) \quad (8)$$

In the polymath software, Eq. (8) is written using finite difference methods as:

$$\frac{dC_{A(n)}}{dt} = \frac{De, p}{\varepsilon_p + \rho_p (dq / dC_{A(n)})} \left(\frac{C_{A(n+1)} - 2C_{A(n)} + C_{A(n-1)}}{\Delta r^2} + \frac{2}{R - (n-1)\Delta r} \frac{C_{A(n+1)} - C_{A(n-1)}}{2\Delta r} \right) \quad (9)$$

the boundary conditions are

$$C_{A(n)} - C_{A(n-1)} = 0 \quad \text{at} \quad r = 0, \quad (10)$$

$$\frac{dC_{A(1)}}{dt} = \frac{mSD_{e,p}}{-V} \frac{C_{A(1)} - C_{A(2)}}{\Delta r} \quad \text{at} \quad r = R, \quad (11)$$

$dq / dC_{A(n)}$ is calculated by Langmuir equation as mentioned above.

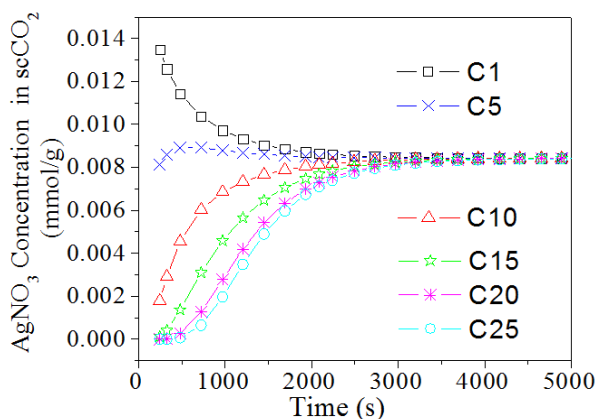


Figure 5. Demonstration of concentration decay curves of AgNO_3 on SBA-15 from the outermost point (C1) to the center of the adsorbent (C25).

Twenty five points in the radial direction from the outside of the spherical adsorbent particle to the center were used. As seen in Figure 5, the concentration of the precursor at the outermost point of the adsorbent particle decreased as the time increased (C1 curve), while that inside the adsorbent increased with time (C5, C10, C15, C20, C25 curves). The concentration at the location near the outside of the adsorbent particle increased faster than that far away from it. After 10000s (about 2.8 h) the concentration at the outermost point of the adsorbent particle was the same as that inside even at the center of the adsorbent, and the adsorption reached equilibrium. The equilibrium time was consistent with the experimental data (2.5 h).

CONCLUSION

In summary, SCFD is an effective method to prepare Ag nanostructures in mesoporous silica using inorganic AgNO_3 as precursor. Co-solvent has a significant influence on the metal loading and the morphology of the nanostructures. The addition of ethylene glycol as co-solvent leads to a large metal loading within very short deposition time. Moreover, only nanowires are found instead of small nanoparticles in all the samples when the mixture of ethanol and ethylene glycol is used as co-solvent. The underlying reason could be attributed to the reduction of a small amount of AgNO_3 into Ag^0 , leading to a rapid non-equilibrium adsorption of AgNO_3 . In addition, deposition temperature, pressure and time are found to influence the metal loading and the morphology of the nanocomposites. Higher pressure and moderate temperature are suggested. As for the deposition time, the metal loading usually increases with the increase of the deposition time before the adsorption of the precursor reaches the equilibrium. But the morphology changes from small nanoparticles, nanowires to big nanoparticles along with the increase of the deposition time. Finally, it is also found that the adsorption isotherm data of AgNO_3 from $\text{scCO}_2/\text{co-solvent}$ on SBA-15 are well fitted by Langmuir model. The kinetics study using a mass balance differential equation shows that the adsorption reaches equilibrium after 10000 s (about 2.8 h) which is comparable to the experimental result (2.5 h).

ACKNOWLEDGMENTS

The work was financially supported by the National Natural Science Foundation of China (21376045, 21506027), Chinese Postdoctoral Science Foundation (2015M571307) and the Fundamental Research Funds for the Central Universities.

REFERENCES

- An, G.M., Zhang, Y., Liu, Z.M., Miao, Z.J., Han, B.X., Miao, S.D., Li, J.P. 2008. Preparation of porous chromium oxide nanotubes using carbon nanotubes as templates and their application as an ethanol sensor. *Nanotechnology*, **19**(3).

- Bekyarova, E., Kaneko, K. 2000. Structure and physical properties of tailor-made Ce,Zr-doped carbon aerogels. *Adv. Mater.*, **12**(21), 1625-1628.
- Blackburn, J.M., Long, D.P., Cabanas, A., Watkins, J.J. 2001. Deposition of conformal copper and nickel films from supercritical carbon dioxide. *Science*, **294**(5540), 141-145.
- Bozbag, S.E., Yasar, N.S., Zhang, L.C., Aindow, M., Erkey, C. 2011. Adsorption of Pt(cod)me(2) onto organic aerogels from supercritical solutions for the synthesis of supported platinum nanoparticles. *J. Supercrit. Fluids*, **56**(1), 105-113.
- Cabanas, A., Long, D.P., Watkins, J.J. 2004. Deposition of gold films and nanostructures from supercritical carbon dioxide. *Chem. Mater.*, **16**(10), 2028-2033.
- Chen, C.Y., Chang, J.K., Tsai, W.T., Hung, C.H. 2011. Uniform dispersion of Pd nanoparticles on carbon nanostructures using a supercritical fluid deposition technique and their catalytic performance towards hydrogen spillover. *J. Mater. Chem.*, **21**(47), 19063-19068.
- Do, Q.H., Zeng, C.C., Zhang, C., Wang, B., Zheng, J. 2011. Supercritical fluid deposition of vanadium oxide on multi-walled carbon nanotube buckypaper for supercapacitor electrode application. *Nanotechnology*, **22**(36).
- Erkey, C. 2009. Preparation of metallic supported nanoparticles and films using supercritical fluid deposition. *J. Supercrit. Fluids*, **47**(3), 517-522.
- Haruki, M., Li, S.K., Qian, G., Watkins, J.J. 2016. Reactive deposition of cobalt using bis(2,2,6,6-tetramethyl-3,5-heptanedionato) cobalt(II) from supercritical carbon dioxide. *Journal of Supercritical Fluids*, **107**, 189-195.
- Hong, B.H., Bae, S.C., Lee, C.W., Jeong, S., Kim, K.S. 2001. Ultrathin single-crystalline silver nanowire arrays formed in an ambient solution phase. *Science*, **294**(5541), 348-351.
- Hu, X.S., Bai, J., Hong, H.L., Li, C.P. 2016. Supercritical carbon dioxide anchored highly dispersed silver nanoparticles on 4A-zeolite and selective oxidation of styrene performance. *Crystengcomm*, **18**(14), 2469-2476.
- Huang, M.H., Choudrey, A., Yang, P.D. 2000. Ag nanowire formation within mesoporous silica. *Chem. Commun.*(12), 1063-1064.
- Karanikas, C.F., Watkins, J.J. 2010. Kinetics of the ruthenium thin film deposition from supercritical carbon dioxide by the hydrogen reduction of Ru(tmhd)(2)cod. *Microelectron. Eng.*, **87**(4), 566-572.
- Lei, Y., Mehmood, F., Lee, S., Greeley, J., Lee, B., Seifert, S., Winans, R.E., Elam, J.W., Meyer, R.J., Redfern, P.C., Teschner, D., Schlogl, R., Pellin, M.J., Curtiss, L.A., Vajda, S. 2010. Increased Silver Activity for Direct

- Propylene Epoxidation via Subnanometer Size Effects. *Science*, **328**(5975), 224-228.
- Liu, Z.M., Han, B.X. 2009. Synthesis of Carbon-Nanotube Composites Using Supercritical Fluids and Their Potential Applications. *Adv. Mater.*, **21**(7), 825-829.
- Meng, Y., Su, F.H., Chen, Y.Z. 2015. Synthesis of nano-Cu/graphene oxide composites by supercritical CO₂-assisted deposition as a novel material for reducing friction and wear. *Chemical Engineering Journal*, **281**, 11-19.
- Miller, J.M., Dunn, B., Tran, T.D., Pekala, R.W. 1997. Deposition of ruthenium nanoparticles on carbon aerogels for high energy density supercapacitor electrodes. *J. Electrochem. Soc.*, **144**(12), L309-L311.
- Morere, J., Tenorio, M.J., Torralvo, M.J., Pando, C., Renuncio, J.A.R., Cabanas, A. 2011. Deposition of Pd into mesoporous silica SBA-15 using supercritical carbon dioxide. *J. Supercrit. Fluids*, **56**(2), 213-222.
- Nowack, B. 2010. Nanosilver Revisited Downstream. *Science*, **330**(6007), 1054-1055.
- Pyayt, A.L., Wiley, B., Xia, Y.N., Chen, A., Dalton, L. 2008. Integration of photonic and silver nanowire plasmonic waveguides. *Nature Nanotech.*, **3**(11), 660-665.
- Ralph, K.I. 1979. *Chemistry of Silica: Solubility, Polymerization, Colloid and Surface Properties, and Biochemistry*. John Wiley & Sons Inc., New York
- Saquin, C.D., Cheng, T.T., Aindow, M., Erkey, C. 2004. Preparation of platinum/carbon aerogel nanocomposites using a supercritical deposition method. *J. Phys. Chem. B*, **108**(23), 7716-7722.
- Sun, Y.G., Xia, Y.N. 2002. Shape-controlled synthesis of gold and silver nanoparticles. *Science*, **298**(5601), 2176-2179.
- Sun, Z.Y., Liu, Z.M., Han, B.X., An, G.M. 2007. Supercritical carbon dioxide-assisted deposition of tin oxide on carbon nanotubes. *Mater. Lett.*, **61**(23-24), 4565-4568.
- Sun, Z.Y., Liu, Z.M., Han, B.X., Miao, S.D., Miao, Z.J., An, G.M. 2006. Decoration carbon nanotubes with Pd and Ru nanocrystals via an inorganic reaction route in supercritical carbon dioxide-methanol solution. *J. Colloid Interface Sci.*, **304**(2), 323-328.
- Watkins, J.J., McCarthy, T.J. 1995. Polymer/Metal Nanocomposite Synthesis in Supercritical CO₂. *Chem. Mater.*, **7**(11), 1991-1994.
- Xu, Q.-q., Wang, Y.-q., Wang, A.-q., Yin, J.-z. 2012a. Systematical study of depositing nanoparticles and nanowires in mesoporous silica using supercritical carbon dioxide and co-solvents: morphology control,

- thermodynamics and kinetics of adsorption. *Nanotechnology*, **23**(28), 285602.
- Xu, Q.-Q., Zhang, C.-J., Zhang, X.-Z., Yin, J.-Z., Liu, Y. 2012b. Controlled synthesis of Ag nanowires and nanoparticles in mesoporous silica using supercritical carbon dioxide and co-solvent. *The Journal of Supercritical Fluids*, **62**, 184-189.
- Xu, Q.Q., Ma, Y.L., Gang, X., Yin, J.Z., Wang, A.Q., Gao, J.J. 2014a. Comprehensive study of the role of ethylene glycol when preparing Ag@SBA-15 in supercritical CO₂. *Journal of Supercritical Fluids*, **92**, 100-106.
- Xu, Q.Q., Xu, G., Yin, J.Z., Wang, A.Q., Ma, Y.L., Gao, J.J. 2014b. Preparation of Superhighly Dispersed Co₃O₄@SBA-15 with Different Morphologies in Supercritical CO₂ with the Assistance of Dilute Acids. *Industrial and Engineering Chemistry Research*, **53**(25), 10366-10371.
- Yin, J.-Z., Xu, Q.-Q., Wang, A.-Q. 2010. Controlled Growth of Copper Nanoparticles and Nanorods in the Channels of Sba-15 by Supercritical Fluid Deposition. *Chemical Engineering Communications*, **197**(4), 627-632.
- Zhang, Y., Cangul, B., Garrabos, Y., Erkey, C. 2008. Thermodynamics and kinetics of adsorption of bis(2,2,6,6-tetramethyl-3,5-heptanedionato) (1,5-cyclooctadiene) ruthenium(II) on carbon aerogel from supercritical CO₂ solution. *J. Supercrit. Fluids*, **44**(1), 71-77.
- Zhang, Y., Kang, D.F., Saquing, C., Aindow, M., Erkey, C. 2005. Supported platinum nanoparticles by supercritical deposition. *Ind. Eng. Chem. Res.*, **44**(11), 4161-4164.
- Zhang, Y.M., Jiang, H.X., Li, G.M., Zhang, M.H. 2016. Controlled synthesis of highly dispersed and nano-sized Ru catalysts supported on carbonaceous materials via supercritical fluid deposition. *Rsc Advances*, **6**(20), 16851-16858.
- Zhao, J., Yu, H., Liu, Z.S., Ji, M., Zhang, L.Q., Sun, G.W. 2014. Supercritical Deposition Route of Preparing Pt/Graphene Composites and Their Catalytic Performance toward Methanol Electrooxidation. *Journal of Physical Chemistry C*, **118**(2), 1182-1190.
- Zheng, J., Dickson, R.M. 2002. Individual water-soluble dendrimer-encapsulated silver nanodot fluorescence. *J. Am. Chem. Soc.*, **124**(47), 13982-13983.

Complimentary Contributor Copy

Chapter 4

**FABRICATION OF POROUS SILICON
WITH SILVER NANOPARTICLES
BY ION IMPLANTATION**

***A. L. Stepanov^{1,2,*}, V. V. Vorobev², V. I. Nuzhdin¹,
V. F. Valeev¹ and Y. N. Osin²***

¹Nanooptics and Nanoplasmonics Department, Kazan Physical-Technical
Institute, Russian Academy of Sciences, Kazan, Russia

²Interdisciplinary Center for Analytical Microscopy,
Kazan Federal University, Kazan, Russia

ABSTRACT

Porous silicon (PSi) have attracted remarkable concerns and found tremendous importance widespread in both fundamental research and industrial applications. At modern time PSi is considering as a key material in many industrial sectors such as electronics, sensors and photonics. Additionally, the interest to PSi nanostructures containing noble metal nanoparticles was recently found. Silver nanoparticles are the subject of specific increasing features due to their strongest plasmon resonance in the visible spectrum. Such materials could be widely used for variety applications as solar cells, absorbents, lightings, catalysts, and for biological sensors. At the present report a novel technological approach based on low-energy ion implantation is suggested and realized to create

* Corresponding author Email: aanstep@gmail.com.

PSi layers with silver nanoparticles on the crystalline surface of Si wafers. It is demonstrated that using high-dose Ag-ion implantation of silicon with the energy of 30-60 keV the surface PSi structures with silver nanoparticles can be successfully fabricated. Also the fabricated plasmonic material - Ag:PSi is tested for Surface Enhanced Raman Scattering - SERS sensor application.

Keywords: silver nanoparticles, porous silicon, ion implantation

1. INTRODUCTION

Porous silicon (PSi) is a promising material used in micro-, nano-, and optoelectronics, which is also important for technological applications in sensorics, biosensorics, and solar cells [1]. PSi was first discovered in 1956 at Bell Labs [2] as a by-product of chemical etching of apertures in crystalline Si wafers. The discovery of PSi photoluminescence in the visible range at room temperature [3], which is explained by the quantum size effect for charge carriers, drastically raised interest for PSi over the world. Prior to this discovery, PSi was almost exclusively considered as insulating layer devices in the microelectronics industry. Therefore, finding new ways of PSi formation, as well as improving presently available technologies for synthesis of such structures, offers a very interesting challenge of today.

It is known a method which used to obtain PSi layers at the surface of monocrystalline silicon as a result of its implantation with ions of rare gases. The solubility of rare gases in solids is very low and does not exceed a level of 10^{16} ion/cm². The gettering of gas bubbles from the matrix gas ions in irradiated polymer material leads to the formation of nanopores (free volumes, nanovoids) [4]. In the case of silicon in order to stimulate the nucleation and growth of pores from implanted gas ions, the implanted silicon wafers are subjected to thermal annealing [5]. Such a technique for the formation of pores at the surface of silicon was demonstrated earlier for implantation with ions such as He⁺ [6], H⁺ [7], Ne⁺ [8], Ar⁺ [9] and Kr⁺ [8, 10].

Additionally, the interest to silicon nanostructures containing noble metal nanoparticles was recently found. It was initiated because of metal nanoparticles with localized surface plasmon modes demonstrate a specific option to enhance the recombination rate of the light silicon emitter to increase the efficiency of photoluminescence and internal quantum effectively, etc. [11, 12-14]. Silver nanoparticles (AgNPs) are the subject of specific increasing interests due to their

strongest plasmon resonance in the visible spectrum [15, 16]. For example, PSi samples coated with a layer of AgNPs after their electrochemical etching showed that a photoluminescence intensity becomes remarkably increased [17], the reflection of incident light with wavelength below 1100 nm could be reduced to use them for antireflection devices [18] or surface-enhanced Raman scattering of adsorbed on AgNP-PSi structures some organic molecules [13].

Instead of using simple silicon as the substrate for the AgNPs deposition on the top of a sample, the ion implantation technique can be used to form AgNPs in a volume of silicon as in the case of ion-irradiated silica glass or polymers [16]. Early, in experiments of the works [19, 20] Ag-ion implantation into crystalline silicon wafers and silicon nanocrystal layers at the energy of 30-35 keV and rather lower dose of $5.0 \cdot 10^{15}$ ion/cm² was performed. Then AgNPs in silicon matrix were synthesized after thermal annealing at 500°C of implanted samples. In another work [21] Ag⁺-ion implantation of silicon using a conventional metal vapor vacuum arc - MEVVA ion source, which produced a mixture of Agⁿ⁺ ions, was applied at higher dose of $2.0 \cdot 10^{17}$ ion/cm² to create AgNPs.

As it will be discussed here and as it was shown in the scientific literature [22], the metal-ion implantation technique was not used before 2013 in practice for fabrication of PSi [23]. In the articles [23-25], a first time it was demonstrated a successful experiment on synthesis of PSi with implanted Ag nanoparticles. A detailed description of technological approach and a new result data for AgNP-PSi are demonstrated and explained in this report.

2. EXPERIMENTAL

For an obtaining the structured composite Ag:PSi material, a wafer of single-crystal Si with *p*-type conductivity and crystallographic orientation (100) was used. Before implantation the substrates were cleaned in a wet chemical etching process. The Ag⁺-ion implantation was performed with the energy of 30 keV, ion dose of $1.5 \cdot 10^{17}$ ion/cm², and ion current density of 8 μA/cm² with an ILU-3 ion accelerator (Figure 1) [25] at residual vacuum of 10⁻⁵ Torr and room temperature of the irradiated samples.

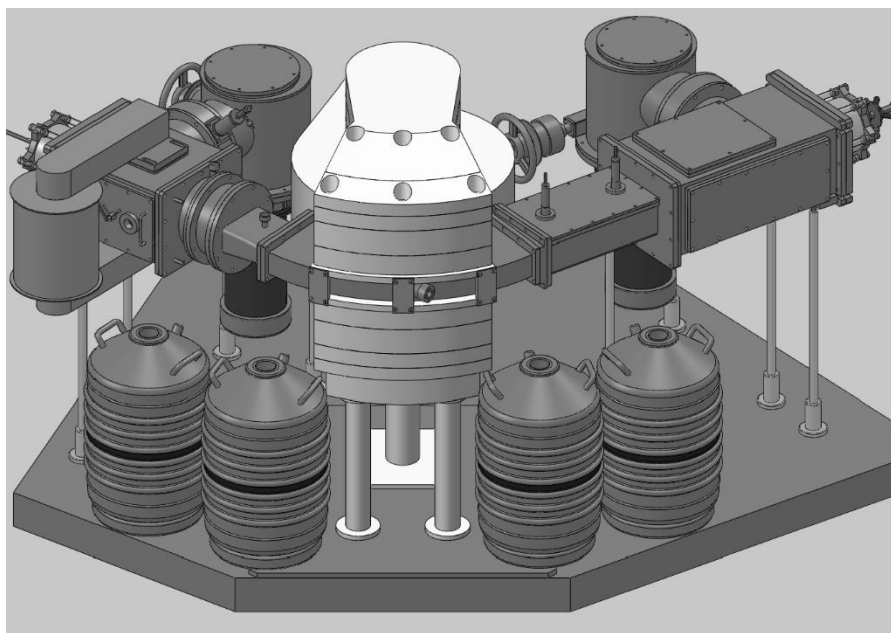


Figure 1. The ion accelerate ILU-3.

Depth distribution profiles of Ag atoms and the damage level in implanted silicon were modeled using the simulation-program the Stopping and Range of Ions in Matter (SRIM-2013) [26]. The morphology of the implanted structured silicon surfaces were characterized in plan-view by scanning electron microscopy (SEM) using high-resolution microscope Merlin Carl Zeiss combined with ASB (Angle Selective Backscattering) and SE InLens (Secondary Electrons in lens direction) detectors, which was also equipped for energy-dispersive X-ray spectroscopy (EDX) analysis with AZTEC X-MAX energy-dispersion spectrometer from Oxford Instruments. The crystallinity of the implanted silicon structure was estimated by the spectra of Raman scattering (RS) registered on a DFS-52 spectrometer at room temperature and excited by a continuous argon laser LGN-502 at a wavelength of 448 nm and radiation power of 50 mW. Surface morphology observation and the measurements of the profile and depth of pores (cross section) in PSi were carried out also by an Innova Bruker atomic-force microscope (AFM).

Raman spectra are measured using optical confocal DXR Raman Microscope (Thermo Scientific). Second harmonic of solid state Nd:YAG laser with the wavelength of 532 nm and the maximum power of 10 mW is used for an excitation. The 0.01 M solution in bidistilled water of Methyl Orange as

testing analyte (MO) is used to study Surface Enhanced Raman Scattering - SERS on the Ag:PSi substrate.

3. RESULTS AND DISCUSSIONS

Ion implantation is a widely applied technique used for the controlled matrix depth doping of various metals, dielectrics, and semiconductors by embedding into them energetically accelerated ions of various chemical elements [1]. According to the SRIM simulations, during ion bombardment an excess vacancy-rich region and accumulation of implanted ions can be formed close to the surface in irradiated matrix (Figure 2). A mean penetration range (R_p^{Ag}) of 30 keV accelerated Ag^+ -ions into silicon substrate is about 26 nm with a longitudinal straggling (ΔR_p^{Ag}) of 8 nm in the Gaussian depth distribution (Figure 2a). Thus, the predicted thickness of the modified silicon surface layer ($R_p + 2\Delta R_p$) is about 42 nm.

It was assumed [27] that during ion implantation porous structures in various semiconductors could be resulted from nucleation of small voids in the irradiated materials by vacancy generations. Therefore, the vacancy depth distribution for silicon implanted with Ag^+ ions was also simulated by the SRIM (Figure 2b), which showed similar profile to ion distribution for such low accelerating energies. Analyzing SRIM modeling, however it should be taking in account that obtained depth distribution of silver and vacancies are corresponded to implantation process of uniform silicon matrix before a nucleation and growth (for ion dose less than $1.0 \cdot 10^{16}$ ion/cm²) of PSi. As it will be shown further, a prolonged irradiation, simultaneously with the formation of PSi and a segregation of silver near the surface.

Figure 3a shows a plane-view SEM image of unimplanted silicon, which looks likes as very smooth without any surface structural inhomogeneity. The results of porosification of the silicon samples are observed by plan-view SEM images (Figure 4). This figure shows the SEM images of the silicon surface implanted with silver ions which demonstrated by different scales. In contrast to unimplanted silicon (Figure 3) the characteristic PSi surface structures show the black hole appearance in the implanted silicon region. The PSi layer formed by ion implantation seems to be homogeneous over a large area (tens of micrometers) of the sample (see Figure 4a), which is an importation characteristic (scalability) for a number of technological applications [1].

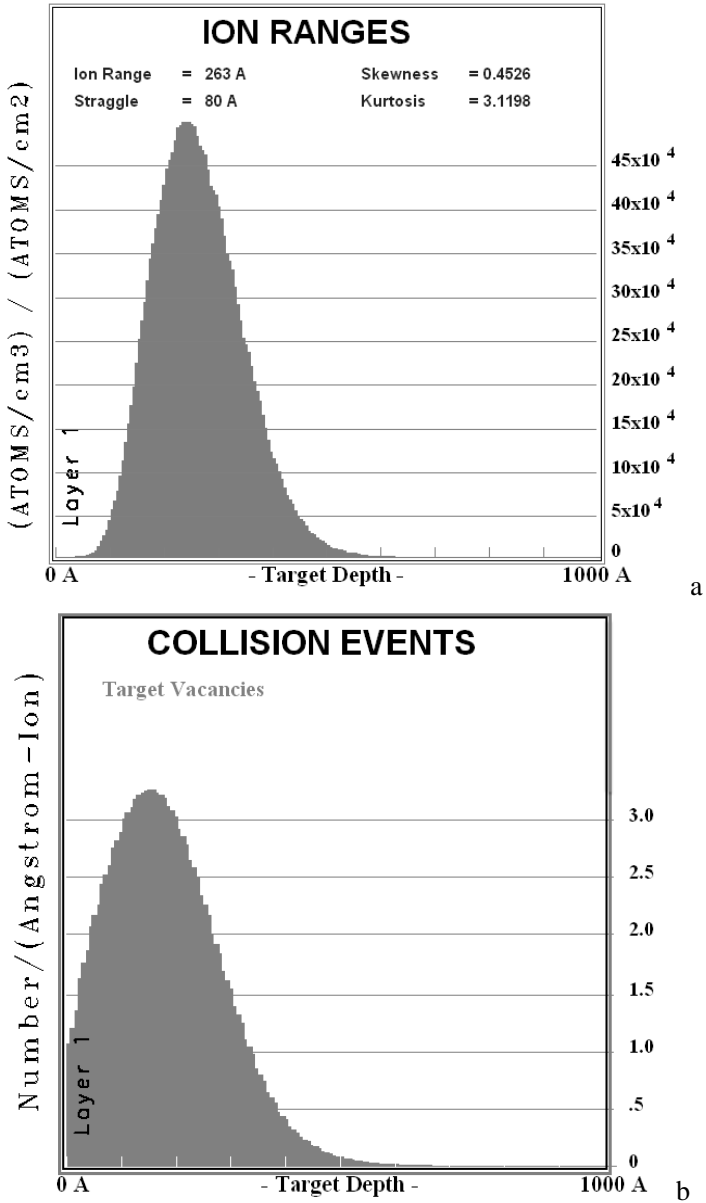


Figure 2. Depth ion distribution of Ag-ions implanted (a) and generated vacancy profiles (b) in silicon with energy of 30 keV calculated using the SRIM code.

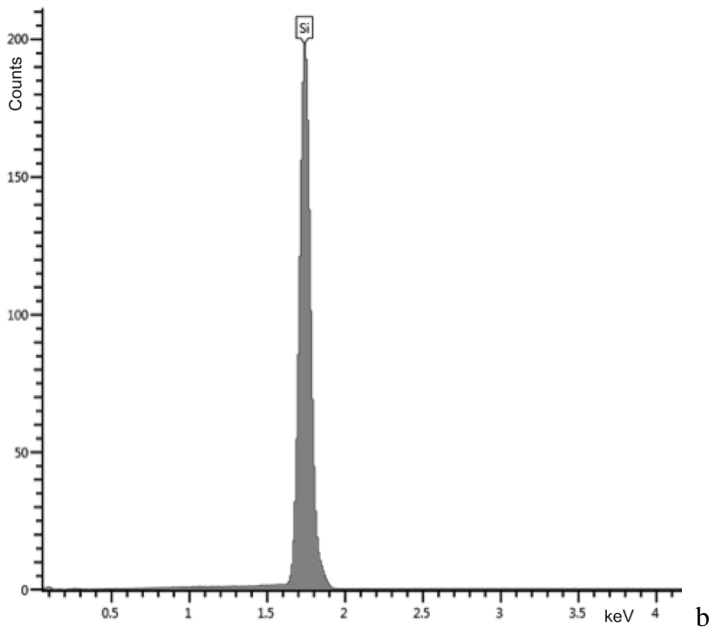
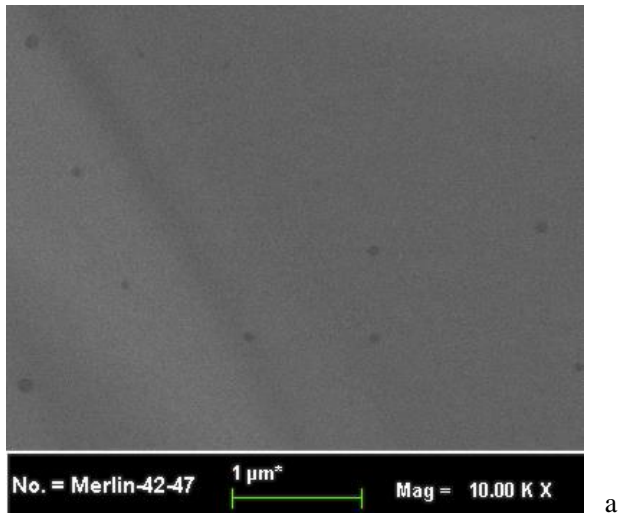


Figure 3. SEM image (a) and EDX characteristic spectrum (b) of unimplanted silicon.

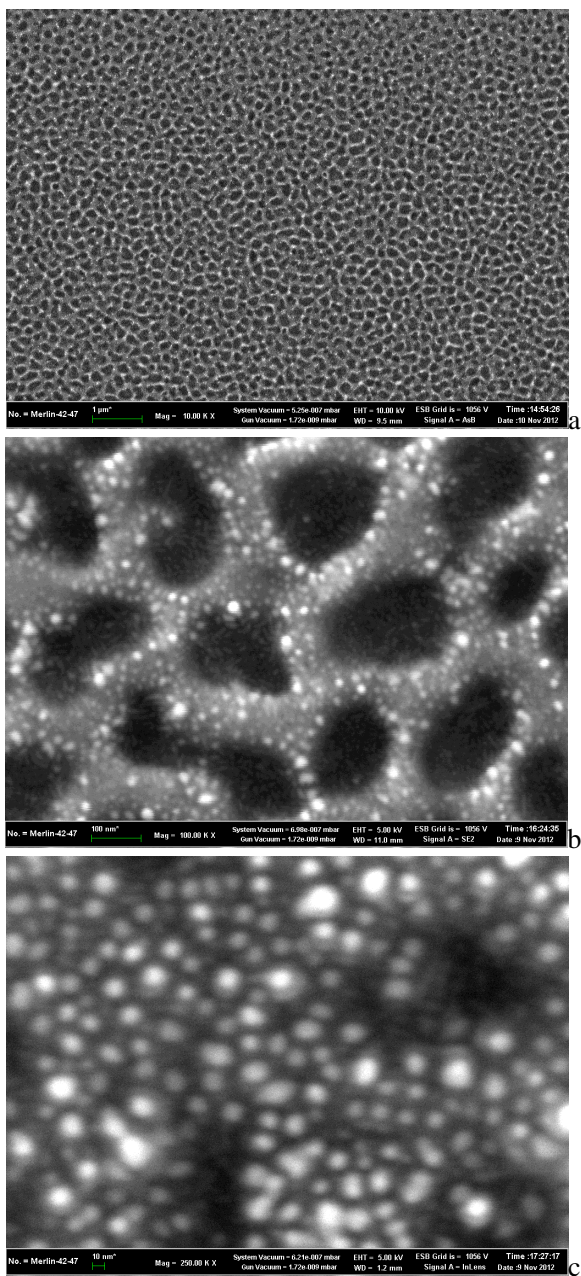


Figure 4. SEM images (in different scales) of the PSi surface layer with silver nanoparticles, which is obtained by Ag^+ -ion implantation of single-crystal Si.

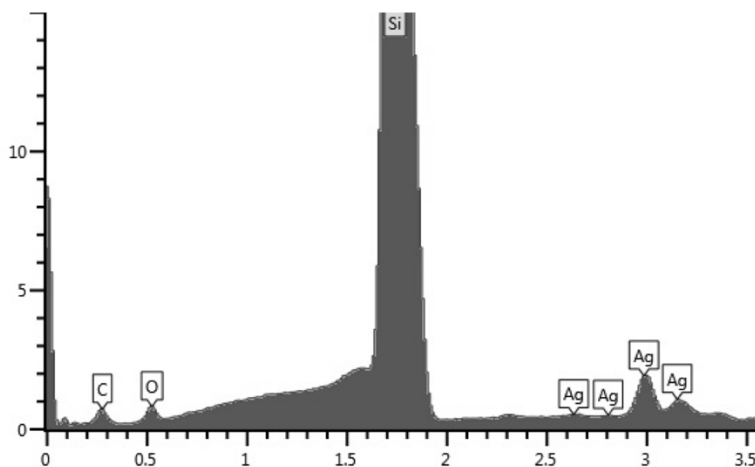


Figure 5. EDX characteristic spectrum of p-Si fabricated at ion dose of $1.5 \cdot 10^{17}$ ion/cm². Visible EDX peaks confirm the presence of Ag in the synthesized p-Si structures.

The magnified image of the surface fragment (Figure 4b) allows to estimate the average size of pores (black regions), which is ~150-180 nm, and the thickness of pore walls (gray regions), which is ~30-60 nm. The next magnified image (Figure 4c) shows the ion-synthesized nanoinclusions with the average size of ~5-10 nm in the structure of p-Si walls (light spots on the gray background of the p-Si matrix). Since heavier (in terms of mass) chemical elements, which are recorded by a detector of backscattered electrons, appear in the SEM images in a lighter tone, thus it possible to conclude that, for the analyzing composite material (which consists only of silicon atoms and implanted silver), the light (bright white) regions on the dark background (signal from silicon) are due to the metallic silver in the form of AgNPs. Note that silver atoms and silicon together do not form any chemical compounds like, for example, metal silicides (with cobalt, iron, etc.).

It is shown in Figure 3b and Figure 5 an EDX spectra recorded on the examined unimplanted silicon and p-Si structures with AgNPs fabricated at highest ion dose, respectively. Such EDX spectra measurements for implanted samples were done in the area on surface outside black holes of the silicon pores. In contrast to EDX data for unimplanted silicon, in the middle part of the presented spectra of p-Si it is clear seen four peaks located between 2.5 and 3.5 keV.

Those maxima are directly related to the Ag characteristic lines. It is observed that the intensity of Ag EDX peaks increases with increasing of ion implantation dose that means a growing of Ag concentrations in the silicon samples. Appearance of Ag peaks is in consistence with white spots in SEM images of the PSi (Figure 4), which are corresponding to AgNPs synthesized in PSi during ion implantation. As shown in the present study, using selected conditions for low-energy Ag-ion irradiation of silicon AgNPs can be fabricated without post-implantation thermal annealing as it was applied in the works [19, 20].

Measuring the optical Raman spectra of the irradiated and nonirradiated silicon (Figure 6) shows that the peak, which is recorded on the frequency of $\sim 520\text{ cm}^{-1}$ and is known to be related with the optical phonon scattering of the crystalline silicon matrix, completely disappears after ion implantation, thus characterizing the formed PSi layer as amorphous.

The additional information confirming the formation of PSi in the process of Ag^+ -ion implantation of Si is obtained from AFM measurements. Figure 7 shows the AFM images of the PSi surface fragment, which are obtained in the imaging and phase contrast modes; these images seem to be typical for PSi structures [1]. The cross-section profile of individual pores, which is measured in the direction marked in Figure 7a, is presented in Figure 7d. It allows to estimate the depth of pores to be $\sim 40\text{-}50\text{ nm}$. Thus, it could be concluded that, as a result of Ag^+ -ion implantation of Si, the typical pores are formed that are comparable with the relatively shallow pores in PSi formed by the electrochemical method in highly dilute solutions of hydrofluoric acid [1]. The AFM image taken at lateral illumination (see Figure 7b) clearly shows that the silver nanoparticles are formed by ion implantation in the PSi structure. It should be noted, however, that, due to the convolution effect, the sizes of the nanoparticles in the AFM images seem to be somewhat overstated as compared to their real sizes observed in SEM images (in Figure 4).

Noble nanoparticles are known to enhance, in particular, Raman signal from organic molecules [28]. Figure 8 compares the Raman spectra of MO solution and MO drop on the Ag:PSi substrate. The bands placed at 1118, 1150, 1200, 1316, 1366, 1392, 1421, 1446 and 1592 cm^{-1} correspond to the vibration frequencies of MO molecules [29]. The intensity of these bands is approximately two times higher for MO layer on the Ag:PSi surface. The band at 520 cm^{-1} corresponds to silicon wafer. It is demonstrate that the laser beam is focused directly at the interface of the SERS-substrate surface of Ag:PSi and drop of dye MO. Enhancement factor (EF) can be estimated as [30]:

$$EF = \frac{I_{SERS}}{I_{SRS}} \frac{C_{SRS}}{C_{SERS}}, \quad (1)$$

where I_{SERS} and I_{SRS} are Raman intensities for SERS on the Ag:PSi substrate and for spontaneous Raman scattering in solution respectively; C_{SERS} and C_{SRS} are corresponding molar concentrations of MO. The frequency and enhancement factor are shown in Table 1.

Thus, a main result of the work is experimental demonstration of a special SERS-substrate with silver nanoparticles, which created by a novel technological approach based on low-energy high-doses ion implantation. It was also observed that Intensity of SERS spectra for MO on Ag:PSi is higher in 2 time than for MO in solution. These results are demonstrate a perspective for using a new SERS-substrate on Ag:PSi as chemical and biological sensors.

Table 1. Frequencies and EFs of SERS bands of MO

ν, cm^{-1}	1118	1150	1200	1316	1366	1392	1421	1446	1592
EF	1.7	1.9	1.6	1.6	1.7	1.7	1.7	1.5	1.5

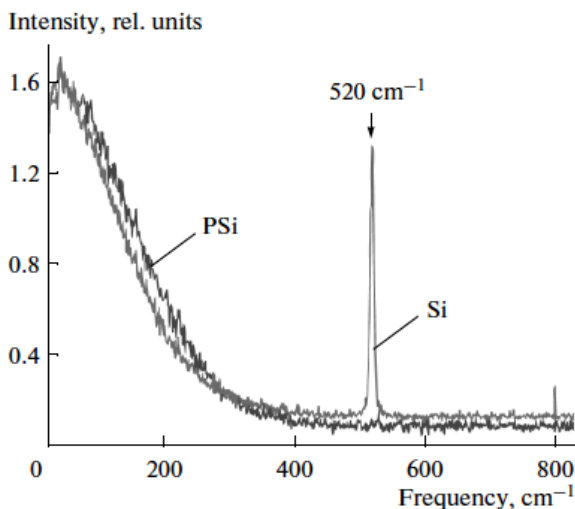


Figure 6. Raman spectra of the unimplanted single-crystal Si and the PSi layer formed by Ag^+ -ion implantation of Si.

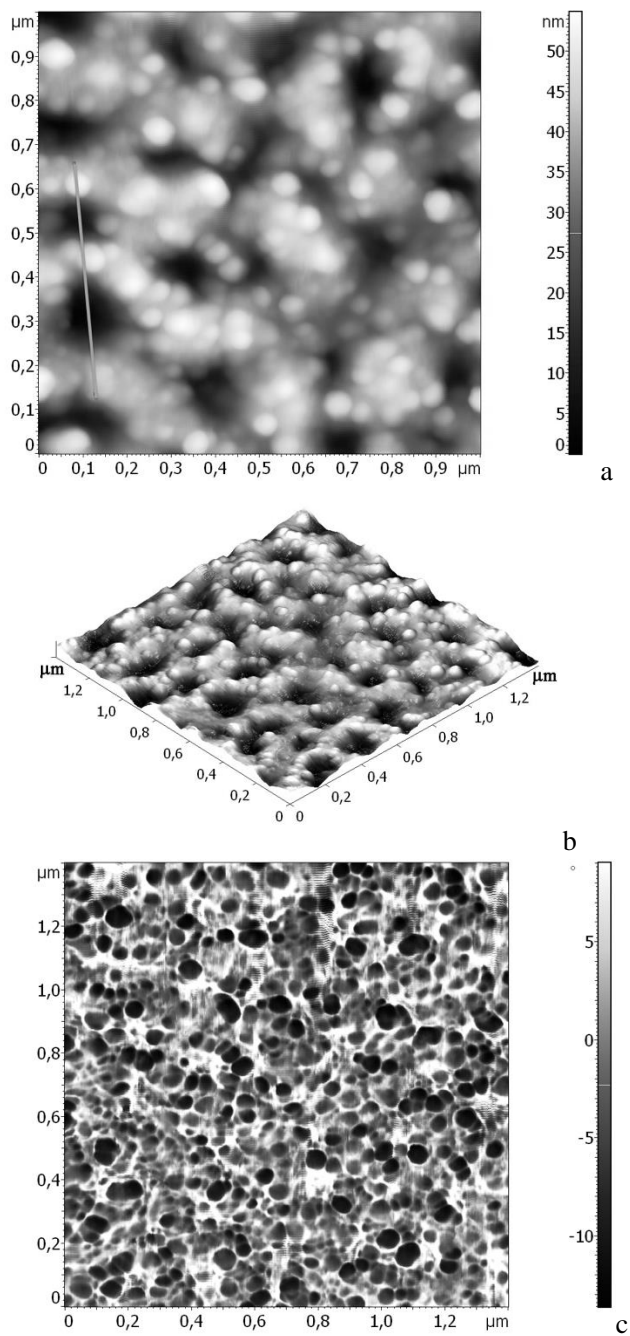


Figure 7. (Continued)

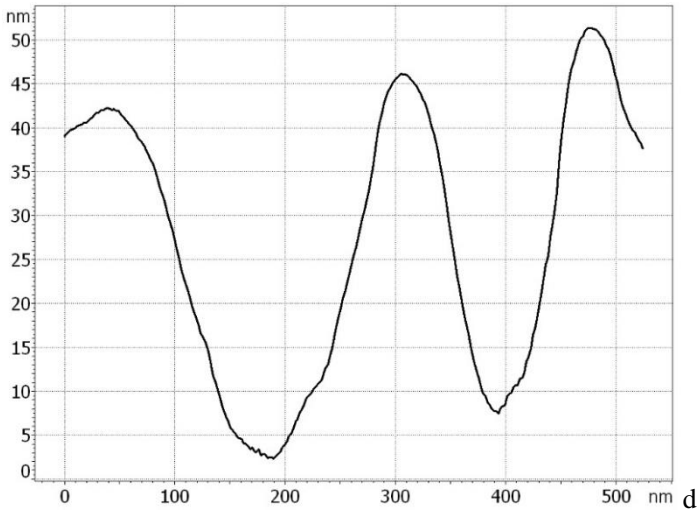


Figure 7. AFM images of the P*Si* surface prepared by low-energy high-dose implantation of single-crystal Si with Ag⁺ ions, which are taken (a, b) in the imaging mode and (c) in the phase contrast mode, and (d) the cross-section profile of individual pores, which is measured in the direction marked in (a).

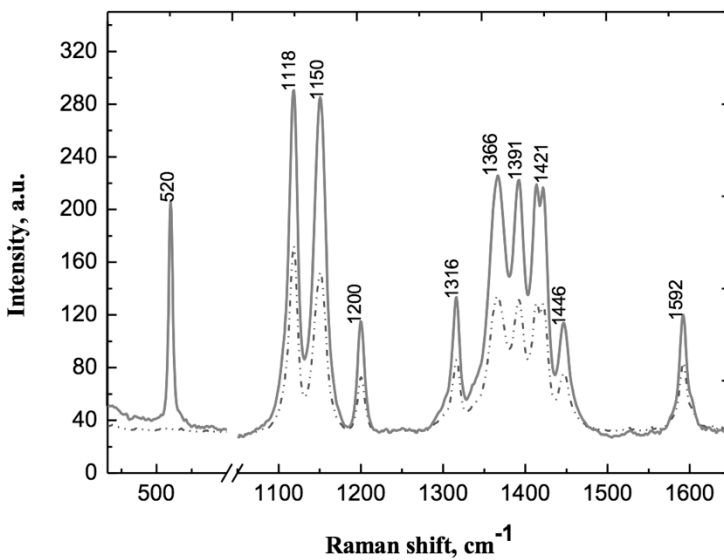


Figure 8. Raman spectra of MO solution (dashed) and MO drop on the Ag:P*Si* substrate (solid).

CONCLUSION

Thus, in this work a completely new technique used to obtain PSi layers with silver nanoparticles at the surface of monocrystalline silicon by a low-energy high-dose implantation was demonstrated. Ion implantation is one of the basic techniques used in industrial semiconductor microelectronics for the formation of various types of silicon nano- and microdevices. Therefore, the proposed new physical technique for the formation of PSi, in contrast to the well-known chemical approaches, rather easily integrated into an industrial modern process for improving the technologies of the fabrication of microcircuits.

As follows from the results presented in this work, in our experiments the PSi structures with silver nanoparticles were first obtained without a chemical technique in solution. Evidently, the further steps in improving such types of composite materials must contain an optimization of the processes of their fabrication and, in particular, searching for correlation features between structural parameters and the characteristics of optical, plasmon, photoluminescence, and sensor properties of new porous structures.

ACKNOWLEDGMENTS

Authors would like to thank N. N. Branbt from Lomonosov Moscow State University for help with SERS measurements and N. V. Kurbatova for her assistance in taking Raman spectrum measurements. This work was partly supported by the Russian Foundation for Basic Research No. 16-29-06137 and UMNIK.

REFERENCES

- [1] Torres-Costa V.; Martin-Palma R. J. *J. Mater. Sci.* 2010, 45, 2823-2838.
- [2] Uglir A. *Bell Syst. Tech. J.* 1956, 35, 333-347.
- [3] Canham L. T. *Appl. Phys. Lett.* 1990, 57, 1046.
- [4] Kavetsky T.; Tsmots V.; Kinomura A.; Kobayashi Y.; Suzuki R.; Mohamed H. F. M.; Sausa O.; Nuzhdin V.; Valeev V.; Stepanov A. L. *Phys. Chem. B* 2014, 118, 4194-4200.

-
- [5] Kozlovskii V. V.; Kozlov V. A.; Lomasov V. N. *Semiconductors* 2000, 34, 123-140.
- [6] Stein H. J.; Myers S. M.; Follstaedt D. M. *J. Appl. Phys.* 1993, 73, 2755-2664.
- [7] Cerofolini G. F.; Meda L.; Balboni R.; Corni F.; Frabboni S.; Ottaviani G.; Tonini R.; Anderle M.; Canteri R. *Phys. Rev. B* 1992, 46, 2061-2070.
- [8] Wittmer M.; Roth J.; Revesz P.; Mayer J. M. *J. Appl. Phys.* 1978, 49, 5207-5212.
- [9] Revesz P.; Wittmer M.; Roth J.; Mayer J. M. *J. Appl. Phys.* 1978, 49, 5199-5206.
- [10] Galyautdinov M. F.; Kurbatova N. V.; Buinova E. Y.; Shtyrkov E. I.; Bukharaev A. A. *Semiconductors* 1997, 31, 970-978.
- [11] Oskam G.; Long J. G.; Natarajan A.; Searson P. C. *J. Phys. D: Appl. Phys.* 1998, 31, 1927-1949.
- [12] Amran T. S. T.; Hashim M. R.; Al-Obaidi N. K.; Yazid H.; Adnan R. *Nanoscale Research Lett.* 2013, 8, 35-1-35-6.
- [13] Chan S.; Kwon S.; Koo T.-W.; Lee L. P.; Berlin A. A. *Adv. Mat.* 2003, 15, 1595-1598.
- [14] Wang M.; Wang X.; Ghoshal S. *Micro and Nano Lett.* 2013, 8, 465-469.
- [15] Kreibig, U.; Vollmer, M. *Optical properties of metal clusters*; Springer: Berlin, 1995; p. 463.
- [16] Stepanov A. L. *Ion-synthesis of silver nanoparticles and their optical properties*; Nova Sci. Publ., New York, 2010; p. 89.
- [17] Cao D. T., Ngan L. T. Q.; Anh C. T. *Surf. Interface Anal.* 45 (2013) 762-766.
- [18] Wang Y.; Liu Y. P.; Liang H. L.; Mei Z. X.; Du X. L. *Phys. Chem. Chem. Phys.* 2013, 15, 2345-2350.
- [19] Sing A. K.; Gryczynski K. G.; McDaniel F. D.; Park S. Y.; Kim M.; Neogi A. *Appl. Phys. Express* 2010, 3, 102201-1-102201-3.
- [20] Sing A. K.; Gryczynski K. G.; Neogi A. *Opt. Mater. Express* 2012, 2, 501-509.
- [21] Seo H. W.; Chen Q. Y.; Rusakova I. A.; Zhang Z. H.; Wijesundera D.; Yeh S. W.; Wang X. M.; Tu L. W.; Ho N. J.; Wu Y. G.; Zhang H. X.; Chu W. K. *Nucl. Instr. Meth. Phys. Res. B* 2012, 292, 50-54.
- [22] Romano L.; Impellizzeri G.; Tomasello M. V.; Giannazzo F.; Spinella C.; Grimaldi M. G. *J. Appl. Phys.* 2010, 107, 84310-1-84310-5.
- [23] Stepanov A. L.; Trifonov A. A.; Osin Y. N.; Valeev V. F.; Nuzhdin V. I. *Optoelecton. Adv. Mater. - Rapid Comm.* 2013, 7, 692-697.

- [24] Stepanov A. L.; Osin Y. N.; Trifonov A. A.; Valeev V. F.; Nuzhdin V. I. *Nanotechnologies in Russia* 2014, 9, 163-167.
- [25] Stepanov A. L.; Nuzhdin V. I., Valeev V. F.; Vorobev V. V.; Kabetsky T. S.; Osin Y. N. *Rev. Adv. Mater. Sci.* 2015, 40, 155-164.
- [26] Ziegler J. F.; Biersack J. P.; Littmark U. *The stopping and range of ions in solids*; Pergamon Press, New York, 1985; p. 416. <http://www.srim.org>.
- [27] Wang L. M.; Birtcher R. C. *Appl. Phys. Lett.* 1989, 55, 2494-2496.
- [28] Chursanova M. V.; Germash L. P.; Yukhymchuk V. O.; Dzhagan V. M.; Khodasevich I. A.; Cojoc D. *Appl. Surf. Sci.* 2010, 256, 3369-3373.
- [29] Zhang A.; Fang Y. *J. Coll. Interf. Sci.* 2007, 305b, 270-278.

Chapter 5

**ANTIFUNGAL ACTIVITIES OF SILVER
NANOPARTICLES OBTAINED BY PULSED
LASER ABLATION IN LIQUID**

***E. T. Aréchiga-Carvajal¹, J. M. Adame-Rodríguez¹,
E. L. Lee-Bazaldúa¹, B. Krishnan^{2,3} and S. Shaji^{2,3,*}***

¹Facultad de Ciencias Biológicas, Universidad Autónoma de Nuevo León, Departamento de Microbiología e Inmunología, Pedro de Alba s/n, Ciudad Universitaria, San Nicolás de los Garza, Nuevo León, México, 66455

²Facultad de Ingeniería Mecánica y Eléctrica, Universidad Autónoma de Nuevo León, Av. Pedro de Alba s/n, Ciudad Universitaria, San Nicolás de los Garza, Nuevo León, México, 66455

³CIIDIT- Universidad Autónoma de Nuevo León, Apodaca, Nuevo León, México

ABSTRACT

Nanostructures of noble metals are being investigated for their applications in areas of biology and biotechnology, biological labeling, photothermal, photonics, optoelectronics, catalysis, surface-enhanced Raman scattering (SERS) detection etc. Among the metal nanoparticles, silver nanoparticles are well known for their size dependent properties as well as antibacterial activities. Pulsed laser ablation in liquid (PLAL) is a

* Corresponding author e-mail: sshajis@yahoo.com, sadasivan.shaji@uanl.edu.mx.

physical synthesis technique to obtain ultra-pure nanoparticles of metals, semiconductors and ceramics which is a green synthesis compared to other chemical methods. In this chapter, we describe antifungal activities of silver nanoparticles produced by pulsed laser ablation of a high purity silver target in distilled water. The chapter includes details of the synthesis of silver nanocolloids using PLAL and their characterization using various techniques. Antifungal activities of these silver nanocolloids on fungi such as *Aspergillus niger* and *Penicillium spp* are explained. These filamentous fungi are responsible for the deterioration of storage life of fruits and vegetables worldwide. The effects of heterogeneous shaped silver nanoparticles produced by PLAL in these two fungal species probed in vitro are discussed. The nanoparticle concentrations from 31.8 to 74.2 mg/L were able to delay mycelium growth and sporulation in both species at the conditions probed. These results open up more biological applications of nanoparticles synthesized by PLAL.

Keywords: silver nanoparticles, pulsed laser ablation in liquid, structure and morphology, antifungal properties

INTRODUCTION

In Mexico's economy, agriculture plays an important role because it is oriented to exportation, hence a very competitive activity in the country. According to the Secretariat of Agriculture, Livestock, Rural Development, Fisheries and Food (SAGARPA for its acronym in Spanish) 350 varieties of agricultural products are exported annually; among them main fruits are avocados, watermelon and lemon, while others are mainly corn and other fruits and vegetables. From its production value, avocados register an annual average value of \$1,108,143,334.50 Mexican pesos, cataloging it as Mexico's best seller fruits, whereas wheat registers an average of \$225,085,609 Mexican pesos and tomato an annual value of \$1,782,499,326 Mexican pesos. As we know, their post-harvest refers to the time between crop maturity and its consumption, presents the agricultural cycle, harvesting, shipping from one place to another (from state to state or different countries), storage, display, buy and consumption.

In developing countries like Mexico, 40% of food loss is present after food process and harvesting (Gustavsson et al., 2011); for instance, the loss of roots and tubers in regions of Latin America happen in the post-harvest period, process and distribution, since these products are more likely to get damaged. In between the stage of process and post-harvest, about 50-55% of fruits and

vegetable are wasted due to wrong management and also the weather in these regions affects directly to the product's physical, chemical and biological (Gustavsson et al., 2011) properties.

Another official record reports 40 million tons of lessening is lost, calculated around 252 billion Mexican pesos. In the post-harvest period, between 5-8% of loss occur during harvest, 15-20% while pre-storage, 5-10% in the course of storage and 10-20% during shipping (Diario Oficial de la Federación). The main causes of loss during post-harvest are the wrong handling of product, senescence, quick maturing crop, chemical damage, inefficient cooling systems with temperature variations, bad selection of product before storage, inadequate packaging, decomposition due to microorganisms (Kiaya, 2014; Kitinoja and Kader, 2002) etc.

As mentioned, storage and shipping are stages from post-harvest with a high incident rate of waste, due to factors such as humidity, temperature and air, which play an important role for the product's stability and affects directly the product's life span. Damage caused from microorganisms to fruits and vegetables is of major interest since bacteria and fungi are opportunistic microorganisms and are present ubiquitously. Fungi are versatile microorganisms that are capable of growing in any kind of place and/or condition; for example, it is registered that fungi that affect fruits and vegetables during post-harvest have an optimum temperature rate from 20 to 25°C even when they can endure temperature rates up to 38°C, in other situations, can grow in temperatures like 15°C even though other type of fungi such as *Penicillium expansum*, *Botrytis cinerea*, *Alternaria alternata* and *Cladosporium herbarum* can grow and cause damage in temperatures as low as -1 and 1°C. Humidity is an important factor for fungal growth, which can be found in the post-harvest processes (Agrious, 2005; FHIA, 2007).

Alternaria, *Botrytis*, *Fusarium*, *Geotrichum*, *Sclerotinia*, *Penicillium* and *Aspergillus* are fungal genus associated to post-harvest diseases. It has been reported that *Aspergillus* affects mainly grains, legumes, wheat, hay and cotton, while the genus *Penicillium* is linked to 90% of fruits decomposition such as apples, tomatoes, pears, quince, grapes, onions, fig, sweet potato, among others, during shipping, storage and display (Agrious, 2005). Some of the alternatives that have been implemented to prevent fungi infections are: having a good management of the product during harvesting, chemical treatments, phytosanitary measures and appropriate constant temperature for a satisfactory product preservation. Although some of these measures have been carried out during the storage and shipping stage are still considered (M. K. Rai, Deshmukh, Ingle and Gade, 2012). With the increasing use of antifungal, disinfectants, etc.

microorganisms are becoming more resistant, reason why new alternatives for the solution of these problems have been sought out and are fundamental to decrease the economic loss due to contamination from micro-organisms during post-harvest.

At this context, nanomaterials are of special interest because of their size, shape and surface chemistry as well as their size dependent properties like high reactivity, catalytic activities, optical properties etc. The smaller size and other unique properties of nanoparticles (NPs) lead to their use in biological systems and medicine. Enhanced surface activities of the nanoparticles provide conjugation and interaction of nanoparticles with different biomolecules. Applications of nanomaterials in biology and medicine are mainly in biomolecular recognition, sensing, drug delivery, biocatalyst, imaging, MRI, biomolecule purification and biocompatible surface coatings. Nanoparticles of silver and gold can function as useful antimicrobial agents. Other nanomaterials having antimicrobial activities reported are TiO₂, ZnO, Pt, Copper and Copper oxide, carbon nanotubes (CNT), MgO, Iron Oxide, SiO₂, CdSe, chitosan etc. Through nanotechnology's progress and development of new synthesis techniques, nanoparticles boomed in different areas such as technology, science and market. It has been proved that metal nanoparticles have size dependent physicochemical characteristics such as catalytic, optical and electronic activity (Kordestani, Nayebhabib, Saadatjo and Kordestani, 2015). Throughout history it has been observed that silver is an antimicrobial agent widely used as well that it was discovered that silver nanoparticles have a powerful antifungal properties (Rivera and Ramos, 2014).

The synthesis method of silver nanoparticles is the main factor that affects their shape and size. There exist different synthesis techniques that vary from physical, chemical and biological methods (Hasan, 2015). In 2009, Panáček and collaborators made an antifungal study in different species from the genus *Candida*. The nanoparticles were synthesized by the chemical method Tollen with an average diameter of 25 nm; the antifungal tests were made in microplates with a range of nanoparticle concentration of 0.05mg/L to 54mg/L. For the *C. albicans II* it was observed a minimum inhibitor concentration of 21mg/L, for *C. albicans I* 0.42 mg/L, *C. tropicalis* of 0.84 mg/L and *C. parapsilosis* 1.69 mg/L; as a result, the *C. parapsilosis* was the less sensitive, showing a loss of 100% of the species in a concentration of 27 mg/L silver nanoparticles (Panáček et al., 2009). In 2015 Lara and collaborators observed an inhibitor effect in the biofilm produced by the *C. albicans* with the use of silver nanoparticles (Lara et al., 2015).

For biological synthesis of silver nanoparticles, the synthesis catalyzed by *Fusarium oxysporum*, resulted particle size range of 5-60 nm (Selvi and Sivakumar 2012). Another fungus capable to produce silver nanoparticles is *Aspergillus foetidus*, obtaining heterogeneous shapes in a size range of 20-40 nm. Nanoparticles produced by *Aspergillus foetidus* had shown an inhibitory effect in *Aspergillus niger*, *Aspergillus flavus*, *Aspergillus foetidus*, *Aspergillus oryzae*, *Aspergillus parasiticus* and *Fusarium oxysporum* (Roy et al., 2013). Gajbhiye and co-workers (Gajbhiye et al., 2009) found that *Alternaria alternata* have the capacity to produce silver nanoparticles using 1 mM de AgNO_3 in the growth medium, obtaining spherical nanoparticles with heterogeneous size between 20 and 60 nm (an average of 32.5 nm). The antifungal activity of these nanoparticles was proved against *Phoma glomerata*, *Phoma herbarum*, *Fusarium semitectum*, *Trichoderma sp.*, and *Candida albicans*, resulting in a significant decrease in the growth inhibition when fluconazol and silver nanoparticles were combined.

Among the physical methods for synthesis, an interesting one is pulsed laser ablation in liquid, which consists of an explosive evaporation of solid materials (target) immersed in a liquid. The laser output is focused onto the target using a lens and as a result of ablation a plasma plume is produced. For a nanosecond pulsed laser, the main mechanism for production of nanoparticles is heating and evaporation of the target. The laser ablation plasma will be quenched by the surrounding liquid medium and as a result the release of nanoparticles are into the liquid resulting in a nanocolloid (Tsuji, 2012). The production efficiency of nanoparticles through this technique is related to the laser wavelength, the incident energy on the target, pulse duration (femto-, pico-, or nano), laser energy fluence, ablation time, liquid medium and the presence or absence of surfactants. The main advantage of this type of synthesis is the absence of toxic precursors or surfactants compared to chemical methods as well as it is faster than the biological methods (Iravani et al., 2014). This technique's main disadvantage is that the limitations in controlling the shape and size of the silver nanoparticles that are non-homogenous and the size distribution vary from 10 nm to 120 nm (Simakin et al., 2004; Dolgaev et al., 2002).

Mafune and co-workers (Mafune et al., 2000) studied silver nanoparticle synthesis by the PLAL method where the liquid media was water with different concentrations of SDS (sodium dodecyl sulfate). They attributed the size of the nanoparticle with the concentration of SDS, the laser power and the number of laser shots. Simakin and his group (Simakin et al., 2004) under their synthesis conditions observed more optical density of silver nanoparticles using acetone

in comparison with water and ethanol. The average nanoparticles size reported was of 60 nm but the actual sizes of the nanoparticles varied from 20 a 120 nm.

Taking into consideration the importance of improved storage and utile life time for the agricultural products (mainly fruits and vegetables) in Mexico, investigations on synthesis and use of nanomaterials, especially on antibacterial and antifungal properties of nanomaterials are extremely significant. In this chapter, we describe studies on the growth inhibitory effect of PLAL synthesized silver (Ag) nanoparticles against fungi from commercial interest as *Penicillium* and *Aspergillus*. *Penicillium spp.* and *Asperguillus niger* are members of the Ascomycota fungal group. *Asperguillus niger* has an asexual reproduction trough asexual spores called conidia just as *Penicillium spp.*, but this last one has also a sexual reproductive phase. Their spore inactivation has been always a challenge due to their strong cell wall prepared to deal with extreme conditions as desecration or sudden temperature changes (Pinto et al. 2013).

METHODS AND RESULTS

Silver nanoparticles were produced by PLAL technique in distilled water using 532 nm output wavelength. Pulsed laser ablation experiment was performed using a q-switched Nd: YAG pulsed laser (Solar Laser System LQ629-100) of 10 ns, 100 Hz and output energy of 90 mJ/pulse for 532 nm of wavelength. The target used for ablation was Ag metal plate (99.99% pure). The metal target was placed at the bottom of a glass beaker (50 ml of volume) containing 30 ml of distilled water. The 532 nm output was focused with a convex lens to the target at its focal distance (150 mm). After 10 minutes ablation, yellow colored solution of silver nanoparticles (Figure 1) was obtained. Immediately after the experiment, a TEM grid was prepared by placing a drop of the colloidal solution on a copper grid and dried it at ambient temperature. Morphology and size of the silver NPs were analyzed using Transmission Electron Microscopy (TEM, Model FEI Titan G2 80-300). UV-Visible absorption measurements were carried out in a UV-Vis-NIR spectrophotometer (Shimadzu UV-1800). Silver nanoparticles used in our study has a non-uniform shapes, but the majority are spherical in shape and the size between 20 to 60 nm (TEM micrographs in Figure 1). The UV-Visible absorption spectrum resulted with an absorption peak at 400 nm which is the characteristic surface plasmon resonance absorption of Ag nanoparticles. Yellow color of the nanocolloid as well as characteristic plasmon resonance

absorption at 400 nm were the first confirmations for the presence of Ag NPs in solution after ablation experiment.

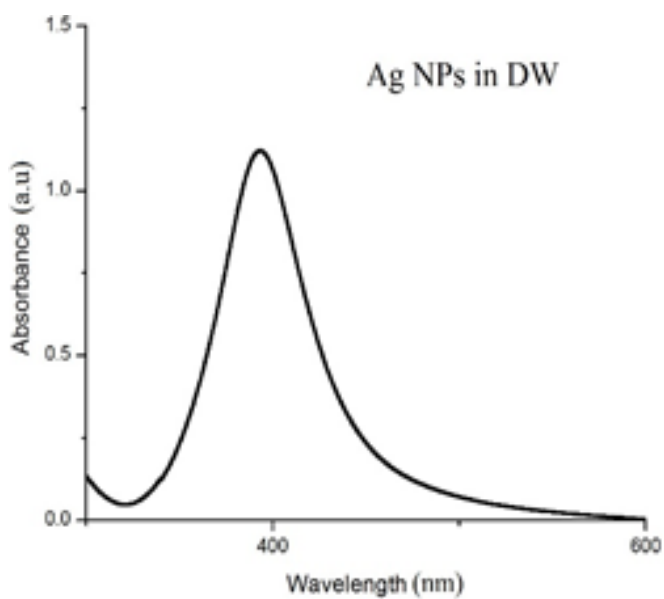
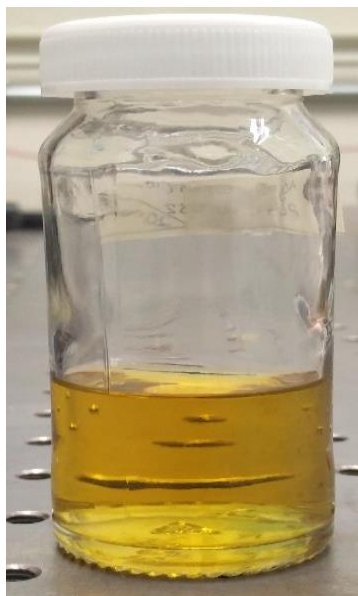


Figure 1. (Continued)

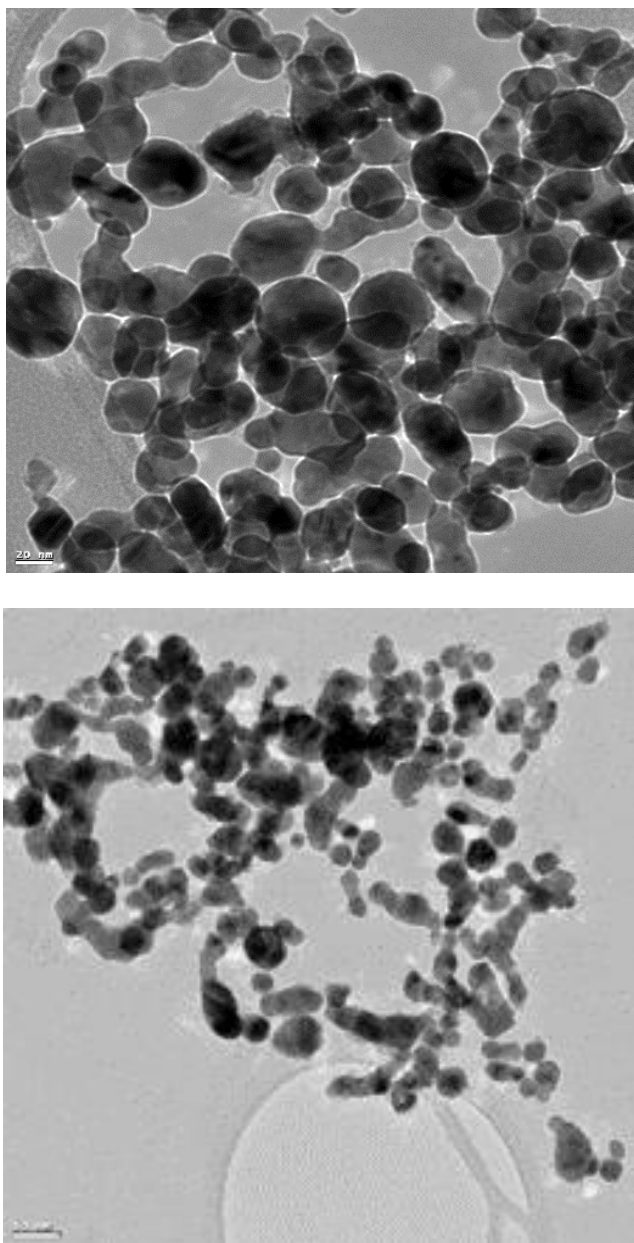


Figure 1. Photo of the silver nanocolloids prepared by pulsed laser ablation of silver target in distilled water, UV-Visible absorption spectrum and Transmission electron micrographs of silver nanoparticles. Ag nanoparticles are not of uniform shape/size pattern and their size vary between 20 nm to 60 nm.

In our research, the *poison plate* technique was employed (Thenmozhi, Kannabiran, Kumar and Gopiesh Khanna, 2013), which was modified using different concentrations of silver nanoparticles (31.8 µg/ml, 42.4 µg/ml, 63.6 µg/ml, 74.2 µg/ml) synthesized by PLAL method. Sterilized PDA (potato dextrose agar) was mixed homogeneously with different nanoparticle concentrations in petri dishes. The mix was inoculated with 100µl of *Penicillium spp.* (3250 spores) and *Asperguillus niger* (2250 spores) after their solidification.

The values obtained were assigned by a qualitative scale, where the low values show less growth compared with positive control and higher values present more growth than that one presented in positive control (Table 1). A sporulation time had a delay in *Penicillium spp.* until 14th day in silver nanoparticles concentrations of 31.8 µg/ml and 63.6 µg/ml with no sporulation signals (Table 2). It is also observed that there is no 100% growth inhibition.

Table 1. Growth inhibition values followed from 9 days of fungal growth in PDA medium amended with different nanoparticle concentrations

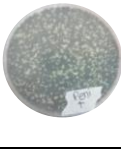
	Sporulation inhibition					
	(+) control	31.8 µg/ml	42.4 µg/ml	63.6 µg/ml	74.2 µg/ml	(-) control
<i>Penicillium spp.</i>	23	13	27	13	22	0
<i>Asperguillus niger</i>	22	19	19	19	18	0

A sporulation delay was observed for *Asperguillus niger* until day 5 at a nanoparticle concentration of 74.2 µg/ml, micelial growth was present at all concentrations.

Some of the main factors associated with antimicrobial/antifungal properties of nanoparticles are their surface charge, metal composition, incubation time or exposure, dose and nanoparticles oxidation capacity (Thenmozhi et al., 2013). It was reported that antifungal activity on silver nanoparticles in phytopathogen fungi as *B. sorokiniana* and *M. grisea* affecting its colonial formation (Jo et al., in 2009). Both species showed differences in their sensibility to nanoparticle concentrations, that could be explained by their spore size of 60 µm for *B. sorokiniana*, bigger than the one presented by *M. grisea* (17 to 28 µm), *M. grisea* showed incremented susceptibility. It was also observed differences between species, for *B. sorokiniana* the inhibition effect presented between 500 ppm and 125 ppm and for *M. grisea* between 200 ppm

and 25 ppm. Differences among maximal concentrations is fungal specie related. In our study it is observed that for *Penicillium spp.* lower silver nanoparticle concentrations were needed (31.8 mg/L y 63.6 mg/L) and for *Aspergillus niger*, higher concentration (74.2 mg/L). *Aspergillus* spore size was reported of 1.8 a 3.5 μm diameter (Buttner and Stetzenbach 1993) while *Penicillium spp.* is of 3.5 to 5.0 μm (Petrikou et al., 2001). Also there are some reports of very near spore diameters between both species; 2.5 a 5.0 μm (*Aspergillus niger*) and 2 to 4 μm (*Penicillium spp.*) (Kanaani et al., 2007).

Table 2. Sporulation inhibitory effect of silver nanoparticles in *Penicillium spp.*

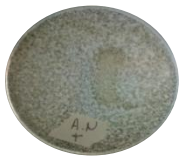


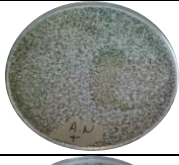

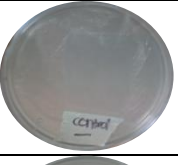
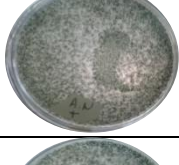
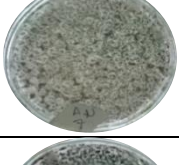




<i>Penicillium spp.</i>				
Growth time (days)	(+) control	31.8 $\mu\text{g/ml}$	63.6 $\mu\text{g/ml}$	(-) control
10				
11				
14				

Thenmozhi et al. synthesized silver nanoparticles by interaction with the actinobacteria *Streptomyces sp.* VITSTK7, they presented a spherical shape with diameters from 20 to 60 nm with 35.2 nm average size. In this work nanoparticles were used after oxidation at 50 $\mu\text{g/ml}$ in PDA solid media inoculated with *A. niger* (MTCC 281), *A. fumigatus* (MTCC 343) and *A. flavus* (MTCC 277) mycelia, and grew for 7 days. 62-75% was observed probing a fungistatic effect (Thenmozhi et al., 2013). In this study, using the antimicrobial assay reported by Thenmozhi et al, obtained a fungistatic effect. On *A. niger*,

with a delay on 5th day at a concentration of 74.2 mg/L, to *Penicillium spp.* we observed the presence of sporulation until the 14th day at a concentration of 31.8 mg/L and 63.6 mg/L.

In comparison with the results obtained by Kim and his research group (Kim et al., 2012) where they used different growth medium, PDA, MEA (malt extract agar) y CMA (corn meal agar) mixed with different types of silver nanoparticles (10, 25, 50 and 100 ppm). Then, the mix was incubated for 48 hours at room temperature. Before this processes, the plates were inoculated at the same time and incubated at 28 °C for 14 days. As a result, they observed an inhibition effect depending the nanoparticle concentrations, type of nanoparticle and agar type. They did not notice any correlation between the concentration of silver nanoparticles and the growth inhibition.

Table 3. Sporulation inhibitory effect of silver nanoparticles in *Aspergillus niger*

<i>Aspergillus niger</i>			
Growth time (days)	(+) control	74.2 µg/ml	(-) control
4			
5			
6			
8			

Comparing with another antimicrobial technique, in which the silver nanoparticles and spores interact themselves in a liquid media and then were inoculated on a PDA petri dish, they observed a decrement in the colonies of *B. sorokiniana* and *M. grisea* in relation to the silver nanoparticles concentration increment (Jo *et al.*, 2009). These studies remark the importance of a good diffusion media to have more superficial contact between the silver nanoparticles and the spores, showing that the liquid media have a major relation between the concentration of silver nanoparticles and the growth of the microorganism (Le Ouay and Stellacci, 2015).

Other studies (Mahdizadeh, Safaie and Khelghatibana, 2015) discussed that some fungi could develop some kind of resistance after being treated with silver nanoparticles, because in *M. phaseolina* an initial growth inhibition was observed after the first 3 days of growth at nanoparticle concentrations between 6 and 8 ppm. But after 5 days, fungal growth initiated again. For higher concentrations (up to 10 ppm) growth was inhibited until 10th day. This behavior changed depending on the specie; for example, in *S. sclerotiorum* growth was inhibited the first 10 days of exposure at NP concentrations from 8 to 16 ppm except for 6ppm, *T. harzianum* couldn't grow the first and second (in the case of 10ppm) day of incubation at 10, 12, 14 and 16 ppm. But after that the growth was restored.

This behavior was observed in both fungi, on *Asperguillus niger* before the 5th day in a concentration of 74.2 $\mu\text{g/ml}$ started to show sporulation effect and *Penicillium spp.* until the 14th day did not show sporulation effect to the 31.8 $\mu\text{g/ml}$ and at the concentration of 63.6 $\mu\text{g/ml}$ started to show a sporulation. That can be due to some type of adaptation to the presence of the silver nanoparticles in the growth media. This activity is directly related with size and shape of such nanoparticle. The size gives the nanoparticle the contact surface with the microorganism; if the nanoparticle size is small the contact surface is bigger (Kordestani *et al.*, 2015). The nanoparticle's shape plays an important role in the antifungal effect while in a truncated triangular shape it was only needed 1 μg to observe the antimicrobial effect, for the bar shape it was needed between 50-100 μg and the spherical shape a total of 12.5 μg proving that it does exist a significant relation between the shape and microbial effect of nanoparticles (Pal, Tak and Song, 2015; M. Rai, Yadav and Gade, 2009).

CONCLUSION

The antimicrobial effect of silver nanoparticles is mainly by their size because when smaller the size of the nanoparticle, more contact area they have. Other important characteristic is the material from which the nanoparticle was made and silver is an important material because it is well recognized like a strong antimicrobial agent. However, there exist a lot of factors that impact the effects of nanoparticles like efficient antimicrobial agent that vary from synthesis technique, dose, exhibition time, type of microorganism, charge of the metal, inoculation method and incubation, size, shape of the nanoparticle among others. The synthesis method is one of the most important factors that affect the characteristics of the nanoparticles. The PLAL method got a number of variable parameters that give different types of nanoparticles in biocompatible solutions through a green process.

ACKNOWLEDGMENTS

The authors are thankful to CONACYT – México (Project 214282) for the research funding.

REFERENCES

- Agrious, G. N. (2005). *Plant Pathology* (Fifth). Elsevier Academic Press. [http://doi.org/10.1002/1521-3773\(20010316\)40:6<9823::AID-ANIE9823>3.3.CO;2-C](http://doi.org/10.1002/1521-3773(20010316)40:6<9823::AID-ANIE9823>3.3.CO;2-C).
- Fundación Hondureña de investigación Agrícola. Deterioro de las frutas y hortalizas frescas en el periodo de poscosecha (2007).
- Gustavsson, J., Cederberg, C., van Otterdijk, R., Meybeck, A., (2011), Global food losses and food waste – Extent, causes and prevention, Roma, FAO.
- Hasan, S. (2015). A Review on Nanoparticles: Their Synthesis and Types. *Research Journal of Recent Sciences*, 4(February), 1–4.
- Jo, Y.-K., Kim, B. H. and Jung, G. (2009). Antifungal Activity of Silver Ions and Nanoparticles on Phytopathogenic Fungi. Retrieved from <http://apsjournals.apsnet.org/doi/abs/10.1094/PDIS-93-10-1037>.
- Kiaya, V. (2014). Post-Harvest losses and Strategies to Reduce Them. *ACF International*, (January), 1–25.

- Kim, S. W., Jung, J. H., Lamsal, K., Kim, Y. S., Min, J. S. and Lee, Y. S. (2012). Antifungal effects of silver nanoparticles (AgNPs) against various plant pathogenic fungi. *Mycobiology*, *40*(1), 53–58. <http://doi.org/10.5941/MYCO.2012.40.1.053>.
- Kitinoja, L. and Kader, A. A. (2002). Técnicas de Manejo Poscosecha a Pequeña Escala : Manual para los Productos Hortofrutícolas. *Series de Horticultura Postcosecha*, (8).
- Kordestani, S., Nayebhabib, F., Saadatjo, M. H. and Kordestani, S. S. (2015). A novel wound rinsing solution based on nano colloidal silver. *Nanomed J*, *1*(5), 315–323. Retrieved from <http://nmj.mums.ac.ir>.
- Lara, H. H., Romero-Urbina, D. G., Pierce, C., Lopez-Ribot, J. L., Arellano-Jiménez, M. J. and Jose-Yacaman, M. (2015). Effect of silver nanoparticles on *Candida albicans* biofilms: an ultrastructural study. *Journal of Nanobiotechnology*, *13*, 91. <http://doi.org/10.1186/s12951-015-0147-8>.
- Le Ouay, B. and Stellacci, F. (2015). Antibacterial activity of silver nanoparticles: A surface science insight. *Nano Today*, *10*(3), 339–354. <http://doi.org/10.1016/j.nantod.2015.04.002>.
- Mafune, F., Kohno, J., Takeda, Y., Kondow, T. and Sawabe, H. (2000). Formation and size control of silver nanoparticles by laser ablation in aqueous solution. *Journal of Physical Chemistry B*, *104*(39), 9111–9117. <http://doi.org/10.1021/jp001336y>.
- Mahdizadeh, V., Safaie, N. and Khelghatibana, F. (2015). Evaluation of antifungal activity of silver nanoparticles against some phytopathogenic fungi and *Trichoderma harzianum*. *Journal of Crop Protection*, *4*(April), 291–300.
- Pal, S., Tak, Y. K. and Song, J. M. (2015). Does the antibacterial activity of silver nanoparticles depend on the shape of the nanoparticle? A study of the gram-negative bacterium *Escherichia coli*. *Journal of Biological Chemistry*, *290*(42), 1712–1720. <http://doi.org/10.1128/AEM.02218-06>.
- Panáček, A., Kolar, M., Vecerova, R., Pucek, R., Soukupová, J., Krystof, V., ... Kvítek, L. (2009). Antifungal activity of silver nanoparticles against *Candida* spp. *Biomaterials*, *30*(31), 6333–6340. <http://doi.org/10.1016/j.biomaterials.2009.07.065>.
- Pinto, R. J. B., Almeida, A., Fernandes, S. C. M., Freire, C. S. R., Silvestre, A. J. D., Neto, C. P. and Trindade, T. (2013). Antifungal activity of transparent nanocomposite thin films of pullulan and silver against *Aspergillus niger*. *Colloids and Surfaces B: Biointerfaces*, *103*, 143–148. <http://doi.org/10.1016/j.colsurfb.2012.09.045>.

- Rai, M. K., Deshmukh, S. D., Ingle, A. P. and Gade, A. K. (2012). Silver nanoparticles: The powerful nanoweapon against multidrug-resistant bacteria. *Journal of Applied Microbiology*, 112(5), 841–852. <http://doi.org/10.1111/j.1365-2672.2012.05253.x>.
- Rai, M., Yadav, A. and Gade, A. (2009). Silver nanoparticles as a new generation of antimicrobials. *Biotechnology Advances*, 27(1), 76–83. <http://doi.org/10.1016/j.biotechadv.2008.09.002>.
- Rivera, L. E. C. and Ramos, A. P. (2014). Actividad antimicótica de nanopartículas, 7(12).
- Simakin A. V., Voronov V. V., Kirichenko N. A., and S. G. A. (2004). Nanoparticles Produced by Laser Ablation of Solids in Liquid Environment,. *Applied Physics A*, 791(127), 546–551.
- Thenmozhi, M., Kannabiran, K., Kumar, R. and Gopiesh Khanna, V. (2013). Antifungal activity of Streptomyces sp. VITSTK7 and its synthesized Ag₂O/Ag nanoparticles against medically important Aspergillus pathogens. *Journal de Mycologie Medicale*, 23(2), 97–103. <http://doi.org/10.1016/j.mycmed.2013.04.005>.
- Tsuji T. (2012) Preparation of Nanoparticles Using Laser Ablation in Liquids: Fundamental Aspects and Efficient Utilization, Guowei Yang, (1), Laser Ablation in Liquids: Principles and Applications in the Preparation of Nanomaterials, (pp 207-257), Singapore, Pan Stanford Publishing Pte. Ltd.

Complimentary Contributor Copy

Chapter 6

**SILVER NANOPARTICLES:
ADVANCES IN RESEARCH
AND APPLICATIONS IS APPROACHING**

I. Alghoraibi and R. Zein*

Department of Physics, Damascus University, Syria

ABSTRACT

The field of nanotechnology has gained momentum over the past two decades with a broad range of potential applications, such as increasing bioavailability of a drug, biological labeling, cancer treatment, biosensing, antibacterial activity, antiviral activity, detection of genetic disorders and gene therapy. Advances in this field are mainly dependent on the ability to form nanoparticles of various materials, sizes, and shapes, and to efficiently assemble these particles into complex architectures. Nanoparticles are particles with a maximum size of 100 nm. These particles have unique properties, which are quite different than those of larger particles. The most prominent nanoparticles for medical uses are noble metal nanoparticles such as nanosilver which are well recognized for their remarkable physical, chemical, optical, electronic, magnetic, catalytic and anti-microbial properties of silver nanomaterial allows for their utilization in various scientific applications such as sensors, nanophotonics devices biology, drug delivery, cancer treatment, photothermal therapy, diabetic healing, solar cells, catalysis, cooling system, surface-enhanced

* Corresponding Author address Email: Ibrahim.Alghoraibi@gmail.com.

Raman spectroscopy, inkjet-printer, imaging sensing, biology and medicine, optoelectronics and magnetic devices. There are many methods for the synthesis of silver nanoparticles such as chemical reduction, electrochemical reduction, photochemical reduction, microemulsion, chemical vapor deposition, microwave assisted, hydrothermal method, spray pyrolysis, laser ablation, radiolysis and sonochemical method, etc.

From a practical point of view, the method of chemical reduction from aqueous silver nitrate solution is most preferable for obtaining silver nanoparticles which involve the reduction of relevant metal salts in the presence or absence of surfactants, which is necessary in controlling the growth of metal colloids through agglomeration.

The synthesized nanoparticles were characterized using Atomic Force Microscopy (AFM), UV-visible spectrophotometer; X-ray diffraction (XRD) and Fourier transform infrared spectrometry (FTIR).

Keywords: silver nanoparticles (Ag-NPs), properties of Ag-NPs, nanosilver toxicity, applications of Ag-NPs, synthesis of Ag-NPs, atomic force microscopy (AFM), X-ray diffraction (XRD)

1. INTRODUCTION

This chapter gives an introduction of silver nanoparticles and some of their unique properties. Some possible applications of silver nanoparticles will be described, and finally focuses on the experimental procedure which provides a general concerns on synthesizing silver nanoparticles by wet chemistry and a discussion of the experimental results will be included.

1.1. Why Silver Nanoparticles?

One of the first and most natural questions to ask when starting to deal with silver nanoparticles is: “why are silver nanoparticles so interesting?.” The answer lies in the nature and unique properties possessed by nanosilver. Silver nanoparticles (Ag-NPs) have attracted increasing interest due to their unique physical, chemical and biological properties compared to their macro-scaled counterparts. Ag-NPs have distinctive physico-chemical properties, including a high electrical and thermal conductivity, surface-enhanced Raman scattering, chemical stability, catalytic activity and nonlinear optical behavior. When silver exists in its nanometer size scale (nanosilver), its antimicrobial properties are

amplified because of the much larger surface-to-volume ratio and small their size. The one of the most potent uses of nanosilver as antimicrobial agent that is toxic to bacteria, fungi, and viruses. Due to their large surface area and their size which typically results in greater biological activity, chemical reactivity and catalytic behavior compared to larger particles of the same chemical composition. The size of silver nanoparticles is compared to that of other “small” particles showed in Figure 1, where the bacterium is huge in comparison [1].

Nanosilver is not a new discovery; it has been known for over 100 years. Previously, nanosilver or suspensions of nanosilver were referred to as colloidal silver. Before the invention of penicillin in 1928, colloidal silver had been used to treat many infections and illnesses. By converting bulk silver into nanosized silver, its effectiveness for controlling bacteria and viruses was increased, primarily because of the nanomaterials have extremely large surface to volume ratio compared to bulk silver, thus resulting in increased the area of contact with bacteria and fungi. In 1951, Turkevich et al. reported a wet chemistry technique to synthesize nanosilver using silver nitrate as a silver ion source and sodium citrate as the reducing agent for the first time [2]. Recent advances in nonmaterials science in the last two decades have enabled scientists to control silver nonmaterials size and shape which in turn control the chemical, physical and optical properties of nanosilver. The unique properties of silver nanoparticles have been exploited in a wide range of potential applications in medicine, cosmetics, renewable energies, environmental remediation and biomedical devices. According to the novel properties of Ag-NPs over 250 products containing nanosilver are now available for public use, this has made nanosilver the largest and fastest growing class of Ag-NPs in consumerproducts applications.

1.2. Properties of Nanosilver

Two primary factors cause nanomaterials to behave significantly differently than bulk materials: surface effects and quantum effects. These factors affect the chemical reactivity of materials as well as their physical, optical, mechanical, electric, and magnetic properties.

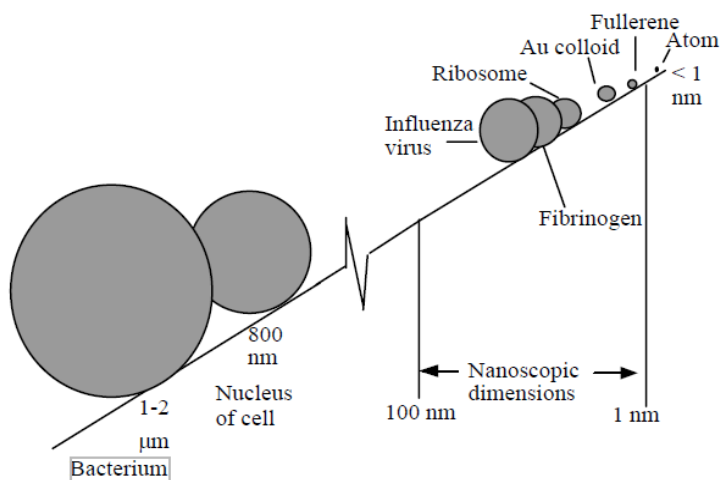


Figure 1. Size comparison of small particles.

1.3. Optical Properties

There is growing interest in utilizing the optical properties of silver nanoparticles as the functional component in various products and sensors. Silver nanoparticles are extraordinarily efficient at absorbing and scattering light and, unlike many dyes and pigments, have a color that depends upon the size and the shape of the particle see Figure 2.

The interaction of light incident on the NP surface with the conduction electrons of the metal lead to surface plasmon resonance (SPR) band. If the particle size is much smaller than the incident light wavelength, the electron motion leads to the appearance of a dipole that oscillates with the frequency of the exciting electric field as showed in Figure 3. If the frequency of incident light oscillations coincides with the intrinsic frequency of conduction electrons near the particle surface, then the resonance light absorption and scattering are observed, which is referred to as SPR.

This oscillation results in unusually strong scattering and absorption properties. The strong scattering cross section allows for sub 100 nm nanoparticles to be easily visualized with a conventional microscope. When 60 nm silver nanoparticles are illuminated with white light they appear as bright blue point source scatterers under a dark field microscope (Figure 3, inset). The bright blue color is due to an SPR that is peaked at a 450 nm wavelength. A unique property of spherical silver nanoparticles is that this SPR peak

wavelength can be tuned from 400 nm (violet light) to 530 nm (green light) by changing the particle size and the local refractive index near the particle surface. Even larger shifts of the SPR peak wavelength out into the infrared region of the electromagnetic spectrum can be achieved by producing silver nanoparticles with rod or plate shapes [3]. Of all metals, silver has the greatest SPR band intensity; for gold and copper, the intensity is much weaker. Silver exhibits the highest extinction ratio in the SPR band peak among not only metals, but also the other known materials that absorb in the same spectral range (i.e., in this spectral range, silver NP transmit light to the lesser extent as compared with any other particles of the same size).



Figure 2. Nanoparticles of various shape and size in solution – the plasmon resonance determines the color.

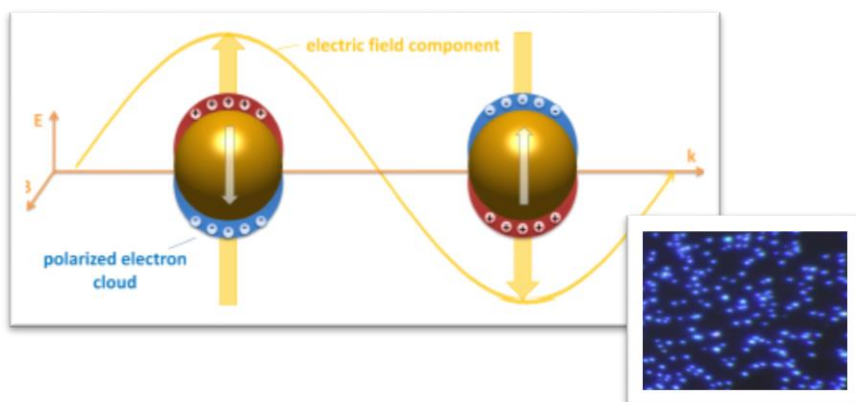


Figure 3. Surface plasmon resonance where the free electrons in metal nanoparticles are driven into oscillation due to a strong coupling with specific wave length of the incident light, (inset) Dark field microscopy image for 60 nm silver nanoparticles.

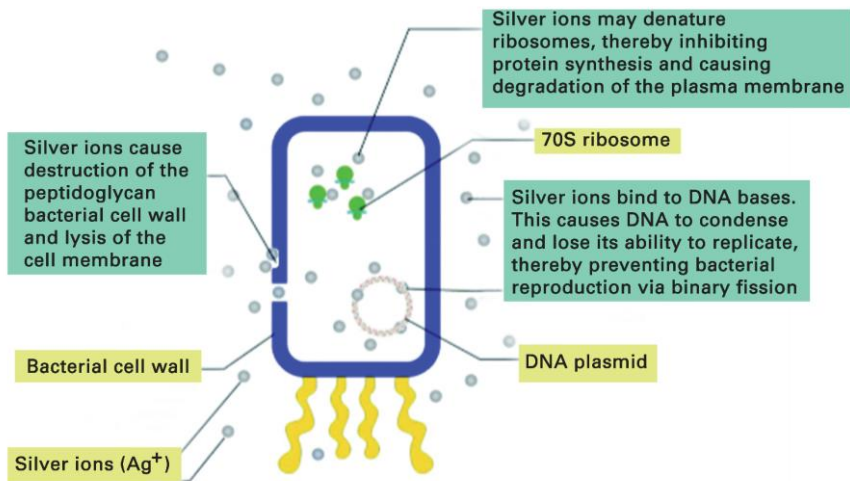


Figure 4. Diagram showing mechanism of action of silver ions [5].

1.4. Antibacterial Properties

Antibacterial properties of silver nanoparticles are attributed to their large surface to volume ratio which provides more efficient for enhanced antibacterial activity. Nanosilver is an effective killing agent against a broad spectrum of Gram-negative bacteria such as *Acinetobacter*, *Escherichia*, *Pseudomonas*, *Salmonella*, and *Vibrio*. *Acinetobacter* and Gram-positive bacteria like *Bacillus*, *Clostridium*, *Enterococcus*, *Listeria*, *Staphylococcus*, and *Streptococcus* [4]. There are however various theories are put forwarded on the possible mechanism for the antimicrobial action of nanosilver (see Figure 4) [5]. Nanosilver interacts with sulphur containing proteins on microbial cell membrane causing disruption [6]. The surface of microbes having phosphorus containing compound like DNA, nanosilver inhibit their functions [7].

Nanosilver release Ag^+ ion inside the microbial cell which may create free radicals and induce oxidative stress, thus further enhancing their bactericidal activity [8]. Based on studies that show that silver nanoparticles anchor to and penetrate the cell wall of Gram-negative bacteria, it is reasonable to suggest that the resultant structural change in the cell membrane could cause an increase in cell permeability, leading to an uncontrolled transport through the cytoplasmic membrane, and ultimately cell death. Bases on the presence of silver nanoparticles inside the cells it is likely that further damage could be caused by interactions with compounds such as DNA. This interaction may prevent cell

division and DNA replication from occurring, and also ultimately lead to cell death [9].

1.5. Antifungal Properties

Silver nanomaterials have been shown to have antifungal properties against a broad spectrum of common fungi [10, 11] including genera such as *Aspergillus*, *Saccharomyces*, and the most important findings were related to toxic effects toward *Candida albicans* species [12, 13]. It was shown that colloidal silver nanoparticles in very low concentrations may have substantial antifungal impact in vitro. The exact mechanisms of action of silver nanoparticles against fungi are still not clear, but mechanisms similar to that of the antibacterial actions have been proposed for fungi.

1.6. Antiviral Properties

Silver nanoparticles (diameter 5-20 nm, average diameter ~10 nm) inhibit HIV-1 virus replication [14]. Gold nanoparticles (average diameter ~10 nm) showed relatively low anti HIV-1 activity (6-20%) when compared to silver nanoparticles (98%). Size-dependent antiviral activity of silver nanoparticles has been shown with HIV-1 virus [15]. Interaction of silver nanoparticles with HIV-1 was exclusively within the range of 1-10 nm.

1.7. Anti-Inflammatory Properties

Nanosilver dressings as well as nanosilver-derived solutions proved to have anti-inflammatory activity [16]. In animal models, nanosilver alters the expression of matrix metallo-proteinases (proteolytic enzymes that are important in various inflammatory and repair processes), suppresses the expression of tumor necrosis factor (TNF)-interleukin (IL)-12, and IL-1, and induces apoptosis of inflammatory cells. Silver nanoparticles (diameter 14 ± 9.8 nm) modulate cytokines involved in wound healing. The results indicate the possibility of achieving scar-less wound healing even though further studies using other animal models are required to confirm this. It is evident that nanosilver due to its biological and physiochemical properties is potent as

antimicrobials and therapeutic agents. They can be used for many challenges in the field of nanomedicine.

2. APPLICATIONS

The remarkable physical, chemical and optical properties of silver nanomaterials allows for their utilization in various applications. These properties significantly depend on the size, shape and surface chemistry of the nanomaterials.

2.1. Medical Applications

Nanosilver has many medical applications including diagnosis, treatment, drug delivery. Nanosilver is used for coating medical tools and materials used in the areas of surgery, anesthesiology, cardiology and urology. It is also incorporated in wound dressings [17, 18] diabetic socks, scaffolds, sterilization materials in hospitals, medical textiles and medical catheters. Nanosilver is used in dentistry for making artificial teeth and in eye care for coating contact lenses. Silver has possible applications in the treatment of cancer. HIV-1 virus was reported to be inhibited from binding to the host cells through the use of silver nanoparticles [14].

2.2. Used for Surface Enhanced Raman Scattering

Raman scattering by molecules could be enhanced if the analyte molecules are adsorbed on rough metal surfaces, silver thin films and NPs. The enhancement factor increases in Raman scattering ($10^5 - 10^{10}$) by aggregates of silver NP prepared by different methods, which allows for enough sensitivity to detect single molecules. SERS using nanosilver can be used for biological imaging, trace analysis of pesticides, anthrax, prostate-specific antigen glucose, and nuclear waste, identification of bacteria, genetic diagnostics and detection of nitro-explosives [19, 20].

2.3. Used for Metal Enhanced Fluorescence Applications

The intrinsic spectral properties of fluorophores can be altered by metallic nanostructures. The proximity of metallic nanosilver results in an increase in the intensity of low quantum yield fluorophores. The effects include fluorophore quenching at short distances, spatial variation of the incident light field, and change in the radioactive decay rate. These characteristics enable nanosilver to be used in applications such as immunoassays and DNA/RNA detection [21, 22].

2.4. Catalysis

The high surface area to volume ratio of silver nanomaterials provides high surface energy, which promotes surface reactivity such as adsorption and catalysis. This has resulted in the use of silver nanomaterials and silver nanocomposites to catalyze many reactions in industrial processes such as CO oxidation, benzene oxidation to phenol and the reduction of the p-nitrophenol to p-aminophenol.

2.5. Electronics

The high electrical and thermal conductivity of nanosilver along with the enhanced optical properties result in various applications in electronics. Nanosilver is used in electronic equipment, Silver nanowires [23] are used as Nano connectors and Nano electrodes for designing and fabricating Nano-electronic devices Other applications include data storage devices, nonlinear optics, making micro-interconnects in integrated circuits (IC) and integral capacitors inks for printed circuit board and optoelectronics [24].

2.6. Applications in Consumer Products

Besides, Ag-NPs exhibit broad spectrum bactericidal and fungicidal activity [8] that has made them extremely popular in a diverse range of consumer products, including sprays, socks, pillows, slippers, face masks, wet wipes, detergent, soap, shampoo, toothpaste, plastic [25], air filters, coatings of refrigerators, vacuum cleaners, washing machines [26], food storage containers,

cellular phones...etc, increasing their market value. To date, nanosilver technologies have appeared in a variety of manufacturing processes and end products. Nanosilver can be used in a liquid form, such as a colloid (coating and spray) or contained within a shampoo (liquid) and can also appear embedded in a solid such as a polymer master batch or be suspended in a bar of soap (solid). Nanosilver can also be utilized either in the textile industry by incorporating it into the fiber (spun) or employed in filtration membranes of water purification systems. In many of these applications, the technological idea is to store silver ions and incorporate a time-release mechanism. This usually involves some form of moisture layer that the silver ions are transported through to create a long-term protective barrier against bacterial/fungal pathogens [27, 28].

3. NANOSILVER TOXICITY

The rapid expansion of nanotechnology and its commercial products is threatening to outpace the research on the potential of adverse ecological and health effects should these materials or their degradation products be released into the environment. Increasingly widespread use of nanosilver in consumer products will lead to an amplified risk of exposure to both nanosilver and ionic silver (Ag^+) in the aquatic environments receiving wastewater effluent. There is evidence that fabrics with embedded nanosilver such as socks have a potential to release silver ions and silver nanoparticles into wastewater when they are washed [29, 30]. The biological mechanism of the nanosilver toxicity is not completely clear. It is still an ongoing discussion whether toxicity is caused by particles as such, or by silver ion release from silver nanoparticles, or both [31]. It has been suggested that nanosilver particles, as well as the released silver ions from their surface destroy sulfur and phosphorus containing compounds such as DNA and proteins. This has vast ramifications on the membrane stability of the cell as well as on the functions of proteins leading to cell death. The Ag^+ ion release of the nanosilver particle surface plays a major role on their toxicity.

Therefore, the mechanism of toxicity of nanosilver is not agreed upon in the literature, but three possibilities are commonly discussed or implied. (i) Toxicity may be caused directly by Ag^+ associated with the particles. Ag^+ may be left over from the synthesis of the particles, released from the particles, or displayed on the surface of the particles. (ii) Nanosilver possesses a unique mechanism of toxicity related to properties that emerge at the nano-scale. (iii) Nanosilver acts to increase the exposure to Ag^+ above that indicated by the dissolved concentration of Ag^+ in the bulk solution. This could be due to interactions

between nanosilver and biomolecules or membranes that result in an exposure to a higher concentration of Ag^+ than that in the surrounding media. While this represents a pathway of silver toxicity that may be unique to nanosilver, it is not a novel mechanism of action.

Actually, there is a debate in the literature on identifying the toxicity induced by nanosilver or the released Ag^+ ions from its surface. Some of them claim that the effect of the nanosilver particles themselves is negligible, and thus the toxicity stems mostly from the released Ag^+ ions. Others find that the ions do not really participate in the toxic effect, while some claim that both particles and ions induce toxicity. More specifically, Navarro et al. attributed the toxicity of nanosilver to the free Ag^+ ions and not the particles [32]. In contrast, Fabrega et al. showed that the released Ag^+ ions did not participate in the toxicity that was observed against aquatic bacteria and attributed that the particles themselves played the major role [33]. A number of publications showed that the both Ag^+ ions and particles contribute to this toxic effect [34, 35]. These different results make it difficult to establish a good understanding of the toxicity mechanism of nanosilver particles and their released Ag^+ ions. Recently, by systematically varying the nanosilver size, it has been shown that Ag^+ ions dominate the toxicity of nanosilver less than about 10nm in diameter [36] (Figure 5).

Some authors have argued convincingly that there is not enough evidence to suggest separate mechanisms of toxicity for nanosilver and Ag^+ , and that the toxic action of nanoparticles is more likely to be due to their delivery of Ag^+ . Lok et al. found that the toxicity of nanosilver increased with the addition of Ag^+ to its surface, a condition created by bubbling the nanosilver with oxygen [37]. These authors found that bacteria strains with a resistance to Ag^+ were equally resistant to nanosilver, led to the conclusion that the mechanism of toxicity of nanosilver is identical to that of Ag^+ . Navarro et al. also found that both ionic and particulate silver influence toxicity in algae [32].

A consensus does exist that nanosilver is less acutely toxic than ionic Ag^+ . However, there appears to be valid evidence in favor of two conflicting proposals, that nanoparticles possess a unique mechanism of toxicity, or that all toxicity can be accounted for by the presence or delivery of ionic Ag^+ . The third option, that nanosilver simply provides a unique pathway for ionic Ag^+ toxicity and may account for the findings of other authors who claim that the toxicity of nanosilver is above that explainable by the dissolved Ag^+ portion of the exposure.

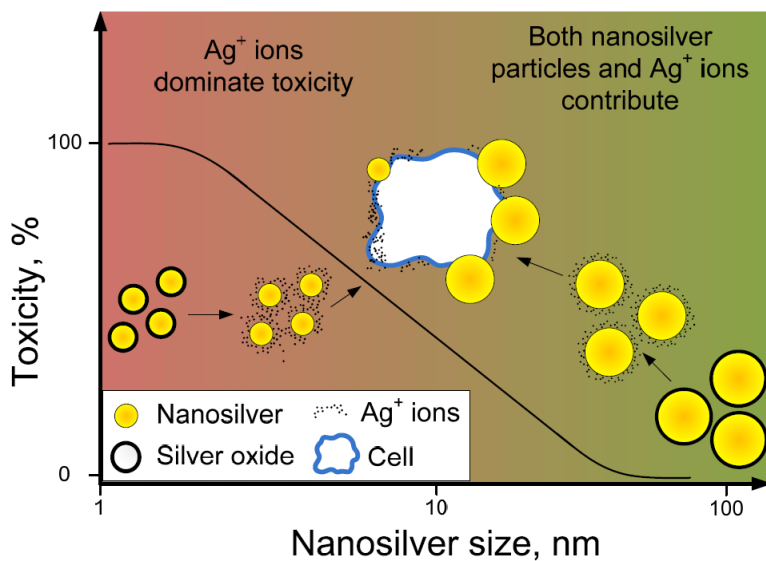


Figure 5. The toxicity of nanosilver as a function of particle size. For small (<10 nm) nanosilver, a large fraction of Ag^+ ions is released from their oxidized and highly convex surface (Kelvin effect) dominating the Ag toxicity. Silver oxide is readily dissolved in liquids in contrast to metallic Ag . For larger (>10 nm) particles, a small fraction of Ag^+ ions is released so the Ag toxicity is affected by both ions and direct contact with the nanosilver particle surface [36].

All above results indicate that the toxicity of nanosilver particles is a very complex system and cannot be explained by simple models and by the same mechanisms of toxicity. Therefore, the Ag^+ ion release mechanism in aqueous solutions needs to be investigated in detail, as well as the parameters that influence it, in order to connect the observed toxicity with specific physico-chemical properties. In fact, it has been observed that the oxidation state of nanosilver strongly influences its Ag^+ ion release and therefore, its toxicity, since oxidized nanosilver exhibited much stronger antibacterial activity. This is associated with the Ag^+ ion release from oxidized nanosilver, since silver oxide has higher solubility in water than metallic silver [38]. Alternatively, if the mechanism of toxicity is the same in nanosilver and Ag^+ , some properties of nanosilver, especially its size, shape, and surface chemistry, are likely to be related to its toxicity because they may influence the effective concentration of the Ag^+ exposure. In addition, water chemistry parameters such as pH, ionic strength, and dissolved organic carbon are known to affect the surface chemistry and aggregation state of nanosilver and to influence its bioavailability. The size

of nanoparticles is on the same scale as proteins, antibodies, and other biological macromolecules, so under certain conditions they may interact with and penetrate the cell membrane more easily than larger particles of the same material [39, 40, 9]. Conversely, Hussain et al. reported a slight decrease in vitro toxicity of nanosilver with decreasing particle size [41].

It is likely that surface area and surface atoms are correlated with biological reactivity, and that therefore, the toxicity of nanoparticles is dependent on particle size, shape, and surface chemistry. The surface chemistry of a nanoparticle -its charge and chemical composition-influences its ability to interact with biomolecules, chelating agents, and other nanoparticles, which in turn may affect its bioavailability. The surface area of an aggregate will be smaller than that of the combined surface area of the individual particles. Unaggregated particles may be more likely to be transported into cells, and may display a larger bio-reactive surface area than aggregated particles. Specifically, nanosilver has been found to have decreasing toxicity corresponding to the increased aggregation due to the presence of dissolved organic carbon or increasing ionic strength [36]. Conversely, there is also some laboratory evidence that dissolved organic carbon in natural waters has the effect of coating silver nanoparticles and decreasing their aggregation, leading to increased toxicity [42]. Many methods of nanosilver synthesis include a step that adds a surface coating, capping agent, or stabilizer in order to reduce their tendency to form aggregates. The presence and type of capping agent influences the aggregation behavior of nanosilver in response to the environmental conditions such as pH and ionic strength, and will therefore affect its toxicity. The surface coating on a silver nanoparticle may either increase its toxicity by maintaining a suspension of individual particles with higher surface area, or decrease toxicity by reducing the bioavailability of the nanoparticles.

4. SYNTHESIS METHODS OF SILVER NANOPARTICLES

There are an extensive number of synthesis methods of silver nanoparticles that are readily available in the literature. There are generally two main approaches to fabricate nanostructure materials, i.e., “top-down” and “bottom-up” (Figure 6). Top-down techniques rely on the generation of isolated atoms and molecules from the bulk materials using various distribution techniques, this route is usually not very well suited to the preparation of uniformly shaped particles; in addition, very small sizes are especially difficult to realize. On the

contrary, bottom-up procedures start with atoms that aggregate in solution or even in the gas phase to form particles of definite size, if appropriate experimental conditions (e.g., solvents, stabilizers, and temperature) are applied. Bottom-up methods are more preferable for generating uniform nanoparticles, of distinct size, shape, and structure. However this method always face the stability issue more than the top-down method because, in most of the cases, the particles are dispersed in aqueous suspension, the as-synthesized particles possess high mobility, and thus have better chance to collide with each other and form clusters or aggregations, With the bottom-up strategies, the use of capping agents is crucial to control the particle size and shape, and to provide stability for the synthesized nanomaterials.

There are basically two broad areas of synthetic techniques for nanostructure materials, namely, physical methods and chemical methods (see Figure 7). A brief introduction and comparison on two major types are discussed below [43, 44]:

- Physical methods:

The physical method is the top-down approach, and it is also called a high-energy method. It is a process in which microsized particles are broken down to nanosized particles, either by mechanical force or evaporation/condensation [45]. The synthesis of Ag -NPs by physical approach is accomplished by techniques such as evaporation–condensation [46], laser ablation [47, 48], mechano-chemical synthesis [49, 50], pulsed wire discharge [51], spray pyrolysis [52], lithography [53], sputtering, thermal decomposition [54, 55], etc. These techniques fall under the top-down approach. Even though NPs obtained through the physical approach have some advantages, such as uniform particle growth, restriction of solvent contaminants, and the preparation of highly pure NPs with negligible agglomeration, the physical approach is prone to disadvantages such as use of expensive equipment, increased time to synthesize NPs, high energy consumption, etc. Out of the methods listed above, evaporation– condensation and laser ablation are the most widely used [56].



Figure 6. The Top- down approach versus bottom- up approach.

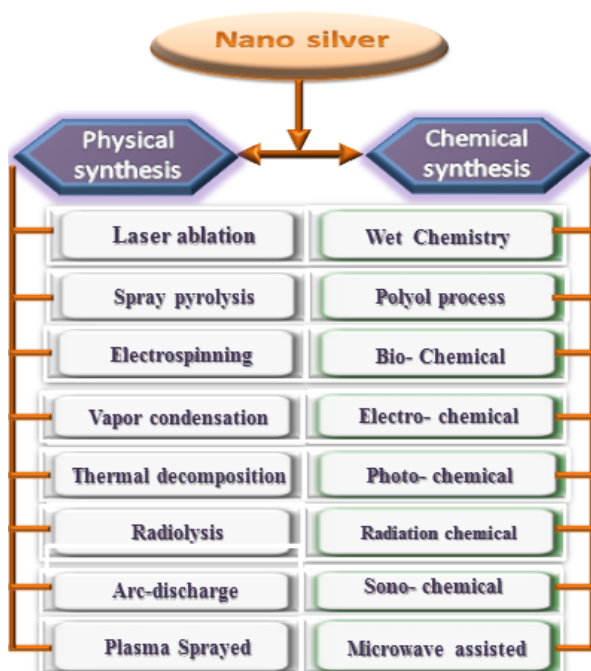


Figure 7. Some of the physical and chemical techniques for synthesize nanostructure materials.

- chemical methods:

This method is the bottom-up approach, where the nanoparticles are formed by precursors. The precursor supplies the ions and molecules, which are built up into nanoparticles by the influence of a suitable reducing agent. For instance, chemical reduction method is the most common synthetic pathway to produce

nanostructure materials due to their straight forward nature and their potential to produce large quantities of the final product [57]. The particle sizes of the nanoparticles can be controlled by systematically adjusting the reaction parameters, such as time, temperature, and the concentration of reagents and stabilizing agents. There are a variety of chemical preparation methods available for the fabrication of silver nanoparticles including radiation [58, 59], chemical precipitation [60], photochemical method [61] and electrochemical [62]. The silver nanoparticles synthesized by chemical method hold good stability and have numerous applications [63].

Chemical and physical methods are often extremely expensive and non-environmental friendly due to the use of toxic, combustible, and hazardous chemicals, which may pose potential environmental and biological risk and high energy requirement. Biological method of nanoparticles provides advancement over chemical and physical methods [64]. Several matrixes for the biogenic synthesis of such nanoparticles are reported so far, and they include microorganisms such as bacteria [65], fungi [66], enzymes, and useful medicinal plant extracts [67, 68]. Among these natural sources, plant materials are the most readily available template-directing matrix offering cost effectiveness, eco-friendliness, and easy handling much suitable for scaling up processes [69].

5. SYNTHESIS OF COLLOIDAL SILVERNANOPARTICLES BY USING WET CHEMISTRY

In this study silver nitrate AgNO_3 was used as Precursor to prepare Ag-NPs provided by Hubei Xinying Noble Metal Co. Ltd, Dextrose as reducing agent and polyvinyl pyrrolidone (PVP) of four different molecular weights (MW = 10000, 29000, 40000, 55000) as stabilizing agent were obtained from Sigma Aldrich. The sodium hydroxide was used to promote the reduction reaction at room temperature and purchased from Tianjin Chemical Reagent Corp.

5.1. Preparation of Colloidal Nanosilver

We prepared three separate solutions, (A), (B) and (C). Solution A contained 0.156 M AgNO_3 with variable quantities of urea (the molar ratio of [Urea]/ $[\text{Ag}^+]$ was between 0 and 12. Solution (B) contained fixed quantity of

polyvinyl pyrrolidone (PVP) with mass ratio 1gPVP/1g AgNO₃ and variable quantities of NaOH change from 0.2 to 1M. Solution C contained 0.334 M dextrose (C₆H₁₂O₆).

Different molecular weights (M_w) of PVP (10,000, 29,000, 40,000 and 55,000) were tested in this work for their capability to stabilize the silver colloidal suspensions. The Particular experimental conditions are listed in Table 1. With stirring and at room ambient temperature, solution (A) was rapidly poured into solution B, light yellow solution formed instantly. After 10 min, solution (C) was poured into the mixed solution. After 5 minutes of interaction we transferred the mixture to water bath at 70°C to accelerate the reduction reaction. The color changed from yellow to black. After half an hour, the silver colloidal was separated from solution by centrifugation at 10,000 rpm for 60 min to remove any excess protecting agent and then re-dispersed in DI water. The operation was repeated many times to remove as much of PVP as possible. For further analysis, the precipitate was also separated by centrifugation at 10000 rpm for another 30 min and dewatered by heating at 100°C for several hours.

Table 1. Experimental parameters for synthesis silver NPs at 70°C

NO.	AgNO ₃ (mol/l)	PVP/AgNO ₃ (g/g)	M _w PVP	Urea/AgNO ₃ (mol/mol)	Dextrose (mol/l)	NaOH (mol/l)
1G	0.156	1	10000	0	0.334	0.0125
2G	0.156	1	29000	0	0.334	0.0125
3G	0.156	1	40000	0	0.334	0.0125
G4	0.156	1	55000	0	0.334	0.0125
5G	0.156	1	10000	4	0.334	0.025
6G	0.156	1	29000	4	0.334	0.025
7G	0.156	1	40000	4	0.334	0.025
8G	0.156	1	55000	4	0.334	0.025
9G	0.156	1	10000	12	0.334	0.05
10G	0.156	1	29000	12	0.334	0.05
11G	0.156	1	40000	12	0.334	0.05
12G	0.156	1	55000	12	0.334	0.05

5.2. Result and Discussion

For analysis, the colloidal silver nanoparticles were performed as thin films on glass substrates of the dimension of 25.4 mm × 76.2 mm × 1 mm using spin-

coating technique. Typically, a few drops of solution are placed on to the surface of the substrate; the initial amount of silver sol has little effect on the final film properties. The substrate is then rotated at several thousand rpm in order to obtain a homogeneous film. The deposited films were characterized by Atomic Force Microscopy and X-ray diffraction. Infrared (IR) spectrum was measured on an EQUINAX55 Fourier transform infrared (FTIR) spectrometer, where the particles were grind with MgBr₂ particles together, and pressed to a circle flake.

5.2.1. UV-IV Spectroscopy Study

Figure 8 assumed optical absorption spectrum for synthesized silver nanoparticles at different preparation conditions. The UV–Vis spectra revealed the appearance of single and strong absorption peaks ranged from 397- 408 nm for different samples. This beak is known as the surface plasmon resonance (SPR) and indicates the formation of silver nanoparticles.

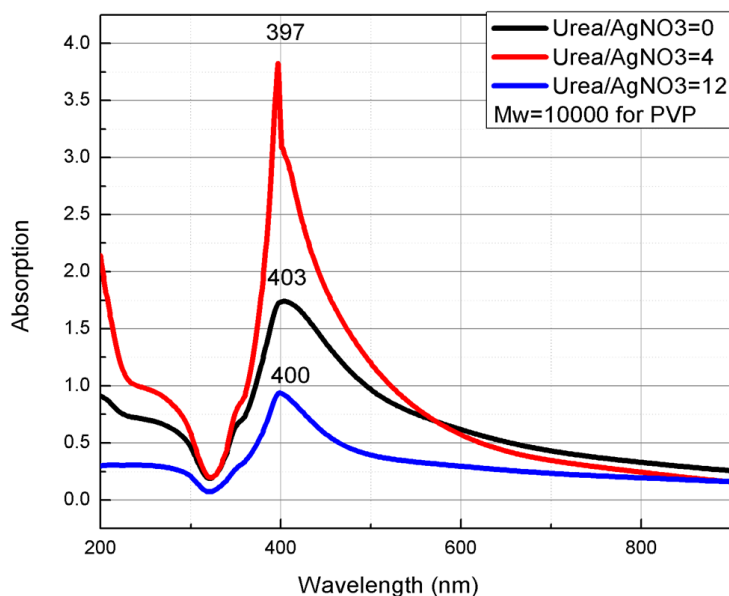


Figure 8. (Continued)

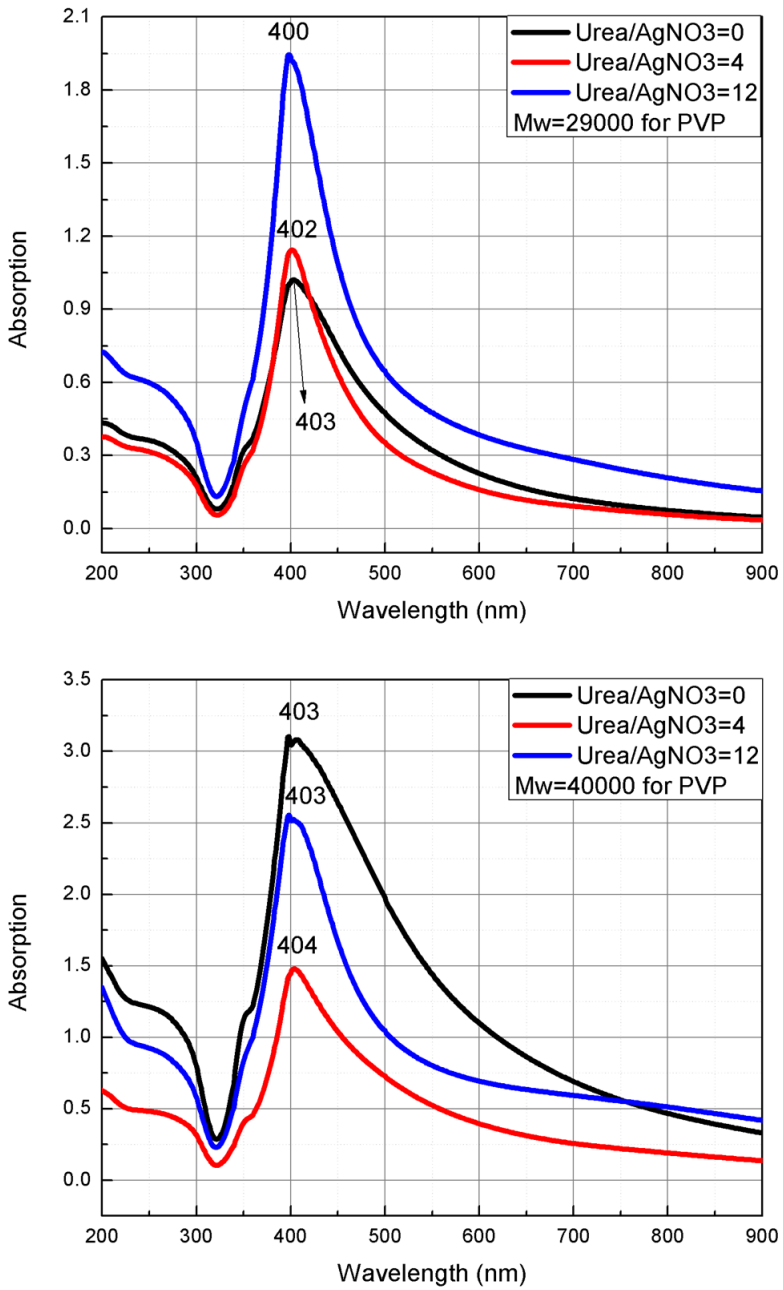


Figure 8. (Continued)

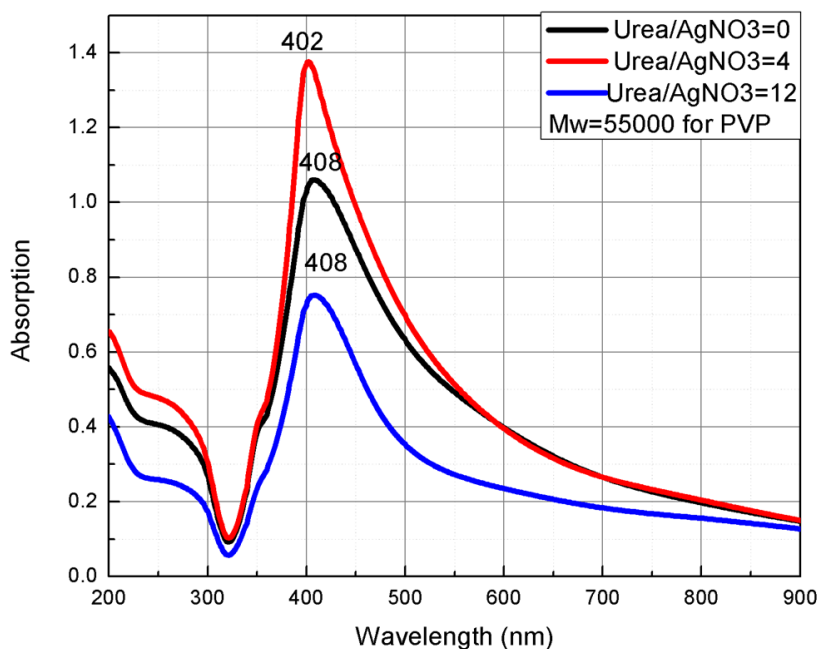


Figure 8. UV-Vis spectra of silver colloids synthesized at different preparation conditions.

5.2.2. X-Ray Diffraction Study

The structural properties of NSPs were investigated by X-ray diffraction (Philips, PW1710, Netherlands) that was operated at a voltage of 40 kV and a current of 30mA with an excitation source of CuK_{α} radiation ($\lambda = 1.54060\text{\AA}$), in the range of scanning angle 30 to 85° at a scan rate of $1^{\circ}/\text{min}$ with the step width 0.02° . The XRD measurements were performed in order to investigate the structural properties of the NSPs. Figure 9 shows x-ray diffraction patterns of pure silver sample and prepared silver thin films.

XRD patterns was showed five distinct peaks at $2\theta = 38^{\circ}, 44^{\circ}, 64^{\circ}, 77^{\circ},$ and 81° . The discernible peaks can be indexed to (111), (200), (220), (311) and (222) planes of a cubic unit cell, which corresponds to face centered cubic structure of silver (JCPDS card. No. 89-3722). The value of the Ag lattice constant has been estimated to be $a = 4.078 \text{\AA}$, a value which is consistent with $a = 4.0862 \text{\AA}$ reported by the (JCPDS cards 4-0783). Crystallite size calculations were done at (111) plane for all samples using Scherrer equation:

$$D = \frac{K\lambda}{\beta \cos\theta}$$

K is a constant (K = 0.9), $\lambda=1.54060 \text{ \AA}$ is a wavelength for the radiation source CuK_α used and θ is the Bragg angle, $\beta = \sqrt{\beta_m^2 - \beta_a^2}$, where β_m is full width at half maximum (FWHM) in degree (get it from fitting peaks according to Gaussian), β_a indicates an instrument broadening, it has been calculated using Rietveld method through the assistance program X'Pert High Score Plus (Version 3), this program allows to stimulate measured X-Ray spectrum and compare it with a database to infer the potential structure for studied materials. We measured an XRD pattern of a bulk sample of Si furnished with our PW3710 XRD-PHILLIPS system, then we refined its profile to determine the Caglioti-Paoletti-Ricci coefficients (U, V, W):

$$\beta_\alpha = \sqrt{U \tan^2\theta + V \tan\theta + W}$$

We obtained U = 0.02591, V = -0.02159 and W = 0.01398 (units: rad^2). Figure 10 shows stimulation of instrument broadens by Caglioti functions.

Particles size, diffraction angle and FWHM of synthesized silver nanoparticles were showed in Table 2.

Table 2. Particle size, diffraction angle and FWHM for synthesized silver nanoparticles using X-Ray diffraction pattern

Sample	2θ	$\beta_m(\text{FWHM})$	Crystal size (nm)
G1	38.134	0.322	27
G2	38.386	0.235	16
G3	38.254	0.245	39
G4	38.224	0.446	20
G5	37.775	0.372	28
G6	38.229	0.341	32
G7	38.3122	0.332	35
G8	37.837	0.476	21
G9	37.581	0.356	33
G10	38.205	0.236	47
G11	38.135	0.253	42
G12	38.109	0.239	34

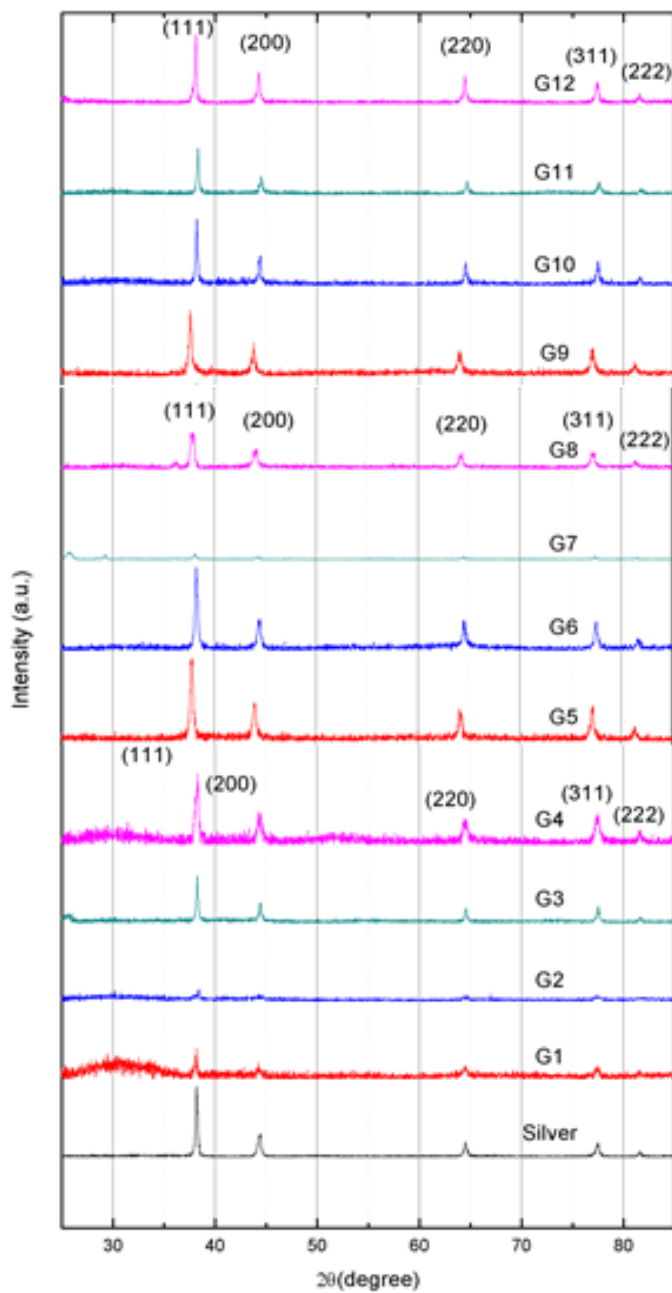


Figure 9. XRD patterns for colloidal silver NPs and reference sample (pure silver).

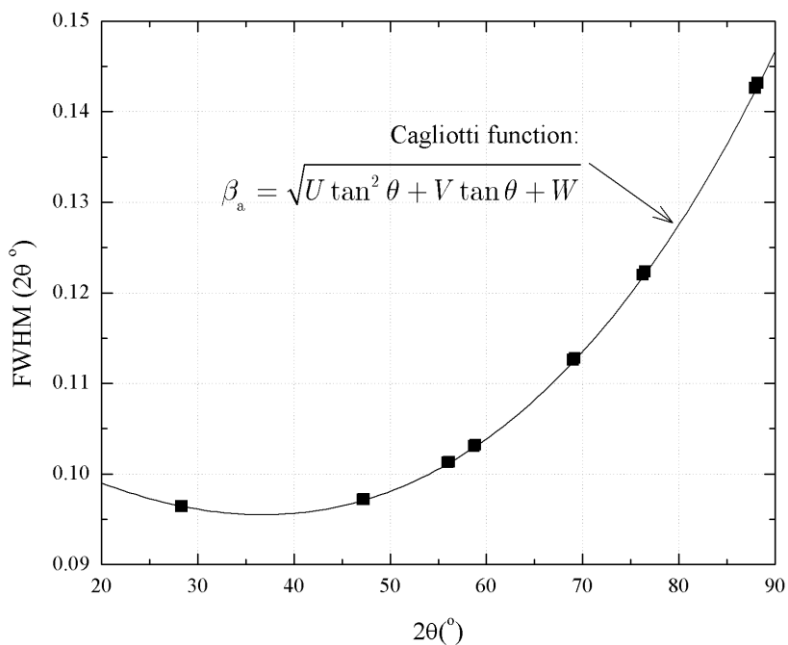
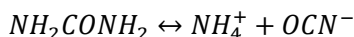
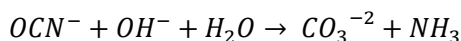


Figure 10. stimulation of instrument broaden by Cagliotti functions.

Theoretically, urea in solution can decompose to ammonium and cyanate ions:



In an alkaline solution, cyanate ions react with hydroxide ions to form carbonate ions and ammonium according to:



The alkaline solution accelerated the urea decomposition greatly and immediately produced many cyanate ions and carbonate ions. In addition, the K_{sp} values of $AgOCN$ and Ag_2CO_3 were both smaller than that of Ag_2O . As a result, the intermediates of $AgOCN$ and Ag_2CO_3 were observed, instead of Ag_2O . In the presence of a reducing agent (i.e., after adding solution C), this intermediate proved unstable, and it gradually converted into silver. Here, in the case of a chemical reduction to synthesize silver colloids, when only Ag^+ , $NaOH$ and dextrose were used, the initial precipitate was obtained very quickly upon

the mixing of these reagents, often within seconds. This period of time was too short for the PVP molecules to uniformly adsorb onto the silver surfaces. Therefore, more PVP had to be added to circumvent this situation. However, the extra PVP molecules subsequently became a burden in the later stages of the process. Yet, when urea was added to the system, the reaction path was significantly changed, first by forming AgOCN and Ag₂CO₃ composite intermediates whose quantity was mainly determined by the quantity of NaOH. The intermediates were then reduced by dextrose to silver at a relatively slow rate. During this period of time, there was also sufficient time for the PVP molecules to adsorb onto the silver surfaces. As a result, we did not need to add many PVPs to obtain a uniform dispersion of silver colloids as final products. The quantity of PVP used here.

The role of NaOH in this chemical reduction process was to accelerate the reduction rate as discussed earlier. In theory, the particle size and distribution from a chemical synthesis process depend upon the relative rates of nucleation and growth processes, as well as the agglomeration. However, these rates are also influenced by the chemical reaction rates and the rate of protective agents adsorbing onto the colloidal surfaces to provide effective barrier against agglomeration, which are influenced, in turn, by the many parameters of the chemical process adopted.

Here in the case of the reaction rate is very fast (without using urea), and when the molecular weight of PVP was 10000, so the smaller PVP molecules would not have sufficient time to coat these newly formed silver colloids, thus unable to prevent the agglomerating into large particles as shown in Table 2. On the other hand, larger PVP molecules (55000) might provide some physical barrier to slow down the agglomeration process, thus enabling the coating and stabilization process to those silver colloids. That is appearing for sample G4 with smaller diameter (20 nm) than G1 (27 nm). For same reason the diameter of sample G5 (28 nm) is smaller than G8 (21 nm) for the molar ratio [urea]/[AgNO₃] = 4. In the case of [urea]/[AgNO₃] = 12 mol/mol, the rate of reaction was very slow so two type of PVP have same affect (We get the same diameters 33 and 34 nm for G9 and G12 respectively).

5.2.3. AFM Study

The atomic force microscopy (AFM) allows us to get microscopic information on the surface structure and to plot topographies representing the surface relief. AFM imaging is performed on the Nanosurf system (easyScan2) operating in a dynamic mode in air at room temperature.

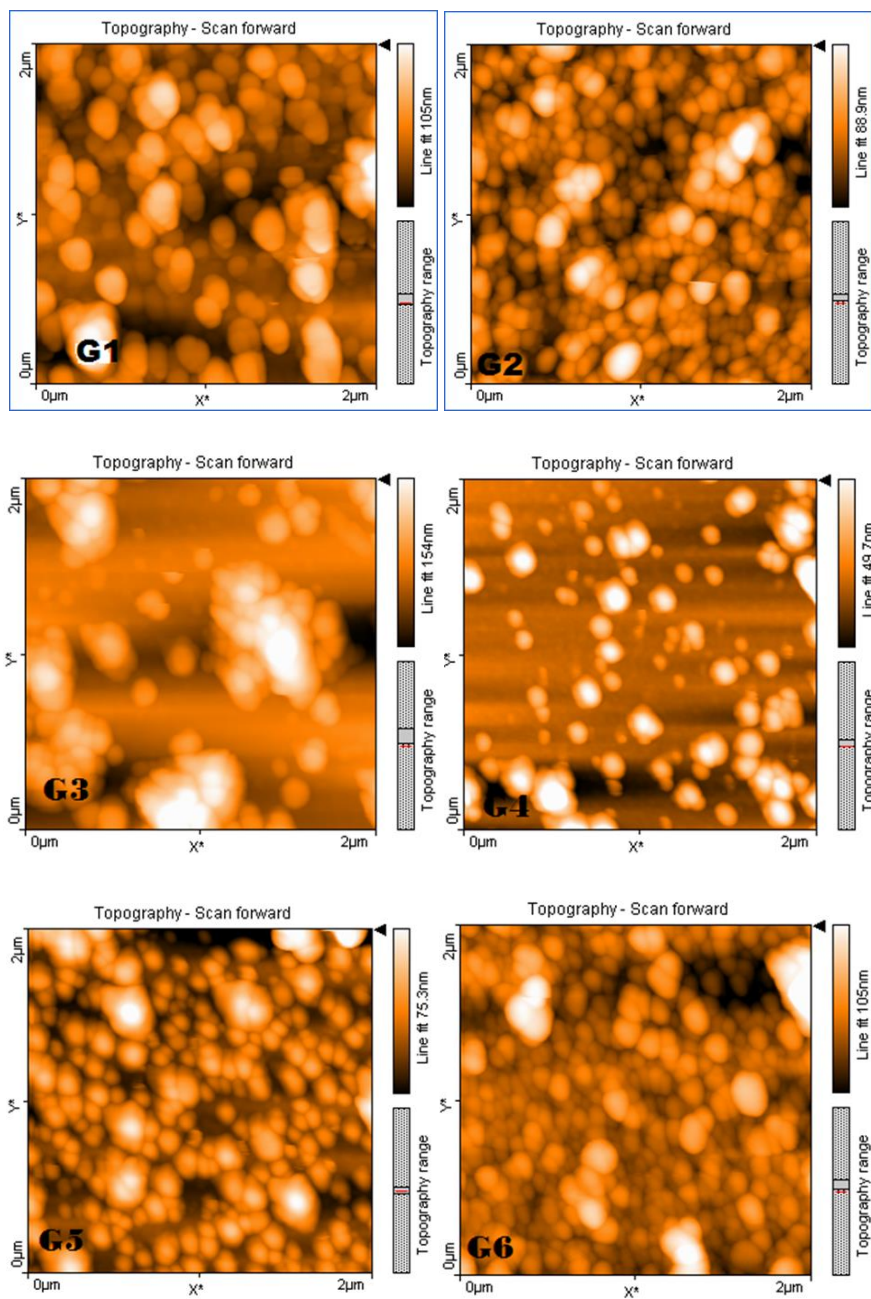


Figure 11. (Continued)

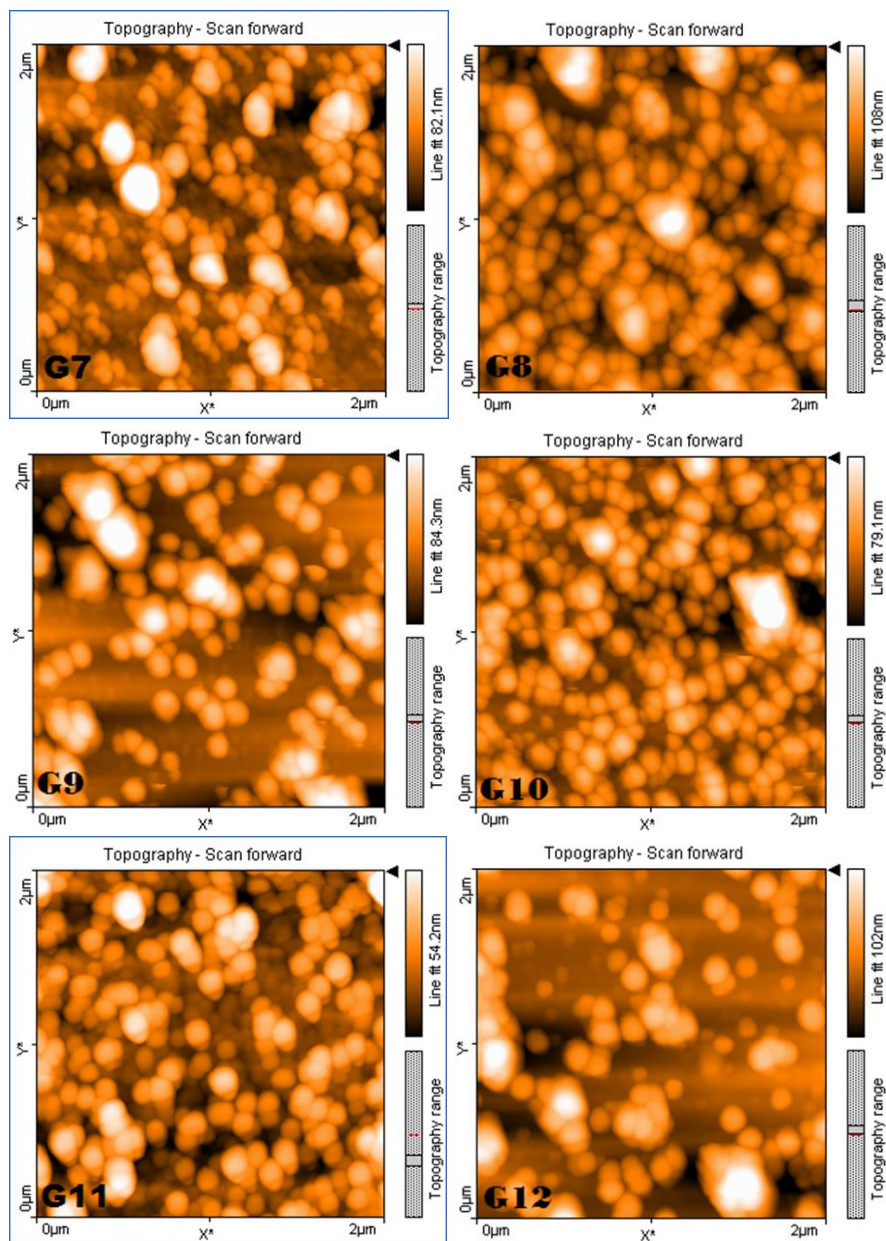


Figure 11. 2μm x 2μm AFM images for colloidal silver deposited on glass substrates using spin coating method.

Table 3. Measured diameters and heights of silver nanoparticles using AFM and X-Ray diffraction method

NO.	Mean diameter using AFM (nm)	Mean height using AFM (nm)	Diameter using X-Ray (nm)
G1	86	9	27
G2	79	10	16
G3	114	26	39
G4	81	10	20
G5	93	13	28
G6	95	12	32
G7	102	14	35
G8	90	10	21
G9	95	13	33
G10	103	14	47
G11	116	12	42
G12	98	11	34

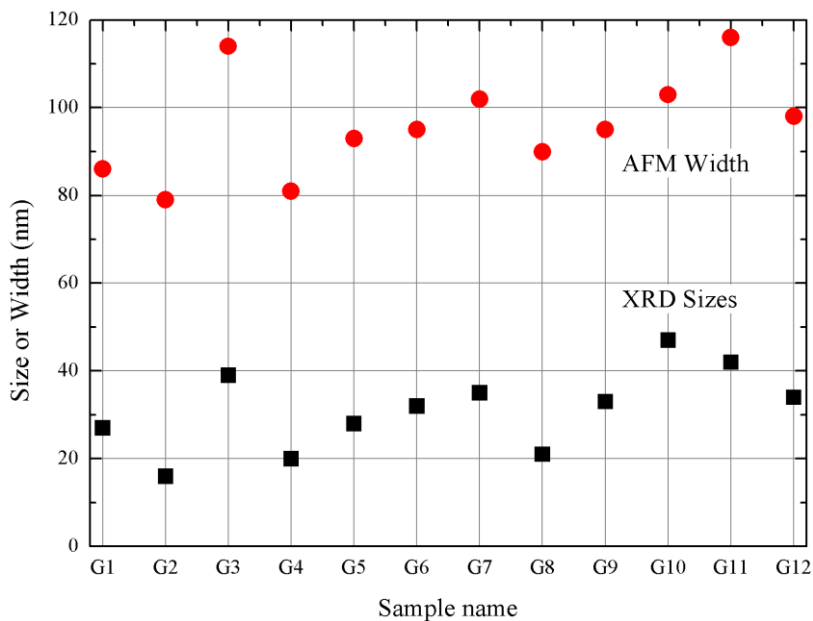


Figure 12. Comparison between diameters of silver nanoparticles using AFM and X-Ray diffraction method.

Figure 11 showed surface morphology of colloidal silver deposited on glass substrates using spin-coating method. The surface is covered with uniform, spherical silver nanoparticles and has relatively low size and narrow size distribution.

The calculated diameters using AFM are ranging from 81 nm to 116 nm and the mean heights are between 9nm and 26nm. Table 3 shows mean diameters and heights of silver nanoparticles using Atomic force microscope and compare it with diameter measured using X-Ray diffraction method.

It is assumed that the diameter calculated using AFM is bigger than one calculated using X-Ray as shown in Figure 12, which is due to many reasons:

- In some cases the aggregated particles could appear as one particle i.e., Figure 13(a) showed two particles so close together, but when we use the attachment software to find diameters, two particles seem as one as shown in Figure 13(b).

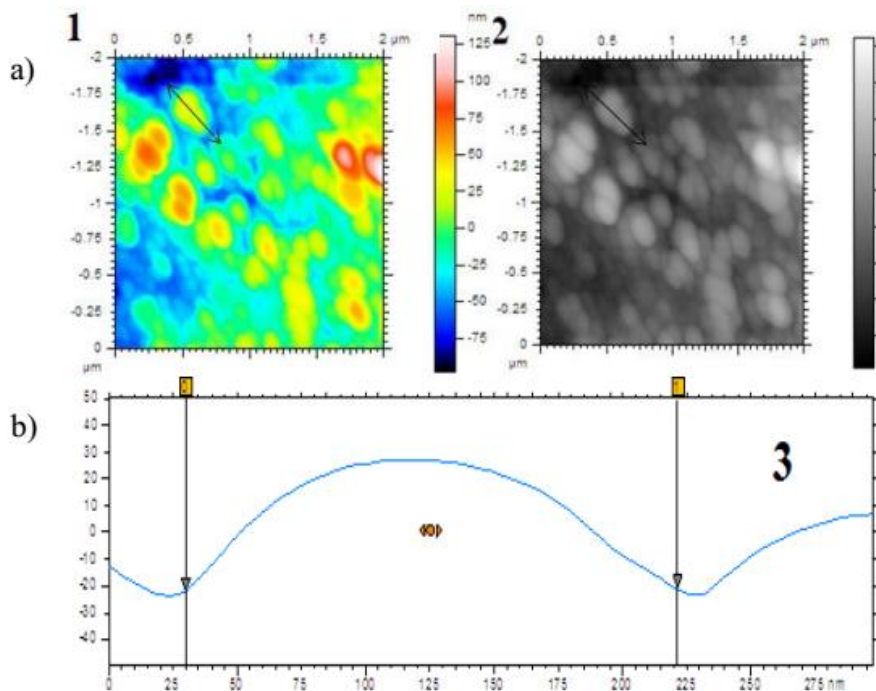


Figure 13. Calculation of diameter for two particles.

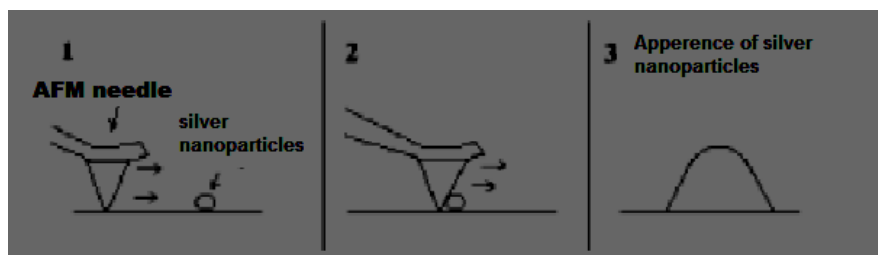


Figure 14. A schematic demonstration of disadvantage of AFM.

- Sometime the surface of thin films was not completely cleaned from PVP even after washing with DI water, and that deludes the size of particle.
- The shape of AFM tip may cause misleading cross sectional views of the sample as demonstrated (Figure 14).

5.2.4. FTIR Analysis

FTIR spectrum of different molecular weights of PVP is presented in Figure 15. The strong band NO. 5 at 1658 cm^{-1} corresponds to C-O stretching bond of amide, band NO. 9 at 1288 cm^{-1} correspond to complex N-OH bend and the bands NO. 12 and NO. 13 at 1074 cm^{-1} and 1013 cm^{-1} respectively correspond to C-N stretching bond.

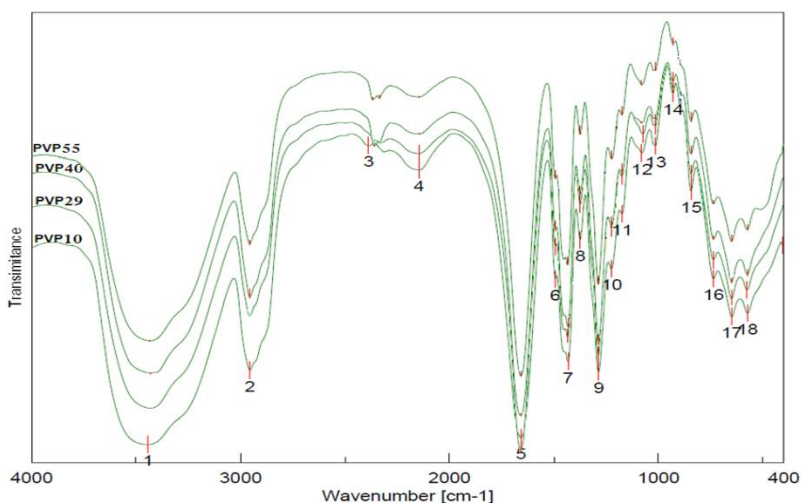


Figure 15. FTIR spectrum of different molecular weights of PVP: 10000, 29000, 40000, 55000).

Figure 16 shows FTIR spectrum of synthesized Ag nanoparticles and compare it with FTIR spectrum of used PVP with different molecular weights (10000, 29000, 40000, 55000).

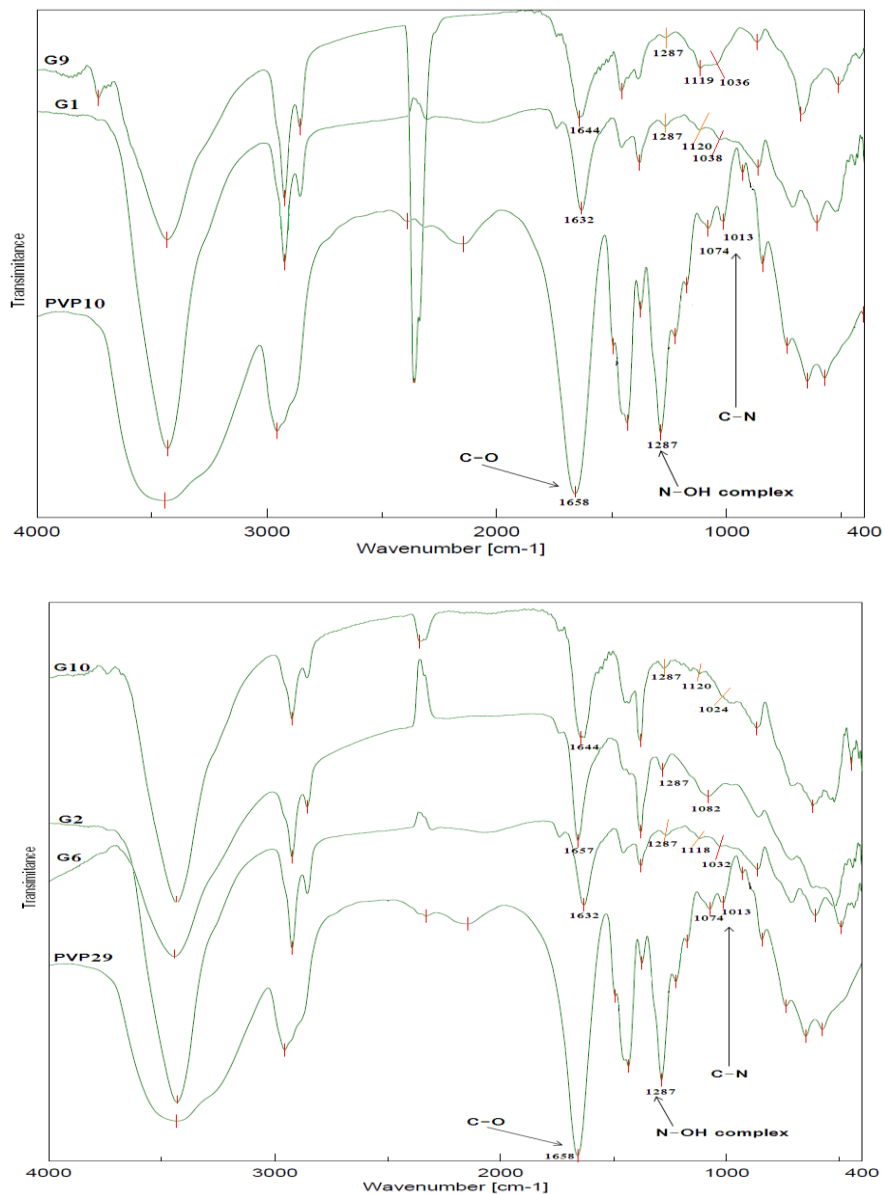


Figure 16. (Continued)

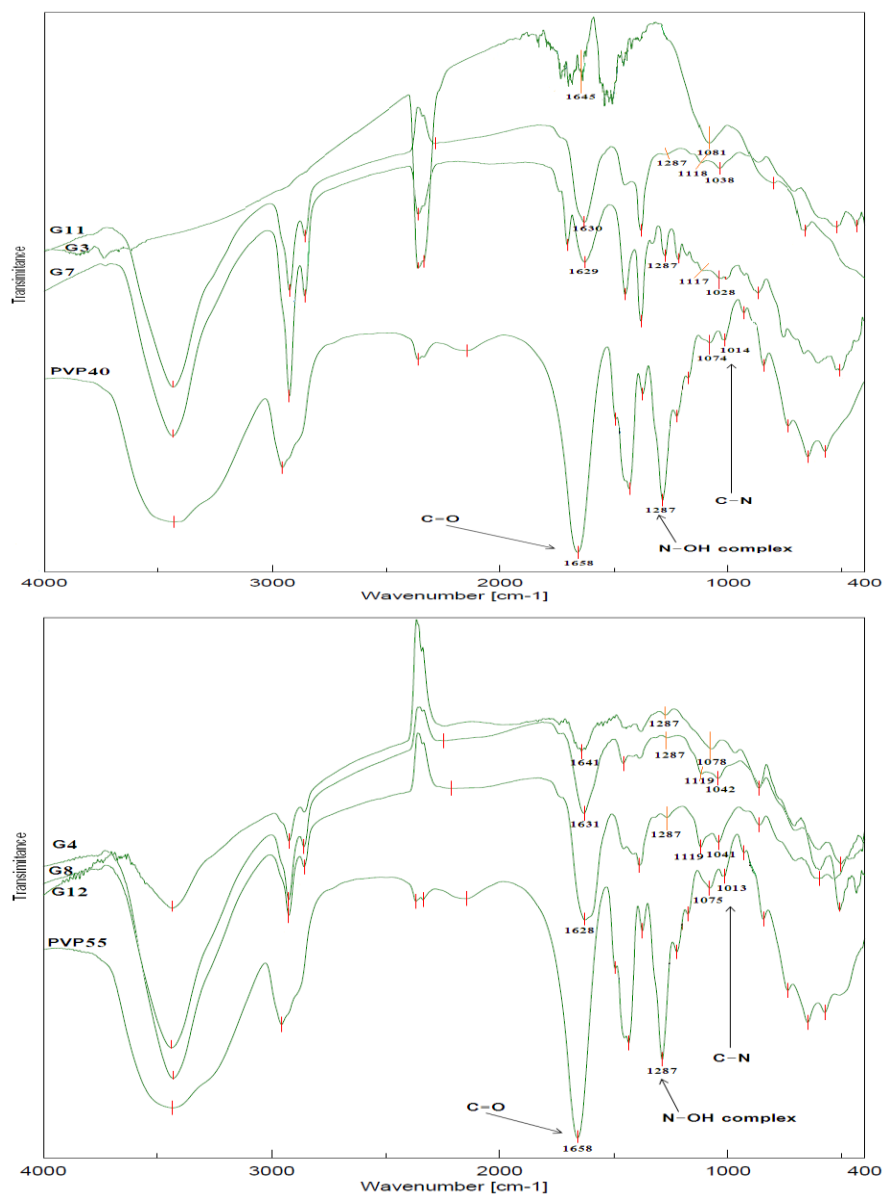


Figure 16. FTIR spectrum of synthesized Ag nanoparticles and compare it with FTIR spectrum of used PVP with different molecular weights (10000, 29000, 40000, 55000).

We noticed the displacement (shift) of absorption peak at 1658 cm^{-1} to the lower wave-numbers, that indicates the weakness of C=O bond which is a result

of formation a molecular bond with Ag nanoparticles. While the displacement of peaks at 1074 cm^{-1} and 1013 cm^{-1} to the high wave-numbers is due to chemical coordination between nitrogen atom and silver nanoparticles surface.

In conclusion, the Ag nanoparticles have been prepared by the wet chemical technique under optimized conditions of preparation. Deposition of silver sols was carried out from aqueous solutions using silver nitrate, dextrose, PVP and sodium hydroxide. XRD as well as Atomic AFM image studies confirmed the nanometer size Ag particles. XRD analysis showed the nanoparticles were crystalline and metallic with minimum size $\sim 16\text{ nm}$. AFM analysis showed that most of the particles were spherical in shape with and their size appears larger than the calculated value from XRD. However, the nano-size particles calculated by XRD correspond reasonably well with the real values of the size Ag-NPs. In summary, we have shown a drastic effect of the molar ratio of $[\text{Urea}]/[\text{Ag}^+]$ and the molecular weight of PVP on the size of silver nanoparticles. FTIR spectra were analyzed to study the mechanism of adsorption of PVP on the silver nanoparticles.

REFERENCES

- [1] Mozghan Bahadory, thesis (2008) "Synthesis of Noble Metal Nanoparticles," Drexel University.
- [2] Turkevich, J., Stevenson, P., Hillier, J. (1951). A Study of the Nucleation and Growth Processes In The Synthesis Of Colloidal Gold. *Discuss. Faraday Soc.*, 55–75.
- [3] Andreas Trügler, thesis (2011), "Optical Properties of Metallic Nanoparticles," Institut Für Physik, Fachbereich Theoretische Physik Karl–Franzens–Universität Graz.
- [4] Wijnhoven Swp, Peijnenburg Wjgm, Herberts Ca, Hagens Wi, Oomen Ag, Heugens Ehw, Roszek B, Bisschops J, Gosens I, Van De Meent D, Dekkers S, De Jong Wh, Zijverden M, Sips Ajam, Geertsma Re (2009). Nanosilver - A Review Of Available Data And Knowledge Gaps In Human And Environmental Risk Assessment. *Nanotoxicology*. 3(2):109-138.
- [5] S. A. Brennan, C. NíFhoghlú, B. M. Devitt, F. J. O'mahony, D. Brabazon, A. Walsh, (2015) "Silver nanoparticles and their orthopaedic applications," *Bone Joint J*; 97-B:582–9.

-
- [6] Liao Sy, Read Dc, Pugh Wj, Furr Jr, Russell Ad (1997). Interaction of Silver Nitrate with Readily Identifiable Groups: Relationship to the Antibacterial Action of Silver Ions. *Lett. Appl. Microbiol.* 25:279-283.
- [7] Matsumura Y, Yoshikata K, Kunisaki Si, Tsuchido T (2003). Appl. Mode of Bactericidal Action of Silver Zeolite and Its Comparison with That Of Silver Nitrate. *Environ. Microbiol.* 69:4278-4281.
- [8] Kim Js, Kuk E, Yu Kn, Kim Jh (2007). Antimicrobial Effects of Silver Nanoparticles, *Nanomed: Nanotechnol, Biol. Med.* 3:95-101.
- [9] Morones Jr, Elechiguerra JI, Camacho A, Holt K, Kouri Jb (2005) "The Bactericidal Effect Of Silver Nanoparticles." *Nanotechnology* 16: 2346-2353.
- [10] Wright Jb, Lam K, Hansen D, Burrell Re (1999). "Efficacy of topical silver against fungal burn wound pathogens." *Am. J. Infect. Control* 27:344-350.
- [11] Valiollah Mahdizadeh, Naser Safaie and Fatemeh Khelghatibana, (2015) "Evaluation of Antifungal Activity of Silver nanoparticles Against Some Phytopathogenic Fungi And *Trichoderma Harzianum*," *J. Crop Prot*, 4 (3): 291-300.
- [12] P. MukhaIu, A. M. Eremenko, N. P. Smirnova, A. I. Mikhienkova, G. I. Korchak, V. F. Gorchev and A. Chunikhin, (2013) "Antimicrobial Activity Of Stable Silver Nanoparticles Of A Certain Size," *Prikl. Biokhim. Mikrobiol.* 49, 215.
- [13] D. R. Monteiro, L. F. Gorup, S. Silva, M. Negri, E. R. De Camargo, R. Oliveira, D. B. Barbosa And M. Henriques, (2011) "Silver Colloidal Nanoparticles: Antifungal Effect Against Adhered Cells And Biofilms Of *Candida Albicans* And *Candida Glabrata*," *Biofouling* 27 711.
- [14] Sun Rw, Chen R, Chung Np, Ho Cm, Lin Cl, Che Cm (2005). "Silver Nanoparticles Fabricated In Hepes Buffer Exhibit Cytoprotective Activities Toward Hiv-1 Infected Cells." *Chem. Commun.* (Camb.): 5059-5061.
- [15] ElechiguerraJI, Burt JI, MoronesJr, Camacho-Bragado A, Gao X, Lara Hh, YacamanMj (2005). "Interaction of Silver Nanoparticles with Hiv-1." *J. Nanobiotechnol.*, June 29:3-6.
- [16] T. R. Suganya, T. Devasena, (2015) "Exploring The Mechanism Of Anti-Inflammatory Activity Of Phyto- Stabilized Silver Nanorods," *Digest Journal Of Nanomaterials And Biostructures* Vol. 10, P. 277 -282.
- [17] D. J. Leaper, (2006) "Silver Dressings: Their Role In Wound Management" *International Wound Journal*, 3, 282-294.

-
- [18] J. Fong and F. Wood, (2006) "Nanocrystalline Silver Dressings In Wound Management: A Review," *Int. J. Nanomed.*, 1, 441–9.
- [19] Balaprasad Ankamwar, a Ujjal Kumar Sur B and Pulak Dasb, (2016) "Sers Study Of Bacteria Using Biosynthesized Silver Nanoparticles As The Sers Substrate," *Anal. Methods*, 8, 2335-2340.
- [20] Meikun Fan And Alexandre G. Brolo, (2009) "Silver Nanoparticles Self Assembly As Sers Substrates With Near Single Molecule Detection Limit," *Phys. Chem. Chem. Phys.*, 11, 7381–7389.
- [21] Xia Wei, Hui Li, Zhonghui Li, Maika Vuki, Yu Fan, Wenying Zhong, Danke Xu, (2012) "Metal-Enhanced Fluorescent Probes Based On Silver Nanoparticles And Its Application In Ige Detection," *Anal Bioanal Chem* 402: 1057.
- [22] Bihua Xia, Fang He, Lidong Li, (2014)" Metal-Enhanced Fluorescence Using Aggregated Silver Nanoparticles," *Colloids And Surfaces A Physicochemical And Engineering Aspects* 444:9–14.
- [23] Cai-Hong Liu and Xun Yu, (2011) "Silver Nanowire-Based Transparent, Flexible, and Conductive Thin Film," *Nanoscale Research Letters* 6:75.
- [24] Surya Prakash Singh et al. (2015) "Conductive Silver Inks and Their Applications in Printed And Flexible Electronics" *Rsc Adv.*, 5, 77760.
- [25] Blaser Sa, Scheringer M, Macleod M, Hungerbuhler K, (2008)" Estimation Of Cumulative Aquatic Exposure and Risk Due To Silver: Contribution Of Nanofunctionalized Plastics and Textiles." *Sci Total Environ*, 390:396–409.
- [26] Farkas J, Peter H, Christian P, Gallego UrreaJa, Hassell V M, Tuoriniemi J, Gustafsson S, Olsson E, Hylland K, Thomas Kv(2011) "Characterization Of The Effluent From A Nanosilver Producing Washing Machine." *Environ Int*, 37:1057–1062.
- [27] Garc Ia-Barrasa J, L'Opez-De-Luzuriaga J M And Monge M, (2011) *Cent. Eur. J. Chem.* 9 17.
- [28] Dallas P, Sharma V K and Zboril R,(2011), *Adv. Colloid Interface Sci.* 166 119.
- [29] Benn Tm, Westerhoff P (2008) "Nanoparticle Silver Released Into Water from Commercially Available Sock Fabrics." *Environmental Science and Technology* 42: 4133-413.
- [30] Geranio L, Heuberger M, Nowack B, (2009) "The Behavior of Silver Nanotextiles during Washing." *Environmental Science and Technology* 43: 8113-8118.
- [31] Lubick N, (2008)" Nanosilver Toxicity: Ions, Nanoparticles or Both?" *Environ. Sci. Technol.* 42 8617.

- [32] Navarro, E., Piccapietra, F., Wagner, B., Marconi, F., Kaegi, R., Odzak, N., Sigg, L. & Behra, R, (2008) "Toxicity of Silver Nanoparticles To *Chlamydomonas Reinhardtii*." *Environ. Sci. Technol.* 42, 8959-8964.
- [33] Fabrega, J., Fawcett, S. R., Renshaw, J. C. and Lead, J. R, (2009) "Silver Nanoparticle Impact on Bacterial Growth: Effect of PH Concentration and Organic Matter." *Environ. Sci. Technol.* 43, 7285-7290.
- [34] Kawata, K., Osawa, M. and Okabe, S, (2009) "In Vitro Toxicity of Silver Nanoparticles at Noncytotoxic Doses To Hepg2 Human Hepatoma Cells." *Environ. Sci. Technol.* 43, 6046-6051.
- [35] Powers, C. M., Badireddy, A. R., Ryde, I. T., Seidler, F. J. & Slotkin, T. A, (2011) "Silver Nanoparticles Compromise Neurodevelopment In Pc12 Cells: Critical Contributions Of Silver Ion, Particle Size, Coating, And Composition." *Environ. Health Perspect.* 119, 37-44.
- [36] Sotiriou, G. A. & Pratsinis, S. E. (2010) "Antibacterial Activity of Nanosilver Ions and Particles." *Environ. Sci. Technol.* 44, 5649-5654.
- [37] Lok et al. Lok Cn, Ho Cm, Chen R, He Qy, Yu Wy (2007) "Silver Nanoparticles: Partial Oxidation and Antibacterial Activities." *Journal of Biological and Inorganic Chemistry* 12: 527-534.
- [38] Lide, D. R, book (2010) "Handbook of Chemistry and Physics," Crc Press/Taylor and Francis.
- [39] Buzea C, Pacheco Ii, Robbie K (2007) "Nanomaterials and Nanoparticles: Sources, And Toxicity." *Iointerphases* 2: 17-71.
- [40] Asharani Pv, Wu Yl, Gong Z, Valiyaveettil S (2008) "Toxicity Of Silver Nanoparticles In Zebrafish Models." *Nanotechnology* 19: 1-8.
- [41] Hussain Sm, Hess Kl, Gearhart Jm, Geiss Kt, Schlager Jj (2005) "In Vitro Toxicity Of Nanoparticles In Brl 3a Rat Liver Cells." *Toxicology In Vitro* 19: 975-983.
- [42] Handy Rd, Kammer Fvd, Lead Jr, Hasselov M, Owen R (2008) "The Ecotoxicology and Chemistry of Manufactured Nanoparticles." *Ecotoxicology* 17: 287-314.
- [43] Abou El-Nour Kmm, Aa Eftaiha, Al-Warthan A, Ammar Raa (2010) "Synthesis And Applications Of Silver Nanoparticles." *Arab J Chem* 3(3):135-140.
- [44] R. S. Jawaad, K. F. Sultan And A. H. Al-Hamadani (2014), Asian Research Publishing Network, 9, 586.
- [45] Y. D. Tretyakov, A. V. Lukashin and A. A. Eliseev, (2004) "Synthesis of Functional Nanocomposites Based On Solid-Phase Nanoreactors" *Russ. Chem. Rev.*, 73, 899.

- [46] J. Harra, J. Makitalo, R. Siikanen, M. Virkki, G. Genty, T. Kobayashi, M. Kauranen And J. M. Makela, (2012) "Size-Controlled Aerosol Synthesis Of Silver Nanoparticles For Plasmonic Materials," *J. Nanopart. Res.*, 14, 870.
- [47] F. Mafune, J. Kohno, Y. Takeda, T. Kondow And H. Sawabe,(2000) "Formation And Size Control Of Silver Nanoparticles By Laser Ablation In Aqueous Solution." *J. Phys. Chem. B*, 104, 9111.
- [48] Y.-H. Chen and C.-S. Yeh, (2000) "Laser Ablation Method: Use Of Surfactants To Form The Dispersed Ag Nanoparticles" *Colloids Surf., A*, 197, 133–139.
- [49] Bo Lu, Fangyi Zhan, Guodong Gong, Yali Cao, Qiang Zhen And Pengfei Hu.(2016) "Room Temperature Mechanochemical Synthesis Of Silver Nanoparticle Homojunction Assemblies For The Surface-Enhanced Raman Scattering Substrate," *Rsc Adv.*, 6, 74662-74669.
- [50] Takuya Tsuzuki and Paul G. McCormick, (2004) "Mechanochemical Synthesis Of Nanoparticles," *Journal Of Materials Science*, 39, P 5143–5146.
- [51] Y Tokoi, K Josho, Y M Izuari, T Suzuki, T Nakayama, H Suematsu, S W Lee2, Z Fu, And K Niihara.(2011) "Particle Size Control Of Silver Nanoparticles Prepared By Pulsed Wire Discharge In Liquid Media," *Iop Conf. Series: Materials science and engineering* 20, 012008.
- [52] Kalyana C. Pingali, David A. Rockstraw, and Shuguang Deng, (2005) "Silver Nanoparticles from Ultrasonic Spray Pyrolysis Of Aqueous Silver Nitrate," *Aerosol Science And Technology*, 39:1010–1014.
- [53] John C. Hulteen, David A. Treichel, Matthew T. Smith, Michelle L. Duval, Traci R. Jensen, and Richard P. Van Duyne, (1999) "Nanosphere Lithography: Size-Tunable Silver Nanoparticle and Surface Cluster Arrays," *J. Phys. Chem. B*, 103, 3854-3863.
- [54] Togashi T, Saito K, Matsuda Y, Sato I, Kon H, Uruma K, Ishizaki M, Kanaizuka K, Sakamoto M, Ohya N, Kurihara M,(2014) "Synthesis Of Water-Dispersible Silver Nanoparticles By Thermal Decomposition Of Water-Soluble Silver Oxalate Precursors." *J Nanosci Nanotechnol.* 14(8):6022-7.
- [55] Le Thi Tam, Vu Ngoc Phan, Hoang Lan, Nguyen Thanh Thuy, Tran Minh Hien, Tran Quang Huy, Nguyen Van Quy, Huynh Dang Chinh, Le Minh Tung, Pham Anh Tuan, Vu Dinh Lam, Anh-Tuan Le. (2013) "Characterization and Antimicrobial Activity of Silver Nanoparticles Prepared By A Thermal Decomposition Technique," *Applied Physics A*, Volume 113, Issue 3, Pp 613–621.

- [56] Guangyin Lei, Master Of Science In Materials Science and Engineering, (2007) "Synthesis Of Nano-Silver Colloids And Their Anti- Microbial Effects," Blacksburg, Virginia.
- [57] Pal Sovan Lal, Utpal Jana Pk, Manna Gp, Mohanta Manavalan R, (2011) "Nanoparticle: An Overview of Preparation and Characterization." *J Appl Pharma Sci* 1(6):228–234.
- [58] K. Hareesh, R. P. Joshi, S. S. Dahiwale, V. N. Bhoraskar, S. D. Dhole, (2016) "Synthesis of Ag-Reduced Graphene Oxide Nanocomposite By Gamma Radiation Assisted Method And Its Photocatalytic Activity," *Vacuum* 124, 40-45.
- [59] Van Phu D, Le Quoc A, DuyNn, LanNt, Du Bd, Le Luan Q, Hien Nq (2014) "Study On Antibacterial Activity Of Silver Nanoparticles Synthesized By Gamma Irradiation Method Using Different Stabilizers." *Nanoscale Res Lett* 9(1):162.
- [60] Anna Zielinska A, Ewa Skwarekb, Adriana Zaleska A, Maria Gazdac, Jan Hupkaa, (2009) "Preparation of Silver Nanoparticles with Controlled Particle Size," *Procedia Chemistry* 1, 1560–1566.
- [61] Moussa Zaarour, Mohamad El Roz, Biao Dong, Richard Retoux, Roy Aad, Julien Cardin, Christian Dufour, Fabrice Gourbilleau, Jean-Pierre Gilson, And Svetlana Mintova,(2014) "Photochemical Preparation Of Silver Nanoparticles Supported On Zeolite Crystals," *American Chemical Society*, 30 (21), Pp 6250–6256.
- [62] Maria Starowicz, Barbara Stypuła, Jacek Banaś, (2006) "Electrochemical Synthesis of Silver Nanoparticles," *Electrochemistry Communications*, Volume 8, Issue 2, Pages 227–230.
- [63] Ibrahim Alghoraibi, Abdalrahim Alahmad, (2014) "Colloidal Synthesis and Structural Characterizations of Silver Nanoparticles by using Wet Chemistry" *International Journal of ChemTech Research* Vol. 6, No. 1, pp 871-880.
- [64] S. Iravani, H. Korbekandi, S. V. Mirmohammadi, and B. Zolfaghari, (2014) "Synthesis of Silver Nanoparticles: Chemical, *Physical and Biological Methods Res Pharm Sci*. Nov-Dec; 9(6): 385–406.
- [65] Hebbalalu D, Lalley J, Nadagouda Mn, Varma Rs, (2013) "Greener Techniques For The Synthesis Of Silver Nanoparticles Using Plant Extracts, Enzymes, Bacteria, Biodegradable Polymers, And Microwaves" *Acs Sustainable ChemEng* 1:703–712.
- [66] Srivastava P, Bragança J, Ramanan Sr, Kowshik M, (2013) "Synthesis Of Silver Nanoparticles Using Haloarchaeal Isolate Halococcus Salifodinae Bk3". *Extremophiles* 17:821–831.

- [67] Huang J, Li Q, Sun D, Lu Y, Su Y, Yang X, Wang H, Wang Y, Shao W, He N, Hong J, Chen C, (2007) "Biosynthesis Of Silver And Gold Nanoparticles By Novel Sundried Cinnamomum Camphora Leaf *Nanotechnology* 18:105104–105114.
- [68] Vijayaraghavan K, NaliniSp, Prakash Nu, Madhankumar D, (2012)" One Step Green Synthesis Of Silver Nano/Microparticles Using Extracts Of *Trachyspermum Ammi* And *Papaver Somniferu*" *Colloids Surf B Biointerfaces* 94:14–17.
- [69] M. C. Moulton, L. K. Braydich-Stolle, M. N. Nadagouda, S. Kunzelman, S. M. Hussaina And R. S. Varma,"Synthesis, Characterization And Biocompatibility Of, (2010) "Green Synthesized Silver Nanoparticles Using Tea Polyphenols," *Nanoscale*, 2, 763–770.

BIOGRAPHICAL SKETCH

Name: Ibrahim Alghoraibi

Affiliation: Physics Department/Damascus University

Education: PhD

Business Address: Physics Department/ Physics Building, Damascus University

Research and Professional Experience: Nanotechnology

Professional Appointments: Physics Assistant Professor in Damascus University

Honors: Assistant Professor/ leader of the Nanotechnology activity

Publications:

1. Ibrahim Alghoraibi "InAs(Sb)/InGaAs(P) Quantum Nanostructures on InP (100) for Mid infrared Emitters" *International Journal of science Georesorce* 1 (12) 2012.
2. Faten Alfeel, Fowzi Awad, Ibrahim Alghoraibi and Fadi Qamar "Using AFM to Determine the Porosity in Porous Silicon" *Journal of Materials Science and Engineering A* 2 (9) (2012) 579 583.
3. Faten Alfeel, Fowzi Awad, Ibrahim Alghoraibi and Fadi Qamar "Change of diffused and scattered light with surface roughness of p-type Porous Silicon" *International Journal of Nano Dimension Materials* A-13-04-24.
4. Abdul Razzak Ghazal¹, Rabab sabbagh¹, Ibrahim alghoraibi², "Using atomic force microscope to compare the surface roughness of superelastic

- and thermal activated Nickel-Titanium wire for orthodontics application” Journal of Hadramout, University for Natural and Applied Sciences, Vol 2 (2013).
5. Ahmed Abdul-Kareem, Ibrahim Alghoraibi, Mohamed-Ali Alsayed-Ali “ Effect of applied voltage and needle size on morphology of Polyamide 66 nanofiber Formed by Electrospinning Technique “ Journal of Engineering Science, Damascus University, N2, 2013
 6. Abdalrahim Alahmad¹, Mustafa Eleoui¹, Ahmad Falah² and Ibrahim Alghoraibi² “Preparation of colloidal silver nanoparticles and structural characterization ”Physical Sciences Research International Vol. 1(4), pp. 89-96, October 2013.
 7. Ibrahim Alghoraibi¹, Abdalrahim Alahmad², “Colloidal Synthesis and Structural Characterizations of Silver Nanoparticles by using Wet Chemistry” International Journal of ChemTech Research Vol.6, No.1, pp 871-880, (2014).
 8. Raghad Zein, Ibrahim Alghoraibi*, Effect of Deposition Time on Structural and Optical Properties of ZnS Nanoparticles Thin Films Prepared by CBD Method”, Int.J. ChemTech Res, Vol.6, No.5, pp 3220-3227 (2014).
 9. Ibrahim Alghoraibi, “Effect of Deposition Time on the Nanocrystalline PbS Thin Films Synthesized by Chemical Solution Deposition Method: Structural Characterization”, Int.J. ChemTech Res, Vol.6, No.5, pp 2725-2731, (2014)
 10. Ibrahim Alghoraibi, “ Fabrication and Characterization of polyamide-66 Nanofibers Via Electrospinning technique : Effect of Concentration and viscosity”, Int.J. ChemTech Res, Vol.7, No.01, pp 20-27, (2014)
 11. Abdul Razzak A. Ghazal¹, Mohammad Y. ^{2*}, Rabab Al-Sabbagh¹, Ibrahim Alghoraibi³ and Ahmad Aldiry⁴ “An evaluation of two types of nickel-titanium wires in terms of micromorphology and nickel ions’ release following oral environment exposure” Progress in Orthodontics (2015) 16:9
 12. Zoalfakar Almahmoud^{1*}, Ibrahim Alghoraibi², Tarek Zaerory¹,” Influence of complexing agent on the Morphology Properties of PbS Thin Films Studied by Atomic Force Microscopy”, IJAP, vol. (11), no. (2), April-June 2015, pp. 13-18.
 13. Zoalfakar Almahmoud^{1*}, Ibrahim Alghoraibi², Tarek Zaerory¹,” Controllable Synthesis of Lead sulfide Nanoparticles using HXAHc as Complexing Agen: Effect of the Concentration complexing Agent on

- Particle Size and Crystallinity”, Research Journal of Aleppo University. Basic Sciences Series, Vol.109 (2015).
14. Zoalfakar Almahmoud^{1*}, Ibrahim Alghoraibi², Tarek Zaerory¹,” study of the complexing agent (TEA) effect on the nanostructure and optical properties of PbS thin film”, Research Journal of Aleppo University. Basic Sciences Series, accepted, (2015).
 15. Zoalfakar Almahmoud^a, Ibrahim Alghoraibi^{b*}, Tarek Zaerory^a,” Investigation of Structure and Optical Properties of Chemically Deposited Nanoparticles PbS Thin Film at different Lead Concentrations”, Journal for the Basic Sciences, Damascus University accepted, (2015).
 16. Zoalfakar Almahmoud^a, Ibrahim Alghoraibi^{b*}, Tarek Zaerory^a,” Effect of the hydrazine hydrate concentration on structural and optical Properties of PbS nanostructures films synthesized by chemical solution deposition, “Journal for the Basic Sciences, Damascus University accepted, (2015).
 17. Zoalfakar Almahmoud¹, Ibrahim Alghoraibi²,” Influence of Complexing Agents on Structural Properties of PbS Thin Films Prepared by CSD Method”, IJAP, vol. (12), no. (1), January-March 2016, pp. 23-26.

Chapter 7

**RISKS AND BENEFITS OF SILVER
NANOPARTICLES FOR NANOMEDICINE
APPLICATIONS**

Elisa Panzarini, PhD and Luciana Dini, PhD*

University of Salento,
Department of Biological and Environmental Sciences and Technologies
Lecce, Italy

ABSTRACT

The unique physicochemical characteristics of metal nanoparticles (NPs) (i.e., catalytic activity, optical properties, electronic properties, antibacterial properties, magnetic properties) are gaining the interest of scientists for their wide applications (from microelectronics to human health). In particular, silver (that is the most studied and used), gold, titanium, zinc, etc. NPs are largely exploited for nanomedicine applications. The AgNPs antibacterial and antifungal properties allow them to be extensively used in medical devices and to be also present in several daily use commercialized products such as food and cosmetics. Indeed, silver and AgNPs are largely applied in the preparation of skin ointments and creams to prevent infection of burns and bloody wounds and silver-impregnated polymers are nowadays present in several implants. The most recent AgNPs applications for human health, are in the field of high sensitivity biomolecular detection, diagnostics, antimicrobials and

* Corresponding author: elisa.panzarini@unisalento.it.

therapeutics. During recent years, AgNPs have received significant attention in cancer management, being also suitable as theranostic agents.

Regardless of the broad potentiality of the AgNPs use, there is still a lack of information concerning the increase exposure to AgNPs of humans, animals, plants and environments and their eventual short- and long-term toxicity. Indeed, *in vitro* studies indicate toxicity of AgNPs for skin, liver, lung, blood, and germ mammalian cells, by inducing cell cycle progression genes, Reactive Oxygen Species (ROS) production, DNA damage and cell deaths that suggest the application of AgNPs as anticancer agent. It is known that AgNPs have a better cytotoxic effects on liver cancer cell lines compared to normal ones. AgNPs in *in vivo* studies in adult rats and mice can reach several organs and cause toxicity while elicit developmental and structural malformations in non-mammalian embryos. Thus, to overcome toxicity (largely due to the release of Ag ions from the NPs) and improve AgNPs performance a particular attention has been paid to the modality of synthesis. There is an increasing demand for *green synthesis* that ensures the absence of toxic byproducts. In fact, the approach used to synthesize AgNPs influences the response of cells by influencing the NPs surface characteristics. The NPs coating with molecules chosen among starch, glycans, PVP (poly(N-vinyl-2-pyrrolidone), citrate, polymers, etc. is pivotal to block the release of Ag ions.

In this work we will discuss the risks and the benefits of AgNPs to human health, in relation to nanomedicine by reviewing *in vitro* literature data and current applications in cancer theranostic.

INTRODUCTION

The field of nanotechnology, dealing with design, synthesis, and manipulation of particles structures ranging from approximately 1-100 nm in at least one dimension, is one of the upcoming areas of research in the modern field of material science. Novel applications of nanoparticles (NPs) and nanoproducts, by possessing novel and size-related physico-chemical properties compared their macro-scaled counterparts (Ju-Nam and Lead, 2008), are emerging rapidly in various fields, such as medicine, cosmetics, renewable energies, environmental remediation, biomedical devices and aerospace engineering (Gerber and Lang, 2006; Singh et al., 2009). Because of their widespread application, the nanotechnology market value is growing on a rapid and consistent basis with a predicted increase to \$3 trillion by 2020 (Sargent, 2012). Among the engineered NPs, silver-based ones (AgNPs) are the hit of the highest point as they are used in biosensing and imaging (Habouti et al., 2010), photonics (Hu and Chan, 2004), electronics (Alshehri et al., 2012), antimicrobial

(Chen et al., 2014), medical and consumer (Ahamed et al., 2010) products. The widespread exploitation of AgNPs is based on their distinctive physico-chemical properties (high electrical and thermal conductivity, surface-enhanced Raman scattering, chemical stability, catalytic activity and non linear optical behavior) (Krutayakov et al., 2008) and broad spectrum bactericidal and fungicidal activity (Ahamed et al., 2010). Recently, AgNPs have gained increased attention also in cancer applications including drug delivery, treatment, diagnosis, monitoring and control of disease and positive outcomes have been achieved rendering them very attractive also as theranostic agents (Sharma et al., 2015).

The counterpart of the positive effects of AgNPs use is their release into the environment, estimated at 14% of AgNPs used in consumer products, and their interactions with animals, including humans (Ahamed et al., 2010).

Thus, an understanding of the interactions between NPs and biological systems is of significant interest. In fact, the scientific community and industry has paid special attention to the research topic of AgNPs: from the database PubMed by using the keyword “silver nanoparticle”, it was found that there are a total of 10658 records up to 05 August 2016; in particular, the number of published papers has grown by nearly 93% from 2001 to 2011.

The *in vitro* toxicity of AgNPs has been evaluated in a wide range of studies but there is still a lack of consistent and reliable data; conversely, few data are still present about the effect *in vivo* mammalian models. Data *in vitro*, recently reviewed by Kim and Ryu (2013), corroborate that increased oxidative stress, apoptosis and genotoxicity are the main outcomes upon exposure to AgNPs. However, experimental design, i.e., manufacturing of NPs, purity of NPs solution, size distributions and coatings, cell lines tested, cell culture conditions, is different in each study. Moreover, there is in general a lack of thorough characterization of the AgNPs in cell medium. Ultimately, the synthesis method and the presence of residual contaminants could also account for the observed toxicity. In addition, three possible hypotheses about the toxicity created by AgNPs are still discussing: i) the toxicity depends on Ag ions released in aqueous environment, ii) the toxicity is independent on metal ions presence, iii) NPs release Ag ions inside cells as they dissolve, iv) AgNPs are toxic *per se* (Beer et al., 2012). Chemistry and material science are now the largest disciplines in the research areas of AgNPs; in fact, more and more studies in literature concord that particularly important in determining the biological interaction and impacts of AgNPs are their physico-chemical properties, including size, surface area, coating, charge, shape, agglomeration and dissolution rate that, in turn, are strictly dependent on synthesis methods

(Johnston et al., 2010). Currently, many methods have been reported for the synthesis of AgNPs, which can be categorized as chemical, physical, photochemical and biological (Tran et al., 2013). In recent years, the development of green processes, ensuring a synthesis free from the use of toxic chemicals as byproducts, is evolving into an important branch of nanotechnology.

In this chapter, we focus on reviewing the most important findings, both positive and negative, related to AgNPs use in medicine field, with particular attention to cancer management.

1. SYNTHESIS METHODS AND PROPERTIES OF AGNPs

Methods of synthesis of AgNPs. Many approaches have been introduced for the synthesis of silver nanostructures, including chemical, physical, photochemical and biological methods. Each of ones has advantages and disadvantages with common problems being cost, scalability, particle sizes and size distribution.

Chemical approach, including chemical reduction reactions, electrochemical techniques, and pyrolysis, represents the mostly used method and provides an easy way for synthesizing AgNPs in solution. The chemical synthesis of silver nanostructures in solution usually employs three main components: i) metal precursor, generally silver nitrate-AgNO₃, ii) reducing agents, widely used borohydride, sodium citrate, ascorbic acid, alcohol, and hydrazine compounds, iii) stabilizing/capping agents, e.g., glycans, PVP (poly(N-vinyl-2-pyrrolidone), citrate and polymers. The formation of colloidal silver from metal precursor requires two stages of nucleation and subsequent growth, that strictly dictate the size and the shape of AgNPs. In particular nucleation stage is pivotal to obtain monodispersed and uniform in size AgNPs and it can be controlled by acting on the temperature of reaction, pH, precursors, reducing and stabilizing agents (Chen et al., 2012; Dang et al., 2012).

By contrast, physical approach is the most useful method to produce AgNPs powder with nearly narrow size distribution by utilizing the physical energies, such as vapor condensation, Arc-discharge, energy ball milling method, and direct current (DC) magnetron sputtering as reducing agent (Asanithi et al., 2012). These methods permit to obtain large quantities of AgNPs in a single process without involvement of toxic chemicals. The major drawbacks are their high energy consumption for raising the environmental temperature around the

source material, a lot of time to achieve thermal stability and the costs for equipments.

Another method to synthesize AgNPs is represented by photochemical reactions, a clean process with high spatial resolution, that permit to control *in situ* generation of reducing agents and enable to fabricate the NPs in different mediums, such as emulsions, surfactant micelles, polymer films, etc. (Christy et al., 2012). The photochemical synthesis includes two distinct approaches: photophysical (top down) that prepares the NPs through subdivision of bulk metals and photochemical (bottom up) that generates the NPs from ionic precursors. Thus, the NPs can be formed in two ways: by direct photoreduction of a metal source or by reduction of metal ions using photo-chemically generated excited molecules and radicals (Christy et al., 2012).

Conversely to the methods above reported, biological synthesis method represents a very new and promising approach in green nanotechnology because it replaces the toxic reducing agents and stabilizer with nontoxic molecules (proteins, glycans, antioxidants, etc.) produced by living organisms, i.e., bacteria (e.g., *Shewanella oneidensis*, *Bacillus* species), fungi (e.g., *Trichoderma viride*, *Aspergillus terreus*), yeasts (e.g., *Lactobacillus* species) and plants (lemongrass, *Aloe vera*, tea, neem, lotus, *Cassia angustifolia*, *Daucus carota*) (Sintubin et al., 2012). Biological synthesis can be considered as an environmentally friendly approach and a low cost technique. Also, it is much faster respect chemical and physical techniques and it occurs at ambient temperature and pressure conditions. Irrespectively of organism used as source of molecules, cell wall is pivotal in biological synthesis; in fact, the negatively charged cell wall by reacting with positively charged Ag^+ bioreduces the metal ions to NPs (Sintubin et al., 2012). This process results from a defense mechanism of organisms against the metal toxicity. The major drawback of this approach is the low quantity of AgNPs produced.

Properties of AgNPs. As above reported, the widespread use of AgNPs in different products depends on the peculiar physico-chemical properties (Krutakov et al., 2008) of nanostructured silver and on its broad spectrum bactericidal and fungicidal activity. Silver nanoparticles have unique optical, electrical, and thermal properties deriving of their small size and are being incorporated into products that range from photovoltaics to biological and chemical sensors. Examples include conductive inks, pastes and fillers which utilize silver nanoparticles for their high electrical conductivity, stability, and low sintering temperatures. Additional applications include molecular diagnostics and photonic devices, which take advantage of the novel optical properties of these nanomaterials. An increasingly common application is the

use of silver nanoparticles for antimicrobial coatings, and many textiles, keyboards, wound dressings, and biomedical devices now contain silver nanoparticles that continuously release a low level of silver ions to provide protection against bacteria. There is growing interest in utilizing the optical properties of AgNPs as the functional component in various products and sensors. They are extraordinarily efficient at absorbing and scattering light and, unlike many dyes and pigments, have a color that depends upon the size and the shape of the particle. The strong interaction of the silver nanoparticles with light occurs because the conduction electrons on the metal surface undergo a collective oscillation when excited by light at specific wavelengths. Known as a localized surface plasmon resonance (LSPR), this oscillation results in unusually strong scattering and absorption properties. Oscillation of the free electrons results in radiative or nonradiative decay, which cause a strong visible light scattering or the conversion of photon energy into thermal energy respectively. The first decay mechanism is utilized in biodiagnostic and imaging, the latter one is exploited in therapeutic applications (Austin et al., 2014).

A unique property of spherical silver nanoparticles is that this LSPR peak wavelength can be tuned from 400 nm (violet light) to 530 nm (green light) by changing the particle size and shape, the local refractive index near the particle surface, the dielectric environment (Huang et al., 2010). Therefore, LSPR enables the development of photothermal and thermolytic laser therapies (Shi et al., 2014) as well as radiation therapy (Zhao et al., 2012) based on AgNPs exploitation. Also, LSPR property has been indicated as very attractive in photodynamic therapy (PDT), a process that encompasses the combined use of light, a light sensitive drug/compound (photosensitizer) and singlet oxygen, and is widely used in the treatment of several diseases (Agostinis et al., 2001). For example, Zhang et al. (2007) indicated that silver surface plasmons facilitates enhanced singlet oxygen generation by photosensitizer.

The most important property of AgNPs in biological context is their antimicrobials effects, including bacteria and fungi as well documented in literature (Ahamed et al., 2010) and viruses. Briefly, the AgNPs are effective biocide against a broad-spectrum bacteria including both Gram-negative and Gram-positive (Gram-negative > Gram-positive) in a dose dependent manner and the effect is independent of acquisition of resistance to antibiotics. Data about the antibacterial mechanism has not been fully understood, but concord that the AgNPs anchor to and penetrate the bacterial cell wall and modulate growth and death *via* three processes: 1) free silver ions inside the bacteria disrupt ATP production and DNA replication; 2) both silver ions and AgNPs

trigger generation of ROS; 3) AgNPs *per se* damage cell membrane (Jones et al., 2010). The antifungal activity of AgNPs is well-known, the mechanism has not yet been studied adequately and data include still few fungal species, including *Candida albicans*, *Candida glabrata*, *Trychophyton rubrum* and *Trychophyton mentagrophytes*, that are the major involved in nosocomial fungal infections in critically ill patients. AgNPs disrupt the integrity of cell membrane and, consequently, inhibit the normal budding process (Kim et al., 2009). In recent years, it has been reported a possible antiviral activity of AgNPs suggesting them as potential antiviral agents in the future (Galdiero et al., 2011). Most publication have suggested that AgNPs *in vitro* inhibit HIV-1, Tascaribe virus (TCRV), hepatitis B virus (HBV), recombinant respiratory syncytial virus (RSV), monkey pox virus, murine norovirus (MNV)-1, influenza A/H1N1 and H3N2 virus, Vaccinia virus and Herpes simplex virus (HSV)-1(Wei et al., 2015). The researchers concord that AgNPs could bind to outer proteins of viral particles, resulting in inhibition of binding and the replication of viral particles in cultured cells. For example, Elechiguerra et al. (2005) demonstrated that AgNPs interact with the HIV-1 by binding to the gp120 surface virus glycoprotein, resulting in the inhibition of the binding of virus to host cells and the consequent viral entry and replication. In this manner, AgNPs inhibit post-entry stages of the HIV-1 life cycle.

Apart from being an excellent anti-bacterial, fungal and viral agent, handful of studies claiming that AgNPs have immunomodulatory effects as well. They may change the production and release of some cytokines, and impact molecular signaling of immune cells although the intracellular pathways involved still remains largely not elucidated. Particularly interesting are the potential interactions between AgNPs and peripheral blood mononuclear cells (PBMCs), mainly consisting of lymphocytes (e.g., T-cells) and monocytes, that represent a well-defined subpopulation of host defense cells. They are able to release various inflammatory mediators, mainly pro-inflammatory cytokines, after interaction with metallic nanoparticles (Ercal et al., 2001). PBMCs respond differentially towards 24h of exposure to 70 nm-sized AgNPs with non-toxic concentrations dependent on the subtype (monocytes or lymphocytes). Primarily, monocytes accumulate AgNPs more than lymphocytes and release IL-6, IL-8 and TNF α , typical pro-inflammatory cytokines. In parallel, a significant decrement in the release of anti-inflammatory cytokine IL-1ra is detected. Conversely, AgNPs do not influence the release of T-cell-specific cytokines IL-2 and IL-4 (Greulich et al., 2011). Monocytes are perturbed by AgNPs exposure by increasing the release of interleukin 1 β , a cytokine that modulate lymphocytes proliferation and maturation (Yang et al., 2012).

Moreover, also in macrophages it has been demonstrated that AgNPs may modulate the pro-inflammatory IL-6 secretion, whose regulation is very important during infection and wound healing, by acting on Toll-like receptor (TLR) signaling (Castillo et al., 2008).

Very important, Nadworny et al., (2010) demonstrated that AgNPs have direct anti-inflammatory effects and improve the healing process in a porcine model of contact dermatitis. In fact, the presence of AgNPs reduce the production of pro-inflammatory cytokines interleukin-6 (IL-6), Tumor necrosis factor (TNF α) and interferon-gamma (IFN γ). Also in a human model it has been demonstrated the positive action of AgNPs on wound healing process. In fact, by using blood and skin biopsy samples from healthy male non-smoking volunteers undergoing plastic surgery it has been demonstrated that AgNPs sized 2 nm accelerate proliferation of keratinocytes, fibroblasts and lymphocytes (Joksic et al., 2016).

Moreover, AgNPs of 15 nm are able to reduce the release of IL-1 β , an important mediators of inflammatory response, when exposed to the human THP-1 monocytes (Simard et al., 2015).

Tian and coworkers (Tian et al., 2007) investigate the wound-healing properties of AgNPs in an animal model and found that rapid healing and improved cosmetic appearance occur in a dose-dependent manner. They demonstrate that AgNPs exert positive effects through their antimicrobial properties, reduction in wound inflammation, and modulation of fibrogenic cytokines. Moreover, it has been reported the ability of AgNPs to control collagen deposition and direct collagen alignment and spatial arrangement, that improv in the tensile properties of the repaired skin (Kwan et al. 2011). Nonetheless, the beneficial effects of AgNPs on wound healing remain unknown but data in literature provide a novel therapeutic direction for wound treatment in clinical practice.

2. APPLICATION OF AGNPs IN MEDICINE: BENEFITS

The wide availability of AgNPs has ensured their rapid application on medical practice, that can be grouped in diagnostic and therapeutic uses. Recently, an exploitation in theranostics is emerging.

Diagnostic application. Early diagnosis to any disease condition is vital to ensure an early treatment start that could result in a better chance of cure. This is particularly true for cancer, whose cases around the world is expected to increase to 21 million by 2030. In recent years, spectroscopic techniques has

been explored to distinguish benign and malignant lesions at the molecular level by reducing the number of biopsies patient trauma and medical cost. Moreover, the coupling to nanoproducts seems to be very promising. At the moment, AgNPs are exploited in two spectroscopic techniques: Surface-enhanced (anelastic) Raman Spectroscopy (SERS) and enhanced Rayleigh (elastic) scattering.

Surface-enhanced Raman Spectroscopy (SERS) is one of the highly sensitive analytical techniques for biomolecules (proteins, DNA and RNA) widely applied in a multitude of interdisciplinary scientific investigations such as chemistry, biology, medicine, environmental sciences and archeological applications (Tu et al., 2012). SERS consists in an anelastic scattering process in which a molecule simultaneously adsorbs a photon incident and emits a photon Raman with an energy level transition, leading to a frequency shift (wavelength, cm^{-1}) of the emitted photon. Because the energy levels are specific for each molecule, the peaks in the Raman spectra are representative of the underlying molecular structures and serve as molecular “fingerprints” for the analyte under investigation (Raman and Krishnan, 1928). Two approaches for SERS-based biomolecule detection exist: label-free, that directly acquires SERS spectra of biomolecules in the absence of Raman dyes, and extrinsic SERS labeling, that indirectly detect biomolecules by employing Raman labels (Han et al., 2012). Blood is an ideal analyte for the diagnosis of cancer since it is able to provide information on-going processes in various internal organs. The characteristics of cancer cells are expressed in specific changes in the quantity and/or conformation of nucleic acids, proteins, glycans and lipids. These changes are visualized in Raman spectra as changes in the intensities of the bands/peaks. There are several studies about the use of Raman spectroscopy on blood sample to detect breast cancer (Pichardo-Molina et al., 2006), cervical (Gonzalez-Solis et al., 2009), gastric (Shangyuan et al., 2011), leukemia (Gonzalez-Solis et al., 2010) as well as results obtained on biopsies to detect breast cancer (Gonzalez-Solis et al., 2011). One of the main problems of label-free SERS is its low sensitivity in detecting biological molecules at low concentrations because of the rather small cross-sections (10^{-30} cm^2) per molecule. Moreover, biological samples generate strong auto-fluorescence background that affects Raman signals, making them difficult or impossible to identify. In recent years, the SERS technique has been coupled to nanoengineered products, in particular AuNPs and AgNPs for their chemical inactivity, to enhance scattered intensity of signals. In fact, it has been demonstrated that the use of sensors of NPs of noble metals, such as Ag, Au, and Cu, improves the sensitivity of conventional SERS of 6-10 orders of

magnitude (Chan et al., 2003). AgNPs, AuNPs and CuNPs show an intense absorption band in the UV-vis when the frequency of incident photons is in resonance with the collective oscillation of conduction electrons. This implies a strong enhancement of the electromagnetic field on the surface of NPs that, in turn, enhances the Raman signals (Haes et al., 2004).

Several groups have applied AuNPs (Huang et al., 2010) or AgNPs (Feng et al., 2010; Feng et al., 2011; Lin et al., 2011; Li et al., 2014; Gonzales-Solis et al., 2013; Feng et al., 2015) to SERS technique for the diagnosis of several cancer types.

SERS coupled to AgNPs was reported for the first time in 2010 by Feng (Feng et al., 2010) to develop a simple blood test for non-invasive detection of nasopharyngeal cancer. AgNPs were directly mixed with blood plasma of patients with pathologically confirmed nasopharyngeal carcinomas (WHO type I, II, and III) and from healthy volunteers. The results from this study demonstrated the great potential of SERS blood plasma analysis as a tool for non-invasive detection of nasopharyngeal cancers. In fact, the Raman bands in the SERS spectra suggest cancer specific biomolecular differences in the blood plasma of nasopharyngeal cancer patients as compared to that of healthy subjects: an increase in the relative amounts of nucleic acid, collagen, phospholipids and phenylalanine and a decrease in the percentage of amino acids and saccharide contents. The sensitivity and the specificity of the test are 90.7% and 100% respectively (Feng et al., 2010). The same results have been obtained from Feng and coworkers by applying SERS technique and AgNPs on blood plasma samples from gastric cancer patients (Feng et al., 2011) and colorectal cancer and adenomatous polyps patients (Feng et al., 2015). Lin's group evaluated the usability of combining membrane electrophoresis with AgNPs-based SERS for detection and screening of gastric cancer. In this method, total serum proteins are isolated from blood plasma by membrane electrophoresis and mixed with AgNPs to perform SERS spectral analysis. The gastric cancer samples are unambiguously distinguished from healthy volunteers samples with both diagnostic sensitivity and specificity of 100% (Lin et al., 2011). A high diagnostic accuracy (around 90%) of SERS based on AgNPs technology in detection and screening has been demonstrated also for esophageal cancer. In particular, SERS bands indicated specific biomolecular changes (i.e., increase in the amounts of nucleic acids and phenylalanine, and decrease of saccharides and proteins contents) associated with cancer transformation (Li et al., 2014). Moreover, AgNPs-based SERS allows to early detect hepatocellular carcinoma (HCC), very difficult to diagnose due to the absence of recognizable physical symptoms, with less time-consumed and cost

then other traditional methods. The diagnostic sensitivity and specificity both were 84.6%. Finally, Gonzalez-Solis suggested that SERS could be a new technique to identify breast cancer cells. The study involved the tumor biopsies obtained from 5 patients who were clinically diagnosed with breast cancer. The isolated ill cells were added with AgNPs of 40 nm by sonication and subjected to Raman spectroscopy; chemical constituents of the cells, as phenylalanine, tyrosine, tryptophan and protein, and changes in the structure of DNA (adenine and guanine) in cancer patients are specifically detected (Gonzalez-Solis et al., 2013).

The major drawback in using AgNPs in SERS spectroscopy is the tendency of nanoparticles to form clusters and/or aggregates. Thus, recently it has been suggested the efficacy of nanostructured silver surfaces in the detecting both albumin and globulin in blood serum. The advantage of nanostructured surfaces consists in size and morphology simply tuning and this could be very promising in detecting cancer pathologies (Kralova et al., 2013).

Noble metal (Au and Ag)-based nanostructures exhibit enhanced Rayleigh (elastic) scattering originating from their LSPR, whose resulting scattered light is heavily dependent on the nanostructure shape and size (Jain et al. 2008). The enhanced scattered light provides several advantages when used as a biological imaging or sensing agent to visualize cancer cells. In fact, it is much brighter (4–5 orders of magnitude) than the most efficient fluorophores, resistant to photobleaching, and does not require expensive strong excitation sources. For example, Austin et al. (2011) utilized AgNPs enhanced Rayleigh light scattering process to image human oral squamous carcinoma (HSC-3) cells at dark field microscopy by using nuclear-targeted AgNPs, which are also capable to induce apoptosis.

Therapeutic application. Recently, studies about therapeutic applications of AgNPs in cancer management as antiproliferative agents in conventional, chemotherapeutic or radiotherapeutic, and non conventional, photodynamic and photothermal, therapies have gained increased attention. In fact, toxicity itself, that created a negative perception of the AgNPs use, is very interesting in cancer therapies since it can counteract cancer progression through two processes: directly, by directly killing ill cells, or indirectly, by inhibiting angiogenesis. Positive outcomes have been achieved when incorporating AgNPs into cancer medicine (Austin et al., 2014).

Silver nanoparticles (AgNPs) provide a unique approach to induce antiproliferative effect on several cancer cell lines, including leukemia, breast, hepatocellular, lung, skin and oral. AgNPs size, shape, surface coatings, cell type, time of treatment and dose. Table 1 summarizes the potential therapeutic

applications of AgNPs as antiproliferative treatment reported in recent publications.

In summary data reported in the studies in Table 2 indicate that exposure to AgNPs causes cytotoxicity by elevating ROS levels and increasing lipid peroxidation, and genotoxicity by inducing DNA and chromosomal damage (Figure 1).

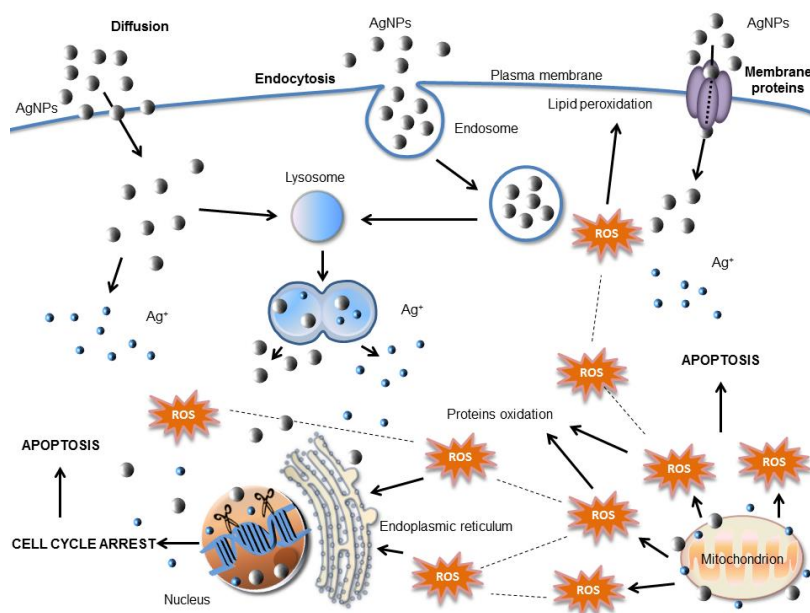


Figure 1. Mechanism of toxicity of AgNPs. AgNPs enter into the cells *via* three different routes: diffusion, endocytosis and membrane proteins. Into the cytoplasm, AgNPs can pass into lysosomes, nucleus or mitochondria. In cytoplasm or into lysosomes, AgNPs can also dissolve in Ag⁺ that amplify the cell damage. Into mitochondria, AgNPs cause imbalance of respiratory chain and formation of ROS, leading to apoptosis. ROS can also negatively interfere with endoplasmic reticulum, oxidize proteins, such as cytoskeleton and plasma membrane proteins, and peroxide the plasma membrane proteins, leading to necrosis. Finally, into the nucleus, AgNPs and Ag⁺ damage the DNA causing cell cycle arrest and apoptosis.

Table 1. Anticancer effect of AgNPs *in vitro*

Cancer type	Cell line	Size (nm)	Surface coating	Dose	Exposure time (h)	Effects	Refs.
Leukemia	AML	3, 11, 30	PVP	Up to 10 µg/mL	24	Size and dose dependent reduced cell viability Oxidative stress Mitochondrial damage	Guo et al., 2013
	HL-60	4.7, 42		Up to 500 µg/mL	24	Size and dose dependent reduced cell viability (4,7 > 42) Oxidative stress	Avalos et al., 2014
	Jurkat T	<100		Up to 1 mg/L	24	Cell cycle arrest DNA damage Apoptosis	Eom et al., 2010
Breast	MCF7	N.D.	Grenetine	3.5 µg/mL	5	Dose dependent Reduced cell viability	Franco-Molina et al., 2010
	MCF7	14.74		500 µg/mL	4	Reduced cell viability Apoptosis	Jang et al., 2016
	MCF7	12	PEG-methotrexate	Up to 500 µg/mL	24	Dose dependent reduced cell viability Apoptosis	Muhammad et al., 2016
	MDAMB-231	5		6 µg/mL	24	Reduced cell viability Plasma membrane leakage	Gurunathan et al., 2013a
	MDAMB-231	2-10		8,7 µg/mL	24	Dose dependent cell growth inhibition	Gurunathan et al., 2013b
Hepatoma	HepG2	30	β-D-Glucose/Sucrose	1,35 µg/mL 6,75 µg/mL	Up to 24	Dose and time dependent reduced cell viability Dose and time dependent oxidative stress	Vergallo et al., 2016
	HepG2	20		1-20 µg/mL	24	Oxidative stress	Sahu et al., 2014

Table 1. (Continued)

Cancer type	Cell line	Size (nm)	Surface coating	Dose	Exposure time (h)	Effects	Refs.
	HepG2	20		1-20 µg/mL	24	Oxidative stress	Sahu et al., 2014
	HepG2	5.9, 23.8, 47.5		Up to 50 µg/mL	24	Oxidative stress Cell cycle arrest Apoptosis	Liu et al., 2010
	HepG2	20-40		2,764 µg/mL	24	Cell growth inhibition	Faedmaleki et al., 2014
	HepG2	50	Citrate PVA	50 mg/L	24	Dose and coating dependent reduced cell viability (cit-AgNPs > PVA-AgNPs) oxidative stress	Vrcek et al., 2016
	HepG2	4.7, 42		0,84-500 µg/mL	24	Size dependent reduced cell viability (4,7 > 42) Oxidative stress	Avalos et al., 2014
	HepG2	10, 75	Citrate PVP	0,001-30 µg/mL	24	Size and coating dependent reduced cell viability (10 > 75; cit-AgNPs > PVP-AgNPs) Oxidative stress Inflammatory response	Prasad et al., 2013
	HepG2	20, 50		12.5, 25, 50, 100, 200 µg/mL	48	Dose dependent reduced cell viability Oxidative stress Mitochondrial damage	Xin et al., 2015
Lung	A549	30-50	PVP	0-20 µg/mL	24	Dose dependent mitochondrial function reduction	Foldbjerg et al., 2011
	A549	100		Up to 200 µg/mL	24, 48	Reduced cell viability Oxidative stress	Chairuangkitti et al., 2013

Cancer type	Cell line	Size (nm)	Surface coating	Dose	Exposure time (h)	Effects	Refs.
						mitochondrial function reduction subG1 population increase cell cycle arrest in S phase	
	A549	20, 50		12.5, 25, 50, 100, 200 µg/mL	48	Dose dependent reduced cell viability Oxidative stress Mitochondrial damage	Xin et al., 2015
	A549	21,74	PVP	10 µg/mL	Up to 72	DNA methylation Time and dose dependent reduced cell viability	Blanco et al., 2016
	A549	N.D.		Up to 50 µg/mL	48	Cell migration inhibition Apoptosis Oxidative stress	Aceituno et al., 2016
	H157	10-20	Sugar	3,6 µM	48	Cell growth inhibition	Nazir et al., 2011
Oral	HT144	10-20	Sugar	0,36 µM	48	Cell growth inhibition	Nazir et al., 2011
Skin	HSC-3	35	Peptide	0,1 nM	24	DNA break subG1 population increase	Austin et al., 2011
	HaCat	35	Peptide	0,1 nM	24	DNA fragmentation subG1 population increase	Austin et al., 2011
Lymphoma	Dalton's lymphoma ascites cell lines	50		500 nM	6	DNA fragmentation Apoptosis	Sriram et al., 2010
	U937	13.2		Up to 8 µg/mL	4, 24	Dose and time dependent reduced cell viability	Kaba et al., 2015
Colon	HT29	172.6	Chitosan	Up to 48 µg/mL	Up to 24	Oxidative stress Apoptosis Mitochondrial damage	Sanpui et al., 2011

Complimentary Contributor Copy

Table 1. (Continued)

Cancer type	Cell line	Size (nm)	Surface coating	Dose	Exposure time (h)	Effects	Refs.
	HCT-116	24-150		100	24	Apoptosis subG1 population increase	Kuppusamy et al., 2016
Cervix	HeLa	30	β -D-Glucose	1.35, 13.5 μ g/ml	Up to 48	Oxidative stress Cell cycle arrest (G2/m and S phases) subG1 population increase Dose and time dependent reduced cell viability Morphological changes	Panzarini submitted
	HeLa	30	β -D-Glucose/ sucrose	1.35, 13.5 μ g/ml	Up to 48	Apoptosis Autophagy Necrosis Oxidative stress Dose and time dependent reduced cell viability Morphological changes	Panzarini et al., 2015
	HeLa	30	β -D-Glucose, β -D-Glucose/ sucrose	Up to 13.5 μ g/ml	Up to 72	Dose, time and coating (β -D-Glucose > β -D-Glucose /sucrose) dependent reduced cell viability	Dini et al., 2011
	HeLa	N.D.		Up to 0,16 mg/mL	48, 72	Morphological changes Oxidative stress Mitochondrial damage	Pandurangan et al., 2016
	HeLa	13.2		Up to 8 μ g/mL	4, 24	Dose and time dependent reduced cell viability	Kaba et al., 2015
	HeLa	40		Up to 250 μ g/mL	24	Morphological changes Oxidative stress Dose and time dependent	Vasanth et al., 2015

Cancer type	Cell line	Size (nm)	Surface coating	Dose	Exposure time (h)	Effects	Refs.
						reduced cell viability Apoptosis	
Ovarian	A2780	16-20	Salinomycin	4 µg/mL	24	Oxidative stress Apoptosis Mitochondrial damage Autophagy	Zhang et al., 2016
Cancer type	Cell line	Size (nm)	Surface coating	Dose	Exposure time (h)	Effects	Refs.
Prostate	PC3	35-98	tannins, phenols, flavonoids, triterpenoids	Up to 98 µg/mL	48	Dose dependent reduced cell viability Apoptosis	Prasannaraj et al., 2016
	PC3	9-32		2–30 µg/mL	72	Dose dependent reduced cell viability Apoptosis	He et al., 2016
Osteosarcoma	U2Os, Saos-2	10-70	Citrate	15–20 µM	24, 48	Mitochondrial damage Apoptosis	Kovacs et al., 2016

PVP: polyvinylpyrrolidone; PVA: polyvinylalcohol; PEG: polyethylene glycol

The interaction between nanomaterials and cells, the cellular uptake, and subsequent toxic effects are crucial issues in AgNPs-induced toxicity. To induce biological effects NPs must be attached to or enter into and distribute within cells. Literature data report that NPs can be internalized by the cells and different mechanisms of entrance, both endocytosis (like macropinocytosis, clathrin-mediated, caveolae-mediated and caveolae-independent pathways), passive diffusion, and pore-mediated transfer, have been found, mainly depending on the specific NPs investigated (chemical nature, method of synthesis, size, shape, surface coating, etc.) (Sahay et al., 2010). The major target organelles are endosomes and lysosomes (Zhang et al., 2014). Upon interaction with acidic environment of lysosomes, AgNPs induce ROS, including superoxide anions (O_2^-), hydroxyl radicals ($\bullet OH$), and hydrogen peroxide (H_2O_2), production (Singh et al., 2012). Thus, ROS diffuse into the cytoplasm and result in oxidative damage to proteins and other organelles, such as mitochondria. In particular, H_2O_2 leads to dissolution of AgNPs and to accumulation of Ag^+ in lysosomes. AgNPs and Ag^+ can escape from lysosomes, amplifying the increase of ROS in cytoplasm, that, in turn, allow to further dissolution of AgNPs and production of Ag^+ . Both silver nanoform and ionic one interact with thiol groups of molecules present in cytoplasm, plasma membrane and mitochondrial membranes causing the release of lipid peroxide which amplifies the permeability of membranes (Zhang et al., 2014). In addition, ROS mediate the release of Ca^{2+} from endoplasmic reticulum (ER) leading to imbalance of calcium homeostasis (Asharani et al., 2009). In this manner four death pathways can be elicited: i) necrosis, via rupture of plasma membrane; ii) mitochondrion-dependent apoptosis, via alteration of electron transfer; iii) lysosome-mediated apoptosis via rupture of lysosomal membrane; iv) ER-mediated apoptosis. Moreover, AgNPs present in cytoplasm can diffuse into the nucleus through nuclear pore complexes leading directly to DNA and chromosomal damage (Asharani et al., 2009). In the nucleus, AgNPs can dissolve and form Ag^+ , able itself to damage DNA (Guo et al., 2013).

Proliferation, as well as metastatic spread, of cancer cells strictly depend on the construction around the tumor mass of a blood vessels network, a process called angiogenesis that plays a crucial role in several pathological conditions, including tumor growth and metastasis. Tumor cells demand higher oxygen and their glucose requirement is also higher than normal cells, and during the growth of solid tumor new blood vessels also arise rapidly to fulfil the raised requirement of nutrients. Hence targeting the formation of new blood vessel formation leading to deprived nutrition and oxygen supply leads to inhibit growth of tumor. Currently, several antiangiogenic drugs are used but still there

is a modest positive outcome with the use of these drugs on some clinical trials and no long-term survival benefits have been documented as yet. Moreover, when used in combination with chemotherapy or radiation therapy, these drugs tend to increase survival since the destruction of blood vessels also impairs that chemotherapeutics reach tumor mass (Nishida et al., 2006). New therapeutic strategies are urgently required. In the last decade, some studies reported the anti-angiogenic property of noble metal nanoparticles, including silver, that can be explored as a potential therapeutic against pathological angiogenesis and solid tumors by targeting the vasculature. Gurunathan et al. (Gurunathan et al. 2009) reported the anti-angiogenesis activity of 50 nm AgNPs in bovine retinal epithelial cells (BREC) as well as in a matrigel mouse model. AgNPs inhibited cellular proliferation and migration in VEGF-induced angiogenesis, in BRECs, due to PI3K/Akt pathway inhibition. The effect is similar to this induced by a natural antiangiogenic molecule PDGF. 16 nm biogenic AgNPs synthesized using *Saliva officinalis* extract as reducing agent display anti-angiogenesis properties on chick chorioalantoic membrane (CAM). In fact, the number and length of the blood vessels, as well as the weight of the embryos and hemoglobin content reduced significantly compared to the control, dose dependently (Baharara et al., 2014). The same results have been observed on chick CAM by using AgNPs manufactured by green synthesis using *Azadirachta indica* (neem) leaves extract (Khandia et al., 2015). A poly(lactic-co-glycolic acid) (PLGA)-based uniform (50–100 nm) hybrid nanoparticle (QAgNP), prepared by single emulsion solvent evaporation method with bioactive small molecule quinacrine (QC) in organic phase and silver (Ag) in aqueous phase, possess anti tumor activity and reduce angiogenesis in H-357 oral cancer cells and OSCC-cancer stem cells (Satapathy et al., 2015).

Newly emerging applications of AgNPs are as photosensitizers (PSs) in photodynamic therapy (PDT) or in photothermal therapy (PTT) and/or radiosensitizers in radiation therapy. In fact, silver, like gold, is a high-Z element that has potential to react with both nonionizing and ionizing radiation on the basis of the LSPR.

PDT is an approach that has gained a significant clinical applications in cancer treatment in the last quarter of a century because of its selectivity and thanks to the high PSs affinity to tumor tissue, and the local illumination of the tumor area and finally to the normal tissue regeneration at the end of the treatment after applying PDT (Agostinis et al., 2011). PDT killing of cancer cells is based on the formation of highly reactive toxic singlet oxygen ($^1\text{O}_2$) upon photoirradiation of PSs. Yet PDT appears to have its own limitations that vary from the penetration limit of the light itself, skin sensitivity and the sub

therapeutic dose accumulated in the cancerous tissue. Nanotechnology-based PS delivery represents an emerging approach to improve the outcome of cancer PDT as development of the nanotechnology-based drug delivery systems can facilitate precise and therapeutically effective PS intracellular delivery (Panzarini and Dini., 2015). In 2007, Zhang (Zhang et al., 2007) report for the first time silver enhanced $^1\text{O}_2$ generation by Rose Bengal, an efficient PS for PDT (Panzarini et al., 2011a and 2011b; 2013; 2014). The study demonstrated that Rose Bengal in close proximity to Silver Island Films can generate more $^1\text{O}_2$ (three-fold increase than control sample without silver) due to coupling to silver surface plasmons (Zhang et al., 2007). In the recent years it has been demonstrated the potentiality of AgNPs in improving PDT outcomes but the studies are yet very few. AgNPs used in conjunction with protoporphyrin IX (PpIX), a photosensitizer, enhance photodynamic treatment efficiency by two orders of magnitude compared to free PpIX. PDT enhancement depends on the spectral overlap between the LSPR of the AgNPs and PpIX, which increased the quantum yield of $^1\text{O}_2$ produced by PpIX in HSC-3 human squamous carcinoma cells (Hayden et al. 2013). El-Hussein demonstrate that also AgNPs activated at 635 nm alone are photodynamically efficient in killing breast (MCF-7) and lung (A549) cancer cells (Mfouo-Tynga et al., 2014; El-Hussein et al., 2015; 2016). The PDT-induced cytotoxicity of Ag NPs has shown to be size and shape dependent (Vankayala et al., 2013).

It has been revealed that AgNPs show potential for photothermal therapy (PTT) upon laser illumination. PTT is a minimally-invasive therapy in which photon energy is converted into heat to kill cancer. AgNPs have a high ability to absorb NIR irradiation and perform PTT of the A549 cells without destroying the healthy cells and the surrounding normal tissues (Wu et al., 2013). Moreover, also grapheneoxide@AgNPs coated with PEG2000 and loaded with doxorubicin show very high chemophotothermal therapeutic efficacy against an *in vivo* murine tumor model without toxic effects to normal organs (Shi et al., 2014).

Given the physicochemical LSPR property AgNPs have attracted much interest also in radiotherapy. Xu et al. (2009) tested the radiosensitization effects of AgNPs with different sizes (20, 50, and 100 nm) in glioma cells (rat C6 and human SHG-44 glioma cells, human glioblastoma U251 cells) and demonstrated that AgNPs could function to enhance radiation-induced necrosis of cells. Thenceforth, several similar studies proved that AgNPs had radiation sensitization effect on MGC803 cancer gastric cells (Huang et al., 2011), U231 breast cancer cells (Lu et al., 2012), C6 cells (Liu et al., 2012) and A549 lung cancer cells (Ma et al., 2013) and MCF7 breast cancer cells (Elshaw et al.,

2016). The effects of AgNPs in combination with ionizing radiation (IR) leads to death via DNA damage in triple-negative breast cancer (TNBC), an aggressive, heterogeneous subclass of breast cancer typically of basal origin (Swanner et al., 2015). Finally, AgNPs loaded with C225 epidermal growth factor receptor combined with X-ray treatment increase the sensitivity of human nasopharyngeal carcinoma cells (CNE) to irradiation (Zhao et al., 2012).

Theranostic application. The term “theranostics” is the combination of the words, therapeutics and diagnostics, and represents a fairly new but revolutionary in the field of cancer therapy. Theranostics is the last frontier in nanomedicine: the nanosystems used in theranostics have multiple functions, such as diagnosis, delivery of targeted therapy and monitoring of the therapeutic response in a single setting by using combinational strategies. In this manner, the clinicians can identify responders and nonresponders by imaging tumors during the course of therapy allowing personalized medicine and take diagnosis from the laboratory to the “point of care” (Caldorera-Moore et al., 2011). A comprehensive review of the preclinical most relevant application of theranostic nanomedicines are reported in (Lammers et al., 2011). In general, classical drug delivery systems, such as liposomes, micelles, and NPs, can be double co-loaded with drugs and contrast agents. In general, in designing multifunctional nanosystems for cancer therapy drugs, DNA and different imaging agents, including fluorescent dyes, near-infrared (NIR) dyes, and radioisotopes can be attached at the surface of particles by using chemical functional groups present on the surface of particle or on the coated polymeric matrix. To improve the specificity of functionalized particles, antibodies against specific receptors present on the surface of cancer cells can be attached. When particles interact with cancer cells, they are internalized; by applying an external stimulus, such as magnetic field or light, tumor imaging can be obtained whereas attached drugs trigger cancer cell death.

In recent years, metal NPs, including iron, gold, silver, and titanium, have gained significant attention as theranostics because of their unique physical and chemical properties (Sharma et al., 2015). For example, the photoluminescence or superparamagnetic properties of metal NPs are useful for imaging, whereas the ability to kill cancer cells *via* ROS production or hyperthermia generation can be exploited as therapeutics.

As above reported, AgNPs are plasmonic structures capable to absorb and scatter the incident light: the portion of absorbed light can be explored to photothermally kill the cancer cells, whereas the scattered one can be used to image cancer cells. Moreover, Ag is a free electrons system that oscillate coherently at a plasma frequency, upon irradiation by an electromagnetic field.

The oscillations (plasmon) by interacting with visible light exhibit SPR that can be tuned to any wavelength in the visible spectrum (Evanoff et al., 2005).

In the therapeutic field (reported above), the main properties of AgNPs exploitable as theranostics is represented by the ability of NPs to deplete proteins involved in antioxidant defense mechanism, like glutathione and thioredoxin. In this manner, ROS accumulate into the cells and initiate responses leading to cell death *via* destruction of mitochondria (Mohammadzadeh, 2012).

Although AgNPs are indicated as very promising in theranostics because of their properties, there are very few studies about cancer theranostics that make them suitable for cancer diagnosis and therapy. For example, it has been demonstrated that biocompatible chitosan-coated AgNPs labeled with para-aminothiophenol (pATP) Raman reporter molecule and conjugated with folic acid were efficiently targeted inside NIH: OVCAR-3 human ovary cancer cells, where the SERS identity of the particles is highly conserved. An efficient specific therapeutic response has achieved by irradiating the nanoparticle-treated cells with a continuous wave-nearinfrared (cw-NIR) laser in resonance with their plasmonic band allowing a hyperthermia treatment (Boca-Farcau et al., 2014). Mukherjee and coworkers (Mukherjee et al., 2014) have designed a simple and efficient bio-synthesized silver AgNPs (4-in1-system) obtained by the reduction of AgNO₃ solution by using *Olox scandens* leaf extract in a green chemistry approach. The synthesized AgNPs exhibit multifunctional biological activities (4-in-1 system): anti-bacterial, anti-cancer, drug delivery vehicle, and imaging facilitator. In fact, these AgNPs: (i) show enhanced antibacterial activity compared to chemically synthesized ones; (ii) show anti-cancer activities against different cancer cells, i.e., A549 human lung cancer cells, B16 mouse melanoma cells, and MCF7 human breast cancer cells; (iii) are biocompatible to H9C2 rat cardiomyoblast normal cells, HUVEC human umbilical vein endothelial cells and CHO Chinese hamster ovary cells which indicates a promising application as drug delivery vehicle; (iv) conserve bright red fluorescence once internalized by the cells that could be utilized to detect the localization of drug molecules inside the cancer cells (diagnostic approach). The role of the *Olox scandens* leaf extract in synthesizing AgNPs used in this study is pivotal to reach the advantageous properties above reported. The phytochemicals, as oleanolic acid, oleanolic acid, β -sitosterol, octacosanol, glucosides of β -sitosterol, etc. stabilize the AgNPs ensuring their good biocompatibility (Balakrishna et al., 1983) and exhibit antiproliferative activity against cancer cell lines (Ju et al., 2004; Awad et al., 2000; Thipperswamy et al., 2008). The *Olox scandens* leaf extract is an important herbal plant useful in traditional medicine as anti-cancer (Ju et al., 2004; Awad et al., 2000;

Thipperswamy et al., 2008), anti-bacterial (Duraipandiyan et al., 2006) and to treat headache (Jeyaprakash et al., 2011) and psoriasis (Venkata Subbaiah et al., 2012). Finally, *Olex scandens* leaf extract contain molecules red fluorescent that allow to localize AgNPs inside the cells. Locatelli and coworkers have reported the synthesis of novel theranostic agent based on a multifunctional nanocomposite formed by polymeric nanoparticles (PNPs) containing two cytotoxic agents, the drug alisertib (Ali@) and AgNPs, conjugated with a chlorotoxin (Cltx), an active targeting 36-amino acid-long peptide that specifically binds to MMP-2, a receptor overexpressed by brain cancer cells, and ^{99m}Tc-radiolabeling that allow to see the *in vivo* biodistribution. The effects of this formulation has been evaluated on U87MG human glioblastoma astrocytoma epithelial like cells (*in vitro*) and on U87MG tumor bearing mice (*in vivo*). This AgNPs-based device promotes a specific targeting by Cltx, a synergistic toxic effect of Ali@ and AgNPs after 48 and 72h of the treatment eliciting the death of ill cells and the reduction of cancer mass, and image of cancer cells (Locatelli et al., 2014). Recently, a formulation of paracetamol dimer, generally considered as nontoxic, encapsulated with fluorescent silver nanocluster (AgNCs) embedded composite nanoparticles where it acts as a prodrug has been demonstrated to be very promising as theranostic nanocarriers. In fact, ROS produced inside HeLa and A549 lung cancer cells by silver nanocluster convert prodrug into a toxic metabolites that kill the cells via apoptotic cell death (therapeutic approach). Moreover, it is possible to conjugate folic acid with these composite NPs allowing to distinguish between two different cancer cell lines such as HeLa, which overexpresses folic acid receptors, and A549, which down-regulates its expression, on the basis of the fluorescence intensity of AgNCs (diagnostic approach) (Kumar et al., 2016).

3. APPLICATION OF AGNPs IN MEDICINE: RISKS

Although AgNPs have been found to be promising for diagnostic, therapeutic and theranostic purposes in cancer field, their toxicity remains an issue. Physico-chemical and biological activities of AgNPs dictate their widespread use in different fields, from environmental treatments (e.g., air disinfection, water disinfection, groundwater and biological wastewater disinfection) to surface disinfection (e.g., silver-nanoparticle-embedded antimicrobial paints, antimicrobial surface functionalization of plastic catheters, antimicrobial gel formulation for topical use, antimicrobial packing paper for

food preservation, silver-impregnated fabrics for clinical clothing) (Tran et al., 2013).

The use of AgNPs for the purposes above reported and the same characteristics rendering AgNPs so attractive ignite to concerns that the fate of NPs could create a new risk for humans and/or the environment. For example, the high surface to volume ratio of NPs by enhancing the surface properties increases the interaction with serum, saliva, mucus, or lung fluid components making them potentially more reactive than larger particles (Maynard et al., 2011). Also, the main doubt relies on the release of silver metal ions (Ag^+), since the high surface area increases the probability that silver ions are released from the NPs as both solubility and dissolution kinetics may vary as a function of size (Mudunkotuwa and Grassian, 2011). It is well known that silver is very toxic for biological organisms and yet it is not clear to which degree the toxicity depends on silver ions or AgNPs. To overcome this, AgNPs can be synthesized by design a capping/functionalization around the nanoparticle that, by interfering with dissolution process, limit or inhibit the release of Ag^+ . Recently, among surface coatings, such as starch, glycans, PVP (poly(N-vinyl-2-pyrrolidone), citrate, polymers, etc. there is an increasing interest in using carbohydrates as biomimetic molecules on the surface of NPs because of their double function: glycans functionalization results in NPs without traces of toxic chemicals, glycans on the NPs surface serves as targeting molecules and mediates cellular responses (Kennedy et al., 2014; Marradi et al., 2013; Chiodo et al., 2014). In addition, also media chemical composition could interfere with dissolution degree of AgNPs. A number of papers collected in Table 2 report studies on the dissolution behavior in different media, from water to complex culture media (Sotiriou et al., 2011; Xiu et al., 2012; Liu et al., 2010; Liu et al., 2010; Li et al., 2010; Kittler et al., 2010; Ho et al., 2010; Sotiriou et al., 2010; Levard et al., 2011; Ho et al., 2011; Zook et al., 2011; Zhang et al., 2011; Xiu et al., 2011).

In general, the dissolution degree strictly depends on AgNPs size, capping molecules, chemical composition of medium, and molecular oxygen (O_2) and hydrogen peroxide (H_2O_2) content. In fact, dissolved O_2 oxidizes metallic silver at low extent, conversely a complete oxidation occurs in the presence of H_2O_2 ; reducing agents as thiol- or selenide-containing molecules, such as cysteine, prevent the dissolution by blocking the surface of AgNPs whereas glucose only

Table 2. Results of dissolution experiments in different media reported in literature (Adapted from Loza et al., 2014)

AgNPs Coating	Diameter (nm)	Immersion medium	Temperature (°C)	Immersion time (h)	Dissolution degree (%)	Refs.
Citrate	4,8	Air-saturated distilled water [O ₂] = 9,1 mg/L; pH = 5,68	4	120	36	Liu et al., 2010a
		Air-saturated distilled water [O ₂] = 9,1 mg/L; pH = 5,68	25	120	100	Liu et al., 2010a
		Air-saturated distilled water [O ₂] = 9,1 mg/L; pH = 5,68	37	120	96	Liu et al., 2010a
		Air-saturated distilled water [O ₂] = 9,1 mg/L; pH = 5,68	25	240	100	Liu et al., 2010a
		Air-saturated distilled water [O ₂] = 9,1 mg/L; pH = 5,68	25	3000	100	Liu et al., 2010a
		Acetate buffer, pH = 5,6	25	24	15	Liu et al., 2010b
		Acetate buffer 0,4 mM citrate, pH = 5,6	25	24	9	Liu et al., 2010b
		Acetate buffer 10 mM citrate, pH = 5,6	25	24	7	Liu et al., 2010b
		Acetate buffer 0,4 mM Na ₂ S, pH = 5,6	25	24	<1	Liu et al., 2010b
		Acetate buffer 4 mM 11-mercaptoundecanoic acid pH = 5,6	25	24	0	Liu et al., 2010b
		Boric acid and bicarbonate low ionic strength seawater buffer, pH = 7,90	25	192	54	Liu et al., 2010a
Natural seawater, pH = 7,90	25	192	38	Liu et al., 2010a		

Table 2. (Continued)

AgNPs Coating	Diameter (nm)	Immersion medium	Temperature (°C)	Immersion time (h)	Dissolution degree (%)	Refs.
	20	Modified Hoagland medium [O ₂] = 7,8 mg/L; pH = 5,6	25	336	40	Zhang et al., 2011
	23	DMEM	25	22	7	Zook et al., 2011
	40	Modified Hoagland medium [O ₂] = 7,8 mg/L; pH = 5,6	25	336	21	Zhang et al., 2011
	80	Modified Hoagland medium [O ₂] = 7,8 mg/L; pH = 5,6	25	336	8	Zhang et al., 2011
	85	Water	25	336	15	Kittler et al., 2010
		Water	25	410	12	Kittler et al., 2010
		Water	37	307	56	Kittler et al., 2010
		Water	37	444	53	Kittler et al., 2010
PVP	4-5	Synthetic gastric acid pH = 1,12	37	24	98	Liu et al., 2012
		Pseudoextracellular fluid pH = 7,52	37	24	80	Liu et al., 2012
	23	DMEM	25	22	76	Zook et al., 2011
	39	0,01 M NaNO ₃ pH = 7	25	720	1,9	Levard et al., 2011
	50	Water	5	411	9	Kittler et al., 2010
		Water	5	149	8	Kittler et al., 2010
		Water	25	134	48	Kittler et al., 2010
		Water	25	81	52	Kittler et al., 2010
		Water	25	42	43	Kittler et al., 2010
		Water	37	27	89	Kittler et al., 2010
	Water	37	11	68	Kittler et al., 2010	

AgNPs Coating	Diameter (nm)	Immersion medium	Temperature (°C)	Immersion time (h)	Dissolution degree (%)	Refs.
	70	Oxygen-free water	25	1660	2	Loza et al., 2014
		0,9% NaCl	25	3670	8	Loza et al., 2014
		PBS	25	3670	4	Loza et al., 2014
		10 mM H ₂ O ₂	25	1821	90	Loza et al., 2014
		Cysteine 1g/L	25	4366	0	Loza et al., 2014
		Glucose 1g/L	25	4366	61	Loza et al., 2014
PVP sulphidated	39	0,01 M NaNO ₃ pH = 7	25	730	0-0,27	Levard
5 kDa PEG	23	DMEM	25	22	11	Zook et al., 2011
20 kDa PEG	23	DMEM	25	22	9	Zook et al., 2011
Dextran	23	DMEM	25	22	67	Zook et al., 2011

PVP: poly(N-vinyl-2-pirrolidone); PEG: polyethylene glicole

slows down the dissolution; finally, the presence in the medium of chloride or phosphate salts complex silver ions and precipitate them as silver salts (Loza et al., 2014). The most important question is the real impact of AgNPs to human and his environment. Several studies report the toxic effect of AgNPs on model animals considered as bioindicators, such as crustaceans (*Daphnia magna*), fish (*Danio rerio*), protozoa (*Eisenia fetida*) (Ahamed et al., 2010) and sea urchins (*Paracentrotus lividus*) (Manno et al., 2013; Panzarini et al., 2013). In these animals, AgNPs cause reproductive failure, developmental malformations and morphological deformities. Due to the nanometric sizes, AgNPs possess a great mobility and enter humans through different routes, such as inhalation, ingestion, skin, etc. Since AgNPs easily pass the biologic membranes, they can translocate from the route of exposure to other vital organs and penetrate into cells. Independently on entry routes, the liver is the preferential organ target, followed by spleen, lungs and kidney. AgNPs have no significant biological function in humans and therefore can cause damage to several organs. Data in literature report that AgNPs are toxic for digestive, respiratory, urinary, reproductive, cardiovascular and nervous systems, and sensory organs. AgNPs-induced toxicity includes oxidative stress, DNA damage and apoptosis. For example, the ingestion of AgNPs in mice leads to destruction of microvilli and loss of small intestine mucosa functionality, that affect absorption by intestinal epithelium causing weight loss (Shahare et al., 2013). Similarly, another study states that AgNPs induce changes in histological sections of liver and apoptosis (Al Gurabi et al., 2015). Also, AgNPs exposure causes a dose dependent mitochondrial dysfunction leading to permanent or temporary hearing loss; or destruction of retinal structure (Sodertjerna et al., 2014). Lung cells (Gliga et al., 2014) as well as germ cells (Zhang et al., 2016) are sensitive to AgNPs presence depending on size (smaller AgNPs more toxic than larger ones). Conversely, AgNPs show cytotoxic effects on kidney cells only in higher doses (Milic et al., 2015). In the cardiovascular system of male Hartley-albino guinea pigs, AgNPs cause increase in inflammation, cardiomyocyte deformities, congestion, pericardial edema, circulatory defects, cardiac arrhythmia and hemorrhage (Gonzalez et al., 2016).

CONCLUSION

As highlighted in this chapter, there has been significant interest and researchs conducted on AgNPs for biodiagnostic, imaging and therapeutic applications. Their biologically relevant size, ability to be easily functionalized

with biomolecules and chemo-therapeutic agents, as well as their enhanced optical properties improve therapeutic delivery and noninvasive disease diagnostics. Though AgNPs have prospective biomedical applications, the toxicity studies elucidate that AgNPs are toxic to humans and his environment. The size, dose and route of exposure of AgNPs are major criteria to be taken into consideration for its biomedical appliance. Although the risk of toxicity does not ablate their potential applications in cancer therapy, risk:benefits ratios should be assessed and possibilities must be explored relating to the use AgNPs in cancer without such toxicity.

REFERENCES

- Agostinis, P; Berg, K; Cengel, KA; Foster, TH; Girotti, AW; Gollnick, SO; Hahn, SM; Hamblin, MR; Juzeniene, A; Kessel, D; Korbelik, M; Moan, J; Mroz, P; Nowis, D; Piette, J; Wilson, BC; Golab, J. Photodynamic therapy of cancer: an update. *CA Cancer J Clin*, 2011, 61, 250-281.
- Ahamed, M; Alsalhi, MS; Siddiqui, MK. Silver nanoparticle applications and human health. *Clin Chim Acta*, 2010, 411, 1841-1848.
- Al Gurabi, MA; Ali, D; Alkahtani, S; Alarifi, S. *In vivo* DNA damaging and apoptotic potential of silver nanoparticles in Swiss albino mice. *Oncotargets Ther*, 2015, 8, 295-302.
- Alshehri, AH; Jakubowska, M; Młozniak, A; Horaczek, M; Rudka, D; Free, C; Carey, JD. Enhanced electrical conductivity of silver nanoparticles for high frequency electronic applications. *ACS Appl Mater Interfaces*, 2012, 4, 7007-7010.
- Arora, S; Jain, J; Rajwade, JM; Paknikar, KM. Cellular responses induced by silver nanoparticles: *In vitro* studies. *Toxicol Lett*, 2008, 179, 93-100.
- Asanithi, P; Chaiyakun, S; Limsuwan, P. Growth of silver nanoparticles by DC magnetron sputtering. *J Nanomater*, 2012, 2012, 8.
- AshaRani, PV; Low Kah Mun, G; Hande, MP; Valiyaveetil, S. Cytotoxicity and genotoxicity of silver nanoparticles in human cells. *ACS Nano*, 2009, 3, 279-290.
- Austin, LA; Kang, B; Yen, CW; El-Sayed, MA. Nuclear targeted silver nanospheres perturb the cancer cell cycle differently than those of nanogold. *Bioconjug Chem*, 2011, 22, 2324-2331.
- Austin, LA; Kang, B; Yen, CW; El-Sayed, MA. Plasmonic imaging of human oral cancer cell communities during programmed cell death by nuclear-targeting silver nanoparticles. *J Am Chem Soc*, 2011, 133, 17594-17597.

- Austin, LA; Mackey, MA; Dreaden, EC; El-Sayed, MA. The optical, photothermal, and facile surface chemical properties of gold and silver nanoparticles in biodiagnostics, therapy, and drug delivery. *Arch Toxicol*, 2014, 88, 1391-1417.
- Avalos, A; Haza, AI; Mateo, D; Morales, P. Cytotoxicity and ROS production of manufactured silver nanoparticles of different sizes in hepatoma and leukemia cells. *J Appl Toxicol*, 2014, 34, 413-423.
- Awad, AB; Chan, KC; Downie, AC; Fink, CS. Peanuts as a source of beta-sitosterol, a sterol with anticancer properties. *Nutr Cancer*, 2000, 36, 238-241.
- Baharara, J; Namvar, F; Mousavi, M; Ramezani, T; Mohamad, R. Anti-angiogenesis effect of biogenic silver nanoparticles synthesized Using *Saliva officinalis* on chick chorioalantoic membrane (CAM). *Molecules*, 2014, 19, 13498-13508.
- Balakrishna, K; Natarajan, RK; Purushothaman, KK. Chemical examination of *Olaax scandens* Roxb. *Bmebr*, 1983, 4, 167-169.
- Beer, C; Foldbjerg, R; Hayashi, Y; Sutherland, DS; Autrup, H. Toxicity of silver nanoparticles - nanoparticle or silver ion? *Toxicol Lett*, 2012, 208, 286-292.
- Blanco, J; Lafuente, D; Gómez, M; García, T; Domingo, JL; Sánchez, DJ. Polyvinyl pyrrolidone-coated silver nanoparticles in a human lung cancer cells: time- and dose-dependent influence over p53 and caspase-3 protein expression and epigenetic effects. *Arch Toxicol*, 2016, DOI: 10.1007/s00204-016-1773-0.
- Boca-Farcau, S; Potara, M; Simon, T; Juhem, A; Baldeck, P; Astilean, S. Folic acid-conjugated, SERS-labeled silver nanotriangles for multimodal detection and targeted photothermal treatment on human ovarian cancer cells. *Mol Pharm*, 2014, 11, 391-399.
- Caldorera-Moore, ME; Liechty, WB; Peppas, NA. Responsive theranostic systems: integration of diagnostic imaging agents and responsive controlled release drug delivery carriers. *Acc Chem Res*, 2011, 44, 1061-1070.
- Castillo, PM; Herrera, JL; Fernandez-Montesinos, R; Caro, C; Zaderenko, AP; Mejías, JA; Pozo, D. Tiopronin monolayer-protected silver nanoparticles modulate IL-6 secretion mediated by Toll-like receptor ligands. *Nanomedicine*, 2008, 3, 627-635.
- Castro Aceituno, V; Ahn, S; Simu, SY; Wang, C; Mathiyalagan, R; Yang, DC. Silver nanoparticles from *Dendropanax moribifera* Léveillé inhibit cell migration, induce apoptosis, and increase generation of reactive oxygen species in A549 lung cancer cells. *In Vitro Cell Dev Biol Anim*, 2016, DOI: 10.1007/s11626-016-0057-6.

- Chairuangkitti, P; Lawanprasert, S; Roytrakul, S; Aueviriyavit, S; Phummiratch, D; Kulthong, K; Chanvorachote, P; Maniratanachote, R. Silver nanoparticles induce toxicity in A549 cells via ROS-dependent and ROS-independent pathways. *Toxicol in vitro*, 2013, 27, 330-338.
- Chan, S; Kwon, S; Koo, TW; Lee, LP; Berlin, AA. Surface-Enhanced Raman Scattering of Small Molecules from Silver Coated Silicon Nanopores. *Adv Mater*, 2003, 15, 1595-1598.
- Chen, G; Lu, J; Lam, C; Yu, Y. A novel green synthesis approach for polymer nanocomposites decorated with silver nanoparticles and their antibacterial activity. *Analyst*, 2014, 139, 5793-579.
- Chen, SF; Zhang, H. Aggregation kinetics of nanosilver in different water conditions. *Adv Nat Sci: Nanosci Nanotechnol*, 2012, 3, 035006.
- Chiodo, F; Marradi, M; Calvo, J; Yuste, E; Penadés, S. Glycosystems in nanotechnology: Gold glyconanoparticles as carrier for anti-HIV prodrugs. *Beilstein J Org Chem*, 2014, 10, 1339-1346.
- Christy, AJ; Umadevi, M. Synthesis and characterization of monodispersed silver nanoparticles. *Adv Nat Sci: Nanosci Nanotechnol*, 2012, 3, 035013.
- Dang, TMD; Le, TTT; Fribourg-Blanc, E; Dang, MC. Influence of surfactant on the preparation of silver nanoparticles by polyol method. *Adv Nat Sci: Nanosci Nanotechnol*, 2012, 3, 035004.
- Dini, L; Panzarini, E; Serra, A; Buccolieri, A; Manno, D. Synthesis and *in vitro* cytotoxicity of glycans-capped silver nanoparticles. *Nanomater Nanotech*, 2011, 1, 58-63.
- Duraipandiyan, V; Ayyanar, M; Ignacimuthu, S. Antimicrobial activity of some ethnomedicinal plants used by Paliyar tribe from Tamil Nadu, India. *BMC Compl Altern Med*, 2006, 6, 35.
- Elechiguerra, JL; Burt, JL; Morones, JR; Camacho-Bragado, A; Gao, X; Lara, HH; Yacaman, MJ. Interaction of silver nanoparticles with HIV-1. *J Nanobiotech*, 2005, 3, 6.
- El-Hussein, A. Study DNA Damage after Photodynamic Therapy Using Silver Nanoparticles with A549 Cell Line. *J Mol Nanot Nanom*, 2016, 1, 101.
- El-Hussein, A; Mfouo-Tynga, I; Abdel-Harith, M; Abrahamse, H. Comparative study between the photodynamic ability of gold and silver nanoparticles in mediating cell death in breast and lung cancer cell lines. *J Photochem Photobiol B*, 2015, 153, 67-75.
- Elshaw, OE; Helmy, EA; Rashed, LA. Preparation, Characterization and *in vitro* Evaluation of the Antitumor Activity of the Biologically Synthesized Silver Nanoparticles. *Adv Nanopart*, 2016, 5, 149-166.

- Eom, HJ; Choi, J. p38 MAPK activation, DNA damage, cell cycle arrest and apoptosis as mechanisms of toxicity of silver nanoparticles in Jurkat T cells. *Environ Sci Technol*, 2010, 44, 8337-8342.
- Ercal, N; Gurer-Orhan, H; Aykin-Burns, N. Toxic metals and oxidative stress part I: mechanisms involved in metal-induced oxidative damage. *Curr Top Med Chem*, 2001, 1, 529-539.
- Evanoff, DD; Chumanov, G. Synthesis and optical properties of silver nanoparticles and arrays. *Chemphyschem*, 2005, 6, 1221-1231.
- Faedmaleki, F; Shirazi, F; Salarian, AA; Ahmadi Ashtiani, H; Rastegar, H. Toxicity Effect of Silver Nanoparticles on Mice Liver Primary Cell Culture and HepG2 Cell Line. *Iran J Pharm Res*, 2014, 13, 235-242.
- Feng, S; Chen, R; Lin, J; Pan, J; Chen, G; Li, Y; Cheng, M; Huang, Z; Chen, J; Zeng, H. Nasopharyngeal cancer detection based on blood plasma surface-enhanced Raman spectroscopy and multivariate analysis. *Biosens Bioelectron*, 2010, 25, 2414-2419.
- Feng, S; Chen, R; Lin, J; Pan, J; Wu, Y; Li, Y; Chen, J; Zeng, H. Gastric cancer detection based on blood plasma surface-enhanced Raman spectroscopy excited by polarized laser light. *Biosens Bioelectron*, 2011, 26, 3167-3174.
- Feng, S; Wang, W; Tai, IT; Chen, G; Chen, R; Zeng, H. Label-free surface-enhanced Raman spectroscopy for detection of colorectal cancer and precursor lesions using blood plasma. *Biomed Opt Express*, 2015, 6, 3494-3502.
- Foldbjerg, R; Dang, DA; Autrup, H. Cytotoxicity and genotoxicity of silver nanoparticles in the human lung cancer cell line, A549. *Arch Toxicol*, 2011, 85, 743-750.
- Franco-Molina, MA; Mendoza-Gamboa, E; Sierra-Rivera, CA; Gómez-Flores, RA; Zapata-Benavides, P; Castillo-Tello, P; Alcocer-González, JM; Miranda-Hernández, DF; Tamez-Guerra, RS; Rodríguez-Padilla, C. Antitumor activity of colloidal silver on MCF-7 human breast cancer cells. *J Exp Clin Cancer Res*, 2010, 29, 148-154.
- Galdiero, S; Falanga, A; Vitiello, M; Cantisani, M; Marra, V; Galdiero M. Silver nanoparticles as potential antiviral agents. *Molecules*, 2011, 16, 8894-8918.
- Gerber, C; Lang, HP. How the doors to the nanoworld were opened. *Nat Nanotechnol*, 2006, 1, 3-5.
- Gliga, AR; Skoglund, S; Wallinder, IO; Fadeel, B; Karlsson, HL. Size-dependent cytotoxicity of silver nanoparticles in human lung cells: the role of cellular uptake, agglomeration and Ag release. *Part Fibre Toxicol*, 2014, 11, 1-17.

- Gonzalez, C; Rosas-Hernandez, H; Ramirez-Lee, MA; Salazar-García, S; Ali SF. Role of silver nanoparticles (AgNPs) on the cardiovascular system. *Arch Toxicol*, 2016, 90, 493-511.
- González-Solís, J; Luévano-Colmenero, G; Vargas-Mancilla, J. Surface enhanced Raman spectroscopy in breast cancer cells. *Laser Ther*, 2013, 22, 37-42.
- González-Solís, JL; Aguiñaga-Serrano, BI; Martínez-Espinosa, JC; Ocegüera-Villanueva, A. Stage determination of breast cancer biopsy using Raman spectroscopy and multivariate analysis. *AIP Conference Proceedings*, 2011, 1364, 33-40.
- González-Solís, JL; Martínez-Espinosa, JC; Frausto-Reyes, C; Miranda-Beltrán, ML; Soria-Fregoso, C; Medina-Valtierra, J. Detection of Leukemia with Blood Samples Using Raman Spectroscopy and Multivariate Analysis. *AIP Conference Proceedings*, 2010, 1142, 99-103
- González-Solís, JL; Rodríguez-López, J; Martínez-Espinosa, JC; Frausto-Reyes, C; Jave-Suárez, LF; Aguilar-Lemarroy, AC; Vargas-Rodríguez, H; Martínez-Cano, E. Detection of Cervical Cancer Analyzing Blood Samples with Raman Spectroscopy and Multivariate Analysis. *AIP Conference Proceedings*, 2009, 1126, 91-95.
- Greulich, C; Diendorf, J; Gessmann, J; Simon, T; Habijan, T; Eggeler, G; Schildhauer, TA; Epple, M; Köller, M. Cell type-specific responses of peripheral blood mononuclear cells to silver nanoparticles. *Acta Biomater*, 2011, 7, 3505-3514.
- Guo, D; Zhao, Y; Zhang, Y; Wang, Q; Huang, Z; Ding, Q; Guo, Z; Zhou, X; Zhu, L; Gu, N. The cellular uptake and cytotoxic effect of silver nanoparticles on chronic myeloid leukemia cells. *J Biomed Nanotechnol*, 2014, 10, 669-678.
- Guo, D; Zhu, L; Huang, Z; Zhou, H; Ge, Y; Ma, W; Wu, J; Zhang, X; Zhou, X; Zhang, Y; Zhao, Y; Gu, N. Anti-leukemia activity of PVP-coated silver nanoparticles via generation of reactive oxygen species and release of silver ions. *Biomaterials*, 2013, 34, 7884-7894.
- Gurunathan, S; Han, JW; Eppakayala, V; Jeyaraj, M; Kim, JH. Cytotoxicity of biologically synthesized silver nanoparticles in MDA-MB-231 human breast cancer cells. *Biomed Res Int*, 2013a, 2013, 535796.
- Gurunathan, S; Lee, KJ; Kalishwaralal, K; Sheikpranbabu, S; Vaidyanathan, R; Eom, SH. Antiangiogenic properties of silver nanoparticles. *Biomaterials*, 2009, 30, 6341-6350.
- Gurunathan, S; Raman, J; Abd Malek, SN; John, PA; Vikineswary, S. Green synthesis of silver nanoparticles using *Ganoderma neo-japonicum* Imazeki:

- a potential cytotoxic agent against breast cancer cells. *Int J Nanomedicine*, 2013, 8, 4399-4413.
- Habouti, S; Solterbecka, CH; Es-Souni, M. Synthesis of silver nano-fir-twigs and application to single molecules detection. *J Mater Chem*, 2010, 20, 5215-5219.
- Haes, AJ; Zou, S; Schatz, GC; Van Duyne, RP. A Nanoscale Optical Biosensor: The Long Range Distance Dependence of the Localized Surface Plasmon Resonance of Noble Metal Nanoparticles. *J Phys Chem B*, 2004, 108, 109-116.
- Han, XX; Ozaki, Y; Zhao, B. Label-free Detection in Biological Applications of Surface-enhanced Raman Scattering. *Trends Anal Chem*, 2012, 38, 67-78.
- Hayden, SC; Austin, LA; Near, RD; Ozturk, R; El-Sayed, MA. Plasmonic enhancement of photodynamic cancer therapy. *J Photochem Photobiol A*, 2013, 269, 34-41.
- He, Y; Du, Z; Ma, S; Cheng, S; Jiang, S; Liu, Y; Li, D; Huang, H; Zhang, K; Zheng, X. Biosynthesis, Antibacterial Activity and Anticancer Effects Against Prostate Cancer (PC-3) Cells of Silver Nanoparticles Using Dimocarpus Longan Lour Peel Extract. *Nanoscale Res Lett*, 2016, 11, 300.
- Ho, CM; Wong, CK; Yau, SKW; Lok, CN; Che, CM. Oxidative Dissolution of Silver Nanoparticles by Dioxygen: A Kinetic and Mechanistic Study. *Chemistry-An Asian Journal*, 2011, 6, 2506-2511.
- Ho, CM; Yau, SK; Lok, CN; So, MH; Che, CM. Oxidative dissolution of silver nanoparticles by biologically relevant oxidants: a kinetic and mechanistic study. *Chem Asian J*, 2010, 5, 285-293.
- Hu, XH; Chan, CT. Photonic crystals with silver nanowires as a near-infrared superlens. *Appl Phys Lett*, 2004, 85, 1520-1522.
- Huang, P; Yang, DP; Zhang, C; Lin, J; He, M; Bao, L. Protein directed one-pot synthesis of Ag microspheres with good biocompatibility and enhancement of radiation effects on gastric cancer cells. *Nanoscale*, 2011, 3, 3623-3626.
- Huang, T; Nancy Xu, XH. Synthesis and Characterization of Tunable Rainbow Colored Colloidal Silver Nanoparticles Using Single-Nanoparticle Plasmonic Microscopy and Spectroscopy. *J Mater Chem*, 2010, 20, 9867-9876.
- Huang, X; El-Sayed, MA. Gold nanoparticles: Optical properties and implementations in cancer diagnosis and photothermal therapy. *J Adv Res*, 2010, 1, 13-28.
- Jain, PK; Huang, XH; El-Sayed, IH; El-Sayed, MA. Noble metals on the nanoscale: optical and photothermal properties and some applications in

- imaging, sensing, biology, and medicine. *Acc Chem Res*, 2008, 41, 1578-1586.
- Jang, SJ; Yang, IJ; Tettey, CO; Kim, KM; Shin, HM. *In-vitro* anticancer activity of green synthesized silver nanoparticles on MCF-7 human breast cancer cells. *Mater Sci Eng C Mater Biol Appl*, 2016, 68, 430-435.
- Jeyaprakash, K; Ayyanar, M; Geetha, KN; Sekar, T. Traditional uses of medicinal plants among the tribal people in Theni District (Western Ghats), Southern India. *Asian Pacific Journal of Tropical Biomedicine*, 2011, S20-S25.
- Johnston, HJ; Hutchison, G; Christensen, FM; Peters, S; Hankin, S; Stone, V. A review of the *in vivo* and *in vitro* toxicity of silver and gold particulates: particle attributes and biological mechanisms responsible for the observed toxicity. *Crit Rev Toxicol*, 2010, 40, 328-346.
- Joksić, G; Stašić, J; Filipović, J; Šobot, AV; Trtica, M. Size of silver nanoparticles determines proliferation ability of human circulating lymphocytes *in vitro*. *Toxicol Lett*, 2016, 247, 29-34.
- Ju, YH; Clausen, LM; Allred, KF; Almada, AL; Helferich, WG. beta-Sitosterol, beta-Sitosterol Glucoside, and a Mixture of beta-Sitosterol and beta-Sitosterol Glucoside Modulate the Growth of Estrogen-Responsive Breast Cancer Cells *in vitro* and in Ovariectomized Athymic Mice. *J Nutr*, 2004, 134, 1145-1151.
- Ju-Nam, Y; Lead, JR. Manufactured nanoparticles: an overview of their chemistry, interactions and potential environmental implications. *Sci Total Environ*, 400, 396-414.
- Kaba, SI; Egorova, EM. *In vitro* studies of the toxic effects of silver nanoparticles on HeLa and U937 cells. *Nanotechnol Sci Appl*, 2015, 8, 19-29.
- Kennedy, DC; Orts-Gil, G; Lai, CH; Müller, L; Haase, A; Luch, A; Seeberger, PH. Carbohydrate functionalization of silver nanoparticles modulates cytotoxicity and cellular uptake. *J Nanobiotechnology*, 2014, 12, 59.
- Khandia, R; Munjal, A; Bangrey, RS; Mehra, R; Dhama, K; Sharma, NC. Evaluation of silver nanoparticle mediated reduction of neovascularisation (angiogenesis) in chicken model. *Adv Anim Vet Sci*, 2015, 3, 372-376.
- Kim, KJ; Sung, WS; Suh, BK; Moon, SK; Choi, JS; Kim, JG; Lee, DG. Antifungal activity and mode of action of silver nano-particles on *Candida albicans*. *Biometals*, 2009, 22, 235-242.
- Kim, S; Choi, JE; Choi, J; Chung, KH; Park, K; Yi, J; Ryu, DY. Oxidative stress-dependent toxicity of silver nanoparticles in human hepatoma cells. *Toxicol In Vitro*, 2009, 23, 1076-1084.

- Kim, S; Ryu, DY. Silver nanoparticle-induced oxidative stress, genotoxicity and apoptosis in cultured cells and animal tissues. *J Appl Toxicol*, 2013, 33, 78–89.
- Kittler, S; Greulich, C; Diendorf, J; Koller, M; Epple, M. Toxicity of Silver Nanoparticles Increases during Storage Because of Slow Dissolution under Release of Silver Ions. *Chem Mater*, 2010, 22, 4548-4554.
- Kovács, D; Igaz, N; Keskeny, C; Bélteky, P; Tóth, T; Gáspár, R; Madarász, D; Rázga, Z; Kónya, Z; Boros, IM; Kiricsi, M. Silver nanoparticles defeat p53-positive and p53-negative osteosarcoma cells by triggering mitochondrial stress and apoptosis. *Sci Rep*, 2016, 6, 27902.
- Králová, ZO; Oriňák, A; Oriňáková, R; Škantárová, L; Radoňák, J. Enhanced Detection of Human Plasma Proteins on Nanostructured Silver Surfaces. *Nanomater Nanotechnol*, 2013, 3, 17, 2013.
- Krut'yakov, YA; Kudrynskiy, AA; Olenin, AY; Lisichkin, GV. Synthesis and properties of silver nanoparticles: advances and prospects. *Russ Chem Rev*, 2008, 77, 233.
- Kumar, AS; Goswami, U; Dutta, D; Banerjee, S; Chattopadhyay, A; Ghosh, SS. Silver Nanocluster Embedded Composite Nanoparticles for Targeted Prodrug Delivery in Cancer Theranostics. *ACS Biomater Sci Eng*, 2016, 2, 1395-1402.
- Kuppusamy, P; Ichwan, SJ; Al-Zikri, PN; Suriyah, WH; Soundharrajan, I; Govindan, N; Maniam, GP; Yusoff, MM. *In vitro* Anticancer Activity of Au, Ag Nanoparticles Synthesized Using Commelina nudiflora L. Aqueous Extract Against HCT-116 Colon Cancer Cells. *Biol Trace Elem Res*, 2016, DOI: 10.1007/s12011-016-0666-7.
- Kwan, KH; Liu, X; To, MK; Yeung, KW; Ho, CM; Wong, KK. Modulation of collagen alignment by silver nanoparticles results in better mechanical properties in wound healing. *Nanomed Nanotechnol Biol Med*, 2011, 7, 497-504.
- Lammers, T; Aime, S; Hennink, WE; Storm, G; Kiessling, F. Theranostic nanomedicine. *Acc Chem Res*, 2011, 44, 1029-1038.
- Levard, C; Reinsch, BC; Michel, FM; Oumahi, C; Lowry, GV; Brown, GE. Sulfidation processes of PVP-coated silver nanoparticles in aqueous solution: impact on dissolution rate. *Environ Sci Technol*, 2011, 45, 5260-5266.
- Li, D; Feng, S; Huang, H; Chen, W; Shi, H; Liu, N; Chen, L; Chen, W; Yu, Y; Chen, R. Label-free detection of blood plasma using silver nanoparticle based surface-enhanced Raman spectroscopy for esophageal cancer screening. *J Biomed Nanotechnol*, 2014, 10, 478-484.

- Li, X; Lenhart, JJ; Walker, HW. Dissolution-accompanied aggregation kinetics of silver nanoparticles. *Langmuir*, 2010, 26, 16690-16698.
- Lin, J; Chen, R; Feng, S; Pan, J; Li, Y; Chen, G; Cheng, M; Huang, Z; Yu, Y; Zeng, H. A novel blood plasma analysis technique combining membrane electrophoresis with silver nanoparticle-based SERS spectroscopy for potential applications in noninvasive cancer detection. *Nanomedicine*, 2011, 7, 655-663.
- Liu, J; Hurt, RH. Ion release kinetics and particle persistence in aqueous nano-silver colloids. *Environ Sci Technol*, 2010, 44, 2169-2175.
- Liu, J; Sonshine, DA; Shervani, S; Hurt, RH. Controlled release of biologically active silver from nanosilver surfaces. *ACS Nano*, 2010, 4, 6903-6913.
- Liu, J; Wang, Z; Liu, FD; Kane, AB; Hurt, RH. Chemical transformations of nanosilver in biological environments. *ACS Nano*, 2012, 6, 9887-9899.
- Liu, P; Huang, Z; Chen, Z; Xu, R; Wu, H; Zang, F; Wang, C; Gu, N. Silver nanoparticles: a novel radiation sensitizer for glioma? *Nanoscale*, 2013, 5, 11829-11836.
- Locatelli, E; Naddaka, M; Uboldi, C; Loudos, G; Fragozeorgi, E; Molinari, V; Pucci, A; Tsoakos, T; Psimadas, D; Ponti, J; Franchini, MC. Targeted delivery of silver nanoparticles and alisertib: *in vitro* and *in vivo* synergistic effect against glioblastoma. *Nanomedicine*, 2014, 9, 839-849.
- Loza, K; Diendorf, J; Sengstock, C; Ruiz-Gonzalez, L; Gonzalez-Calbet, JM; Vallet-Regi, M; Köller, M; Epple, M. The dissolution and biological effects of silver nanoparticles in biological media. *J Mater Chem B*, 2014, 2, 1634-1643.
- Lu, R; Yang, D; Cui, D; Wang, Z; Guo, L. Egg white-mediated green synthesis of silver nanoparticles with excellent biocompatibility and enhanced radiation effects on cancer cells. *Int J Nanomedicine*, 2012, 7, 2101-2107.
- Ma, J; Xu, R; Sun, J; Zhao, D; Tong, J; Sun, X. Nanoparticle surface and nanocore properties determine the effect on radiosensitivity of cancer cells upon ionizing radiation treatment. *J Nanosci Nanotechnol*, 2013, 13, 1472-1475.
- Manno, D; Serra, A; Buccolieri, A; Panzarini, E; Carata, E; Tenuzzo, BA; Izzo, D; Vergallo, C; Rossi, M; Dini, L. Silver and carbon nanoparticles toxicity in sea urchin *Paracentrotus lividus* embryos. *BioNanoMat*, 2013, 14, 229-238.
- Marambio-Jones, C; Hoek, EMV. *J Nanopart Res*, 2010, 12, 1531.
- Marradi, M; Chiodo, F; García, I; Penadés, S. Glyconanoparticles as multifunctional and multimodal carbohydrate systems. *Chem Soc Rev*, 2013, 42, 4728-4745.

- Maynard, AD; Warheit, DB; Philbert, MA. The new toxicology of sophisticated materials: nanotoxicology and beyond. *Toxicol Sci*, 2011, 120, S109-29.
- Milić, M; Leitinger, G; Pavičić, I; Zebić Avdičević, M; Dobrović, S; Goessler, W; Vinković Vrček, I. Cellular uptake and toxicity effects of silver nanoparticles in mammalian kidney cells. *J Appl Toxicol*, 2015, 35, 581-592.
- Mohammadzadeh, R. Hypothesis: silver nanoparticles as an adjuvant for cancertherapy. *Adv Pharm Bull*, 2012, 2, 133.
- Mudunkotuwa, IA; Grassian, VH. The devil is in the details (or the surface): impact of surface structure and surface energetics on understanding the behavior of nanomaterials in the environment. *J Environ Monit*, 2011, 13, 1135-1144.
- Muhammad, Z; Raza, A; Ghafoor, S; Naeem, A; Naz, SS; Riaz, S; Ahmed, W; Rana, NF. PEG capped methotrexate silver nanoparticles for efficient anticancer activity and biocompatibility. *Eur J Pharm Sci*, 2016, 91, 251-255.
- Mukherjee, S; Chowdhury, D; Kotcherlakota, R; Patra, S; Bhadra, MP; Sreedhar, B; Patra, CR. Potential theranostics application of bio-synthesized silver nanoparticles (4-in-1 system). *Theranostics*, 2014, 4, 316-335.
- Nadworny, PL; Landry, BK; Wang, J; Tredget, EE; Burrell, RE. Does nanocrystalline silver have a transferable effect? *Wound Repair Regen*, 2010, 18, 254-265.
- Nazir, S; Hussain, T; Iqbal, M; Mazhar, K; Muazzam, AG; Ismail, M. Novel and cost-effective green synthesis of silver nano particles and their *in vivo* antitumor properties against human cancer cell lines. *J Biosci Tech*, 2011, 2, 425-430.
- Nishida, N; Yano, H; Nishida, T; Kamura, T; Kojiro, M. Angiogenesis in Cancer. *Vasc Health Risk Manag*, 2006, 2, 213-219.
- Pandurangan, M; Enkhtaivan, G; Venkitasamy, B; Mistry, B; Noorzai, R; Jin, BY; Kim, DH. Time and Concentration-Dependent Therapeutic Potential of Silver Nanoparticles in Cervical Carcinoma Cells. *Biol Trace Elem Res*, 2016, 170, 309-319.
- Panzarini, E; Dini, L. Nanotechnology-Based Cancer Photodynamic Therapy. In: *Nova Science Publishers Inc. Photodynamic Therapy: Fundamentals, Applications and Health Outcomes*, 2015, 103-122.
- Panzarini, E; Inguscio, V; Dini, L. Overview of cell death mechanisms induced by Rose Bengal Acetate-Photodynamic Therapy. *Int J Photoen*, 2011, doi:10.1155/2011/713726.

- Panzarini, E; Inguscio, V; Dini, L. Timing the multiple cell deaths pathways initiated by Rose Bengal Acetate photodynamic therapy. *Cell Death Dis*, 2011, 2, e169.
- Panzarini, E; Inguscio, V; Fimia, GM; Dini, L. Rose Bengal Acetate PhotoDynamic Therapy (RBAC-PDT) induces exposure and release of Damage-Associated Molecular Patterns (DAMPs) in human HeLa cells. *PlosOne*, 2014, 9(8), e105778.
- Panzarini, E; Inguscio, V; Tenuzzo, BA; Dini, L. *In vitro* and *in vivo* clearance of Rose Bengal Acetate-PhotoDynamicTherapy-induced autophagic and apoptotic cells. *Exp Biol Med*, 2013, 238, 765-778.
- Panzarini, E; Mariano, S; Dini, L. Glycans Coated Silver Nanoparticles Induce Autophagy and Necrosis in HeLa Cells. *NANOFORUM 2014, AIP Conf Proc*, 2015, 1667, 020017-1–020017-8.
- Panzarini, E; Tenuzzo, BA; Vergallo, C; Dini, L. Biological systems interact with Engineered NanoMaterials (ENMs): possible environmental risks. *Nuovo Cimento C*, 2013, 36, 111-116.
- Pichardo-Molina, JL; Frausto-Reyes, C; Barbosa-García, O; Huerta-Franco, R; González-Trujillo, JL; Ramírez-Alvarado, CA; Gutiérrez-Juárez, G; Medina-Gutiérrez, C. Raman spectroscopy and multivariate analysis of serum samples from breast cancer patients. *Laser Med Sci*, 2016, 10103, 432-438
- Prasad, RY; McGee, JK; Killius, MG; Suarez, DA; Blackman, CF; DeMarini, DM; Simmons, SO. Investigating oxidative stress and inflammatory responses elicited by silver nanoparticles using high-throughput reporter genes in HepG2 cells: effect of size, surface coating, and intracellular uptake. *Toxicol In Vitro*, 2013, 27, 2013-2021.
- Prasannaraj, G; Sahi, SV; Ravikumar, S; Venkatachalam, P. Enhanced Cytotoxicity of Biomolecules Loaded Metallic Silver Nanoparticles Against Human Liver (HepG2) and Prostate (PC3) Cancer Cell Lines. *J Nanosci Nanotechnol*, 2016, 16, 4948-4959.
- Raman, CV; Krishnan, KS. A new type of secondary radiation. *Nature*, 1928, 121, 501-502.
- Sahay, G; Alakhova, DY; Kabanov, AV. Endocytosis of nanomedicines. *J Control Release*, 2010, 145, 182-195.
- Sahu, SC; Zheng, J; Graham, L; Chen, L; Ihrie, J; Yourick, JJ; Sprando, RL. Comparative cytotoxicity of nanosilver in human liver HepG2 and colon Caco2 cells in culture. *J Appl Toxicol*, 2014, 34, 1155-1166.
- Sargent, <http://www.fas.org/sgp/crs/misc/RL34511.pdf>.

- Satapathy, H. Enhancement of Cytotoxicity and Inhibition of Angiogenesis in Oral Cancer Stem Cells by a Hybrid Nanoparticle of Bioactive Quinacrine and Silver: Implication of Base Excision Repair Cascade. *Mol Pharmaceutics*, 2015, 12, 4011-4025.
- Shahare, B; Yashpal, M. Toxic effects of repeated oral exposure of silver nanoparticles on small intestine mucosa of mice. *Toxicol Mech Methods*, 2013, 23, 161-167.
- Shangyuan, F; Rong, Ch; Jianji, P; Yanan, W; Yongzeng, L; Jiesi, Ch; Haishan, Z. Gastric cancer detection based on blood plasm surfaceenhanced Raman spectroscopy excited by polarized laser light. *Biosensors and Bioelectronics*, 2011, 26, 3167-3174.
- Sharma, H; Mishra, PK; Talegaonkar, S; Vaidya, B. Metal nanoparticles: a theranostic nanotool against cancer. *Drug Discov Today*, 2015, 20, 1143-1151.
- Shi, J; Wang, L; Zhang, J; Ma, R; Gao, J; Liu, Y; Zhang, C; Zhang, Z. A tumor-targeting near-infrared laser-triggered drug delivery system based on GO@Ag nanoparticles for chemo-photothermal therapy and X-ray imaging. *Biomaterials*, 2014, 35, 5847-5861.
- Simard, JC; Vallieres, F; de Liz, R; Lavastre, V; Girard, D. Silver nanoparticles induce degradation of the endoplasmic reticulum stress sensor activating transcription factor-6 leading to activation of the NLRP-3 inflammasome. *J Biol Chem*, 2015, 290, 5926-5939.
- Singh, N; Manshian, B; Jenkins, GJ; Griffiths, SM; Williams, PM; Maffeis, TG; Wright, CJ; Doak, SH. NanoGenotoxicology: the DNA damaging potential of engineered nanomaterials. *Biomaterials*, 2009, 30, 3891-3914.
- Singh, RP; Ramarao, P. Cellular uptake, intracellular trafficking and cytotoxicity of silver nanoparticles. *Toxicol Lett*, 2012, 213, 249-259.
- Sintubin, L; Verstraete, W; Boon, N. Biologically produced nanosilver: current state and future perspectives. *Biotechnol Bioeng*, 2012, 109, 2422-2436.
- Söderstjerna, E; Bauer, P; Cedervall, T; Abdshill, H; Johansson, F; Johansson, UE. Silver and gold nanoparticles exposure to *in vitro* cultured retina--studies on nanoparticle internalization, apoptosis, oxidative stress, glial- and microglial activity. *PLoS One*, 2014, 9, e105359.
- Sotiriou, GA; Pratsinis, SE. Antibacterial activity of nanosilver ions and particles. *Environ Sci Technol*, 2010, 44, 5649-5654.
- Sotiriou, GA; Pratsinis, SE. Engineering nanosilver as an antibacterial, biosensor and bioimaging material. *Curr Opin Chem Eng*, 2011, 1, 3-10.
- Swanner, J; Mims, J; Carroll, DL; Akman, SA; Furdui, CM; Torti, SV; Singh, RN. Differential cytotoxic and radiosensitizing effects of silver

- nanoparticles on triple-negative breast cancer and non-triple-negative breast cells. *Int J Nanomed*, 2015, 10, 3937-3953.
- Thippeswamy, G; Sheela, ML; Salimath, BP. Octacosanol isolated from *Tinospora cordifolia* downregulates VEGF gene expression by inhibiting nuclear translocation of NF- κ B and its DNA binding activity. *Eur J Pharmacol*, 2008, 588, 141-150.
- Tian, J; Wong, KK; Ho, CM; Lok, CN; Yu, WY; Che, CM; Chiu, JF; Tam, PK. Topical delivery of silver nanoparticles promotes wound healing. *Chem Med Chem*, 2007, 2, 129-136.
- Tien, DC; Tseng, KH; Liao, CY; Huang JC; Tsung, TT. Discovery of ionic silver in silver nanoparticle suspension fabricated by arc discharge method. *J Alloys Compounds*, 2008, 463, 408-411.
- Tran, QH; Nguyen, VQ; Le, AT. Silver nanoparticles: synthesis, properties, toxicology, applications and perspectives. *Adv Nat Sci: Nanosci*, 2013, 4, 20.
- Tu, Q; Chang, C. Diagnostic applications of Raman spectroscopy. *Nanomedicine*, 2012, 8, 545-558.
- Vankayala, R; Kuo, CL; Sagadevan, A; Chen, PH; Chiang, CS; Hwang, KC. Morphology dependent photosensitization and formation of singlet oxygen ($^1\Delta_g$) by gold and silver nanoparticles and its application in cancer treatment. *J Mater Chem B*, 2013, 1, 4379-4387.
- Vasanth, K; Ilango, K; MohanKumar, R; Agrawal, A; Dubey, GP. Anticancer activity of *Moringa oleifera* mediated silver nanoparticles on human cervical carcinoma cells by apoptosis induction. *Colloids Surf B Biointerfaces*, 2014, 117, 354-359.
- Venkata Subbaiah, KP; Savithamma, N. Bio-prospecting and documentation of traditional medicinal plants used to treat itching, psoriasis and wounds by ethnic groups of kurnool district, Andhra Pradesh, India. *Asian J Pharm Clin Res*, 2012, 5, 127-131.
- Vergallo, C; Panzarini, E; Carata, E; Amhadi, M; Mariano, S; Tenuzzo, BA; Dini, L. Cytotoxicity of β -D-glucose/sucrose-coated silver nanoparticles depends on cell type, nanoparticles concentration and time of incubation. *NANOITALY 2015, AIP Conf Proc 2016*, 1749, 020012-1-020012-9.
- Vrček, IV; Žuntar, I; Petlevski, R; Pavičić, I; Dutour Sikirić, M; Čurlin, M; Goessler, W. Comparison of *in vitro* toxicity of silver ions and silver nanoparticles on human hepatoma cells. *Environ Toxicol*, 2016, 31, 679-692.

- Wei, L; Lu, J; Xu, H; Patel, A; Chen, ZS; Chen, G. Silver nanoparticles: synthesis, properties, and therapeutic applications. *Drug Discov Today*, 2015, 20, 595-601.
- Wu, P; Gao, Y; Lu, Y; Zhang, H; Cai, C. High specific detection and near-infrared photothermal therapy of lung cancer cells with high SERS active aptamer-silver-gold shell-core nanostructures. *Analyst*, 2013, 138, 6501-6510.
- Xin, L; Wang, J; Fan, G; Che, B; Wu, Y; Guo, S; Tong, J. Oxidative stress and mitochondrial injury-mediated cytotoxicity induced by silver nanoparticles in human A549 and HepG2 cells. *Environ Toxicol*, 2015, doi: 10.1002/tox.22171.
- Xiu, ZM; Ma, J; Alvarez, PJ. Differential effect of common ligands and molecular oxygen on antimicrobial activity of silver nanoparticles versus silver ions. *Environ Sci Technol*, 2011, 45, 9003-9008.
- Xiu, ZM; Zhang, QB; Puppala, HL; Colvin, VL; Alvarez, PJ. Negligible particle-specific antibacterial activity of silver nanoparticles. *Nano Lett*, 2012, 12, 4271-4275.
- Xu, R; Ma, J; Sun, X; Chen, Z; Jiang, X; Guo, Z. Ag nanoparticles sensitize IR-induced killing of cancer cells. *Cell Res*, 2009, 19, 1031-1034.
- Yang, EJ; Kim, S; Kim, JS; Choi, IH. Inflammasome formation and IL-1 β release by human blood monocytes in response to silver nanoparticles. *Biomaterials*, 2012, 33, 6858-6867.
- Zhang, T; Wang, L; Chen, Q; Chen, C. Cytotoxic potential of silver nanoparticles. *Yonsei Med J*, 2014, 55, 283-291.
- Zhang, W; Yao, Y; Sullivan, N; Chen, Y. Modeling the primary size effects of citrate-coated silver nanoparticles on their ion release kinetics. *Environ Sci Technol*, 2011, 45, 4422-4428.
- Zhang, XF; Gurunathan, S. Combination of salinomycin and silver nanoparticles enhances apoptosis and autophagy in human ovarian cancer cells: an effective anticancer therapy. *Int J Nanomedicine*, 2016, 11, 3655-3675.
- Zhang, Y; Aslan, K; Previte, MJR; Geddes, CD. Metal-enhanced Singlet Oxygen Generation: A Consequence of Plasmon Enhanced Triplet Yields. *J Fluoresc*, 2007, 17, 345-349.
- Zhao, D; Sun, X; Tong, J; Ma, J; Bu, X; Xu, R; Fan, R. A novel multifunctional nanocomposite C225-conjugated Fe₃O₄/Ag enhances the sensitivity of nasopharyngeal carcinoma cells to radiotherapy. *Acta Biochim Biophys Sin (Shanghai)*, 2012, 44, 678-684.

Zook, JM; Long, SE; Cleveland, D; Geronimo, CL; MacCuspie, RI. Measuring silver nanoparticle dissolution in complex biological and environmental matrices using UV-visible absorbance. *Anal Bioanal Chem*, 2011, 401, 1993-2002.

Complimentary Contributor Copy

INDEX

#

3D images, 40, 46

A

absorption spectra, 16
accelerator, 75
acetone, 58, 93
acid, 10, 82, 148, 154, 163, 166, 169,
170, 174
acidic, 12, 162
activation energy, 33
adenine, 155
adhesion, viii, 31, 32, 33
adhesion properties, viii, 31
adsorption, ix, 32, 37, 42, 56, 57, 60, 62,
63, 64, 65, 66, 67, 68, 71, 113, 136
adsorption isotherms, 57
adverse effects, 3
aerogels, 64, 69, 70
aerospace engineering, 146
AFM, ix, xi, 32, 34, 36, 37, 39, 40, 41,
43, 46, 47, 49, 50, 76, 82, 85, 106,
128, 130, 131, 132, 133, 136, 142
Africa, 1, 21
agar, 19, 97, 99
aggregation, 17, 45, 56, 116, 117, 181
agriculture, 18, 90
albumin, 155

alcohols, 10
aldehydes, 10
algae, 115
alkaloids, 9, 10, 11
amine, 9, 11, 38, 45
amino acid, 11, 154, 167
ammonium, 127
angiogenesis, 155, 162, 174, 179
anthrax, 112
anti-cancer, vii, 1, 5, 19, 20, 166
anticancer activity, vii, 5, 20, 25, 179,
182
anticoagulation, 24
antifungal properties, xi, 90, 92, 94, 97,
111, 145
antigen, 112
anti-inflammatory agents, viii, 32
antioxidant, 5, 11, 26, 166
antitumor, 182
antiviral agents, 151, 176
apoptosis, 20, 111, 147, 155, 156, 162,
172, 174, 176, 180, 184, 185, 186
applications of Ag-NPs, 106
aqueous solutions, 116, 136
aqueous suspension, 118
argon, 76
ascites, 159
ascorbic acid, 148
aseptic, 7
Aspergillus terreus, 149
astrocytoma, 167

atmospheric pressure, 62
 atomic force, ix, 32, 106, 128, 142
 atomic force microscopy (AFM), ix, xi,
 32, 34, 36, 37, 39, 40, 41, 43, 46, 47,
 49, 50, 76, 82, 85, 106, 128, 130, 131,
 132, 133, 136, 142
 atoms, 32, 76, 81, 117

B

Bacillus subtilis, 20
 bacteria, 5, 6, 19, 23, 24, 91, 103, 107,
 110, 112, 115, 120, 149, 150
 bactericidal effects, vii, 5
 bacterium, 102, 107
 base, 146, 164
 beneficial effect, 152
 benign, 3, 11, 56, 153
 benzene, 113
 bicarbonate, 169
 bioavailability, x, 105, 116, 117
 biocompatibility, 6, 33, 142, 166, 178,
 181, 182
 biocompatible materials, 27
 biological activity(ies), 107, 166, 167
 biological media, 181
 biological samples, 153
 biological systems, 18, 92, 147
 biomaterials, vii, 2, 6, 21, 32, 102
 biomedical applications, vii, 1, 5, 173
 biomolecular detection, xi, 145
 biomolecular detection., xi, 145
 biomolecules, 11, 12, 15, 92, 115, 117,
 153, 173
 biopolymers, 6
 biopsy, 152, 177
 biosynthesis, 7, 12, 24
 biotechnological applications, viii, 32
 biotechnology, ix, x, 6, 23, 28, 29, 32,
 89
 blood, xi, 146, 151, 152, 153, 154, 155,
 162, 176, 177, 180, 181, 184, 186
 blood monocytes, 186
 blood plasma, 154, 176, 180, 181
 blood vessels, 162

bonding, 13, 33, 63
 bonds, 15, 37, 38
 brain cancer, 167
 breast cancer, 21, 153, 155, 164, 166,
 176, 177, 178, 179, 183, 185
 budding, 151
 building blocks, 2
 bulk materials, 107, 117

C

Ca²⁺, 162
 calcium, 162
 CAM, 35, 163, 174
 cancer cells, 21, 153, 155, 162, 163, 164,
 165, 166, 174, 176, 177, 178, 179,
 181, 186
 cancer progression, 155
 cancer screening, 180
 cancer stem cells, 163
 cancer therapy, 165, 173, 178
 cancerous cells, 20
 carbohydrate, 11, 168, 181
 carbon, 56, 57, 64, 68, 69, 70, 71, 92,
 116, 117, 181
 carbon dioxide, 56, 69, 70, 71
 carbon nanotubes, 57, 68, 70, 92
 carbonyl groups, 38
 carboxyl, 11, 38, 42, 45
 carcinoma, 20, 24, 154, 155, 164, 165,
 185, 186
 cardiovascular system, 172, 177
 catalysis, vii, x, 1, 18, 56, 89, 105, 113
 catalytic activity, xi, 9, 106, 145, 147
 catalytic properties, 2, 26
 CBD, 143
 cell culture, 147
 cell cycle, xi, 146, 156, 159, 173, 176
 cell death, xi, 20, 110, 114, 146, 165,
 166, 167, 173, 175, 182, 183
 cell division, 111
 cell line, xi, 20, 27, 146, 147, 155, 159,
 166, 175, 176, 182
 cell lines, xi, 20, 146, 147, 155, 159,
 166, 175, 182

- cellulose, 25
ceramic, 57
chemical etching, 74, 75
chemical properties, 106, 116, 146, 147, 149, 165, 174
chemical reactions, 50
chemical reactivity, 107
chemical stability, 106, 147
chemical vapor deposition, xi, 56, 106
chemicals, vii, 1, 3, 5, 7, 120, 148, 168
chemotherapy, 20, 163
chitosan, 92, 159, 166
chromium, 68
classification, 23
clinical application, 163
clinical trials, 163
clusters, 87, 118, 155
C-N, 39, 43, 133
CO₂, ix, 55, 58, 59, 62, 70, 71
coatings, 2, 92, 113, 147, 150, 155, 168
cobalt, 69, 81
collagen, viii, ix, 31, 32, 33, 34, 38, 39, 40, 41, 42, 43, 44, 45, 46, 47, 49, 50, 152, 154, 180
colon, 20, 27, 183
colon cancer, 20, 27
colorectal cancer, 154, 176
compatibility, viii, 3, 31
composites, 70
composition, 17, 48, 49, 97, 107, 117, 168
compounds, 5, 9, 10, 57, 58, 63, 81, 110, 114, 148
condensation, 118, 148
conduction, 108, 150, 154
conductivity, 75, 106, 113, 147, 149, 173
construction, 3, 162
consumption, 90, 118, 148
contact dermatitis, 152
contamination, 7, 92
coordination, 42, 136
copper, 29, 69, 94, 109
correlation, 86, 99
cosmetics, vii, xi, 2, 4, 107, 145, 152, 146
cost, 3, 5, 7, 56, 120, 148, 149, 153, 154, 182
cost effectiveness, 3, 120
crystalline, ix, 15, 69, 74, 75, 82, 136
crystallinity, 17, 76
crystals, 178
CSD, 144
culture, 22, 24, 147, 168, 183
culture conditions, 147
culture media, 168
cytokines, 111, 151, 152
cytoplasm, 156, 162
cytoskeleton, 156
cytotoxic agents, 167
cytotoxicity, 9, 24, 26, 156, 164, 175, 176, 179, 183, 184, 186
- | |
|----------|
| D |
|----------|
- decomposition, 91, 118, 127
degradation, 114, 184
degree of crystallinity, 17
deposition, ix, xi, 55, 56, 57, 58, 59, 60, 61, 62, 63, 68, 69, 70, 71, 75, 106, 144, 152
depth, 76, 77, 82
derivatives, 11
dermatitis, 152
destruction, 163, 166, 172
detection, x, xi, 18, 22, 89, 105, 112, 113, 145, 153, 154, 174, 176, 178, 180, 181, 184, 186
developing countries, 90
diagnostics, xi, 112, 145, 149, 165, 173
diffraction, xi, 106, 122, 124, 125, 131, 132
diffusion, 19, 37, 56, 62, 63, 64, 100, 156, 162
diseases, 5, 18, 20, 91, 150
disinfectant, vii, 1, 5
disinfection, 5, 167
dispersion, ix, 17, 19, 55, 69, 76, 128
distilled water, x, 35, 41, 90, 94, 96, 169

distribution, ix, 16, 17, 39, 41, 55, 56, 58, 63, 76, 77, 78, 90, 93, 117, 128, 132, 148
 diversity, vii, 2, 6, 7
 DNA, vii, xi, 2, 6, 19, 20, 110, 113, 114, 146, 150, 153, 155, 156, 157, 159, 162, 165, 172, 173, 175, 176, 184, 185
 DNA damage, xi, 20, 146, 157, 165, 172, 176
 DOI, 174, 180
 dressings, 111, 112, 150
 drug delivery, x, 92, 105, 112, 147, 164, 165, 166, 174, 184
 dyes, 108, 150, 153, 165

E

electric field, 108
 electrical conductivity, 149, 173
 electrodes, 70, 113
 electromagnetic, 13, 32, 109, 154, 165
 electromagnetic fields, 32
 electron, viii, 12, 15, 32, 35, 76, 96, 108, 162
 electron diffraction, 16
 electron microscopy, 12, 15, 76
 electronics, vii, ix, 3, 4, 56, 73, 113, 146
 electrons, 13, 37, 42, 81, 108, 109, 150, 154, 165
 electrophoresis, 154, 181
 employment, 61
 emulsions, 149
 endothelial cells, 166
 endowments, vii, 2, 6
 energy, ix, 3, 5, 6, 13, 15, 17, 18, 22, 33, 35, 37, 70, 73, 75, 76, 78, 82, 83, 85, 86, 93, 94, 113, 118, 120, 148, 150, 153, 164
 energy consumption, 118, 148
 energy density, 70
 engineering, 140, 146
 environment, viii, 2, 4, 5, 18, 21, 25, 33, 48, 114, 143, 147, 150, 162, 168, 172, 173, 182

environmental conditions, 117
 environmental sustainability, vii, 2, 7
 environments, 45, 114, 181
 enzymes, 24, 29, 111, 120
 epithelial cells, 163
 epithelium, 172
 equilibrium, 59, 60, 63, 64, 67, 68
 equilibrium sorption, 59, 63
 equipment, 113, 118
 ERS, x, 89
 esophageal cancer, 154, 180
 etching, 74, 75
 ethanol, ix, 38, 55, 57, 58, 59, 60, 61, 62, 63, 64, 68, 94
 ethylene glycol, ix, 55, 58, 59, 60, 61, 62, 63, 68, 71
 eukaryotic, 19
 evaporation, 93, 118, 163
 evidence, 3, 19, 114, 115, 117
 excitation, 12, 76, 124, 155
 experimental condition, 118, 121
 experimental design, 147
 expertise, 22
 exploitation, 147, 150, 152
 explosives, 112
 exposure, xi, 2, 21, 23, 45, 97, 100, 114, 115, 116, 143, 146, 147, 151, 156, 172, 173, 183, 184
 extinction, 18, 109
 extracellular matrix, viii, 31
 extracts, viii, 2, 7, 8, 9, 11, 13, 20, 22, 24, 25, 120

F

fabrication, 73, 75, 86, 120, 143
 fiber, 114
 fibroblasts, 152
 films, 27, 34, 38, 39, 41, 42, 49, 50, 56, 69, 102, 112, 122, 124, 133, 144, 149
 filters, 113
 filtration, 114
 flammability, 56
 flavonoids, 9, 10, 11, 15, 161
 fluid, ix, 56, 69, 71, 168, 170

fluorescence, 71, 153, 166
 fluorophores, 113, 155
 folic acid, 166
 food, xi, 3, 7, 23, 32, 90, 101, 113, 145, 168
 force, ix, 32, 35, 76, 106, 118, 128, 132, 142
 formation, 11, 12, 17, 38, 41, 42, 43, 45, 47, 58, 61, 62, 63, 69, 74, 77, 82, 86, 97, 122, 136, 148, 156, 162, 163, 185, 186
 fruits, x, 17, 26, 90, 91, 94
 FTIR, ix, xi, 15, 32, 34, 38, 39, 41, 42, 43, 44, 45, 47, 50, 106, 122, 133, 134, 135, 136
 FTIR spectroscopy, ix, 32, 34, 43
 functionalization, viii, 31, 39, 42, 167, 168, 179
 funding, 101
 fungi, x, 5, 6, 23, 90, 91, 94, 97, 100, 102, 107, 111, 120, 149, 150

G

gel, 56, 167
 gene expression, 185
 gene therapy, x, 105
 genes, xi, 146, 183
 genetic disorders, x, 105
 genus, 91, 92
 genus *Candida*, 92
 glioblastoma, 164, 167, 181
 glioma, 164, 181
 glucose, 9, 112, 162, 168, 185
 glycans, xii, 146, 148, 149, 153, 168, 175
 glycol, ix, 55, 58, 59, 60, 61, 62, 63, 64, 68, 71, 161
 gold (Au) nanoparticles, 14, 22, 24, 184
 groundwater, 167
 growth, viii, x, xi, 12, 19, 20, 24, 27, 32, 45, 59, 60, 74, 77, 90, 91, 93, 94, 97, 99, 100, 106, 118, 128, 148, 150, 157, 158, 159, 162, 165
 growth factor, 165

guanine, 155

H

hazardous substances, vii, 2, 3
 HBV, 151
 HCC, 154
 health, xi, xii, 3, 21, 114, 145, 146, 173
 health effects, 114
 hearing loss, 172
 helium, 32, 34, 50
 helium plasma, 32, 34
 hemoglobin, 163
 hemorrhage, 172
 hepatocellular carcinoma, 154
 hepatoma, 174, 179, 185
 HIV-1, 111, 112, 151, 175
 human, xi, xii, 3, 20, 21, 24, 27, 145, 146, 152, 155, 164, 166, 172, 173, 174, 176, 177, 179, 182, 183, 185, 186
 human health, xi, xii, 3, 21, 145, 146, 173
 hydrazine, 5, 144, 148
 hydrofluoric acid, 82
 hydrogen, 57, 63, 69, 162, 168
 hydrogen peroxide, 162, 168
 hydrophobicity, 35
 hydroxide, 120, 127, 136
 hydroxyl, 11, 38, 162
 hydroxyl groups, 38
 hyperthermia, 165, 166

I

IFN γ , 152
 IL-8, 151
 illumination, 82, 163, 164
 images, 16, 35, 36, 39, 40, 46, 47, 49, 50, 60, 61, 77, 79, 80, 81, 82, 85, 109, 130, 136, 155, 165, 167
 immobilization, viii, 31, 33, 39, 43, 50
 immunomodulatory, 151
 implants, xi, 145

impregnation, ix, 55, 56, 62
in vitro, x, xi, xii, 26, 27, 90, 111, 117,
 146, 147, 151, 157, 167, 175, 179,
 181, 184, 185
in vivo, xi, 146, 147, 164, 167, 179, 181,
 182, 183
 incubation time, 12, 97
 India, 175, 179, 185
 industrial sectors, ix, 73
 industry(ies), 32, 74, 114, 147
 infection, xi, 145, 152
inflammasome, 184
 inflammation, 152, 172
 inflammatory cells, 111
 inflammatory mediators, 151
 inflammatory responses, 183
 infrared spectroscopy, 34
 ingredients, 3, 11, 12
 inhibition, 19, 93, 97, 99, 100, 151, 157,
 158, 159, 163
 inhibitor, 27, 92
 inhomogeneity, 77
 inoculation, 101
 inorganic precursor, 56, 57, 63
 integrated circuits, 113
 integration, 35, 174
 integrity, viii, 32, 151
 interferon, 152
 internalization, 184
 intestine, 172, 184
 ion bombardment, 77
 ion implantation, ix, 73, 74, 75, 77, 80,
 82, 83
 ionizing radiation, 163, 165, 181
 ions, viii, ix, xi, 2, 5, 11, 12, 14, 17, 18,
 24, 32, 42, 74, 75, 77, 78, 85, 88, 110,
 114, 115, 116, 119, 127, 143, 146,
 147, 149, 150, 168, 172, 177, 184,
 185, 186
 iron, 81, 165
 irradiation, 5, 77, 82, 164, 165
 isotherms, 57, 65

K

keratinocytes, 152
 kidney, 172, 182
 kill, 164, 165, 167
 kinetics, ix, 56, 57, 64, 68, 71, 168, 175,
 181, 186

L

labeling, x, 89, 105, 153
Lactobacillus, 149
 laser ablation, x, xi, 89, 90, 93, 94, 96,
 102, 106, 118
 Latin America, 90
 lead, vii, 1, 5, 92, 108, 111, 114
 lens, 76, 93, 94
 lesions, 153, 176
 leukemia, 153, 155, 174, 177
 light, 17, 74, 81, 108, 109, 113, 121,
 142, 150, 155, 163, 165, 176, 184
 light scattering, 17, 150, 155
 lipid peroxidation, 156
Listeria monocytogenes, 19
 lithography, 118
 liver, xi, 146, 172, 183
 liver cancer, xi, 146
 localization, 166
 lubricants, 2
 lung cancer, 164, 166, 174, 175, 176,
 186
 lymphocytes, 151, 152, 179
 lymphoma, 159

M

macromolecules, 19, 117
 macrophages, 152
 magnetic field, 165
 magnetic properties, xi, 107, 145
 magnitude, 154, 155, 164
 malaria, 28
 malt extract, 99
 mammalian cells, xi, 146

management, xi, 91, 146, 148, 155
manipulation, 146
manufacturing, vii, 4, 114, 147
marketability, 7
mass, 60, 64, 66, 68, 81, 121, 162, 167
materials, viii, ix, x, 2, 5, 7, 27, 31, 33, 71, 73, 77, 86, 93, 105, 107, 109, 112, 114, 117, 118, 119, 120, 125, 182
matrix, viii, 32, 74, 75, 77, 81, 82, 111, 120, 165
measurements, 14, 15, 34, 35, 41, 47, 48, 49, 50, 76, 81, 82, 86, 94, 124
mechanical properties, 180
media, 93, 98, 100, 115, 168, 169, 181
medical, viii, x, xi, 2, 31, 32, 33, 105, 112, 145, 147, 152, 153
medicine, vii, x, 4, 5, 7, 29, 33, 56, 92, 106, 107, 146, 148, 153, 155, 165, 166, 179
melanoma, 166
membrane permeability, 19
membranes, 114, 115, 162, 172
mesoporous silica, ix, 55, 56, 57, 58, 62, 68, 69, 70, 71
metabolites, 23, 167
metal ions, 12, 18, 147, 149, 168
metal nanoparticles, vii, viii, ix, x, xi, 4, 5, 7, 12, 18, 23, 27, 28, 29, 32, 55, 73, 74, 89, 92, 105, 109, 145, 163
metal oxides, 57
metal salts, xi, 12, 106
metals, x, 11, 13, 77, 90, 109, 149, 153, 176, 178
metastasis, 162
methanol, 58, 70
methylation, 159
mice, xi, 146, 167, 172, 173, 184
microelectronics, xi, 74, 86, 145
microemulsion, xi, 106
microorganisms, 5, 6, 19, 28, 91, 92, 120
microscope, 76, 108, 132, 142
microscopy, ix, 12, 15, 32, 43, 106, 109, 128, 155
migration, 159, 163, 174
mitochondria, 156, 162, 166

mixing, 12, 128
MMP, 167
models, 111, 116, 147
modifications, 35, 50
moisture, 114
molecular oxygen, 168, 186
molecular structure, 33, 153
molecular weight, 120, 121, 128, 133, 134, 135, 136
molecules, viii, xii, 15, 32, 38, 39, 41, 43, 45, 47, 48, 49, 50, 75, 82, 112, 117, 119, 128, 146, 149, 153, 162, 166, 168, 178
morphology, 7, 15, 37, 47, 56, 60, 61, 62, 63, 68, 70, 76, 90, 132, 143, 155
mucosa, 172, 184
multivariate analysis, 176, 177, 183
mycelium, x, 90

N

NaCl, 171
nanocomposites, viii, 23, 32, 56, 58, 59, 60, 61, 68, 70, 113, 175
nanocrystals, 22, 70
nanomaterials, viii, 2, 5, 18, 24, 25, 27, 28, 92, 94, 107, 111, 112, 113, 118, 149, 162, 182, 184
nanomedicine, ix, xi, xii, 32, 112, 145, 146, 165, 180
nanometer, 106, 136
nanoparticles, vii, viii, ix, x, xi, 1, 2, 4, 5, 6, 7, 8, 9, 11, 13, 14, 15, 17, 18, 19, 20, 21, 22, 23, 24, 25, 26, 27, 28, 29, 32, 41, 43, 44, 45, 47, 50, 55, 57, 58, 59, 60, 61, 62, 68, 69, 70, 71, 73, 74, 75, 80, 82, 83, 86, 87, 89, 90, 92, 93, 94, 96, 97, 98, 99, 100, 101, 102, 103, 105, 106, 107, 108, 109, 110, 111, 112, 114, 115, 117, 119, 120, 121, 122, 125, 131, 132, 134, 135, 136, 137, 143, 145, 146, 149, 150, 151, 155, 163, 167, 173, 174, 175, 176, 177, 178, 179, 180, 181, 182, 183, 184, 185, 186

nanophotonics, x, 105
 nanorods, 58, 60
 nanosilver toxicity, 106, 114
 nanostructures, vii, ix, 4, 48, 55, 56, 58, 60, 68, 69, 73, 74, 89, 113, 142, 144, 148, 155, 186
 nanosystems, 165
 nanotechnology, 1, ii, iii, vii, x, 2, 4, 5, 18, 20, 21, 22, 23, 24, 25, 68, 69, 71, 92, 105, 114, 137, 139, 142, 146, 148, 149, 164, 175, 182
 nanowires, ix, 2, 55, 57, 58, 59, 60, 61, 62, 68, 70, 71, 113, 178
 nasopharyngeal carcinoma, 154, 165, 186
 natural resources, 6
 necrosis, 111, 152, 156, 162, 164
 nervous system, 172
 nickel, 69, 143
 NIR, 94, 164, 165, 166
 nitrogen, 49, 136
 noble metals, x, 89, 153
 nonlinear optics, 113
 NRF, 21
 nucleation, 74, 77, 128, 148
 nuclei, 59, 63
 nucleic acid, 153, 154
 nucleus, 156, 162
 Nuevo León, 89
 nutrients, 162
 nutrition, 162

O

one dimension, 146
 optical density, 93
 optical properties, xi, 18, 87, 92, 107, 108, 112, 113, 144, 145, 149, 173, 176
 optimization, 86
 optoelectronics, x, 74, 89, 106, 113
 organic solvents, 56, 57
 organism, 3, 149
 organs, xi, 146, 153, 164, 172
 oscillation, 108, 109, 150, 154

ovarian cancer, 174, 186
 oxidation, 6, 19, 69, 97, 98, 113, 116, 168
 oxidative damage, 162, 176
 oxidative stress, 110, 147, 157, 158, 172, 176, 180, 183, 184
 oxygen, 37, 48, 115, 150, 162, 163, 168, 174, 177, 185, 186

P

pathogens, 9, 19, 24, 25, 103, 114, 137
 pathway, 4, 115, 119, 151, 162, 163, 175, 183
 PDT, 150, 163, 183
 penicillin, 107
 peptide, 23, 43, 167
 peripheral blood mononuclear cell, 151, 177
 permeability, 19, 110, 162
 permit, 148, 149
 peroxidation, 156
 peroxide, 156, 162, 168
 PET, viii, ix, 31, 32, 33, 34, 35, 36, 37, 38, 39, 40, 41, 42, 43, 47, 48, 49, 50
 pH, 12, 38, 116, 117, 148, 169, 170, 171
 pharmaceutical, 3, 32
 phenol, 113
 phenolic compounds, 10
 phenyl propanoids, 11
 phenylalanine, 154
 phosphate, 172
 phospholipids, 154
 phosphorus, 110, 114
 photobleaching, 155
 photodynamic therapy (PDT), 150, 163, 183
 photoelectron spectroscopy, ix, 32, 35
 photoirradiation, 163
 photoluminescence, 74, 86, 165
 photonics, ix, x, 73, 89, 146
 photosensitizers, 163
 physical properties, 69
 physicochemical characteristics, 92
 PI3K, 163

plants, vii, xi, 2, 6, 7, 11, 22, 23, 24, 25, 28, 146, 149, 175, 179, 185

plasma membrane, 156, 162

plasmonic activity, vii, 5

platinum, 5, 64, 69, 70, 71

PM, 174, 184

pneumonia, 22

polar, 37, 48, 58

polyethylene terephthalate, 32, 37

polymer, viii, 31, 32, 33, 37, 38, 47, 57, 74, 114, 149, 175

polymer chain, 38

polymer films, 149

polymer nanocomposites, 175

polymeric materials, 33

polymers, viii, xi, xii, 23, 24, 25, 29, 32, 33, 75, 145, 146, 148, 168

polypeptide, 44

polyphenols, 9, 11, 17

polysaccharides, 11

polyvinylalcohol, 161

porous silicon, 74

precipitation, 45, 120

preparation, xi, 7, 11, 60, 117, 118, 120, 122, 124, 136, 145, 175

preservation, 5, 91, 168

pro-inflammatory, 151, 152

proliferation, viii, 32, 151, 152, 163, 179

properties of Ag-NPs, 106, 107

protein structure, 45

proteins, vii, viii, 2, 6, 19, 31, 33, 38, 110, 114, 117, 149, 151, 153, 154, 156, 162, 166

proteolytic enzyme, 111

Pseudomonas aeruginosa, 20, 24, 28

psoriasis, 167, 185

pulsed laser ablation in liquid, 90, 93

purification, 5, 27, 92, 114

PVA, 158, 161

PVP, xii, 120, 121, 128, 133, 134, 135, 136, 146, 148, 157, 158, 159, 161, 168, 170, 171, 177, 180

pyrolysis, xi, 106, 118, 148

Q

quartz, 34

quinacrine, 163

R

radiation, 5, 13, 76, 120, 124, 125, 141, 150, 163, 164, 178, 181, 183

radiation therapy, 150, 163

radiation treatment, 181

radicals, 110, 149, 162

radiosensitization, 164

radiotherapy, 20, 164, 186

Raman spectra, 76, 82, 83, 85, 153

Raman spectroscopy, x, 106, 153, 155, 176, 177, 180, 183, 184, 185

reaction medium, 12

reaction rate, 128

reaction time, 14, 16, 34

reactions, 38, 50, 113, 148, 149

reactive oxygen, 174, 177

reactivity, 2, 92, 107, 113, 117

reagents, vii, 2, 5, 120, 128

receptor, 152, 165, 167, 174

refractive index, 109, 150

respiratory syncytial virus, 151

response, viii, xii, 26, 31, 117, 146, 152, 158, 165, 166, 186

reticulum, 156, 162, 184

risk, 3, 25, 114, 120, 146, 168, 173, 183

RNA, vii, 2, 6, 113, 153

room temperature, 12, 25, 28, 34, 35, 62, 74, 75, 76, 99, 120, 128

root-mean-square, 47

roughness, 33, 37, 39, 41, 47, 142

ruthenium, 64, 69, 70, 71

S

Salmonella, 19, 110

salts, xi, 8, 11, 12, 58, 106, 172

SAXS, ix, 32, 35, 48, 50

scanning electron microscopy, 76

- scattering, x, 17, 35, 75, 76, 82, 83, 89,
106, 108, 112, 147, 150, 153, 155
- science, 92, 102, 107, 140, 142, 146, 147
- scientific investigations, 153
- secondary radiation, 183
- secretion, 152, 174
- selected area electron diffraction, 16
- selectivity, 163
- semiconductors, x, 77, 90
- sensing, x, 26, 56, 92, 106, 155, 179
- sensitivity, xi, 112, 145, 153, 154, 163,
165, 186
- sensitization, 164
- sensors, ix, x, 18, 68, 73, 74, 83, 86, 105,
108, 149, 153, 184
- serum, 154, 155, 168, 183
- shape, 10, 12, 13, 16, 19, 35, 92, 93, 94,
96, 98, 100, 101, 102, 107, 108, 109,
112, 116, 117, 118, 133, 136, 147,
148, 150, 155, 162, 164
- silanol groups, 63
- silica, ix, 55, 56, 57, 58, 62, 63, 68, 69,
70, 71, 75
- silicon, ix, 57, 73, 74, 75, 76, 77, 78, 79,
81, 82, 86
- silver nanoparticles (Ag-NPs), vii, viii,
ix, x, xi, 1, 4, 5, 6, 7, 8, 9, 11, 13, 14,
15, 16, 17, 18, 19, 20, 21, 22, 23, 24,
25, 26, 27, 28, 32, 43, 45, 47, 50, 57,
69, 70, 74, 80, 82, 83, 86, 87, 89, 90,
92, 93, 94, 96, 97, 98, 99, 100, 101,
102, 106, 107, 108, 109, 110, 111,
112, 114, 117, 120, 121, 122, 125,
131, 132, 136, 143, 147, 149, 150,
173, 174, 175, 176, 177, 178, 179,
180, 181, 182, 183, 184, 185, 186,
187
- skin, xi, 33, 145, 146, 152, 155, 163, 172
- small intestine, 172, 184
- small-angle X-ray, 35
- sodium, 5, 93, 107, 120, 136, 148
- sodium dodecyl sulfate, 93
- sodium hydroxide, 120, 136
- software, 35, 48, 66, 132
- solar cells, ix, x, 73, 74, 105
- sol-gel, 56
- solid state, 76
- solid tumors, 163
- solidification, 97
- solubility, 58, 62, 74, 116, 168
- solution, xi, 12, 14, 34, 38, 41, 42, 43,
44, 47, 50, 56, 58, 62, 63, 69, 70, 71,
76, 82, 83, 85, 86, 92, 94, 102, 106,
109, 114, 118, 121, 122, 127, 144,
147, 148, 166, 180
- solvents, ix, 3, 55, 56, 57, 58, 62, 63, 64,
65, 70, 118
- sorption, 59, 63
- South Africa, 1, 21
- species, vii, x, 2, 4, 7, 9, 10, 11, 21, 37,
90, 92, 97, 111, 149, 151, 174, 177
- specific surface, ix, 55
- spectroscopic techniques, 152
- spectroscopy, ix, x, 17, 32, 34, 35, 38,
43, 76, 106, 153, 155, 176, 177, 180,
181, 183, 184, 185
- spin, 121, 130, 132
- stability, 17, 28, 91, 106, 114, 118, 120,
147, 149
- stabilization, 11, 15, 27, 29, 128
- starch, xii, 6, 14, 16, 23, 26, 27, 146, 168
- state, 76, 90, 116, 184
- stem cells, viii, 32, 163
- stimulation, 125, 127
- storage, x, 90, 91, 94, 113
- stress, 110, 147, 157, 158, 159, 160, 161,
172, 176, 179, 180, 183, 184, 186
- stretching, 38, 43, 133
- strong interaction, 45, 150
- structure, viii, 31, 32, 33, 41, 42, 43, 44,
45, 47, 50, 76, 81, 82, 90, 118, 124,
125, 128, 155, 172, 182
- structure and morphology, 90
- styrene, 69
- substrate, viii, 32, 33, 41, 42, 47, 55, 56,
57, 58, 59, 60, 62, 63, 75, 77, 82, 83,
85, 121, 122, 130, 132
- sucrose, 160, 185
- Sun, 9, 24, 27, 28, 56, 57, 70, 71, 137,
142, 181, 186

- supercritical carbon dioxide, 56, 69, 70, 71
- superparamagnetic, 165
- surface area, ix, 2, 5, 13, 55, 56, 66, 107, 113, 117, 147, 168
- surface chemistry, viii, 31, 92, 112, 116, 117
- surface layer, 77, 80
- surface modification, viii, 31, 33, 38
- surface properties, 33, 37, 168
- surface structure, 41, 77, 128, 182
- surface tension, ix, 55, 56, 62
- surface treatment, 35, 49, 50
- suspensions, 107, 121
- sustainability, vii, 2, 4, 7
- sustainable development, 4
- sustainable energy, 22
- synergistic effect, 181
- synthesis, vii, x, xi, xii, 1, 3, 4, 5, 6, 7, 9, 11, 13, 14, 15, 17, 19, 20, 21, 22, 23, 24, 25, 26, 27, 28, 29, 57, 59, 69, 70, 71, 74, 75, 87, 90, 92, 93, 94, 101, 106, 114, 117, 118, 120, 121, 128, 146, 147, 148, 149, 162, 163, 167, 175, 177, 178, 181, 182, 185, 186
- synthesis of Ag-NPs, 6, 106
- T**
- target, x, 90, 93, 94, 96, 162, 172
- techniques, x, 5, 12, 13, 14, 15, 20, 24, 33, 37, 50, 86, 90, 92, 117, 118, 119, 148, 149, 153
- TEM, 15, 16, 27, 60, 61, 63, 94
- temperature, ix, 12, 25, 27, 28, 34, 35, 43, 55, 56, 57, 60, 62, 64, 68, 74, 75, 76, 91, 94, 99, 118, 120, 121, 128, 148, 149
- tension, ix, 55, 56, 62
- textiles, 2, 112, 150
- theranostic, xi, xii, 146, 147, 165, 167, 174, 184
- therapeutic agents, 112, 173
- therapeutic use, 152
- therapeutics, xi, 146, 165
- therapy, x, 18, 105, 150, 163, 164, 165, 166, 173, 174, 178, 183, 184, 186
- thermal decomposition, 118
- thermal energy, 150
- thermal properties, 56, 149
- thermal stability, 149
- thermal treatment, 58
- thermodynamics, ix, 56, 71
- thin films, 102, 112, 121, 124, 133
- tin, 70tin oxide, 70
- tissue, viii, 32, 163
- titanium, xi, 143, 145, 165
- toxic effect, 23, 111, 115, 162, 164, 167, 172, 179
- toxicity, vii, xi, 1, 3, 5, 6, 24, 29, 56, 106, 114, 115, 116, 117, 146, 147, 149, 155, 156, 162, 167, 168, 172, 173, 175, 176, 179, 181, 182, 185
- toxicology, 182, 185
- Transmission Electron Microscopy, 94
- treatment, x, 5, 18, 20, 32, 33, 34, 35, 36, 37, 38, 42, 48, 49, 56, 58, 59, 105, 112, 147, 150, 152, 155, 163, 165, 166, 174, 181, 185
- tryptophan, 155
- tumor, 111, 155, 162, 163, 164, 165, 167, 184
- tumor growth, 162
- tumor necrosis factor, 111
- tyrosine, 155
- U**
- underlying mechanisms, 23
- uniform, 77, 94, 96, 118, 128, 132, 148, 163
- urea, 120, 127, 128
- urine, 164
- V**
- vacancies, 77
- vacuum, 34, 75, 113
- valuation, 26, 175

vapor, xi, 56, 62, 75, 106, 148
vegetables, x, 90, 91, 94
VEGF, 163, 185
vessels, 5, 162
virus replication, 111
viruses, 19, 107, 150
viscosity, 62, 143

W

waste, 2, 21, 22, 91, 101, 112
waste disposal, 21
wastewater, 114, 167
water, x, 5, 9, 11, 15, 18, 25, 27, 35, 36,
38, 41, 62, 63, 71, 76, 90, 93, 94, 96,

114, 116, 121, 133, 167, 168, 169,
171, 175
water chemistry, 116
water purification, 27, 114
workers, 57, 59, 61, 62, 63, 64, 93
wound healing, 111, 152, 180, 185

X

X-ray diffraction (XRD), xi, 17, 60, 106,
122, 124, 125, 126, 136
X-ray photoelectron spectroscopy
(XPS), ix, 32, 33, 34, 35, 38, 48, 49,
50